C.P. No. 944

C.P. No. 944

LIBRARY
ROYAL AIRCRAFT ESTABLISHMENT
BEDFORD.

MINISTRY OF TECHNOLOGY

AERONAUTICAL RESEARCH COUNCIL

CURRENT PAPERS

Wind-Tunnel Tests on a Rectangular, Twin-Duct, Variable-Geometry Air Intake at Supersonic Speeds

by

M. D. Dobson

LONDON: HER MAJESTY'S STATIONERY OFFICE

1967

PRICE £1 5*s* 0*d* NET

U.D.C. No.533.697.2 : 533.6.011.5

C.P. No. 944*
April 1966

WIND TUNNEL TESTS ON A RECTANGULAR, TWIN DUCT, VARIABLE GEOMETRY AIR INTAKE AT SUPERSONIC SPEEDS

by

M. D. Dobson

SUMMARY

Tests have been made in the 3 ft × 3 ft supersonic wind tunnel on a rectangular twin duct air intake, which has variable geometry, over the Mach number range 1·7 to 2·2. The design Mach number of the intake was 2·12 and tests included an investigation of the effects of the variable geometry, throat bleed flow, transition fixing, splitter design and afterspill for conditions of equal and unequal throttling of the ducts.

Pressure recovery, duct mass flow and bleed mass flow were measured and the amplitude and frequency of pressure fluctuations were recorded.

Maximum mean pressure recoveries recorded were generally up to 2½% below the theoretical shock recovery. Recovery increases with the introduction of throat bleed and is dependent to some extent on transition of the boundary layer, bleed slot position and splitter design. At reduced duct mass flows both pressure recovery and distribution may be restored to "full flow" levels by careful use of afterspill.

Unequal throttling produces interference effects on the "unthrottled" duct by the "throttled" duct. These effects may be eliminated by the use of afterspill in the "throttled" duct.

---

* Replaces R.A.E. Technical Report No.66141 - A.R.C. 28348

CONTENTS

		Page
1	INTRODUCTION	7
2	EXPERIMENTAL DETAILS	7
	2.1 Model	7
	2.2 Model mounting	8
	2.3 Model systems and instrumentation	9
	2.4 Scope of tests	10
	2.5 Reduction and presentation of results	11
3	RESULTS - EQUAL ENGINE FLOWS	12
	3.1 Intake characteristics	12
	3.2 Intake performance	15
	3.2.1 Pressure recovery	15
	3.2.2 Flow distribution	17
	3.2.3 Flow stability	18
	3.3 Effects of configuration changes	19
	3.3.1 Throat bleed slot	19
	3.3.2 Fixing transition	19
	3.3.3 Splitter design	20
4	RESULTS - UNEQUAL DUCT FLOWS	22
	4.1 General	22
	4.2 Interference effects	22
	4.3 Effects of transition	23
	4.4 Splitter design	23
	4.5 Use and effects of spill vents	24
5	CONCLUSIONS	25
Appendix A	Comparison between model and current aircraft geometries	27
Tables 1-6	(Tables of results)	28-50
Symbols		51
References		52
Illustrations		Figures 1-59
Detachable abstract cards		-

ILLUSTRATIONS

	Fig.
Inlet details - splitter I configuration	1
Additional splitter configurations	2
Intake details	3
Duct details	4
Throat bleed slot configurations	5
Photographs of model	6
Area distribution along duct for $\delta_3 = 20°$	7
Model support	8
Details of flow control and measurement unit	9
Pressure recovery and mass flow ratio - differences in these quantities depending on method of evaluation ($M = 2{\cdot}12$, $\delta_3 = 16{\cdot}25°$)	10
Critical ramp angle - variation with Mach number	11
Possibilities of shock detachment at the cowl lip	12
Schlieren photograph - maximum inlet flow at $M = 1{\cdot}70$, $\delta_3 = 9{\cdot}7°$	13
Theoretical minimum and measured ratios of throat area to entry stream tube area	14
Schlieren photographs - $M = 2{\cdot}12$, splitter I	15
Mass flow ratio - variation with δ_3 at constant values of Mach number	16
Schlieren photographs - intake at full flow	17
Maximum values of mass flow when deflection is by 7° wedge only	18
Typical pressure recovery characteristics for various values of M and δ_3 - splitter I	19
Sketches showing shock systems at $M = 2{\cdot}0$	20
Maximum pressure recovery - variation with throat bleed flow, δ_3 and M - splitter I	21
Variation of bleed efficiency with Mach number for critical ramp angle settings	22
Summary of pressure recovery - variation with M and δ_3	23
Distributions of pressure recovery, $M = 2{\cdot}12$, $\delta_3 = 16{\cdot}25°$ - splitter I	24
Circumferential distribution of $V/\bar{V}$ at $r/R = 0{\cdot}798$, $M = 2{\cdot}12$, $\delta_3 = 16{\cdot}25°$	25
Distribution of $V/\bar{V}$ across a vertical diameter - $M = 2{\cdot}12$, $\delta_3 = 16{\cdot}25°$	26
Distortion parameters D_v and $V_{max}/\bar{V}$ - variation with r/R. $M = 2{\cdot}12$, $\delta_3 = 16{\cdot}25°$, $m_b/m_i = 0{\cdot}042$, splitter I	27
Distortion parameters D_v and R_v - variation with δ_3. $M = 2{\cdot}12$, $m_b/m_i \approx 0{\cdot}04$, splitter I	28

ILLUSTRATIONS (Contd.)

	Fig.
Pressure recovery distributions - inboard duct each with $m_b/m_i \approx 0{\cdot}04$ at the point of maximum P_f/P_∞	29
Circumferential distribution of $V/\bar{V}$ at $r/R = 0{\cdot}798$ - variation with Mach number. $m_b/m_i \approx 0{\cdot}04$, splitter I	30
Distortion parameter D_v - variation with Mach number $r/R = 0{\cdot}798$, $m_b/m_i \approx 0{\cdot}04$, splitter I	31
Fluctuating pressure amplitudes. $m_b/m_i \approx 0{\cdot}04$, splitter I	32
Frequency of L.F. oscillation - variation with throttle position	33
Stability boundaries. $m_b/m_i \approx 0{\cdot}04$, δ_3 critical, splitter I	34
Pressure recovery versus throat bleed flow; effect of throat bleed design. $M = 2{\cdot}12$, $\delta_3 = 16{\cdot}25°$, splitter I	35
Fluctuating pressure amplitudes at various values of throat bleed flow. $M = 2{\cdot}12$, $\delta_3 = 16{\cdot}25°$, splitter I	36
Effects of fixing transition, $M = 2{\cdot}12$, splitter I	37
Pressure recovery distributions - effects of fixing transition. $M = 2{\cdot}12$, splitter I	38
Circumferential distributions of $V/\bar{V}$ at $r/R = 0{\cdot}798$. $M = 2{\cdot}12$, $m_b/m_i \approx 0{\cdot}04$, splitter I	39
Maximum pressure recovery - variation with throat bleed flow and δ_3. $M = 2{\cdot}12$, splitter I	40
Effects of transition on maximum values of pressure recovery and mass flow at $M = 2{\cdot}12$ - variation with δ_3. $m_b/m_i \approx 0{\cdot}04$, splitter I	41
Fluctuating pressure amplitudes. $M = 2{\cdot}12$, $\delta_3 = 16{\cdot}25°$, $m_b/m_i \approx 0{\cdot}04$, splitter I	42
Maximum values of pressure recovery - variation with δ_3 for the three splitter designs, $M = 2{\cdot}12$	43
Maximum values of mass flow ratio - variation with δ_3 for the three splitter designs, $M = 2{\cdot}12$	44
Pressure distributions. $M = 2{\cdot}12$, $\delta_3 = 16{\cdot}25$, $m_b/m_i \approx 0{\cdot}04$	45
Circumferential distributions of $V/\bar{V}$ at $r/R = 0{\cdot}798$. $M = 2{\cdot}12$, $\delta_3 = 16{\cdot}25°$, $m_b/m_i \approx 0{\cdot}04$	46
Maximum pressure recovery - variation with throat bleed flow and δ_3. $M = 1{\cdot}85$	47
Fluctuating pressure amplitudes, splitter II. $M = 2{\cdot}12$, $\delta_3 = 16{\cdot}25°$, $m_b/m_i = 0{\cdot}04$	48
Fluctuating pressure amplitudes, splitter III. $M = 2{\cdot}12$, $\delta_3 = 16{\cdot}25°$, $m_b/m_i = 0{\cdot}04$	49

ILLUSTRATIONS (Contd.)

	Fig.
Curves showing interference effects	50
Changes of pressure recovery in inboard duct for a mass flow ratio in outboard duct 20% below maximum	51
Schlieren photographs	52
Pressure distributions in the inboard duct with throttle set to pass maximum flow. $M = 2{\cdot}12$, $\delta_3 = 16{\cdot}25°$, splitter I	53
Curves showing interference effects. $M = 2{\cdot}12$, $\delta_3 = 17{\cdot}25°$, $m_b/m_i = 0{\cdot}04$	54
Curves showing interference effects, splitter II. $M = 2{\cdot}12$, $\delta_3 = 16{\cdot}25°$	55
Curves showing interference effects, splitter III. $M = 2{\cdot}12$, $\delta_3 = 16{\cdot}25°$	56
Velocity distributions in inboard duct at $r/R = 0{\cdot}877$. $M = 2{\cdot}12$, $\delta_3 = 16{\cdot}25°$, $m_b/m_i \approx 0{\cdot}04$	57
Pressure distributions and schlieren photographs	58
Pressure recovery - variation with mass flow ratio showing effects of opening spill vents. $M = 2{\cdot}12$, $\delta_3 = 16{\cdot}25°$, splitter III	59

1 INTRODUCTION

As a continuation of the work reported in Ref.1 it was felt necessary to use a more highly developed intake and one which was more appropriate to current thinking for the supersonic transport aircraft project. Thus a twin-duct model with external compression, designed for a Mach number of 2·12 was manufactured.

The compression geometry consisted of two surfaces, the first of which was a fixed wedge and the second a variable ramp which included a curved "isentropic compression" portion. Both duct flow and throat bleed flow could be controlled and measured, while afterspillage could be controlled but not measured directly.

The model geometry was different from that proposed subsequently[2] for the supersonic transport in several respects and Appendix I provides a comparison of the main features.

2 EXPERIMENTAL DETAILS

2.1 Model

Drawing of various parts of the model appear in Figs.1 to 5 and two photographic views in Fig.6.

Throughout its length the model is split into two ducts by a central splitter. It is symmetrical about this splitter and the two ducts diverge downstream each at an angle of $\frac{1}{2}^{\circ}$ relative to the splitter centre line. Three interchangeable splitter leading-edge configurations are available. The leading edge of splitter I (Fig.1) lies in the plane of the sidewall leading edges and splitters II and III (Fig.2) are both extended upstream of this.

Each duct inlet is 3·68 inches wide and the height of the lip above the leading edge of the compression wedge is 2·707 inches. The aspect ratio and capture area per duct are therefore 1·36 and 9·95 sq inches respectively. Some slight compression of the flow results from both the splitter and the inside of the outer walls (Fig.1), but the main compression is by the double wedge arrangement shown in Fig.3. There is a fixed angle wedge OA whose oblique shock wave falls on the intake lip at a Mach number of 2·12. This is followed by a ramp AB which provides the variable part of the compression geometry and which is pivoted as indicated in Figs.3 and 4. Immediately behind the first pivot point the ramp surface describes a circular arc turn of 9·3°, which gives roughly focussed isentropic compression, and then is followed by a length of flat surface. Thus with the notation as indicated in Fig.3, the compression geometry is:-

δ_1 fixed 7°

δ_2 variable 0·2° to 12·7°

then 9·3° near isentropic turn giving :-

δ_3 9·5° to 22°.

When the compression geometry is varied, changes in the subsonic diffuser shape occur as a result of the pivoting arrangements shown in Fig.4. Because of a physical connection between pieces AB and CDE across the bleed gap, the part OA is constrained to slide horizontally as BC is moved parallel to itself. Thus at constant Mach number, variation of the ramp geometry alters by parallel motion, the position of the first oblique shock wave relative to the lip. The upstream end of the portion BC contains the throat bleed slot, the various configurations of which are shown in Fig.5.

The portion DE arbitrarily fairs the rectangular duct section into the circular measuring station. Fig.7 shows a duct area distribution for $\delta_3 = 20°$.

To control afterspillage each duct includes a spill vent which is shown in Fig.4 and can be clearly seen in the photograph Fig.6(b).

To distinguish between the two ducts of the model, they are referred to as "outboard" and "inboard" and are as shown in Fig.6(a). Thus their orientation is correct with respect to subsequent tests[3] which have been made with the nacelle mounted on a half-wing model typical of a supersonic transport configuration.

2.2 Model mounting

A sketch of the method of mounting the model in the tunnel is shown as Fig.8. The model was attached to a table which was pivoted towards its upstream end onto a strut fixed to the tunnel floor. The pivot was at the centre of rotation of the tunnel incidence quadrant, to which the rear of the table was attached by a flexible joint. Thus by rotating the quadrant the incidence of the table (and model) could be varied while the aerodynamic and static loads were taken by the strut. Upstream of the inlet, a suitably shaped "Mach" plate was attached to the table which generated a local uniform flow in the region of the inlet, the supersonic Mach number of which was varied by variation of the incidence of the plate. Thus the facility to test the model

at Mach numbers above the tunnel maximum of 2·0 was available, with the added convenience of Mach number variation during a single run.

The "Mach" plate was displaced below the model wedge leading edge to provide a bleed for the plate boundary layer and some difficulty was experienced in finding a suitable point at which to inject this air back into the free stream, particularly at Mach numbers above 2·0. However a suitable arrangement was achieved by collecting it and ducting it to the upper surface of the table on either side of the nacelle where the pressures were low enough to provide suction.

The upper limit of entry Mach number (M) was set by the tunnel normal shock* which gradually moved upstream as incidence was altered in the direction to increase M. At M just greater than 2·2 this shock was sufficiently far upstream to begin to interfere with the inlet shock system and thus M = 2·2 was the upper limit for these tests.

2.3 Model systems and instrumentation

Independent actuation of each of the ramp systems and each of the spill vents was by electromechanical arrangements and in each case a remote reading position indicator was included. Flow through the ducts was controlled by separate conical plugs at the exits but these plugs were moved together by a single motor. Asymmetric throttling conditions could only be achieved by disconnecting one plug from the motor and setting it at a required position. Indication of the throttle position was by a multi-way switch and lamp system.

A drawing showing a main duct flow control and measurement unit is shown in Fig.9. The instrumentation contained therein includes twelve pitot pressure tubes and eight static pressure holes. The pitot tubes were mounted on a rotatable rake across a diameter, with six tubes on each arm positioned radially at the centres of six annuli of equal area. The two rakes (one in each duct) were mechanically linked so that they rotated in unison, driven, through gearing, by a single electric motor. Four of the static holes were located in the outer wall of the duct at angular positions of 0°, 90°, 180° and 270° in the plane of the pitot tubes. The other four statics were positioned in the outer wall further downstream at angular positions of 75°, 165°, 255 and 345° thus avoiding the wakes from the four struts which supported the central hub. Two methods of measuring mean pressure recovery and duct mass flow were thus available. Firstly, using the pitot tubes and their associated statics and secondly, using

* It is thought that the strut was to some extent responsible for the position of the tunnel shock and it is hoped that redesign of this strut will enable M to be increased to 2·4 for future tests.

the remaining four statics together with a sonic exit of known area. The exit of each duct was carefully shaped in order to provide a high discharge coefficient.

To measure transient pressures, capacitance type pressure transducers were located within the control hub of each duct with their diaphragms exposed to the pressure at a small hole on the hub centre line facing directly upstream. The range of the transducers was ±4 psi (free stream total pressure was 6·3 psi), with an upper frequency limit of several kilocycles per second. The amplified output from the transducers was used to drive mirror galvanometers, the ultra-violet light spots from which recorded onto sensitive paper. For calibration purposes the transducer diaphragms were exposed to a series of steady pressures.

Auxiliary suction, external to the tunnel, was provided to operate the throat bleed. Control of this was by hand operated valves (one for each duct) and measurement, by pitot tubes and a static hole at a suitable station in the bleed ducting upstream of the valve.

2.4 Scope of tests

The test values of entry Mach number were 1·70, 1·85, 2·00, 2·12 and 2·20, though some configurations were not tested at all these Mach numbers and others were tested only at the design value of 2·12. Corresponding Reynolds numbers, based on inlet capture height, were:-

M	1·70	1·85	2·00	2·12	2·20
$R_e (\div 10^6)$	0·393	0·374	0·346	0·330	0·319

To fix transition of the boundary layer at the inlet, bands of distributed roughness were applied to the ramp surface, sidewalls and splitter. The bands were about 0·2 inch wide, positioned about 0·2 inch from the leading edges, and consisted of 0·011 inch diameter ballotini, secured with an epoxy resin.

All cases were tested with this artificial fixing of transition except one in which splitter I configuration was tested without for comparison purposes. Five throat bleed configurations were tested, all with splitter I and in all other tests, bleed configuration A0 was used (see Fig.5).

Pitot pressure surveys in the ducts were made, in some cases by taking readings at rake rotation angles of 0° × 30° to 150° and in other cases, by taking readings at 0° and 90° only. The former are referred to as comprehensive surveys and the latter as limited surveys.

The method of obtaining unsteady pressure characteristics was to start with the throttles fully out (inlet well supercritical) and then run them in continuously, at the same time recording the transducer outputs. Event markers on the recorder were used in conjunction with the throttle position indicators so that the traces could be related to throttle positions and hence duct mass flows.

2.5 Reduction and presentation of results

Curves A and B of Fig.10 show typical values of pressure recovery plotted as a function of mass flow ratio. Pressure recovery is quoted as the mean mass flow weighted total pressure compared with the entry stream total pressure*. Curve A shows recovery measured at the compressor entry position using the pitot tubes and their associated static tappings. Curve B shows values measured from choked exit conditions. The loss of 0·02 in recovery from A to B arises from the further aft measurement position, downstream of the pitot rakes and cruciform struts, (see Fig.9). Pressure recovery as measured by the pitots and their associated statics is used throughout this report.

Mass flow ratio is defined as the entry stream tube area, which is the sum of the "engine" mass flow m_e, the throat bleed mass flow, m_b and the afterspill mass flow $m_{s.v.}$, compared with the inlet capture area. The values of m_e/m_i for curves A and B, Fig.10 are measured from choked exit conditions. The values used in curve C are from the pitot measurements, and it will be seen that a less well defined supercritical characteristic is obtained and the "comprehensive" point aligns less well with the other points. This is typical of the results as a whole and therefore the choked exit method of calculating mass flow ratio is used in this report.

To limit the number of figures, only selected experimental results are plotted but all are contained in tables 1 to 6, which list values of m_e/m_i, m_b/m_i, A_∞/A_{en} and P_f/P_∞.

The following is a summary of the tests made:-

---

* This is not necessarily the tunnel total pressure because of the Mach plate.

Splitter Config.	Throat bleed Config.	M	δ_3	Throttling	Table
I	A0	1·70	9·7, 11·3	Equal	1
I	A0	1·85	11·3, 13·25	Equal	1
I	A0	2·00	13·6, 15·75, 16·25, 17·75	Equal	1
I	A0	2·12	15·25,16·25, 17·50, 18·25, 20·0	Equal	1
I	A0	2·20	16·25,17·50, 18·25, 20·25	Equal	1
I	A0	1·70	9·7	Unequal	2
I	A0	1·85	11·3	Unequal	2
I	A0	2·00	13·6	Unequal	2
I	A0	2·12	16·25	Unequal	2
I	A0	2·20	17·50	Unequal	2
II	A0	1·85	11·3, 13·25	Both	3
II	A0	2·12	16·25	Both	3
III	A0	2·12	16·25, 17·25, 18·25	Equal	4
III	A0	2·12	16·25	Unequal	4
I	A0	2·12	16·25, 17·25, 18·25 (No roughness)	Both	5
I	A2	2·12	16·25	Equal	6
I	A4	2·12	16·25	Equal	6
I	B0	2·12	16·25	Equal	6
I	B2	2·12	16·25	Equal	6

Results of fluctuating pressure measurements are not available for every flow condition because the recording equipment was available for only part of the period of the tests. The selection of results presented however, records the main characteristics.

The results presented are peak to peak amplitudes of total pressure fluctuation, P_A/P_∞, as a function of mass flow ratio for unequal throttling cases only. The tests indicated that similar stability characteristics are obtained in the throttled duct if both ducts are throttled together.

3 RESULTS - EQUAL ENGINE FLOWS

3.1 Intake characteristics

Tests commenced with the establishment of a relationship between critical ramp angle and Mach number. With the throttles wide open the schlieren image

was observed while the ramps were moved together to increase the angle δ_3, at each Mach number, until a point was reached at which the inlet normal shock was seen to detach from the cowl lip. The value of δ_3 at this point is called the critical ramp angle and is shown plotted as a function of Mach number in Fig.11.

In general the normal shock could detach from the cowl lip as δ_3 is increased for one of two reasons:-

(i) either internal or external deflection of the flow at the lip,

or (ii) reduction of the duct area below the value at which the full entry stream tube can be passed.

To investigate whether, in this model, shock detachment is caused by (i), Fig.12 has been drawn. At the critical ramp angle for each of the five test Mach numbers, values of flow deflection required for shock detachment at Mach number M_3* are plotted. The variation of external and internal cowl angles relative to δ_3 are also plotted as a function of δ_3. If it is assumed that the Mach number at the lip is M_3 and that the flow direction is parallel to δ_3, then it will be seen that only at $M = 1{\cdot}70$, $\delta_3 = 9{\cdot}7°$ is the (external) deflection at the cowl lip likely to be sufficient to detach the shock. Fig.13 is a schlieren photograph at this condition and although it is difficult to see whether the shock is actually attached or just detached, any displacement there is is extremely small. The conclusion therefore, is that flow deflection at the lip does not cause detachment of the normal shock at any Mach number.

To investigate possibility (ii), estimates have been made of the effective model contraction ratio A_2/A_1 (for notation see Fig.3). The geometrical part of this may be calculated but uncertainty in the estimation lies in the calculation of the growth of the boundary layer between the two planes. However an estimation of this on the appropriate parts of the four bounding surfaces was made and as a check, the amount of boundary layer compression which together with the physical contraction would be required to choke the throat at $M = 2{\cdot}12$, $\delta_3 = 16{\cdot}25°$ was calculated. These two values were found to agree reasonably well and the mean of them was used as the value of the boundary layer contribution to the internal contraction at all Mach numbers.

A curve of the estimated model contraction ratio is shown in Fig.14 plotted as a function of δ_3. Theoretical area ratios required to choke the

---

* M_3 is the pre-normal shock Mach number, i.e. after the oblique shocks and isentropic compression.

subsonic flow downstream of the normal shock (assumed to lie in plane A_1) for various values of Mach number are also plotted as functions of δ_3. It will be seen that observed critical values of δ_3 fall below the estimated curve while corresponding next higher values fall above. This indicates that duct choking is the likely reason for expulsion of the normal shock and thereby determines the limiting value of δ_3 at each Mach number.

Schlieren photographs of the model with various values of δ_3 at a Mach number of 2·12 are shown in Fig.15 for cases with zero and about 4% throat bleed flow. Corresponding photographs of each case show similar external shock configurations and indicate the critical value of δ_3 to be about 16·25°. It appears therefore that the presence of throat bleed flow does not have any large effect on the external shock geometry. This is as might be expected since the bleed slot position is downstream of the geometric throat. However the results do indicate a small effect (not discernible on the schlieren) in that at values of δ_3 greater than critical the total mass flow is generally 1% to 2% greater with throat bleed flow than without. This probably results from the upstream influence of the bleed on the boundary layer, for example, in helping it to turn the corner of the compression surface upstream of the bleed slot (see Fig.3), thus affecting the net throat area. Once throat bleed flow is present any increase of this flow does not alter the total mass flow and is therefore at the expense of engine flow.

By definition, ramp angles greater than critical cause a detached normal shock (Fig.15) and thus forespillage and reduced entry flow. Fig.16 illustrates the reduction in mass flow at constant Mach number as δ_3 is increased above critical. The figure also shows that at Mach numbers of 2·12 and 2·20 the inlet flow remains constant as δ_3 is reduced below the critical value, which result indicates that under these conditions the second ramp does not cause any spillage of the flow.

The dashed line on Fig.16 joins values of A_∞/A_{en} measured at critical settings of δ_3, and these are in fact, the maximum values measured. Maximum values vary from 0·905 at M = 1·70 to 0·934 at M = 2·20. At Mach numbers below the intake design value there will clearly be some two-dimensional forespillage as the first oblique shock passes upstream of the lip, as illustrated by schlieren pictures in Fig.17. However the photographs taken at M = 2·12 and

2·20 show that at these Mach numbers also, the first oblique shock passes upstream of the lip. This modification to the shock angle as compared with design is not uncommon in model tests and could result from effects of compression surface boundary layer. It might be expected that this kind of mismatch would occur, though perhaps to a lesser extent, at full scale. However it is interesting to note that in the tests of Ref.1 the actual shock geometry was obviously close to the theoretical geometry, as evidenced both by schlieren photographs and maximum measured values of mass flow. The implication of this is that mismatching of this kind may be dependent upon intake aspect ratio. It should be pointed out that in wind tunnel schlieren photographs any local distortion of the oblique shock in the region of the sidewalls would be what is "seen" by the schlieren system.

A comparison is made in Fig.18 between maximum measured values of mass flow and those calculated when pre-entry deflection is by a 7° wedge only. The oblique shock angles used in this calculation are those measured on the schlieren photographs of Fig.17 and thus the calculated values of mass flow allow for cowl lip spillage. Since the intake has an aspect ratio near to unity, it might be expected that sidewall spillage would be of similar magnitude to cowl lip spillage and thus could largely account for the residual difference between the calculated and measured values of maximum mass flow.

3.2 Intake performance

The prime objects of an inlet-diffuser system are to provide the engine with air at the highest possible mean total pressure and to present this air as uniformly as possible to the compressor. Both of these aspects have been examined and are discussed in this section.

3.2.1 Pressure recovery

Mean pressure recovery is plotted as a function of mass flow ratio in Fig.19. These curves are typical for the various values of δ_3 at each Mach number and in each case throat bleed flow is 3% to 4% of the total inlet flow. On the curves for M = 1·85, 2·12 and 2·20 letters appear: these correspond with schlieren photographs which are included in the presentation.

At Mach numbers below the design value of 2·12, the maximum pressure recovery is achieved at values of δ_3 greater than the critical. This is thought to be due to the isentropic part of the compression process and is illustrated in Fig.20. The sketch shows the theoretical shock geometries for

δ_3 = 13·6° and 15·75° at a Mach number of 2·0. The critical value of δ_3 is 13·6° and the sketch shows that the isentropic part of the compression meets the normal shock well inside the lip at this value, with the result that, while some of the inlet flow goes through the complete compression process, some goes only through the first oblique shock and the normal shock. At a δ_3 of 15·75° the isentropic fan meets the normal shock nearer the lip and thus, for small displacements of the normal shock, a larger proportion of the inlet flow goes through the isentropic compression, which results in a higher mean pressure recovery.

Data obtained at other values of throat bleed flow are contained in Table 1 but are not plotted. However, curves showing maximum mean pressure recovery plotted as a function of throat bleed flow for each Mach number, are given in Fig.21. In this and similar later figures, curves are drawn as continuous lines when they are defined by three or more experimental points but where tests were made at two values of bleed flow only, (usually zero and about 0·04), the points are joined by a straight dashed line.

In all cases pressure recovery rises with increase of throat bleed flow up to the maximum values tested. The rate of change of recovery with bleed flow varies with Mach number and ramp angle and Fig.22 shows this exchange rate plotted as a function of Mach number, in each case at the critical ramp angle. Below M = 2·0 the exchange rate is well below 1·0 but above this Mach number rises rapidly to 1·5 at M = 2·12.

A summary plot from the pressure recovery results is given in Fig.23. This shows the variation of maximum pressure recovery with δ_3 and M. Three curves are included, the measured recovery at a throat bleed flow of 0·035, the maximum recovery measured (usually at higher values of throat bleed flow) and the recovery as determined from theoretical shock systems for the experimental inlet geometry. The measured values are generally between 1% and 2½% below the theoretical values except at a Mach number of 2·20 where they coincide. As this Mach number is greater than the design value, the first oblique shock would theoretically fall inside the cowl lip. In calculating recovery, allowance has been made for the small portion of inlet flow that would pass through a "free stream" normal shock. However a schlieren photograph (Fig.17(e)) shows that the first oblique shock passes upstream of the cowl lip and therefore this diminution in shock recovery does not apply in the experiment.

The reason for the rapid fall in recovery between a Mach number of 2·0 and the design value of 2·12 is that restriction of δ_3 to the critical value, does not allow the inlet geometry to become optimum and thus the model inlet runs at reduced efficiency.

Summarising the results on pressure recovery, it may be said that with 3½% bleed flow, peak measured recoveries at all Mach numbers investigated are within 2½% of the corresponding theoretical recoveries for the shock configurations actually obtained. Increase of Reynolds number to full scale may be expected to be beneficial in two respects:-

(1) Viscous losses, represented by the 2½% maximum, will be reduced by 30% or so* and will therefore be around 1½%;

(2) the thinner boundary layers on the compression surfaces will allow a shock configuration closer to design to be obtained, which will itself have a higher pressure recovery.

The results therefore confirm the high internal efficiency of this intake design.

3.2.2 Flow distribution

Distributions of flow at the measuring station are presented in the form of isobaric maps of pressure recovery and in terms of distribution of velocity around and across the annulus. Pressure distributions are shown in Fig.24 for a Mach number of 2·12, $\delta_3 = 16{\cdot}25^\circ$ with throat bleed flows of zero and 0·042. Distributions are approximately symmetrical about the vertical centre line of each duct and a region of maximum pressure occurs in the half of the duct adjacent to the cowl lip. Maximum values of pressure recorded are greater than the theoretical shock recovery of 0·914 indicated in Fig.23. This could result either from a more efficient local supersonic compression caused by normal-shock and boundary-layer interaction or from a strong oblique shock adjacent to the cowl lip[4] followed by subsonic flow.

The effect of introducing throat bleed is to reduce pressure gradients over the annulus and also to increase substantially the pressure level on the ramp side in the duct. The low pressure level without bleed results from a separation of the flow in the subsonic diffuser and the introduction of throat bleed substantially reduces it. By comparing the pressure distributions of

---

* By analogy with Reynolds number correction to skin friction.

Fig.24, the presence of throat bleed would appear to produce a marked improvement in the distribution of flow but when this is examined in terms of $V/\bar{V}$, circumferential and radial distributions of which are shown in Figs.25 and 26, the improvement is not as great as might have been expected. From these figures it may be seen that differences in D_v $(V_{max}/\bar{V} - V_{min}/\bar{V})$ between cases with and without throat bleed is only about 10%. Values of D_v and $\left[\frac{V_{max}}{\bar{V}}\right]_{RAD}$ have been have been calculated and are plotted as functions of radial distance r/R in Fig.27. Both parameters are seen to increase up to $r/R \simeq 0{\cdot}8$ above which value they fall. Thus R_v, in which V_{max} is the maximum value measured over the whole duct area, is 1·24. The variations of R_v and $[D_v]_{r/R=0{\cdot}798}$ with δ_3 at a Mach number of 2·12 are shown in Fig.28.

Fig.29 shows a pressure recovery distributions at the four off-design Mach numbers. In each case δ_3 is the critical value and the throat bleed flow is about four per cent. As Mach number is reduced the isobars become increasingly more circular and concentric with the duct axis which results in the increasingly improving circumferential velocity distributions shown in Fig.30. The variation of D_v at $r/R = 0{\cdot}798$ with Mach number is shown in Fig.31.

3.2.3 Flow stability

The effects on duct pressure fluctuations resulting from throttling are shown, at each Mach number, in the lower curves of Fig.32. The lowest level of amplitude at each Mach number occurs in the region of critical flow. Opening the throttle beyond the "critical" position usually leads to an increase in amplitude, as indicated by the dashed part of the curves. The lowest level of fluctuation recorded increases from zero at M = 1·70 and 1·85 to 0·02 at M = 2·12 and 0·05 at M = 2·20. As the throttle is closed from the critical position, a point is reached at which the amplitude begins to increase, usually fairly rapidly. This point varies from about 7½% below full mass flow at M = 1·70 to immediately below full mass flow at M ≥ 2·00. The oscillation here is of high frequency i.e. around 500 cps. As the throttle is further closed the amplitude of this oscillation increases until a point is reached at which a low frequency oscillation starts. This oscillation occurs at Mach numbers greater than 1·85 with a sudden increase of amplitude from the high frequency signal. It is thought to result from shock induced separation of the boundary layer on the ramp surface and here is called "buzz". The frequency of buzz varies with throttle position and is of the order 50-100 cps. A curve showing the variation of frequency over a small range of throttle movement is given

in Fig.33, which also includes details of the throttle geometry. There is generally a region in which both the high and low frequency oscillations occur together but buzz usually dominates. The amplitude of buzz varies from about $0{\cdot}2\ P_\infty$ at $M = 1{\cdot}70$ to $0{\cdot}5\ P_\infty$ at $M = 2{\cdot}20$, while the maximum amplitude of the high frequency instability is about $0{\cdot}15\ P_\infty$. Fig.34 shows the boundaries of A_∞/A_{en} at which both instabilities start, as a function of Mach number.

3.3 Effects of configuration changes

3.3.1 Throat bleed slot

The actual shapes of the front and rear edges of the bleed slot were fixed but the width and position of the slot could be varied to some extent by building up either or both of these edges. The various configurations tested are shown in Fig.5.

The performances of the various bleed configurations in terms of main duct pressure recovery are plotted as a function of bleed flow in Fig.35. The results for the "A" configurations fall reasonably on a single curve indicating that the position of the front edge of the slot is not critical. The points for the "B" configurations also fall reasonably on a curve but at a level rather above the "A" curve indicating that a gain of about ½% in pressure recovery (at 2 to 4% bleed flow ratio) can be achieved by moving the rear edge forward to the "B' position.

Although the presence of throat bleed flow does not affect the amplitude of either type of flow oscillation, it does influence the buzz boundary, as shown in Fig.36. With no bleed flow this boundary is at $A_\infty/A_{en} = 0{\cdot}69$ but with bleed it improves by 5% to $0{\cdot}64$.

3.3.2 Fixing transition

To assess this effect the model was tested without roughness bands at a Mach number of $2{\cdot}12$. The critical value of δ_3 was found to be $17{\cdot}25^\circ$, which is 1° higher than for the case with fixed transition and probably results from a thinner compression surface boundary layer. The nearest test value of δ_3 for the model with transition fixed is $17{\cdot}5^\circ$ and results for the two cases and for the optimum δ_3 ($16{\cdot}25^\circ$) with transition fixed are compared in Fig.37 (a) and (b), for zero and 4% throat bleed flows. The maximum value of pressure recovery with free transition is greater than in both cases of fixed transition at both throat bleed conditions. Since the maximum values of mass flow ratio are not very different for the two transition cases at their respective critical ramp

angle settings, it might be expected that the external shock geometry is not much affected by transition and the schlieren photographs* contained in Fig.37, corresponding to the experimental points as indicated, confirm this. These facts indicate that allowing free transition gives results which are representative of higher Reynolds number conditions and adding roughness artificially thickens and disturbs the boundary layers giving reduced values of peak pressure recovery. Pressure recovery distributions for transition fixed and free with bleed flows of 0 and 4% are shown in Fig.38. At both values of bleed the improved mean recovery due to free transition comes from a general increase of pressure level over the depressed parts of the engine face and with this, particularly at 4% throat bleed flow, comes a much improved distribution. This is demonstrated in the circumferential velocity distribution plot of Fig.39 and the following values of D_v at $r/R = 0{\cdot}798$ are noted:

roughness on	D_v	= 0·757
no roughness	D_v	= 0·493.

The variation of maximum pressure recovery with throat bleed flow for each of the test values of δ_3 for the model with free transition is shown in Fig.40. For comparison the "roughness on" curves are shown and these are seen to be slightly steeper giving a slightly better exchange rate. Fig.41 provides a comparison of peak values of mass flow ratio and pressure recovery measured over a range of δ_3 for the two cases. With free transition, recoveries 1½% to 2½% greater are noted for little change in mass flow ratio.

Fluctuating pressure results are available for the model without roughness with $\delta_3 = 16{\cdot}25°$ and pressure amplitudes are shown as a function of mass flow ratio in Fig.42. Comparison with the results with roughness shows there to be little difference in the buzz boundary but around the critical point, $(A_\infty/A_{en} = 0{\cdot}93)$, there is, without roughness, a slightly smaller amplitude fluctuation which persists to 5% subcritical, as opposed to the case with roughness where the amplitude rises immediately on reduction of mass flow from the critical.

3.3.3 Splitter design

At full scale it is structurally necessary to have some thickness of the centre splitter in the region of the cowl lip, which therefore involves an upstream extension. Results hitherto discussed refer to the case with no extension, designated splitter I and shown in Fig.1. Limited tests have been

* When comparing photographs, $\delta_3 = 17{\cdot}5°$ for the "roughness on" case is 1¼° above the critical value and therefore the normal shock is slightly detached.

made at a Mach number of 2·12 on two extended splitters, designated II and III and illustrated in Fig.2.

Peak values of pressure recovery (Fig.43) and mass flow ratio (Fig.44) are plotted against δ_3 for the three splitters. These results indicate that the critical ramp angle for the model with splitter III is slightly greater than that for splitter I. The reason for this is not clear as it might have been expected that an increased upstream length and consequent increased boundary layer thickness on the splitter wall would have led to a reduced effective throat area.

With 4% throat bleed flow and $\delta_3 = 16{\cdot}25°$, pressure recovery falls with increasing upstream extension of the splitter but the duct passes (to within 1%), the same mass flow in each case. Pressure recovery distributions for splitter cases II and III at these conditions are shown in Fig.45 and are comparable with those of Fig.24 (b) for splitter I. Careful examination of these figures shows that the reduction in recovery with extension of the splitter cases from a lowering of the pressure level in the lip-splitter quadrant. The last continuous isobar running round the periphery of this quadrant in each case is:-

splitter I	0·90
splitter II	0·88
splitter III	0·86 (outboard), 0·84 (inboard).

This quadrant is adjacent to that part of the splitter where the upstream extension is greatest. Circumferential distributions of $V/\bar{V}$ at $r/R = 0{\cdot}798$ for the three cases are shown in Fig.46. The extended splitters produce reductions in $V/\bar{V}$ in the lip-splitter quadrant but slight increases in the lip-sidewall quadrant which results in there being little effect on D_v.

Further limited tests were made with splitter II at a Mach number of 1·85 and peak measured values of pressure recovery are shown as a function of throat bleed flow in Fig.47. Comparison with corresponding splitter I curves, also plotted, shows there to be little difference between the two cases.

Pairs of curves similar to those of Fig.32 showing the variation of fluctuating pressure amplitude with mass flow ratio are presented for splitters II and III in Figs.48 and 49. In each case $\delta_3 = 16{\cdot}25$, $M = 2{\cdot}12$ and $m_b/m_i \simeq 0{\cdot}04$ so they are comparable with the splitter I case, Fig.32(d). The character of the curves for the outboard duct is similar in each of the three cases and the buzz boundary occurs at similar values of A_∞/A_{en}.

4 RESULTS - UNEQUAL DUCT FLOWS

4.1 General

The main purpose of this type of test is to study the effects which throttling of one duct will have on the general performance of the other. This is a situation that could occur if for example the intake control system functioned wrongly or a spill vent failed to open after a single engine failure. Thus it is necessary to check on the stability of the flow in the unthrottled duct as well as its pressure recovery and flow distribution. Accordingly tests were made on the model with the throttle of the inboard duct set to pass approximately full flow, while the outboard duct was throttled progressively.

4.2 Interference effects

Fig.50 shows the basic results for five test Mach numbers, in each case with the appropriate critical value of δ_3. On each graph two curves are plotted, one which shows the variation of mean pressure recovery with inlet mass flow ratio for the throttled outboard duct and one which shows the pressure recovery in the inboard duct (whose throttle is fixed to give the value of A_∞/A_{en} indicated) also plotted as a function of the inlet mass flow ratio of the outboard duct. These curves show that as one duct is throttled there is an initial range in which there is little or no effect on the performance of the adjacent duct but further throttling generally produces an unfavourable effect.

To summarise these results Fig.51 has been drawn to show the change of pressure recovery in the inboard duct when the flow through the outboard duct has been reduced to 80% of its maximum value. The curves show the unfavourable influence which increases both with increase of throat bleed flow and increase of Mach number. At M = 2·12 with 4% throat bleed, reducing the flow through the outboard duct by 20% causes a 3½% reduction in mean pressure recovery in the inboard duct. From Table 2 it will be seen that at this point the flow through the inboard duct is reduced from a maximum value of A_∞/A_{en} = 0·934 to 0·905. In order to reduce the flow through the inboard duct its shock system has to be modified in some way and as suggested for another model in Ref.1, the normal shock position at the inlet of the unthrottled duct is modified by the movement of the normal shock at the inlet of the throttled duct, which results in the interference effects observed. This is clearly shown in schlieren photograph Fig.52(c) which indicates a well detached normal shock at the inlet of the throttled outboard duct and also a detached normal shock for the inboard duct which is nominally running full.

The curves of Fig.19 show that as a duct is throttled the rate of decrease of pressure recovery with mass flow ratio increases as Mach number increases. Thus for a given degree of expulsion of the normal shock, in this context due to interference, a larger loss in recovery will result the higher the Mach number.

Pressure distributions for the inboard duct are shown in Fig.53 for cases with zero and about 4% throat bleed flow, when the outboard duct is throttled to 15% below the maximum flow. Comparison of these with the inboard duct distributions of Fig.24 shows that while there is little difference between cases with no throat bleed and thus little interference effect (see Fig.51), with throat bleed there is a distinct reduction in the intensity of the high pressure region in the upper part of the duct, which results in a substantial loss of recovery as noted. The schlieren photographs show that with throat bleed flow, Fig.52(c), the inboard normal shock is detached further from the cowl lip than with no bleed flow, Fig.52(b). The reason for this influence of bleed flow is not understood but the result is clearly responsible for the loss of recovery noted.

4.3 Effects of transition

Curves showing interference effects for the model with free transition are shown in Fig.54. Comparison with the curves for the model with fixed transition, Fig.50(d) (iii), shows there to be little difference except that the non-interfering mass flow margin* is rather smaller with transition free. (Note the value of δ_3 is 1° different between the two cases.)

4.4 Splitter design

Interference curves for splitters II and III are shown in Figs.55 and 56. Both of these designs appear to be rather worse from an interference point of view than splitter I. Splitter II has no non-interfering mass flow margin and splitter III less than 2%. The inference from this is that the primary interfering influence is located in the region external to the lip, i.e. in the region of confluence of the intake shock system. This conclusion supports the idea that interference effects are transmitted primarily by modification of the normal shock position.

---

* The non-interfering mass flow margin is the amount by which the mass flow through the throttled duct may be reduced before the recovery in the other duct begins to suffer.

Circumferential distributions of $V/\bar{V}$, at $r/R = 0{\cdot}877$ in the inboard duct, for the three splitter cases, with the outboard duct throttled to about 10% below full mass flow, are shown in Fig.57. There is no marked difference in distribution but V_{max} increases slightly and V_{min} decreases slightly in the order splitter I, II, III which gives worsening values of D_v.

Interference effects on the unsteady flow characteristics were included in Figs.48 and 49; these compare with the curves for splitter I in Fig.32(d). In each case $M = 2{\cdot}12$, $\delta_3 = 16{\cdot}25°$ and $m_b/m_i = 0{\cdot}04$. Splitter design does influence conditions in the unthrottled inboard duct; the high frequency oscillation induced is similar in all cases but the amplitude of induced buzz lessens considerably with splitter changes from I to II to III.

From the present tests it would be deduced that by carrying a splitter extension around the cowl lip so as to cover the region of shock confluence, interference effects could be reduced to a low order, satisfactory for practical purposes on the present design. It has been demonstrated elsewhere* that this is in fact the case.

4.5 Use and effects of spill vents

If for any reason an engine passes a reduced mass flow, a means of bringing the inlet shock geometry back to optimum is by the use of afterspillage. This is illustrated by the series of schlieren photographs contained in Fig.58 for the model with splitter III configuration. "A" shows the ducts running just on the critical point (the normal shock appears to have just detached from the cowl lip of one duct). In "B" the outboard duct is throttled. In "C", "D" and "E" the throttle position remains as "B" but the spill vent of the outboard duct is opened successively to positions 1, 2 and 3 (these positions are arbitrary but more air is spilled as the position number increases). In "C" the normal shock appears to be still just detached but in "D" and "E" the outboard duct is once more running full. Graphs of pressure recovery against mass flow ratio are shown in Fig.59 for both ducts, on which the five corresponding points "A" to "E" are plotted. Throttling obviously produces a loss in recovery in the outboard duct but also, by interference, reductions of recovery and mass flow occur in the inboard duct - point "B". Opening the spill vent to position 1, (Fig.58(c)), restores the recovery level in the outboard duct at reduced engine flow but because the inlet flow is still not "full" (see schlieren phot.) the inboard duct is still influenced. Further opening of the spill vent,

---

* In work at the O.N.E.R.A., Paris.

sufficient to allow "full" inlet flow eliminates any interference in the inboard duct. If the spill vent is opened beyond this position, supercritical operation of the outboard duct occurs resulting in the reduced recovery shown by points D and E, though with no further influence on the inboard duct.

Fig.58(c) shows that opening the spill vent to position 1 nearly restores the shock geometry to "full" and produces a distribution pattern very like that which exists when the duct is running normally (distribution A). Hence the only way in which the engine suffers is from reduced flow - recovery and pressure distribution being largely unaffected. Opening the spill vent appreciably beyond this point takes the intake into supercritical flow and hence worsens the distribution of pressure, particularly in the lower part of the duct. It may be worth mentioning, that with this configuration the flow in the lower part of the duct appeared to be rather more sensitive to spill vent opening than it did with the splitter configurations I and II.

To sum up, the experiments show that if a spill vent is opened just sufficiently to restore the inlet shock geometry to optimum after throttling, the pressure recovery and distribution will remain largely unaffected, and any interference effects on the neighbouring duct will be eliminated. Opening the spill vent further than is necessary for this condition causes supercritical operation and consequent deterioration in recovery and pressure distribution.

5 CONCLUSIONS

From tests at Mach numbers 1·7 to 2·0 on a rectangular, twin-duct air intake which has variable geometry, the following conclusions are noted:-

(a) Pressure recovery

(1) Values measured with $3\frac{1}{2}\%$ bleed flow are generally up to $2\frac{1}{2}\%$ lower than those calculated from the theoretical shock geometries. This is a measure of the viscous loss, which therefore at full scale Reynolds number would be around $1\frac{1}{2}\%$ only.

(2) Maximum values measured increase with quantity of throat bleed flow at all Mach numbers; and at M = 2·12 (the only Mach number at which appropriate tests were made) maximum recovery is dependent to a small extent on the position of the downstream edge of the bleed slot.

(3) Higher values are obtained with natural transition of the boundary layer than with transition fixed at the inlet leading edges and no flow loss is incurred.

(4) Extension of the central splitter upstream of the plane of the side-wall leading edges generally causes a loss in recovery.

(5) At reduced duct mass flow both recovery and distribution of pressure can be restored to "full flow" levels by careful use of afterspill.

(b) Flow instability

(6) Two types of instability are found to occur, one at high values of mass flow ratio which is a high frequency, low amplitude pressure fluctuation and the second, which occurs at values of A_∞/A_{en} of about 0·7 to 0·75 and is a lower frequency, higher amplitude fluctuation. The severity of this latter increases with increase of Mach number.

(c) Interference

(7) Throttling one duct interferes with the performance (pressure recovery and mass flow) in the other to some extent, at all Mach numbers. These effects worsen both with increase of Mach number and with the introduction of throat bleed flow. They can however, be eliminated by careful use of afterspill in the throttled duct.

(8) With one duct running in the unstable flow region, an instability of similar frequency but lower amplitude is generally induced into the flow of the other. This interference effect intensifies with increase of Mach number but extending the leading edge of the splitter upstream goes some way towards eliminating it.

Appendix A

COMPARISON BETWEEN MODEL AND CURRENT AIRCRAFT GEOMETRIES

The intake items are listed in tabular form and compression geometry and diffuser lines are shown in sketches.

Item	Model	Aircraft
Lip		
position x/h (see sketch)	1·461	1·458
y/h (see sketch)	1·000	1·000
internal angle	14°	12°
internal radius	2·5 h	2·5 h
included angle	$4\frac{1}{2}$°	$4\frac{1}{2}$°
Compression geometry (shown in sketch A)		
δ_1	7°	7°
isentropic turn	9° 20'	≈ 5° 40'
δ_3	9° to 22°	9° to 22°
Splitter		
wedge semi angle (streamwise)	I 3·75° II 1·5° III 3·75°	2°
leading edge sweep	I 34·4° II 42° III 45°	45°
Duct divergence	1°	≈ 2°
Throat bleed		
slot width	0·42 h (max)	0·58 h at δ_2 = 14·5°
Sidewalls		
external wedge angle	4·75°	5·5°
internal wedge angle	2·75°	0°
Length of duct		
lip to engine face	≈ 4·9h	≈ 3·8 h
Aspect ratio		
w/h per duct	1·36	1·03 to 1·08
Diffuser		
see sketch B		

Table 1

Splitter I, equal throttling

Outboard				Inboard			
m_c/m_i	m_b/m_i	A_∞/A_{en}	P_f/P_∞	m_c/m_i	m_b/m_i	A_∞/A_{en}	P_f/P_∞
$M = 1{\cdot}70$, $\delta_3 = 9{\cdot}7^\circ$							
0·917	0	0·917	0·924	0·919	0	0·919	0·924
0·883	0	0·883	0·943	0·886	0	0·886	0·943
0·874	0	0·874	0·948	0·871	0	0·871	0·946
0·851	0	0·851	0·948	0·848	0	0·848	0·944
0·828	0	0·828	0·945	0·827	0	0·827	0·944
0·791	0	0·791	0·942	0·784	0	0·784	0·935
0·666	0	0·666	0·919	0·658	0	0·658	0·907
0·906	0·019	0·925	0·943	0·908	0·019	0·927	0·943
0·889	0·020	0·909	0·942	0·887	0·020	0·907	0·943
0·862	0·021	0·883	0·942	0·860	0·021	0·881	0·941
0·839	0·022	0·861	0·941	0·839	0·022	0·861	0·941
0·814	0·022	0·836	0·933	0·816	0·022	0·838	0·935
0·803	0·022	0·825	0·932	0·799	0·022	0·821	0·929
Instrumentation fault				0·890	0·029	0·919	0·940
				0·873	0·034	0·907	0·950
				0·853	0·037	0·890	0·949
				0·827	0·038	0·865	0·946
				0·780	0·040	0·820	0·942
$M = 1{\cdot}70$, $\delta_3 = 11{\cdot}3^\circ$							
0·912	0	0·912	0·938	0·906	0	0·906	0·931
0·893	0	0·893	0·936	0·886	0	0·886	0·931
0·872	0	0·872	0·940	0·867	0	0·867	0·935
0·850	0	0·850	0·942	0·846	0	0·846	0·937
0·831	0	0·831	0·939	0·826	0	0·826	0·933
0·809	0	0·809	0·936	0·805	0	0·825	0·933
0·875	0·016	0·891	0·937	0·873	0·016	0·889	0·929
0·855	0·016	0·871	0·943	0·854	0·017	0·871	0·935
0·847	0·019	0·866	0·949	0·844	0·019	0·863	0·945
0·837	0·020	0·857	0·954	0·833	0·021	0·854	0·949
0·828	0·022	0·850	0·954	0·824	0·022	0·846	0·949
0·818	0·022	0·840	0·956	0·815	0·023	0·838	0·952
0·796	0·023	0·819	0·955	0·793	0·024	0·817	0·947
0·737	0·025	0·762	0·940	0·733	0·025	0·758	0·937
0·846	0·028	0·874	0·946	0·847	0·029	0·876	0·942
0·831	0·033	0·864	0·954	0·831	0·033	0·864	0·949
0·823	0·036	0·859	0·958	0·821	0·036	0·857	0·954
0·814	0·038	0·852	0·959	0·811	0·038	0·849	0·955
0·807	0·040	0·847	0·961	0·803	0·039	0·842	0·957
0·794	0·042	0·836	0·961	0·790	0·041	0·831	0·957
0·780	0·042	0·822	0·962	0·777	0·042	0·819	0·955
0·728	0·046	0·774	0·949	0·725	0·044	0·769	0·946

Table 1 (Contd.)

Outboard				Inboard			
m_c/m_i	m_b/m_i	A_∞/A_{en}	P_f/P_∞	m_c/m_i	m_b/m_i	A_∞/A_{en}	P_f/P_∞
			$M = 1{\cdot}85,\ \delta_3 = 11{\cdot}3°$				
0·929	0	0·929	0·885	0·927	0	0·927	0·882
0·924	0	0·924	0·894	0·923	0	0·923	0·893
0·916	0	0·916	0·901	0·909	0	0·909	0·895
0·895	0	0·895	0·902	0·884	0	0·884	0·895
0·861	0	0·861	0·888	0·855	0	0·855	0·883
0·847	0	0·847	0·886	0·840	0	0·840	0·881
0·893	0·017	0·910	0·900	0·893	0·017	0·910	0·901
0·885	0·020	0·905	0·915	0·883	0·020	0·903	0·916
0·880	0·022	0·902	0·918	0·880	0·022	0·902	0·917
0·875	0·025	0·900	0·921	0·871	0·024	0·895	0·918
0·861	0·025	0·886	0·920	0·859	0·025	0·884	0·918
0·842	0·026	0·868	0·913	0·842	0·026	0·868	0·913
0·825	0·026	0·851	0·906	0·826	0·026	0·852	0·907
0·806	0·026	0·832	0·898	0·804	0·026	0·830	0·896
0·891	0·028	0·919	0·909	0·891	0·028	0·919	0·911
0·874	0·031	0·905	0·919	0·875	0·032	0·907	0·921
0·863	0·038	0·901	0·933	0·864	0·038	0·902	0·934
0·851	0·044	0·895	0·931	0·849	0·044	0·893	0·930
0·837	0·045	0·882	0·932	0·834	0·045	0·879	0·930
0·816	0·045	0·861	0·925	0·815	0·045	0·860	0·925
0·800	0·045	0·845	0·920	0·799	0·046	0·845	0·920
0·782	0·046	0·828	0·913	0·779	0·045	0·824	0·910
			$M = 1{\cdot}85,\ \delta_3 = 13{\cdot}25°$				
0·888	0	0·888	0·900	0·883	0	0·883	0·890
0·889	0	0·889	0·908	0·882	0	0·882	0·903
0·877	0	0·877	0·903	0·871	0	0·871	0·899
0·871	0	0·871	0·906	0·868	0	0·868	0·904
0·863	0	0·863	0·908	0·861	0	0·861	0·907
0·841	0	0·841	0·908	0·837	0	0·837	0·907
0·795	0	0·795	0·893	0·788	0	0·788	0·887
0·883	0·015	0·898	0·904	0·884	0·015	0·899	0·898
0·875	0·015	0·890	0·913	0·876	0·015	0·891	0·907
0·869	0·018	0·887	0·927	0·868	0·018	0·886	0·926
0·864	0·019	0·883	0·931	0·863	0·019	0·882	0·929
0·858	0·021	0·879	0·932	0·855	0·021	0·876	0·932
0·842	0·022	0·864	0·931	0·841	0·022	0·863	0·930
0·867	0·028	0·895	0·907	0·870	0·027	0·897	0·905
0·868	0·031	0·899	0·924	0·870	0·031	0·901	0·924
0·849	0·034	0·883	0·938	0·849	0·034	0·883	0·938
0·843	0·038	0·881	0·941	0·844	0·039	0·884	0·940
0·828	0·042	0·870	0·940	0·828	0·042	0·870	0·940
0·819	0·044	0·863	0·944	0·819	0·044	0·863	0·944

Table 1 (Contd.)

Outboard				Inboard			
m_c/m_i	m_b/m_i	A_∞/A_{en}	P_f/P_∞	m_c/m_i	m_b/m_i	A_∞/A_{en}	P_f/P_∞
$M = 2{\cdot}00,\ \delta_3 = 13{\cdot}6°$							
0·921	0	0·921	0·847	0·919	0	0·919	0·848
0·913	0	0·913	0·861	0·912	0	0·912	0·863
0·909	0	0·909	0·862	0·910	0	0·910	0·860
0·919	0	0·919	0·871	0·914	0	0·914	0·866
0·912	0	0·912	0·871	0·903	0	0·903	0·866
0·896	0	0·896	0·870	0·886	0	0·886	0·864
0·857	0	0·857	0·853	0·846	0	0·846	0·843
0·913	0·015	0·928	0·859	0·918	0·014	0·932	0·863
0·902	0·014	0·916	0·869	0·905	0·015	0·920	0·871
0·894	0·019	0·913	0·885	0·894	0·019	0·913	0·888
0·893	0·021	0·914	0·890	0·892	0·021	0·913	0·889
0·875	0·023	0·898	0·885	0·874	0·024	0·898	0·885
0·858	0·024	0·0882	0·878	0·858	0·024	0·882	0·880
0·838	0·024	0·862	0·871	0·835	0·025	0·860	0·870
0·821	0·025	0·846	0·866	0·818	0·025	0·843	0·863
0·903	0·027	0·930	0·882	0·906	0·027	0·933	0·886
0·879	0·031	0·910	0·893	0·883	0·032	0·915	0·895
0·868	0·038	0·906	0·908	0·871	0·038	0·909	0·911
0·859	0·047	0·906	0·908	0·859	0·046	0·905	0·907
0·839	0·048	0·887	0·898	0·839	0·047	0·886	0·899
0·819	0·049	0·868	0·890	0·818	0·047	0·865	0·890
0·799	0·050	0·849	0·888	0·797	0·048	0·845	0·887
0·780	0·051	0·831	0·879	0·766	0·047	0·813	0·867
$M = 2{\cdot}00,\ \delta_3 = 15{\cdot}75°$							
0·876	0	0·876	0·851	0·876	0	0·876	0·836
0·876	0	0·876	0·877	0·874	0	0·874	0·876
0·876	0	0·876	0·878	0·872	0	0·872	0·876
0·863	0	0·863	0·882	0·856	0	0·856	0·876
0·849	0	0·849	0·882	0·838	0	0·838	0·872
0·833	0	0·833	0·879	0·821	0	0·821	0·866
0·819	0	0·819	0·875	0·806	0	0·806	0·862
0·786	0	0·786	0·863	0·774	0	0·774	0·849
0·769	0	0·769	0·857	0·749	0	0·749	0·835
0·875	0·017	0·892	0·864	0·881	0·017	0·898	0·867
0·869	0·017	0·886	0·882	0·871	0·018	0·889	0·886
0·858	0·021	0·879	0·902	0·859	0·022	0·881	0·904
0·851	0·024	0·875	0·902	0·854	0·025	0·879	0·906
0·838	0·026	0·864	0·903	0·840	0·027	0·867	0·905
0·820	0·027	0·847	0·899	0·816	0·028	0·844	0·899
0·783	0·029	0·812	0·885	0·776	0·029	0·805	0·877
0·747	0·031	0·778	0·875	0·734	0·030	0·764	0·862

Table 1 (Contd.)

Outboard				Inboard			
m_c/m_i	m_b/m_i	A_∞/A_{en}	P_f/P_∞	m_c/m_i	m_b/m_i	A_∞/A_{en}	P_f/P_∞
0·877	0·029	0·906	0·883	0·877	0·028	0·905	0·887
0·857	0·029	0·886	0·894	0·859	0·031	0·890	0·897
0·830	0·037	0·887	0·917	0·852	0·038	0·890	0·920
0·835	0·040	0·875	0·914	0·840	0·041	0·881	0·919
0·819	0·043	0·862	0·913	0·828	0·044	0·872	0·921
0·799	0·045	0·844	0·909	0·803	0·047	0·850	0·913
0·778	0·046	0·824	0·903	0·780	0·048	0·828	0·905
0·740	0·050	0·790	0·889	0·735	0·051	0·786	0·880
0·703	0·051	0·754	0·877	0·692	0·051	0·743	0·867
$M = 2·00, \quad \delta_3 = 16·25°$							
0·868	0	0·868	0·859	0·866	0	0·866	0·861
0·849	0	0·849	0·870	0·848	0	0·848	0·873
0·838	0	0·838	0·873	0·835	0	0·835	0·874
0·828	0	0·828	0·874	0·825	0	0·825	0·874
0·817	0	0·817	0·873	0·811	0	0·811	0·868
0·840	0·040	0·880	0·913	0·843	0·042	0·885	0·917
0·821	0·040	0·861	0·913	0·824	0·042	0·866	0·917
0·804	0·043	0·847	0·913	0·805	0·046	0·851	0·916
0·784	0·044	0·828	0·909	0·781	0·047	0·828	0·908
$M = 2·00, \quad \delta_3 = 17·75°$							
0·815	0	0·815	0·854	0·817	0	0·817	0·860
0·818	0	0·818	0·866	0·820	0	0·820	0·870
0·814	0	0·814	0·873	0·815	0	0·815	0·875
0·803	0	0·803	0·878	0·803	0	0·803	0·877
0·798	0·036	0·834	0·909	0·796	0·037	0·833	0·910
0·780	0·037	0·817	0·911	0·780	0·038	0·818	0·911
0·770	0·041	0·811	0·914	0·768	0·043	0·811	0·913
0·750	0·044	0·794	0·912	0·746	0·046	0·792	0·908
$M = 2·12, \quad \delta_3 = 15·25°$							
0·932	0	0·932	0·807	0·918	0	0·918	0·803
0·925	0	0·925	0·819	0·909	0	0·909	0·811
0·906	0	0·906	0·833	0·901	0	0·901	0·832
0·914	0	0·914	0·839	0·916	0	0·916	0·842
0·928	0	0·928	0·843	0·922	0	0·922	0·837
0·917	0	0·917	0·845	0·896	0	0·896	0·829
0·893	0	0·893	0·833	0·870	0	0·870	0·814
0·873	0	0·873	0·823	0·854	0	0·854	0·807
0·852	0	0·852	0·814	0·834	0	0·834	0·799

Table 1 (Contd.)

Outboard					Inboard			
m_c/m_i	m_b/m_i	A_∞/A_{en}	P_f/P_∞		m_c/m_i	m_b/m_i	A_∞/A_{en}	P_f/P_∞
0·899	0·016	0·915	0·849		0·891	0·015	0·906	0·838
0·906	0·021	0·927	0·865		0·897	0·021	0·918	0·859
0·910	0·026	0·936	0·873		0·900	0·026	0·926	0·864
0·892	0·028	0·920	0·869		0·882	0·027	0·909	0·859
0·869	0·028	0·897	0·861		0·857	0·028	0·885	0·849
0·843	0·029	0·872	0·847		0·831	0·028	0·859	0·837
0·922	0·027	0·949	0·860		0·915	0·025	0·940	0·854
0·901	0·030	0·931	0·869		0·897	0·029	0·926	0·863
0·888	0·039	0·927	0·886		0·884	0·039	0·923	0·881
0·872	0·046	0·918	0·879		0·873	0·045	0·918	0·880
0·853	0·048	0·901	0·872		0·850	0·048	0·898	0·869
0·821	0·049	0·870	0·855		0·819	0·048	0·867	0·853
0·804	0·050	0·854	0·851		0·795	0·049	0·844	0·843
$M = 2·12$, $\delta_3 = 16·25°$								
0·919	0	0·919	0·820		0·920	0	0·920	0·819
0·912	0	0·912	0·840		0·912	0	0·912	0·842
0·917	0	0·917	0·840		0·919	0	0·919	0·840
0·914	0	0·914	0·847		0·910	0	0·910	0·844
0·875	0	0·875	0·830		0·872	0	0·872	0·830
0·839	0	0·839	0·814		0·833	0	0·833	0·809
0·804	0	0·804	0·807		0·799	0	0·799	0·803
0·784	0	0·784	0·801		0·778	0	0·778	0·796
0·925	0·017	0·942	0·844		0·933	0·017	0·950	0·850
0·913	0·015	0·928	0·859		0·919	0·020	0·939	0·860
0·904	0·020	0·924	0·873		0·909	0·021	0·930	0·872
0·868	0·022	0·890	0·859		0·850	0·023	0·873	0·840
0·823	0·023	0·846	0·839		0·808	0·025	0·833	0·825
0·783	0·024	0·807	0·826		0·767	0·027	0·794	0·810
0·929	0·020	0·949	0·863		0·925	0·020	0·945	0·855
0·921	0·021	0·942	0·866		0·918	0·021	0·939	0·860
0·918	0·023	0·941	0·871		0·915	0·023	0·938	0·868
0·910	0·026	0·936	0·876		0·909	0·026	0·935	0·872
0·905	0·030	0·935	0·885		0·902	0·029	0·931	0·880
0·888	0·032	0·920	0·877		0·893	0·033	0·926	0·886
0·831	0·034	0·865	0·847		0·833	0·036	0·869	0·852
0·792	0·036	0·828	0·837		0·790	0·037	0·827	0·835
0·746	0·038	0·784	0·824		0·747	0·039	0·786	0·826

Table 1 (Contd.)

Outboard				Inboard			
m_c/m_i	m_b/m_i	A_∞/A_{en}	P_f/P_∞	m_c/m_i	m_b/m_i	A_∞/A_{en}	P_f/P_∞
0·904	0·029	0·933	0·870	0·903	0·028	0·931	0·867
0·899	0·032	0·931	0·879	0·899	0·031	0·930	0·878
0·895	0·037	0·932	0·890	0·894	0·035	0·929	0·892
0·875	0·040	0·915	0·877	0·886	0·040	0·926	0·892
0·837	0·041	0·878	0·853	0·851	0·042	0·893	0·870
0·816	0·042	0·858	0·848	0·819	0·043	0·862	0·854
0·774	0·041	0·815	0·836	0·771	0·041	0·812	0·834
0·750	0·042	0·792	0·828	0·751	0·042	0·793	0·829
0·908	0·029	0·937	0·862	0·912	0·031	0·943	0·859
0·896	0·034	0·930	0·875	0·901	0·036	0·937	0·875
0·889	0·038	0·927	0·882	0·893	0·040	0·933	0·882
0·881	0·042	0·923	0·890	0·585	0·043	0·928	0·895
0·859	0·048	0·907	0·878	0·867	0·050	0·917	0·885
0·833	0·050	0·883	0·865	0·818	0·050	0·868	0·852
0·784	0·052	0·836	0·848	0·773	0·052	0·825	0·838
0·745	0·055	0·800	0·834	0·735	0·054	0·789	0·826
$M = 2·12, \quad \delta_3 = 17·50°$							
0·889	0	0·889	0·820	0·888	0	0·888	0·816
0·885	0	0·885	0·845	0·885	0	0·885	0·848
0·878	0	0·878	0·840	0·879	0	0·879	0·842
0·861	0	0·861	0·834	0·866	0	0·866	0·842
0·849	0	0·849	0·831	0·849	0	0·849	0·833
0·836	0	0·836	0·836	0·830	0	0·830	0·829
0·760	0	0·760	0·806	0·756	0	0·756	0·800
0·880	0·018	0·898	0·847	0·847	0·017	0·902	0·849
0·864	0·021	0·885	0·864	0·867	0·020	0·887	0·868
0·856	0·022	0·877	0·866	0·860	0·022	0·882	0·870
0·835	0·024	0·859	0·862	0·838	0·024	0·862	0·865
0·820	0·025	0·845	0·856	0·812	0·025	0·837	0·848
0·801	0·026	0·827	0·852	0·793	0·026	0·719	0·844
0·709	0·029	0·738	0·819	0·705	0·029	0·734	0·815
0·873	0·031	0·904	0·863	0·879	0·032	0·911	0·869
0·855	0·038	0·893	0·883	0·861	0·039	0·900	0·889
0·838	0·044	0·882	0·878	0·840	0·043	0·883	0·880
0·825	0·047	0·872	0·879	0·821	0·046	0·867	0·875
0·795	0·049	0·844	0·866	0·767	0·049	0·816	0·855
0·681	0·057	0·738	0·829	0·681	0·055	0·736	0·825
0·861	0·034	0·895	0·868	0·865	0·036	0·901	0·872
0·853	0·039	0·892	0·876	0·858	0·040	0·898	0·881
0·845	0·044	0·889	0·889	0·851	0·046	0·897	0·895
0·829	0·047	0·876	0·885	0·830	0·050	0·880	0·886
0·798	0·049	0·847	0·868	0·791	0·052	0·843	0·861
0·777	0·053	0·830	0·862	0·769	0·054	0·823	0·853
0·686	0·058	0·744	0·832	0·687	0·061	0·748	0·833

Table 1 (Contd.)

Outboard					Inboard			
m_c/m_i	m_b/m_i	A_∞/A_{en}	P_f/P_∞		m_c/m_i	m_b/m_i	A_∞/A_{en}	P_f/P_∞
				$M = 2{\cdot}12,\ \delta_3 = 18{\cdot}25^\circ$				
0·830	0	0·830	0·807		0·834	0	0·834	0·834
0·832	0	0·832	0·837		0·829	0	0·829	0·829
0·822	0	0·822	0·833		0·817	0	0·817	0·817
0·809	0	0·809	0·834		0·805	0	0·805	0·805
0·791	0	0·791	0·829		0·788	0	0·788	0·788
0·774	0	0·774	0·824		0·774	0	0·774	0·774
0·686	0	0·686	0·796		0·688	0	0·688	0·688
0·825	0·019	0·844	0·834		0·827	0·018	0·845	0·835
0·813	0·023	0·836	0·857		0·817	0·023	0·840	0·862
0·807	0·026	0·833	0·861		0·806	0·026	0·832	0·860
0·790	0·028	0·818	0·861		0·787	0·028	0·815	0·857
0·764	0·030	0·794	0·851		0·764	0·030	0·794	0·849
0·748	0·031	0·779	0·846		0·749	0·032	0·781	0·846
0·654	0·035	0·689	0·817		0·657	0·036	0·693	0·819
0·812	0·031	0·843	0·851		0·815	0·032	0·847	0·856
0·795	0·040	0·835	0·870		0·799	0·040	0·839	0·874
0·779	0·044	0·823	0·869		0·775	0·044	0·819	0·863
0·763	0·047	0·810	0·864		0·760	0·047	0·807	0·859
0·738	0·050	0·788	0·857		0·737	0·050	0·787	0·856
0·712	0·052	0·764	0·847		0·716	0·053	0·769	0·849
0·627	0·058	0·685	0·825		0·631	0·058	0·689	0·828
				$M = 2{\cdot}12,\ \delta_3 = 20{\cdot}0^\circ$				
0·794	0	0·794	0·803		0·781	0	0·781	0·790
0·791	0	0·791	0·827		0·779	0	0·779	0·814
0·780	0	0·780	0·836		0·772	0	0·772	0·828
0·759	0	0·759	0·826		0·753	0	0·753	0·819
0·725	0	0·725	0·821		0·720	0	0·720	0·818
0·784	0·022	0·806	0·846		0·771	0·021	0·792	0·830
0·771	0·024	0·795	0·855		0·761	0·024	0·785	0·841
0·765	0·028	0·793	0·852		0·757	0·027	0·784	0·843
0·750	0·032	0·782	0·855		0·748	0·032	0·780	0·856
0·704	0·036	0·740	0·839		0·705	0·039	0·744	0·844
0·659	0·041	0·700	0·824		0·664	0·042	0·706	0·833

Table 1 (Contd.)

Outboard					Inboard			
m_c/m_i	m_b/m_i	A_∞/A_{en}	P_f/P_∞		m_c/m_i	m_b/m_i	A_∞/A_{en}	P_f/P_∞
				$M = 2{\cdot}20,\ \delta_3 = 16{\cdot}25°$				
0·937	0	0·937	0·779		0·942	0	0·942	0·781
0·934	0	0·934	0·794		0·934	0	0·934	0·792
0·932	0	0·932	0·817		0·932	0	0·932	0·818
0·931	0	0·931	0·817		0·931	0	0·931	0·817
0·941	0	0·941	0·827		0·933	0	0·933	0·820
0·918	0	0·918	0·813		0·918	0	0·918	0·816
0·888	0	0·888	0·798		0·884	0	0·884	0·793
0·852	0	0·852	0·787		0·849	0	0·849	0·784
0·813	0	0·813	0·775		0·809	0	0·809	0·772
0·934	0·017	0·951	0·824		0·939	0·017	0·956	0·821
0·922	0·018	0·940	0·830		0·928	0·019	0·947	0·828
0·918	0·023	0·941	0·846		0·920	0·024	0·944	0·849
0·910	0·027	0·937	0·851		0·911	0·028	0·939	0·852
0·898	0·031	0·929	0·843		0·900	0·032	0·932	0·845
0·868	0·032	0·900	0·827		0·858	0·033	0·891	0·821
0·841	0·032	0·873	0·822		0·832	0·033	0·865	0·811
0·798	0·034	0·832	0·806		0·792	0·035	0·827	0·799
0·928	0·027	0·955	0·841		0·934	0·028	0·962	0·839
0·911	0·032	0·943	0·851		0·916	0·033	0·949	0·849
0·898	0·044	0·942	0·864		0·901	0·044	0·945	0·869
0·874	0·048	0·922	0·849		0·870	0·050	0·920	0·847
0·847	0·049	0·896	0·836		0·829	0·050	0·879	0·822
0·821	0·050	0·871	0·830		0·806	0·051	0·857	0·817
0·799	0·052	0·851	0·827		0·787	0·052	0·839	0·814
0·753	0·054	0·807	0·809		0·742	0·055	0·797	0·798
				$M = 2{\cdot}20,\ \delta_3 = 17{\cdot}50°$				
0·936	0	0·936	0·820		0·929	0	0·929	0·824
0·900	0	0·900	0·821		0·879	0	0·879	0·806
0·860	0	0·860	0·811		0·844	0	0·844	0·796
0·837	0	0·837	0·798		0·822	0	0·822	0·785
0·816	0	0·816	0·795		0·801	0	0·801	0·781
0·797	0	0·797	0·789		0·783	0	0·783	0·776
0·936	0·024	0·960	0·832		0·940	0·021	0·961	0·829
0·922	0·020	0·942	0·846		0·929	0·021	0·950	0·847
0·905	0·025	0·930	0·861		0·906	0·025	0·931	0·864
0·894	0·028	0·922	0·857		0·888	0·029	0·917	0·852
0·861	0·029	0·890	0·838		0·855	0·030	0·885	0·836
0·838	0·030	0·868	0·828		0·829	0·031	0·860	0·823
0·813	0·031	0·844	0·823		0·805	0·032	0·837	0·816
0·768	0·033	0·801	0·805		0·765	0·034	0·799	0·804
0·740	0·034	0·774	0·795		0·738	0·035	0·773	0·794

Table 1 (Contd.)

Outboard					Inboard			
m_c/m_i	m_b/m_i	A_∞/A_{en}	P_f/P_∞		m_c/m_i	m_b/m_i	A_∞/A_{en}	P_f/P_∞
0·931	0·030	0·961	0·851		0·935	0·031	0·966	0·846
0·907	0·032	0·937	0·859		0·912	0·034	0·946	0·859
0·893	0·042	0·935	0·877		0·895	0·041	0·936	0·882
0·869	0·046	0·915	0·859		0·862	0·047	0·909	0·854
0·834	0·047	0·881	0·840		0·820	0·047	0·867	0·832
0·790	0·050	0·840	0·831		0·780	0·050	0·830	0·821
0·740	0·053	0·793	0·814		0·735	0·054	0·789	0·809
$M = 2·20, \quad \delta_3 = 18·25°$								
0·917	0	0·917	0·815		0·910	0	0·910	0·811
0·902	0	0·902	0·817		0·896	0	0·896	0·814
0·889	0	0·889	0·814		0·877	0	0·877	0·805
0·874	0	0·874	0·812		0·860	0	0·860	0·799
0·906	0·033	0·939	0·856		0·909	0·034	0·943	0·856
0·898	0·034	0·932	0·863		0·899	0·036	0·935	0·863
0·888	0·037	0·925	0·871		0·871	0·040	0·911	0·854
0·870	0·041	0·911	0·864		0·858	0·043	0·901	0·853
$M = 2·20, \quad \delta_3 = 20·25°$								
0·824	0	0·824	0·791		0·816	0	0·816	0·786
0·819	0	0·819	0·805		0·809	0	0·809	0·793
0·811	0	0·811	0·805		0·797	0	0·797	0·793
0·793	0	0·793	0·806		0·777	0	0·777	0·791
0·794	0·035	0·829	0·838		0·783	0·037	0·820	0·827
0·776	0·036	0·812	0·842		0·765	0·040	0·805	0·829
0·760	0·042	0·802	0·842		0·746	0·046	0·792	0·825
0·738	0·046	0·784	0·838		0·722	0·049	0·771	0·821

Table 2

Splitter I Unequal throttling

Outboard					Inboard			
m_o/m_i	m_b/m_i	A_∞/A_{en}	P_f/P_∞		m_o/m_i	m_b/m_i	A_∞/A_{en}	P_f/P_∞
				$M = 1{\cdot}70,\ \delta_3 = 9{\cdot}70°$				
0·935	0	0·935	0·910		0·877	0	0·877	0·914
0·900	0	0·900	0·911		0·877	0	0·877	0·912
0·849	0	0·849	0·906		0·877	0	0·877	0·912
0·828	0	0·828	0·910		0·876	0	0·876	0·910
0·839	0	0·839	0·922	Outboard S.V.* open 1	0·877	0	0·877	0·914
0·815	0	0·815	0·916	Outboard S.V. open 2	0·879	0	0·879	0·916
0·811	0	0·811	0·914		0·880	0	0·880	0·915
0·789	0	0·789	0·909		0·879	0	0·879	0·915
0·801	0	0·801	0·927	Outboard S.V. open 2	0·880	0	0·880	0·915
0·789	0	0·789	0·920	" S.V. open 2·5	0·882	0	0·882	0·917
0·687	0	0·687	0·891		0·881	0	0·881	0·918
0.952	0·016	0·968	0·932		0·896	0·017	0·913	0·928
0·923	0·016	0·939	0·935		0·897	0·016	0·913	0·928
0·888	0·019	0·907	0·943		0·898	0·017	0·915	0·928
0·864	0·019	0·883	0·943		0·899	0·017	0·916	0·934
0·857	0·017	0·874	0·942	Outboard S.V. open 1	0·900	0·017	0·917	0·933
0·841	0·019	0·860	0·942		0·898	0·017	0·915	0·930
0·816	0·020	0·836	0·936		0·898	0·017	0·915	0·931
0·812	0·017	0·829	0·935	" S.V. open 1·5	0·896	0·017	0·913	0·927
0·590	0·021	0·611	0·883		0·893	0·018	0·913	0·929
0·613	0·016	0·629	0·923	" S.V. open 6	0·896	0·016	0·912	0·928
0 902	0·025	0·927	0·932		0·859	0·029	0·888	0·934
0·876	0·027	0·903	0·940		0·860	0·029	0·889	0·935
0·830	0·039	0·869	0·949		0·859	0·030	0·889	0·941
0·828	0·030	0·858	0·951	" S.V. open 1	0·860	0·030	0·890	0·942
0·806	0·040	0·846	0·948		0·860	0·030	0·890	0·937
0·783	0·041	0·824	0·945		0·861	0·030	0·891	0·938
0·790	0·039	0·829	0·953	" S.V. open 1	0·861	0·030	0·891	0·939
0·781	0·029	0·810	0·946	" S.V. open 2	0·858	0·029	0·887	0·935
0·575	0·042	0·617	0·898		0·851	0·035	0·886	0·932
0·593	0·026	0·619	0·928	" S.V. open 6	0·859	0·029	0·888	0·935

* When spill vents are open the figure in the mass flow ratio column is not A_∞/A_{en} as the spill vent flow has not been included.

Table 2 (Contd.)

Outboard					Inboard			
m_c/m_i	m_b/m_i	A_∞/A_{en}	P_f/P_∞		m_c/m_i	m_b/m_i	A_∞/A_{en}	P_f/P_∞
				$M = 1{\cdot}85°,\ \delta_3 = 11{\cdot}3°$				
0·949	0	0·949	0·882		0·915	0	0·915	0·874
0·936	0	0·936	0·886		0·917	0	0·917	0·876
0·913	0	0·913	0·899		0·919	0	0·919	0·876
0·888	0	0·888	0·896		0·922	0	0·922	0·885
0·873	0	0·873	0·895	Outboard S.V. open 1	0·919	0	0·919	0·885
0·861	0	0·861	0·887		0·922	0	0·922	0·877
0·829	0	0·829	0·881		0·923	0	0·923	0·878
0·797	0	0·797	0·871		0·920	0	0·920	0·877
0·818	0	0·818	0·897	" S.V. open 2	0·920	0	0·920	0·876
0·607	0	0·607	0·821		0·922	0	0·922	0·877
0·601	0	0·601	0·850	" S.V. open 6	0·917	0	0·917	0·876
0·893	0·017	0·910	0·901		0·873	0·018	0·891	0·897
0·878	0·019	0·897	0·917		0·873	0·019	0·892	0·896
0·875	0·023	0·898	0·923		0·874	0·019	0·893	0·897
0·865	0·023	0·888	0·923		0·875	0·019	0·894	0·898
0·848	0·024	0·872	0·919		0·875	0·019	0·894	0·905
0·849	0·021	0·870	0·925	Outboard S.V. open 1	0·875	0·019	0·894	0·905
0·786	0·024	0·810	0·895		0·874	0·019	0·893	0·896
0·784	0·018	0·800	0·906	" S.V. open 2	0·875	0·018	0·893	0·898
0·674	0·026	0·700	0·871		0·880	0·019	0·899	0·904
0·685	0·019	0·704	0·891	" S.V. open 4	0·874	0·019	0·893	0·897
0·875	0·027	0·902	0·912		0·845	0·040	0·885	0·921
0·865	0·031	0·896	0·922		0·845	0·041	0·886	0·921
0·860	0·035	0·895	0·927		0·844	0·042	0·886	0·920
0·850	0·041	0·891	0·931		0·843	0·041	0·884	0·919
0·837	0·042	0·879	0·932		0·842	0·041	0·883	0·917
0·818	0·043	0·861	0·929		0·842	0·041	0·883	0·918
0·800	0·044	0·844	0·922		0·842	0·041	0·883	0·923
0·794	0·030	0·824	0·925	Outboard S.V. open 1·5	0·845	0·041	0·886	0·926
0·762	0·044	0·806	0·908		0·841	0·040	0·881	0·915
0·711	0·046	0·757	0·896		0·838	0·040	0·878	0·913
0·667	0·049	0·716	0·890		0·838	0·039	0·877	0·914
0·627	0·049	0·676	0·874		0·833	0·039	0·872	0·911
0·658	0·034	0·692	0·922	" S.V. open 4	0·845	0·041	0·886	0·920
				$M = 2{\cdot}00,\ \delta_3 = 13{\cdot}6°$				
0·923	0	0·923	0·834		0·907	0	0·907	0·843
0·913	0	0·913	0·844		0·911	0	0·911	0·847
0·912	0	0·912	0·862		0·916	0	0·916	0·851
0·918	0	0·918	0·870		0·920	0	0·920	0·854
0·892	0	0·892	0·867		0·921	0	0·921	0·861
0·878	0	0·878	0·868	Outboard S.V. open 1	0·918	0	0·918	0·860
0·855	0	0·855	0·853		0·919	0	0·919	0·852
0·818	0	0·818	0·849	" S.V. open 2	0·914	0	0·914	0·850
0·673	0	0·673	0·794		0·915	0	0·915	0·854
0·653	0	0·653	0·826	" S.V. open 5	0·914	0	0·914	0·850

Table 2 (Contd.)

Outboard					Inboard			
m_c/m_i	m_b/m_i	A_∞/A_{en}	P_f/P_∞		m_c/m_i	m_b/m_i	A_∞/A_{en}	P_f/P_∞
0·917	0·014	0·931	0·860		0·887	0·018	0·905	0·871
0·905	0·015	0·920	0·870		0·886	0·018	0·904	0·871
0·901	0·016	0·917	0·878		0·887	0·018	0·905	0·872
0·894	0·018	0·912	0·883		0·885	0·018	0·903	0·871
0·894	0·020	0·914	0·892		0·885	0·019	0·904	0·871
0·886	0·023	0·909	0·897		0·886	0·019	0·905	0·871
0·847	0·025	0·872	0·883		0·886	0·020	0·906	0·878
0·847	0·021	0·868	0·895	Outboard S.V. open 1	0·886	0·019	0·905	0·879
0·793	0·026	0·819	0·863		0·885	0·019	0·904	0·873
0·729	0·026	0·755	0·845		0·885	0·019	0·904	0·874
0·693	0·028	0·721	0·839		0·886	0·019	0·905	0·874
0·722	0·022	0·744	0·885	" S.V. open 3	0·885	0·019	0·904	0·871
0·896	0·025	0·921	0·880		0·864	0·040	0·904	0·897
0·884	0·030	0·914	0·898		0·870	0·040	0·910	0·902
0·859	0·045	0·904	0·905		0·870	0·042	0·912	0·902
0·839	0·046	0·885	0·896		0·870	0·042	0·912	0·901
0·819	0·047	0·866	0·890		0·870	0·042	0·912	0·899
0·798	0·047	0·845	0·884		0·868	0·042	0·910	0·900
0·789	0·028	0·817	0·891	" S.V. open 2	0·868	0·040	0·908	0·903
0·650	0·053	0·703	0·835		0·854	0·041	0·895	0·886
0·679	0·033	0·712	0·889	" S.V. open 4	0·869	0·040	0·909	0·902
$M = 2·12, \delta_3 = 16·25°$								
0·934	0	0·934	0·798		0·927	0	0·927	0·838
0·927	0	0·927	0·815		0·927	0	0·927	0·840
0·928	0	0·928	0·831		0·930	0	0·930	0·842
0·926	0	0·926	0·845		0·932	0	0·932	0·844
0·901	0	0·901	0·847		0·935	0	0·935	0·846
0·894	0	0·894	0·856	Outboard S.V. open 1	0·936	0	0·936	0·847
0·861	0	0·861	0·823		0·935	0	0·935	0·845
0·827	0	0·827	0·813		0·934	0	0·934	0·843
0·788	0	0·788	0·805		0·933	0	0·933	0·841
0·794	0	0·794	0·816	" S.V. open 1	0·932	0	0·932	0·842
0·793	0	0·793	0·851	" S.V. open 2·3	0·938	0	0·938	0·848
0·707	0	0·707	0·780		0·929	0	0·929	0·836
0·925	0·019	0·944	0·833		0·906	0·018	0·924	0·859
0·914	0·017	0·931	0·854		0·904	0·018	0·922	0·858
0·902	0·019	0·921	0·870		0·904	0·018	0·922	0·856
0·896	0·023	0·919	0·879		0·905	0·018	0·923	0·857
0·885	0·026	0·911	0·877		0·905	0·018	0·923	0·856
0·860	0·027	0·887	0·869		0·903	0·019	0·922	0·863
0·816	0·019	0·835	0·844	Outboard S.V. open 2	0·906	0·018	0·924	0·864
0·598	0·035	0·633	0·767		0·884	0·019	0·903	0·841

Table 2 (Contd.)

Outboard					Inboard			
m_c/m_i	m_b/m_i	A_∞/A_{en}	P_f/P_∞		m_c/m_i	m_b/m_i	A_∞/A_{en}	P_f/P_∞
0·918	0·017	0·935	0·860		0·909	0·021	0·930	0·866
0·912	0·017	0·929	0·867		0·909	0·021	0·930	0·866
0·907	0·020	0·927	0·874		0·907	0·021	0·928	0·864
0·818	0·022	0·840	0·833		0·901	0·021	0·922	0·858
0·780	0·023	0·803	0·823		0·896	0·021	0·917	0·853
0·734	0·024	0·758	0·810		0·889	0·020	0·909	0·846
0·933	0·023	0·956	0·855		0·919	0·031	0·950	0·876
0·922	0·025	0·947	0·866		0·921	0·032	0·953	0·878
0·911	0·030	0·941	0·877		0·922	0·032	0·954	0·879
0·898	0·037	0·935	0·891		0·922	0·032	0·954	0·880
0·817	0·043	0·860	0·851		0·921	0·033	0·954	0·887
0·846	0·036	0·882	0·894	Outboard S.V. open 1	0·924	0·032	0·956	0·888
0·776	0·040	0·816	0·838		0·913	0·031	0·944	0·873
0·737	0·043	0·780	0·828		0·904	0·030	0·934	0·871
0·747	0·040	0·787	0·842	" S.V. open 1	0·913	0·030	0·943	0·874
0·762	0·031	0·793	0·885	" S.V. open 2·3	0·919	0·029	0·948	0·884
0·912	0·028	0·940	0·865		0·895	0·045	0·940	0·894
0·901	0·034	0·935	0·879		0·895	0·045	0·940	0·895
0·862	0·049	0·911	0·879		0·898	0·046	0·944	0·898
0·809	0·050	0·859	0·857		0·894	0·047	0·941	0·900
0·837	0·048	0·885	0·891	" S.V. open 1	0·894	0·045	0·939	0·900
0·763	0·054	0·817	0·842		0·878	0·047	0·925	0·878
0·723	0·058	0·781	0·834		0·869	0·045	0·914	0·874
0·732	0·053	0·785	0·848	" S.V. open 1	0·881	0·047	0·928	0·885
0·739	0·033	0·777	0·878	" S.V. open 3	0·898	0·046	0·944	0·904
0·706	0·060	0·766	0·829		0·863	0·042	0·905	0·866
M = 2·20, δ_3 = 17·5°								
0·915	0	0·915	0·807		0·843	0	0·843	0·793
0·882	0	0·882	0·800		0·843	0	0·843	0·792
0·866	0	0·866	0·799		0·842	0	0·842	0·792
0·830	0	0·830	0·791		0·843	0	0·843	0·792
0·808	0	0·808	0·783		0·843	0	0·843	0·792
0·763	0	0·763	0·768		0·844	0	0·844	0·795
0·781	0	0·781	0·802	Outboard S.V. open 1·5	0·843	0	0·843	0·793
0·724	0	0·724	0·757		0·842	0	0·842	0·791
0·674	0	0·674	0·744		0·841	0	0·841	0·789
0·706	0	0·706	0·787	" S.V. open 3	0·843	0	0·843	0·792
0·936	0·021	0·957	0·833		0·898	0·022	0·920	0·844
0·925	0·022	0·947	0·846		0·897	0·022	0·919	0·842
0·919	0·024	0·943	0·852		0·898	0·023	0·921	0·843
0·896	0·030	0·926	0·856		0·895	0·022	0·917	0·841
0·861	0·032	0·893	0·835		0·898	0·023	0·921	0·843
0·814	0·033	0·847	0·823		0·891	0·023	0·914	0·843
0·839	0·032	0·871	0·858	Outboard S.V. open 1	0·893	0·023	0·916	0·844
0·720	0·036	0·756	0·791		0·876	0·022	0·898	0·825
0·648	0·037	0·685	0·772		0·874	0·022	0·896	0·822
0·693	0·032	0·725	0·841	" S.V. open 3·5	0·892	0·022	0·914	0·840

Table 2 (Contd.)

Outboard					Inboard			
m_c/m_i	m_b/m_i	A_∞/A_{en}	P_f/P_∞		m_c/m_i	m_b/m_i	A_∞/A_{en}	P_f/P_∞
0·927	0·027	0·954	0·849		0·892	0·042	0·934	0·872
0·906	0·031	0·937	0·857		0·891	0·042	0·933	0·871
0·903	0·036	0·939	0·867		0·891	0·042	0·933	0·872
0·878	0·047	0·925	0·870		0·892	0·042	0·934	0·873
0·838	0·049	0·887	0·846		0·889	0·042	0·931	0·871
0·809	0·049	0·858	0·835		0·886	0·044	0·930	0·866
0·789	0·051	0·840	0·828		0·879	0·045	0·924	0·857
0·817	0·044	0·861	0·872	Outboard S.V. open 1·5	0·891	0·042	0·933	0·872
0·717	0·056	0·773	0·811		0·863	0·043	0·906	0·844
0·668	0·058	0·726	0·796		0·856	0·042	0·898	0·838
0·615	0·060	0·675	0·781		0·853	0·041	0·894	0·832

Table 3

Splitter II

Outboard					Inboard			
m_c/m_i	m_b/m_i	A_∞/A_{en}	P_f/P_∞		m_c/m_i	m_b/m_i	A_∞/A_{en}	P_f/P_∞
				$M = 1{\cdot}85,\ \delta_3 = 11{\cdot}3°$				
0·948	0	0·948	0·885	Equal throttling	0·950	0	0·950	0·880
0·931	0	0·931	0·886		0·931	0	0·931	0·883
0·928	0	0·928	0·898		0·928	0	0·928	0·898
0·910	0	0·910	0·898		0·902	0	0·902	0·893
0·857	0	0·857	0·886		0·851	0	0·851	0·883
0·800	0	0·800	0·871		0·792	0	0·792	0·864
0·733	0	0·733	0·862		0·725	0	0·725	0·852
0·657	0	0·657	0·835		0·650	0	0·650	0·825
0·884	0·028	0·912	0·908		0·882	0·029	0·911	0·913
0·868	0·031	0·899	0·916		0·869	0·033	0·902	0·916
0·864	0·034	0·898	0·922		0·866	0·036	0·902	0·923
0·860	0·038	0·898	0·932		0·856	0·041	0·897	0·927
0·847	0·041	0·888	0·929		0·839	0·042	0·881	0·924
0·834	0·042	0·876	0·930		0·823	0·043	0·866	0·919
0·800	0·044	0·844	0·920		0·788	0·044	0·832	0·910
0·731	0·046	0·777	0·900		0·717	0·044	0·761	0·886
0·663	0·047	0·710	0·882		0·653	0·046	0·699	0·869
0·586	0·048	0·634	0·850		0·577	0·047	0·624	0·839
0·862	0·039	0·901	0·928	Unequal throttling	0·823	0·041	0·864	0·912
0·848	0·041	0·887	0·928		0·822	0·041	0·863	0·912
0·816	0·043	0·859	0·927		0·819	0·041	0·860	0·910
0·801	0·044	0·845	0·920		0·820	0·041	0·861	0·911
0·733	0·047	0·780	0·901		0·818	0·040	0·858	0·910
0·663	0·048	0·711	0·884		0·817	0·040	0·857	0·909
				$M = 1{\cdot}85,\ \delta_3 = 13{\cdot}25°$				
0·858	0·031	0·889	0·927	Equal throttling	0·856	0·032	0·032	0·926
0·847	0·033	0·880	0·934		0·847	0·035	0·035	0·933
0·842	0·038	0·880	0·941		0·839	0·040	0·040	0·938
0·826	0·040	0·866	0·939		0·824	0·042	0·042	0·937
0·816	0·043	0·859	0·940		0·810	0·044	0·044	0·935
0·803	0·044	0·847	0·941		0·795	0·044	0·044	0·934
0·753	0·046	0·799	0·928		0·748	0·048	0·048	0·923
0·627	0·050	0·677	0·888		0·619	0·051	0·051	0·876
0·854	0·030	0·884	0·924	Unequal throttling	0·845	0·042	0·887	0·933
0·846	0·031	0·877	0·932		0·846	0·042	0·888	0·936
0·828	0·039	0·867	0·941		0·845	0·041	0·886	0·937
0·817	0·042	0·859	0·942		0·843	0·041	0·884	0·936
0·795	0·046	0·841	0·944		0·843	0·040	0·883	0·938
0·791	0·040	0·831	0·941	Outboard S.V. open 1	0·845	0·041	0·886	0·937
0·695	0·052	0·747	0·919		0·838	0·039	0·877	0·934
0·575	0·054	0·629	0·876		0·831	0·038	0·869	0·926
0·597	0·053	0·650	0·917	" " open 2	0·836	0·039	0·875	0·934
0·595	0·033	0·628	0·920	" " open 5	0·845	0·041	0·886	0·937

Table 3 (Contd.)

Outboard					Inboard			
m_o/m_i	m_b/m_i	A_∞/A_{en}	P_f/P_∞		m_o/m_i	m_b/m_i	A_∞/A_{en}	P_f/P_∞
				$M = 2{\cdot}12,\ \delta_3 = 16{\cdot}25°$				
0·916	0	0·916	0·826	Equal throttling	0·913	0	0·913	0·823
0·915	0	0·915	0·836		0·913	0	0·913	0·832
0·921	0	0·921	0·851		0·920	0	0·920	0·853
0·917	0	0·917	0·849		0·907	0	0·907	0·846
0·898	0	0·898	0·840		0·890	0	0·890	0·838
0·881	0	0·881	0·834		0·866	0	0·866	0·825
0·804	0	0·804	0·806		0·793	0	0·793	0·799
0·635	0	0·635	0·739		0·622	0	0·622	0·726
0·895	0·033	0·928	0·876		0·895	0·034	0·929	0·876
0·886	0·035	0·921	0·882		0·886	0·037	0·923	0·882
0·876	0·036	0·912	0·890		0·874	0·042	0·916	0·888
0·865	0·044	0·909	0·888		0·855	0·046	0·901	0·879
0·842	0·046	0·888	0·878		0·815	0·045	0·860	0·854
0·816	0·047	0·863	0·863		0·789	0·045	0·834	0·838
0·714	0·051	0·765	0·823		0·706	0·052	0·758	0·816
0·610	0·056	0·666	0·784		0·596	0·052	0·648	0·768
0·920	0	0·920	0·830		0·934	0	0·934	0·845
0·919	0	0·919	0·835		0·934	0	0·934	0·845
0·915	0	0·915	0·847		0·928	0	0·928	0·844
0·904	0	0·904	0·844		0·928	0	0·928	0·844
0·886	0	0·886	0·836		0·927	0	0·927	0·841
0·861	0	0·861	0·824		0·928	0	0·928	0·838
0·867	0	0·867	0·848	Outboard S.V. open 1	0·929	0	0·929	0·842
0·753	0	0·753	0·795		0·925	0	0·925	0·840
0·600	0	0·600	0·734		0·908	0	0·908	0·822
0·641	0	0·641	0·778	" S.V. open 1	0·920	0	0·920	0·835
0·621	0	0·621	0·811	" S.V. open 5	0·932	0	0·932	0·844
0·910	0·026	0·936	0·864		0·878	0·049	0·927	0·881
0·900	0·031	0·931	0·880		0·877	0·049	0·926	0·880
0·890	0·036	0·926	0·886		0·876	0·048	0·924	0·879
0·864	0·045	0·909	0·881		0·874	0·046	0·920	0·874
0·833	0·046	0·879	0·865		0·859	0·044	0·903	0·861
0·807	0·047	0·854	0·852		0·857	0·043	0·900	0·861
0·782	0·049	0·831	0·848		0·860	0·043	0·903	0·866
0·809	0·046	0·855	0·886	Outboard S.V. open 1	0·869	0·044	0·913	0·876
0·720	0·053	0·773	0·829		0·870	0·044	0·914	0·872
0·563	0·058	0·621	0·769		0·844	0·039	0·883	0·846
0·603	0·055	0·658	0·822	" S.V. open 2	0·863	0·042	0·905	0·866
0·617	0·039	0·656	0·873	" S.V. open 4·5	0·875	0·046	0·921	0·879

Table 4

Splitter III

Outboard					Inboard			
m_o/m_i	m_b/m_i	A_∞/A_{en}	P_f/P_∞		m_o/m_i	m_b/m_i	A_∞/A_{en}	P_f/P_∞
				$M = 2{\cdot}12,\ \delta_3 = 16{\cdot}25°$				
0·907	0	0·907	0·804		0·909	0	0·909	0·808
0·906	0	0·906	0·812		0·909	0	0·909	0·812
0·906	0	0·906	0·823		0·905	0	0·905	0·825
0·896	0	0·896	0·832		0·399	0	0·899	0·833
0·903	0	0·903	0·831		0·903	0	0·903	0·830
0·901	0	0·901	0·838		0·901	0	0·901	0·837
0·875	0	0·875	0·836		0·875	0	0·875	0·835
0·846	0	0·846	0·824		0·846	0	0·846	0·822
0·819	0	0·819	0·819		0·819	0	0·819	0·820
0·921	0·014	0·935	0·840		0·921	0·014	0·935	0·842
0·911	0·016	0·927	0·853		0·911	0·016	0·928	0·855
0·900	0·018	0·918	0·861		0·900	0·018	0·918	0·863
0·897	0·020	0·917	0·868		0·897	0·021	0·918	0·867
0·869	0·022	0·891	0·861		0·869	0·022	0·891	0·863
0·829	0·024	0·853	0·847		0·829	0·024	0·853	0·847
0·802	0·025	0·827	0·842		0·802	0·026	0·828	0·844
0·917	0·021	0·938	0·851		0·917	0·021	0·938	0·849
0·913	0·022	0·935	0·854		0·913	0·022	0·935	0·855
0·912	0·024	0·936	0·861		0·912	0·025	0·937	0·864
0·903	0·028	0·931	0·870		0·903	0·029	0·932	0·872
0·886	0·032	0·916	0·874		0·886	0·033	0·919	0·867
0·844	0·038	0·882	0·866		0·844	0·038	0·882	0·866
0·809	0·041	0·850	0·854		0·809	0·041	0·850	0·853
0·893	0·027	0·920	0·851		0·904	0·027	0·931	0·854
0·889	0·029	0·918	0·858		0·898	0·030	0·928	0·863
0·883	0·033	0·916	0·867		0·891	0·036	0·927	0·871
0·876	0·037	0·913	0·875		0·880	0·040	0·920	0·874
0·866	0·043	0·909	0·877		0·859	0·043	0·902	0·870
0·834	0·047	0·881	0·869		0·830	0·048	0·878	0·867
0·794	0·050	0·844	0·863		0·791	0·051	0·842	0·859
0·758	0·052	0·810	0·851		0·760	0·055	0·815	0·852
				$M = 2{\cdot}12,\ \delta_3 = 17{\cdot}25°$				
0·913	0	0·913	0·795		0·908	0	0·908	0·792
0·901	0	0·901	0·804		0·900	0	0·900	0·802
0·901	0	0·901	0·829		0·901	0	0·901	0·829
0·896	0	0·896	0·827		0·898	0	0·898	0·830
0·888	0	0·888	0·835		0·892	0	0·892	0·838
0·883	0	0·883	0·851		0·885	0	0·885	0·854
0·861	0	0·861	0·844		0·864	0	0·864	0·850
0·831	0	0·831	0·837		0·834	0	0·834	0·841
0·792	0	0·792	0·824		0·797	0	0·797	0·819

Table 4 (Contd.)

Outboard				Inboard			
m_c/m_i	m_b/m_i	A_∞/A_{en}	P_f/P_∞	m_c/m_i	m_b/m_i	A_∞/A_{en}	P_f/P_∞
0·896	0·018	0·914	0·821	Instrumentation fault			
0·896	0·018	0·914	0·843				
0·893	0·018	0·911	0·855				
0·884	0·018	0·902	0·860				
0·880	0·020	0·900	0·867				
0·866	0·021	0·887	0·864				
0·845	0·025	0·870	0·875				
0·813	0·027	0·840	0·861				
0·768	0·029	0·797	0·849				
0·723	0·031	0·754	0·833				
0·898	0·029	0·927	0·837	0·903	0·028	0·931	0·841
0·886	0·029	0·915	0·856	0·891	0·029	0·920	0·856
0·877	0·034	0·911	0·873	0·882	0·035	0·917	0·875
0·867	0·037	0·904	0·877	0·862	0·036	0·898	0·869
0·846	0·040	0·886	0·873	0·850	0·039	0·889	0·875
0·826	0·046	0·872	0·879	0·829	0·046	0·875	0·884
0·783	0·049	0·832	0·867	0·785	0·051	0·836	0·869
0·741	0·053	0·794	0·855	0·745	0·055	0·800	0·858
0·695	0·055	0·750	0·842	0·694	0·055	0·749	0·840
$M = 2·12$, $\delta_3 = 18·25°$							
0·866	0	0·866	0·798	Instrumentation fault			
0·865	0	0·865	0·813				
0·860	0	0·860	0·818				
0·864	0	0·864	0·841				
0·862	0	0·862	0·838				
0·854	0	0·854	0·844				
0·837	0	0·837	0·853				
0·803	0	0·803	0·837				
0·715	0	0·715	0·803				
0·859	0·018	0·877	0·811				
0·868	0·018	0·886	0·833				
0·868	0·018	0·886	0·846				
0·863	0·018	0·881	0·857				
0·853	0·019	0·872	0·860				
0·846	0·022	0·868	0·870				
0·819	0·027	0·846	0·875				
0·780	0·029	0·809	0·863				
0·709	0·032	0·741	0·837				
0·858	0·028	0·886	0·845				
0·850	0·033	0·883	0·870				
0·836	0·035	0·871	0·875				
0·832	0·041	0·873	0·880				
0·808	0·045	0·853	0·880				
0·790	0·047	0·837	0·879				
0·750	0·050	0·800	0·870				
0·699	0·055	0·754	0·848				
0·651	0·057	0·708	0·834				

Table 4 (Contd.)

Outboard					Inboard			
m_o/m_i	m_b/m_i	A_∞/A_{en}	P_f/P_∞		m_o/m_i	m_b/m_i	A_∞/A_{en}	P_f/P_∞
				$M = 2{\cdot}12$, $\delta_3 = 16{\cdot}25°$				
0·919	0	0·919	0·813		0·923	0	0·923	0·837
0·907	0	0·907	0·818		0·921	0	0·921	0·835
0·909	0	0·909	0·829		0·926	0	0·926	0·839
0·909	0	0·909	0·834		0·922	0	0·922	0·835
0·900	0	0·900	0·848		0·923	0	0·923	0·835
0·872	0	0·872	0·841		0·928	0	0·928	0·849
0·860	0	0·860	0·850	Outboard S.V. open 1	0·925	0	0·925	0·846
0·839	0	0·839	0·830		0·929	0	0·929	0·836
0·899	0·018	0·917	0·856		0·887	0·023	0·910	0·863
0·896	0·019	0·915	0·864		0·888	0·023	0·911	0·864
0·885	0·021	0·906	0·876		0·887	0·023	0·910	0·866
0·872	0·022	0·898	0·865		0·886	0·023	0·909	0·863
0·860	0·023	0·883	0·871		0·887	0·023	0·910	0·865
0·847	0·021	0·868	0·872	Outboard S.V. open 1	0·887	0·023	0·910	0·865
0·822	0·025	0·847	0·857		0·887	0·023	0·910	0·864
0·788	0·027	0·815	0·854		0·885	0·023	0·908	0·862
0·772	0·021	0·793	0·868	" S.V. open 2	0·886	0·023	0·909	0·864
0·898	0·027	0·925	0·853		0·895	0·037	0·932	0·870
0·895	0·030	0·925	0·862		0·899	0·037	0·936	0·874
0·889	0·035	0·924	0·870		0·901	0·037	0·938	0·876
0·882	0·039	0·921	0·877		0·898	0·038	0·936	0·874
0·867	0·044	0·911	0·876		0·895	0·038	0·933	0·874
0·853	0·029	0·882	0·867	Outboard S.V. open 1	0·899	0·038	0·937	0·877
0·835	0·048	0·883	0·871		0·892	0·037	0·929	0·865
0·795	0·053	0·848	0·863		0·890	0·035	0·925	0·868
0·799	0·034	0·833	0·878	" S.V. open 1	0·889	0·037	0·926	0·869
0·781	0·032	0·813	0·868	" S.V. open 2	0·898	0·038	0·936	0·876
0·743	0·023	0·766	0·832	" S.V. open 3	0·899	0·038	0·937	0·877
0·764	0·056	0·820	0·859		0·890	0·035	0·925	0·864

Table 5

Splitter I, no roughness, M = 2·12

Outboard					Inboard			
m_c/m_i	m_b/m_i	A_∞/A_{en}	P_f/P_∞		m_c/m_i	m_b/m_i	A_∞/A_{en}	P_f/P_∞
				δ_3 = 16·25°				
0·922	0	0·922	0·839		0·911	0	0·911	0·824
0·913	0	0·913	0·858		0·895	0	0·895	0·837
0·913	0	0·913	0·866		0·896	0	0·896	0·845
0·913	0	0·913	0·873		0·898	0	0·898	0·852
0·885	0	0·885	0·849		0·882	0	0·882	0·844
0·862	0	0·862	0·839		0·865	0	0·865	0·843
0·843	0	0·843	0·832		0·847	0	0·847	0·840
0·821	0	0·821	0·827		0·825	0	0·825	0·834
0·716	0	0·716	0·786		0·699	0	0·699	0·772
0·644	0	0·644	0·751		0·641	0	0·641	0·755
0·543	0	0·543	0·703		0·570	0	0·570	0·744
0·896	0·031	0·927	0·885		0·887	0·027	0·914	0·879
0·880	0·039	0·919	0·904		0·867	0·034	0·901	0·893
0·867	0·049	0·916	0·909		0·854	0·045	0·899	0·892
0·829	0·049	0·878	0·881		0·831	0·047	0·878	0·884
0·802	0·050	0·852	0·869		0·809	0·049	0·858	0·877
0·779	0·052	0·831	0·861		0·784	0·050	0·834	0·869
0·762	0·054	0·816	0·858		0·750	0·048	0·798	0·847
0·733	0·056	0·789	0·848		0·703	0·045	0·748	0·817
0·616	0·056	0·672	0·791		0·600	0·047	0·647	0·774
0·563	0·056	0·619	0·771		0·563	0·050	0·613	0·771
				δ_3 = 17·25°				
0·919	0	0·919	0·839		0·907	0	0·907	0·830
0·915	0	0·915	0·859		0·903	0	0·903	0·848
0·918	0	0·918	0·870		0·904	0	0·904	0·856
0·913	0	0·913	0·877		0·899	0	0·899	0·866
0·888	0	0·888	0·855		0·892	0	0·892	0·859
0·867	0	0·867	0·847		0·872	0	0·872	0·852
0·848	0	0·848	0·841		0·856	0	0·856	0·850
0·831	0	0·831	0·839		0·839	0	0·839	0·849
0·723	0	0·723	0·792		0·708	0	0·708	0·775
0·662	0	0·662	0·771		0·648	0	0·648	0·757
0·555	0	0·555	0·717		0·576	0	0·576	0·743
0·905	0·032	0·937	0·867		0·901	0·025	0·926	0·864
0·887	0·035	0·922	0·894		0·879	0·030	0·909	0·890
0·879	0·037	0·916	0·903		0·870	0·033	0·903	0·898
0·870	0·042	0·912	0·911		0·860	0·037	0·897	0·904
0·837	0·045	0·882	0·889		0·840	0·045	0·885	0·892
0·809	0·047	0·856	0·879		0·814	0·047	0·861	0·885
0·784	0·050	0·834	0·869		0·795	0·050	0·845	0·882
0·768	0·052	0·820	0·866		0·774	0·050	0·824	0·875
0·633	0·057	0·690	0·814		0·611	0·048	0·659	0·789
0·572	0·057	0·629	0·781		0·570	0·051	0·621	0·781

Table 5 (Contd.)

Outboard					Inboard			
m_c/m_i	m_b/m_i	A_∞/A_{en}	P_f/P_∞		m_c/m_i	m_b/m_i	A_∞/A_{en}	P_f/P_∞
0·918	0·028	0·946	0·879	Unequal throttling	0·886	0·039	0·925	0·905
0·900	0·033	0·933	0·891		0·889	0·039	0·928	0·908
0·892	0·035	0·927	0·898		0·887	0·039	0·927	0·908
0·874	0·034	0·917	0·914		0·886	0·039	0·925	0·907
0·846	0·047	0·893	0·899		0·887	0·040	0·927	0·908
0·817	0·050	0·867	0·887		0·886	0·040	0·926	0·904
0·793	0·052	0·845	0·881		0·878	0·042	0·920	0·897
0·821	0·044	0·865	0·914	Outboard S.V. open 1	0·884	0·039	0·923	0·904
0·753	0·056	0·809	0·868		0·866	0·041	0·907	0·880
0·705	0·058	0·763	0·855		0·862	0·040	0·902	0·875
0·740	0·044	0·784	0·912	" S.V. open 2·5	0·886	0·039	0·925	0·908
0·585	0·060	0·645	0·801		0·848	0·038	0·886	0·866
				$\delta_3 = 18·25°$				
0·864	0	0·864	0·791	Equal throttling	0·874	0	0·874	0·803
0·859	0	0·859	0·806		0·871	0	0·871	0·814
0·860	0	0·860	0·816		0·873	0	0·873	0·824
0·863	0	0·863	0·826		0·872	0	0·872	0·834
0·861	0	0·861	0·835		0·870	0	0·870	0·841
0·857	0	0·857	0·844		0·865	0	0·865	0·849
0·847	0	0·847	0·844		0·853	0	0·853	0·849
0·834	0	0·834	0·843		0·841	0	0·841	0·850
0·764	0	0·764	0·831		0·749	0	0·749	0·818
0·625	0	0·625	0·765		0·621	0	0·621	0·766
0·839	0·029	0·868	0·843		0·854	0·030	0·884	0·856
0·830	0·034	0·864	0·870		0·839	0·035	0·874	0·878
0·829	0·038	0·867	0·884		0·835	0·039	0·874	0·889
0·814	0·043	0·857	0·891		0·818	0·043	0·861	0·891
0·793	0·046	0·839	0·884		0·798	0·047	0·845	0·886
0·775	0·049	0·824	0·879		0·782	0·049	0·831	0·887
0·750	0·052	0·802	0·872		0·756	0·050	0·806	0·878
0·728	0·054	0·782	0·866		0·733	0·051	0·784	0·869
0·580	0·058	0·637	0·793		0·584	0·053	0·637	0·798

Table 6

Various bleed configurations, $M = 2{\cdot}12$, $\delta_3 = 16{\cdot}25°$

Outboard					Inboard			
m_c/m_i	m_b/m_i	A_∞/A_{en}	P_f/P_∞		m_c/m_i	m_b/m_i	A_∞/A_{en}	P_f/P_∞
0·916	0·016	0·932	0·854	Bleed A2	0·919	0·016	0·935	0·853
0·901	0·017	0·918	0·862		0·906	0·018	0·924	0·861
0·898	0·020	0·918	0·863		0·901	0·020	0·921	0·869
0·896	0·024	0·920	0·880		0·900	0·025	0·925	0·883
0·880	0·025	0·905	0·873		0·876	0·026	0·902	0·869
0·855	0·026	0·881	0·860		0·843	0·027	0·870	0·851
0·827	0·026	0·853	0·845		0·815	0·027	0·832	0·834
0·785	0·028	0·813	0·830		0·776	0·028	0·084	0·822
0·761	0·028	0·789	0·823		0·749	0·029	0·778	0·812
0·913	0·028	0·941	0·864		0·917	0·026	0·943	0·863
0·898	0·033	0·931	0·878		0·903	0·034	0·937	0·879
0·888	0·036	0·924	0·884		0·895	0·037	0·932	0·886
0·877	0·040	0·917	0·889		0·882	0·040	0·922	0·896
0·864	0·048	0·912	0·885		0·868	0·049	0·917	0·888
0·829	0·048	0·877	0·865		0·831	0·050	0·881	0·867
0·808	0·049	0·857	0·856		0·800	0·051	0·851	0·848
0·763	0·051	0·814	0·843		0·756	0·053	0·809	0·835
0·717	0·053	0·770	0·828		0·707	0·054	0·761	0·817
0·914	0·018	0·932	0·849	Bleed A4	0·913	0·016	0·929	0·849
0·904	0·018	0·922	0·861		0·904	0·018	0·922	0·859
0·900	0·020	0·920	0·870		0·900	0·020	0·920	0·867
0·899	0·024	0·923	0·884		0·899	0·024	0·923	0·884
0·885	0·026	0·911	0·877		0·882	0·027	0·909	0·874
0·860	0·027	0·887	0·866		0·853	0·027	0·880	0·861
0·832	0·027	0·859	0·850		0·820	0·028	0·848	0·839
0·793	0·029	0·822	0·840		0·782	0·029	0·811	0·828
0·744	0·030	0·774	0·821		0·728	0·030	0·758	0·805
0·909	0·030	0·939	0·865		0·910	0·027	0·937	0·859
0·903	0·034	0·937	0·882		0·903	0·033	0·936	0·877
0·894	0·037	0·931	0·887		0·892	0·036	0·928	0·883
0·887	0·041	0·928	0·895		0·883	0·040	0·923	0·895
0·862	0·047	0·909	0·882		0·865	0·049	0·914	0·886
0·840	0·048	0·888	0·876		0·831	0·050	0·881	0·868
0·815	0·049	0·864	0·866		0·803	0·051	0·854	0·853
0·772	0·051	0·823	0·855		0·757	0·052	0·809	0·838
0·729	0·054	0·783	0·842		0·709	0·053	0·762	0·819

Table 6 (Contd.)

Outboard					Inboard			
m_c/m_i	m_b/m_i	A_∞/A_{en}	P_f/P_∞		m_c/m_i	m_b/m_i	A_∞/A_{en}	P_f/P_∞
0·917	0·016	0·933	0·857	Bleed B0	0·921	0·015	0·936	0·856
0·908	0·016	0·924	0·869		0·911	0·017	0·928	0·867
0·904	0·020	0·924	0·876		0·906	0·020	0·926	0·876
0·900	0·024	0·924	0·883		0·902	0·024	0·926	0·889
0·879	0·025	0·904	0·868		0·872	0·025	0·897	0·865
0·848	0·025	0·873	0·851		0·841	0·025	0·866	0·846
0·829	0·026	0·855	0·845		0·816	0·026	0·842	0·834
0·764	0·028	0·792	0·823		0·751	0·028	0·779	0·811
0·913	0·024	0·937	0·871		0·915	0·025	0·940	0·868
0·899	0·030	0·929	0·883		0·903	0·030	0·933	0·881
0·890	0·035	0·925	0·887		0·895	0·035	0·930	0·894
0·872	0·038	0·910	0·880		0·888	0·039	0·927	0·900
0·842	0·039	0·881	0·859		0·838	0·043	0·881	0·858
0·819	0·039	0·858	0·854		0·810	0·044	0·854	0·845
0·800	0·041	0·841	0·847		0·791	0·045	0·836	0·837
0·737	0·045	0·882	0·818		0·729	0·050	0·779	0·820
0·920	0·017	0·937	0·855	Bleed B2	0·922	0·015	0·937	0·853
0·901	0·016	0·917	0·862		0·903	0·016	0·919	0·859
0·896	0·019	0·915	0·870		0·900	0·019	0·919	0·870
0·893	0·023	0·916	0·876		0·900	0·023	0·923	0·887
0·875	0·024	0·899	0·866		0·872	0·025	0·897	0·866
0·848	0·024	0·872	0·850		0·838	0·025	0·861	0·842
0·827	0·025	0·852	0·845		0·815	0·025	0·840	0·834
0·788	0·026	0·814	0·832		0·777	0·026	0·803	0·823
0·763	0·026	0·789	0·824		0·750	0·027	0·777	0·813
0·910	0·026	0·936	0·871		0·916	0·024	0·940	0·868
0·899	0·029	0·928	0·882		0·902	0·029	0·931	0·880
0·890	0·038	0·928	0·885		0·898	0·035	0·933	0·896
0·870	0·040	0·910	0·878		0·866	0·040	0·906	0·876
0·840	0·040	0·880	0·860		0·831	0·041	0·872	0·851
0·818	0·042	0·860	0·852		0·806	0·042	0·848	0·841
0·800	0·043	0·843	0·847		0·788	0·043	0·831	0·836
0·736	0·047	0·783	0·828		0·721	0·046	0·767	0·811

SYMBOLS

A_2	throat area
A_{en}	intake capture area
A_∞	entry stream tube upstream area
D_v	distortion parameter $\left[\frac{V_{max} - V_{min}}{V_{mean}}\right]_{RAD}$
h	intake capture height
M	"free stream" Mach number (though not necessarily tunnel Mach No.)
M_3	pre-normal shock Mach number
m_b	throat bleed mass flow
m_e	"engine" mass flow
m_i	intake mass flow
$m_{s.v.}$	afterspill mass flow
	lb/sec
P_A	peak to peak amplitude of pressure fluctuations
P_f	mean total pressure at measuring station
p_s	mean static pressure at measuring station
P_∞	"free stream" total pressure (though not necessarily tunnel total pressure)
R_e	Reynolds number
R_v	distortion parameter $\frac{V_{max}}{V_{mean}}$ at measuring station
r/R	radius/measuring station maximum radius
S.V.	spill vent (afterspill)
V	stream velocity
$\bar{V}$	mean velocity at measuring station
W	intake capture width (per duct)
$\frac{d(P_f/P_\infty)}{d(m_b/m_i)}$	bleed efficiency
δ_1, δ_2, δ_3	compression surface angles (see Fig.3)
ϕ	angle of rotation looking downstream (see Fig.24)
$[\ ]_{RAD}$	at constant radius
$[\ ]_{r/R=}$	at constant radius of specific value r/R

REFERENCES

No.	Author	Title, etc.
1	M.D. Dobson	Wind tunnel tests at M = 2·0 on interference effects between intake flows in a four-engine nacelle. A.R.C. C.P.753
2	B.A.C.	Supersonic transport. Definition of nacelle geometry - prototype and interim engine variants. SST/B72A - 05.3/2047 August 1964
3	M.D. Dobson	Unpublished M.O.A. Report
4	M.C. Neale P.S. Lamb	Tests with a two-dimensional intake having all-external compression and a design Mach number of 2·0. A.R.C. C.P.937 September 1963

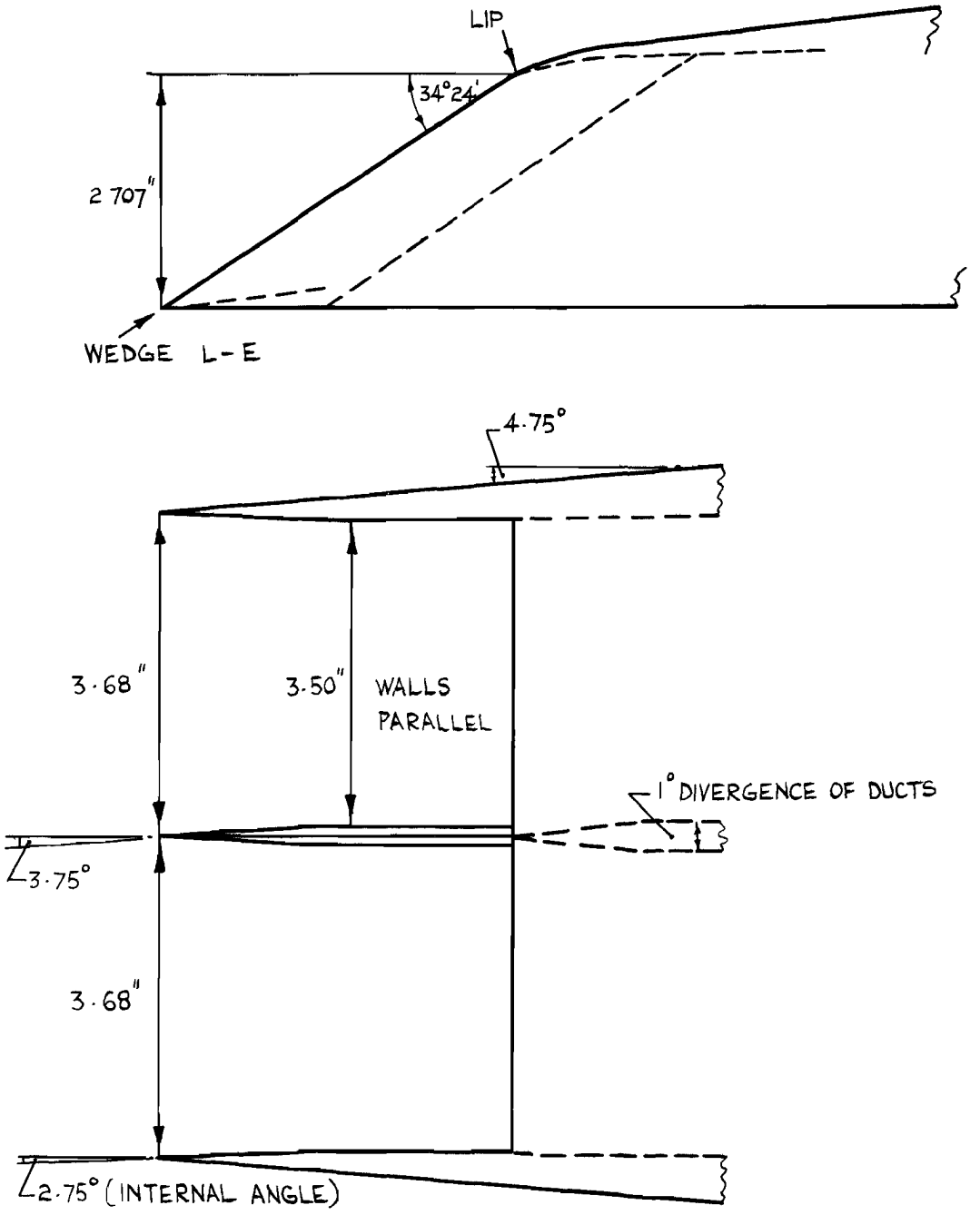

FIG. I. INLET DETAILS SPLITTER I CONFIGURATION

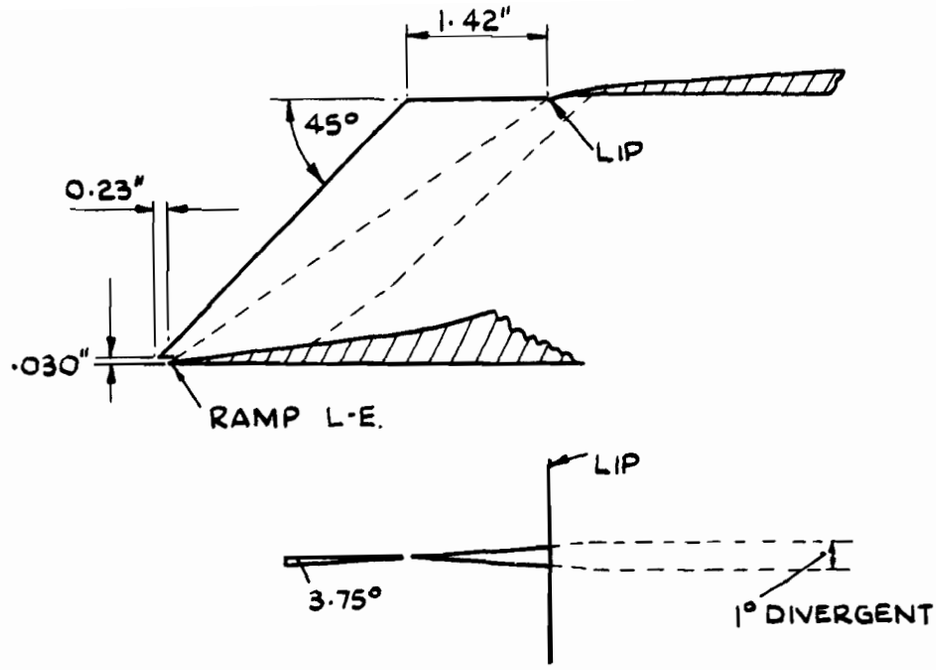

SPLITTER III CONFIGURATION.

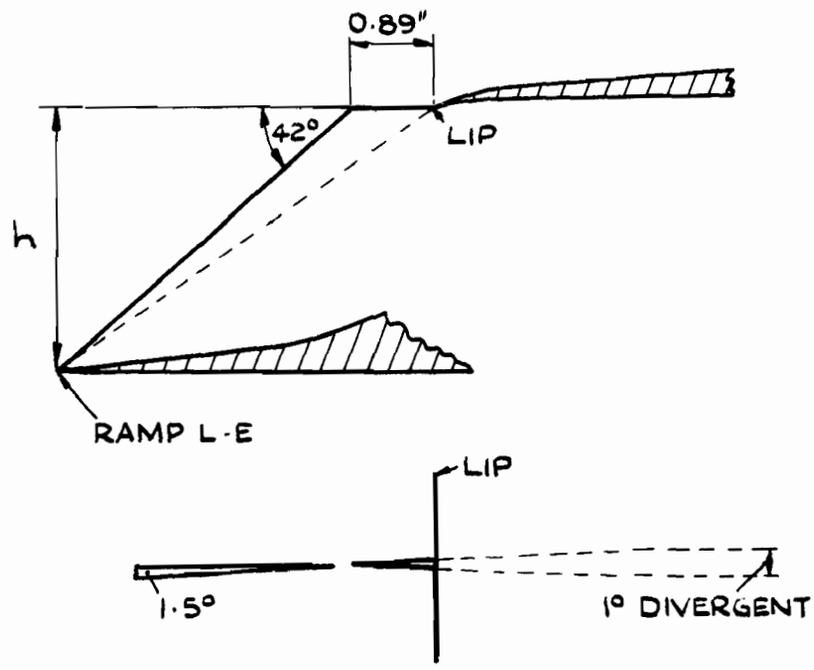

SPLITTER II CONFIGURATION.

FIG. 2 ADDITIONAL SPLITTER CONFIGURATIONS.

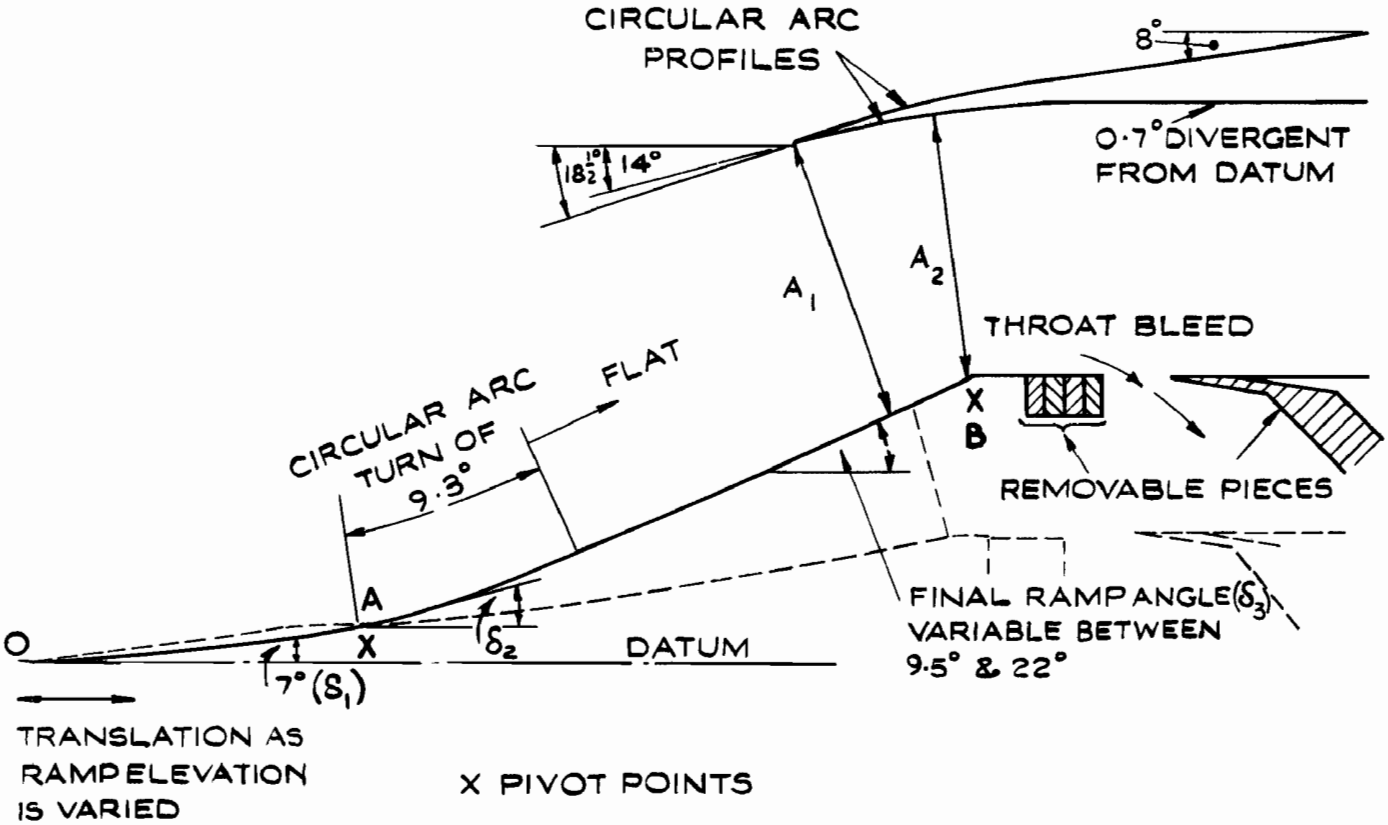

FIG.3 INTAKE DETAILS

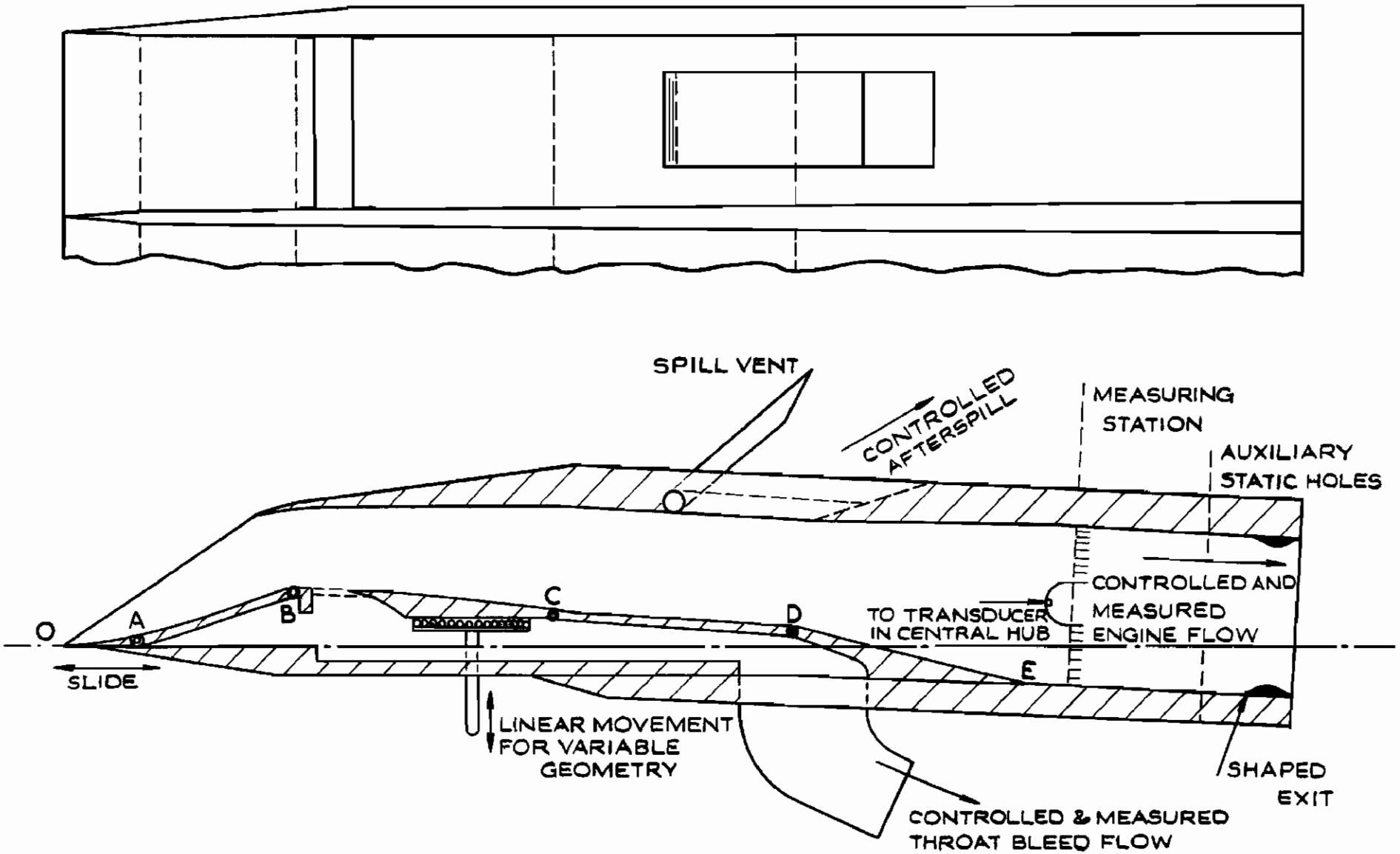

FIG.4 DUCT DETAILS

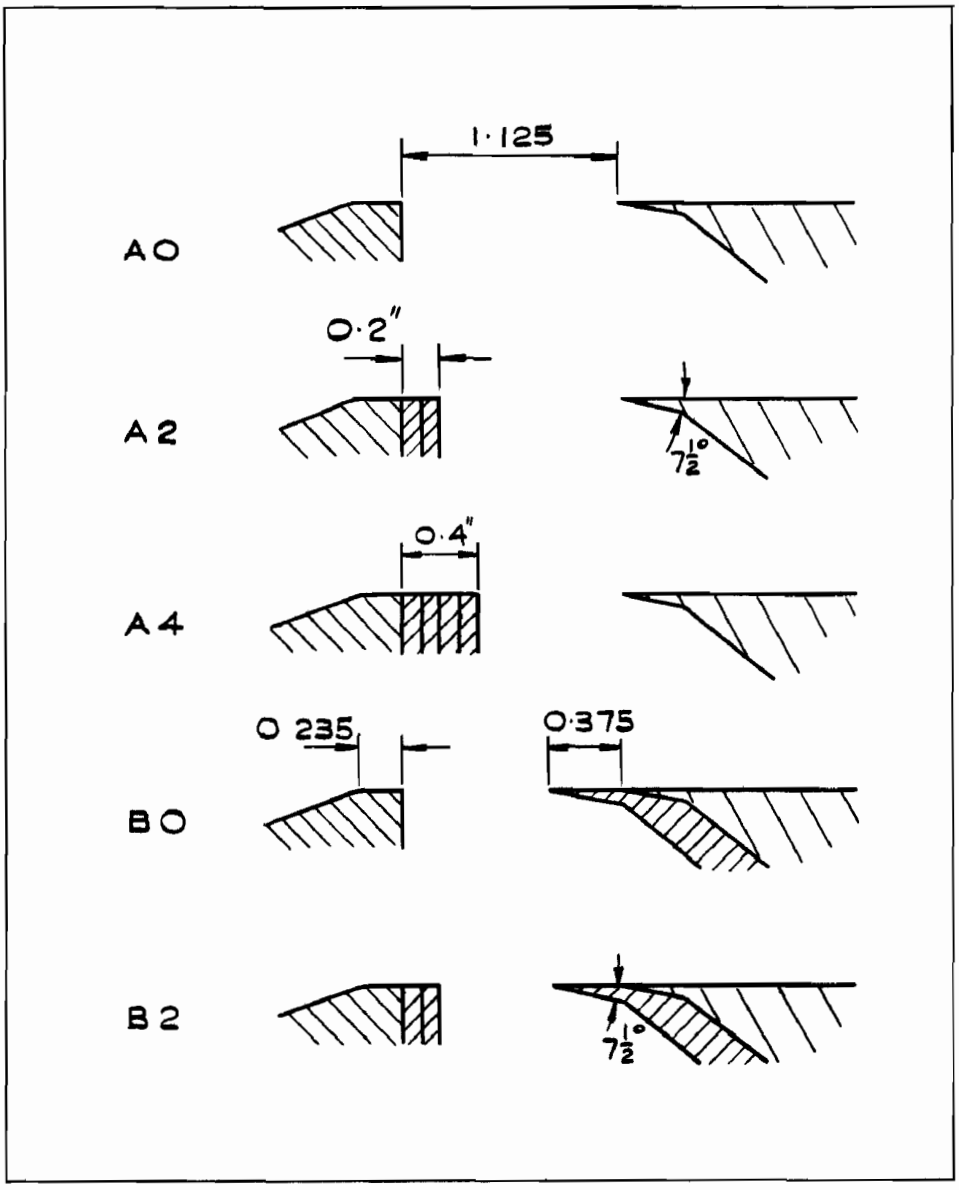

FIG.5 THROAT BLEED SLOT CONFIGURATIONS

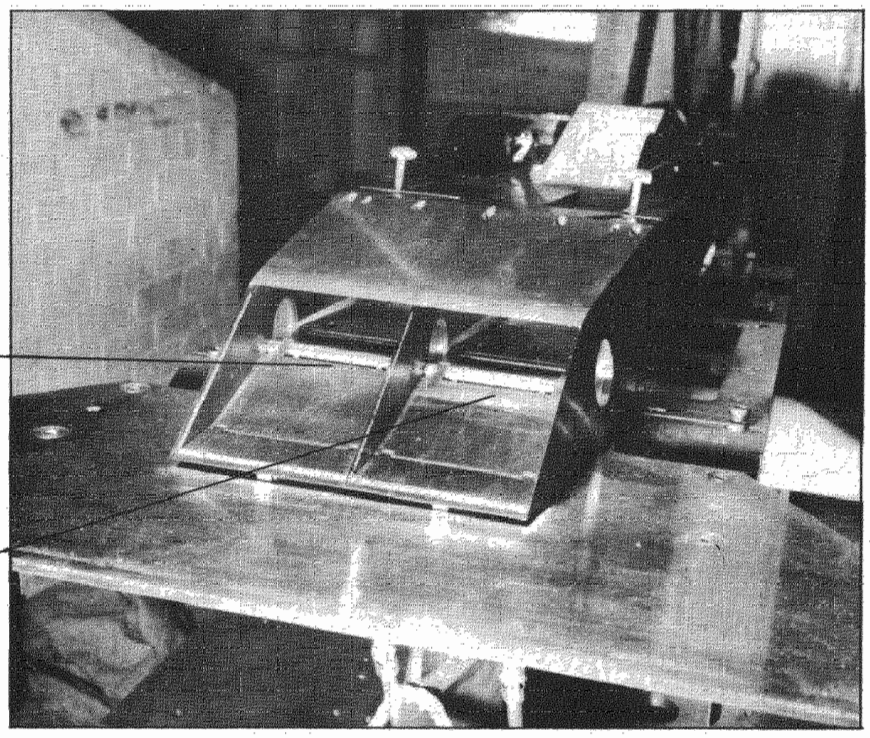

(a)

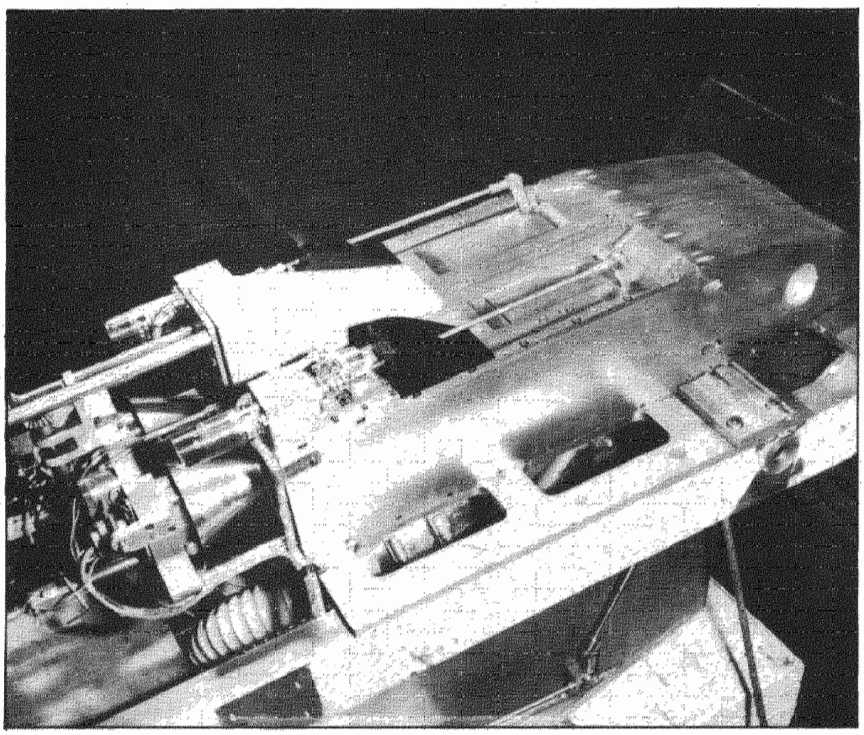

(b)

FIG.6 MODEL

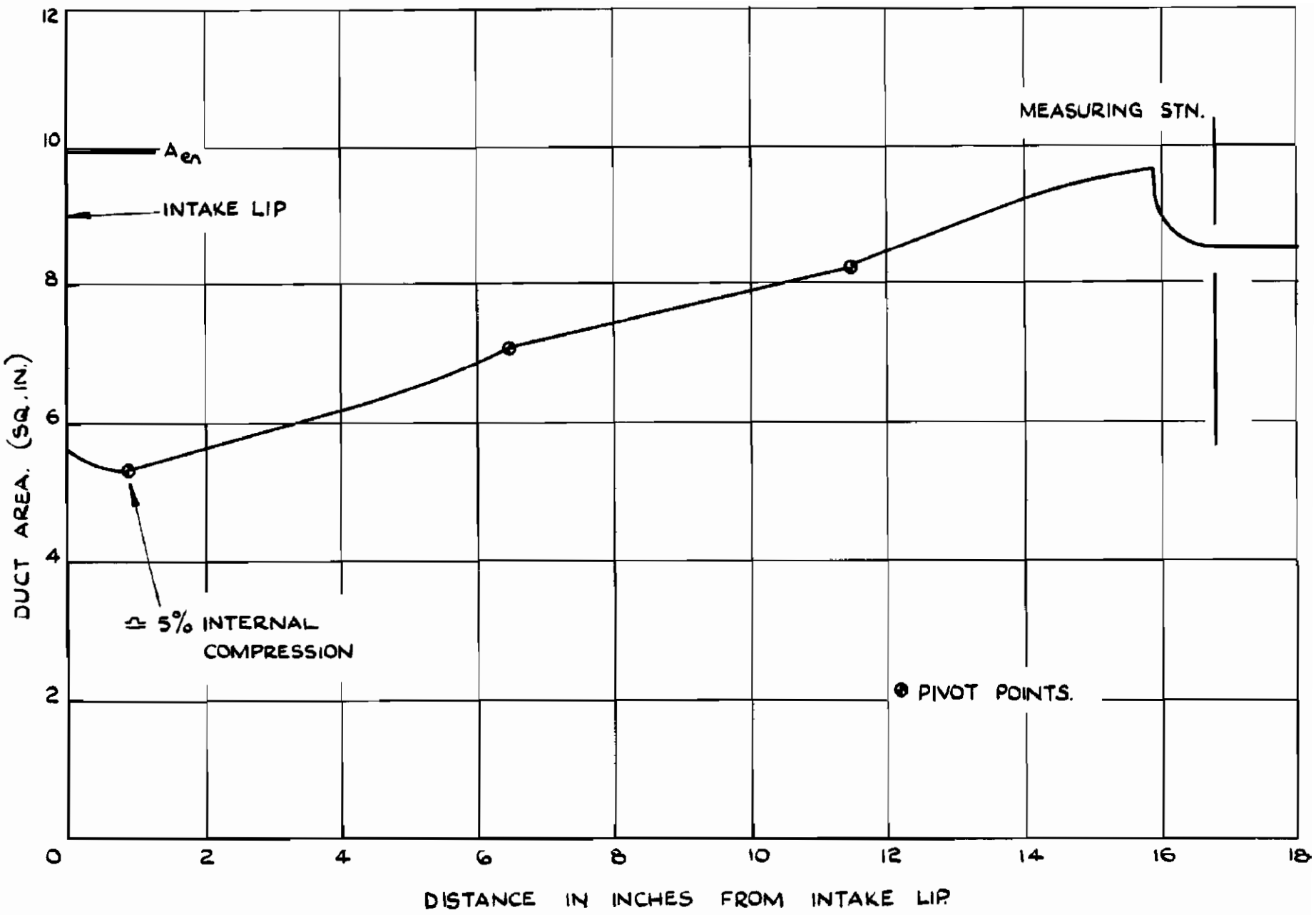

FIG. 7 AREA DISTRIBUTION ALONG DUCT FOR $\delta_3 = 20^\circ$

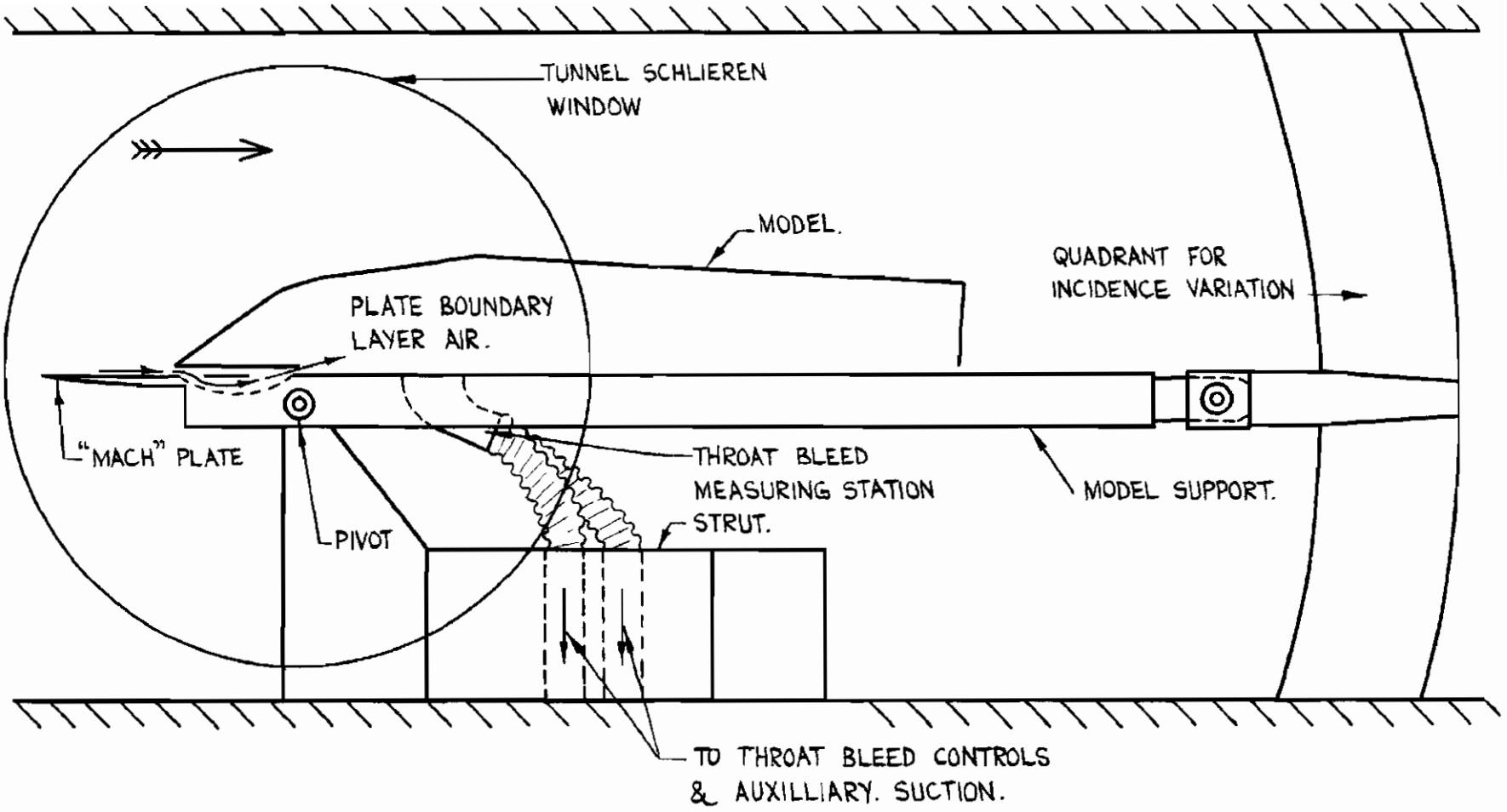

FIG. 8. MODEL SUPPORT.

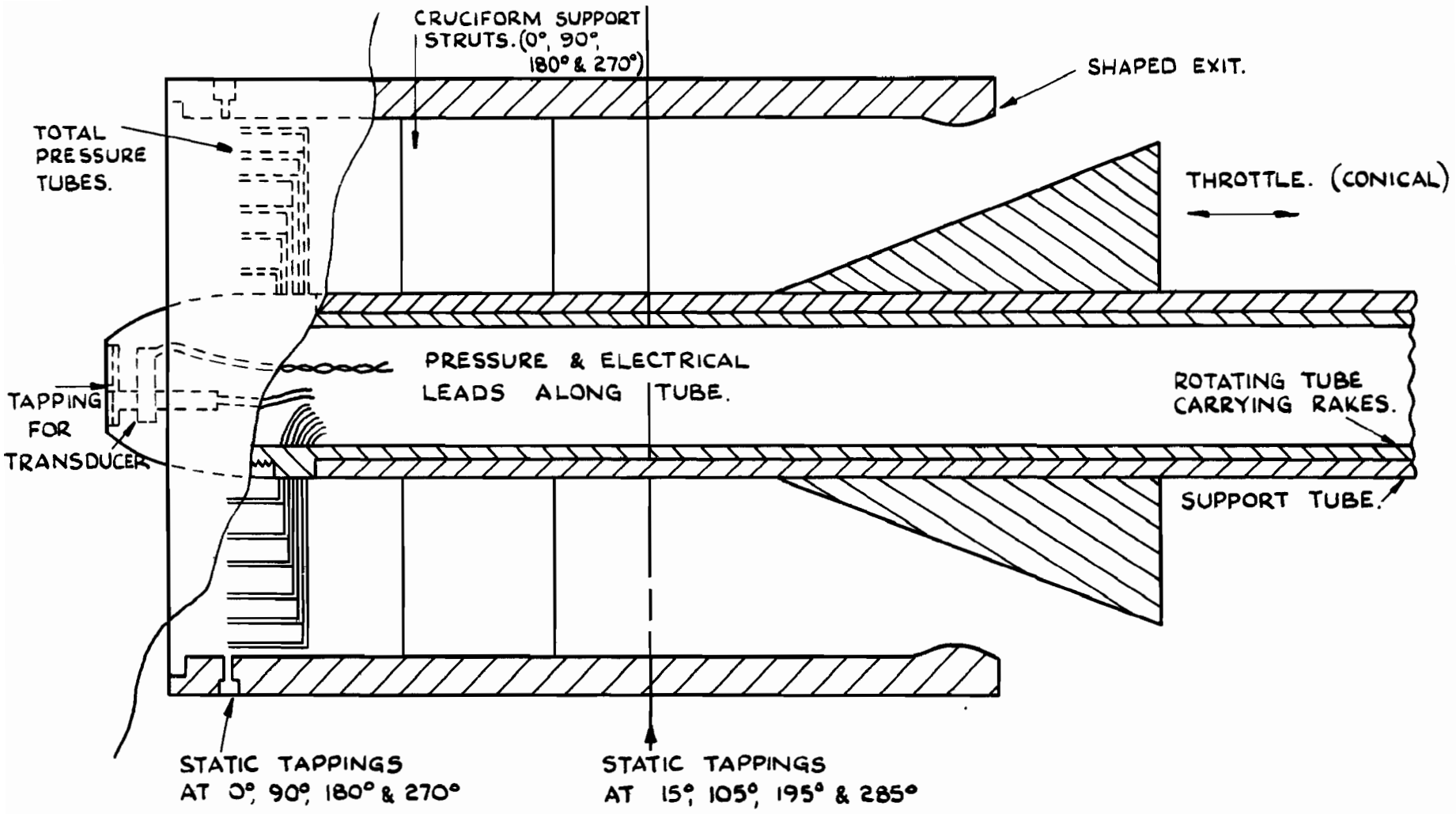

FIG. 9 DETAILS OF FLOW CONTROL & MEASUREMENT UNIT.

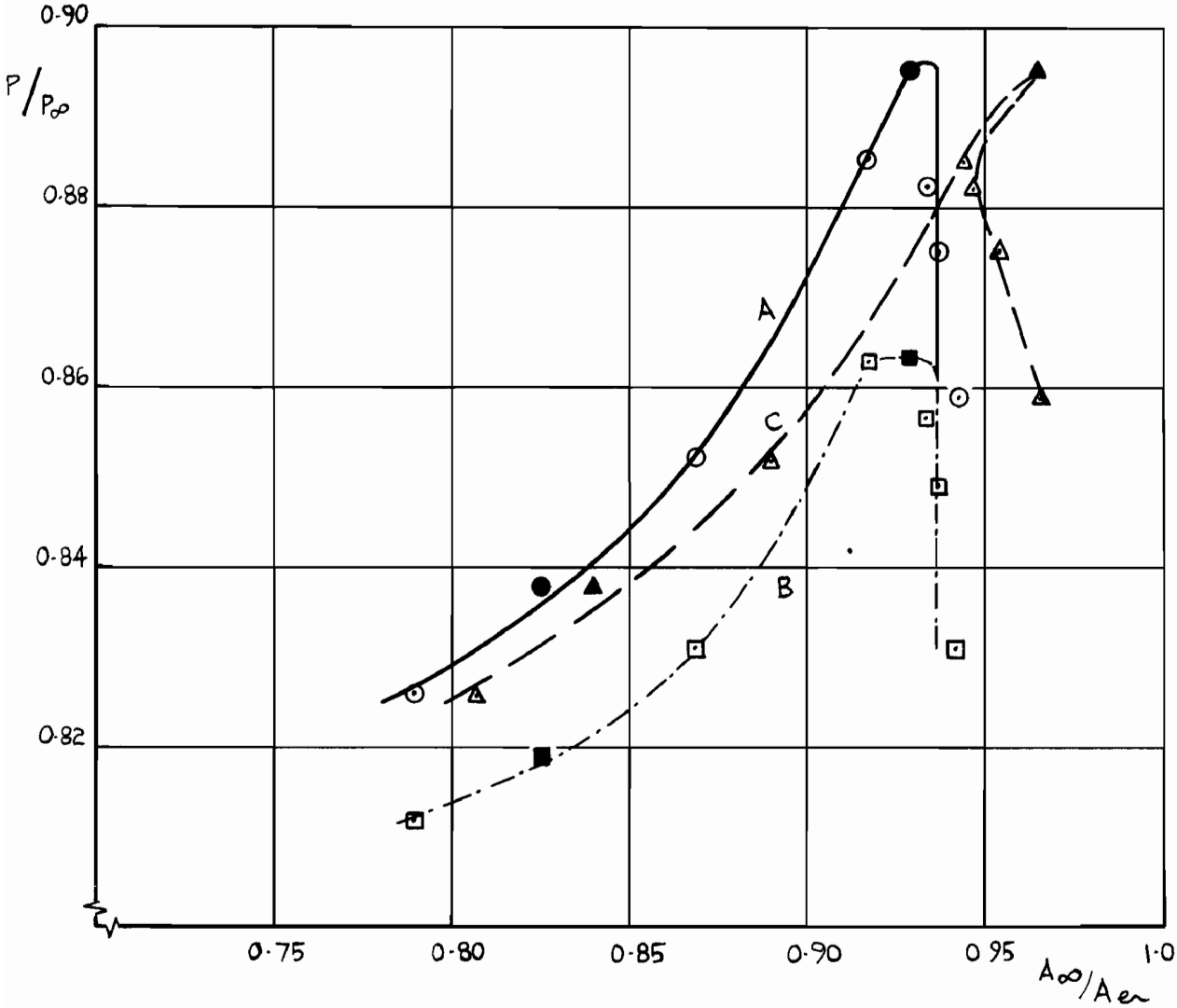

KEY TO CURVES.

	PRESSURE RECOVERY	MASS FLOW
COMPRESSOR ENTRY	①	②
CHOKED EXIT	③	④

① & ④	● ■ ▲ "FILLED" SYMBOLS INDICATE POINTS FROM COMPREHENSIVE SURVEYS
① & ②	
③ & ④	

FIG. 10 PRESSURE RECOVERY & MASS FLOW RATIO-DIFFERENCES IN THESE QUANTITIES DEPENDING ON METHOD OF EVALUATION. ($M = 2 \cdot 12$. $\delta_3 = 16 \cdot 25^\circ$)

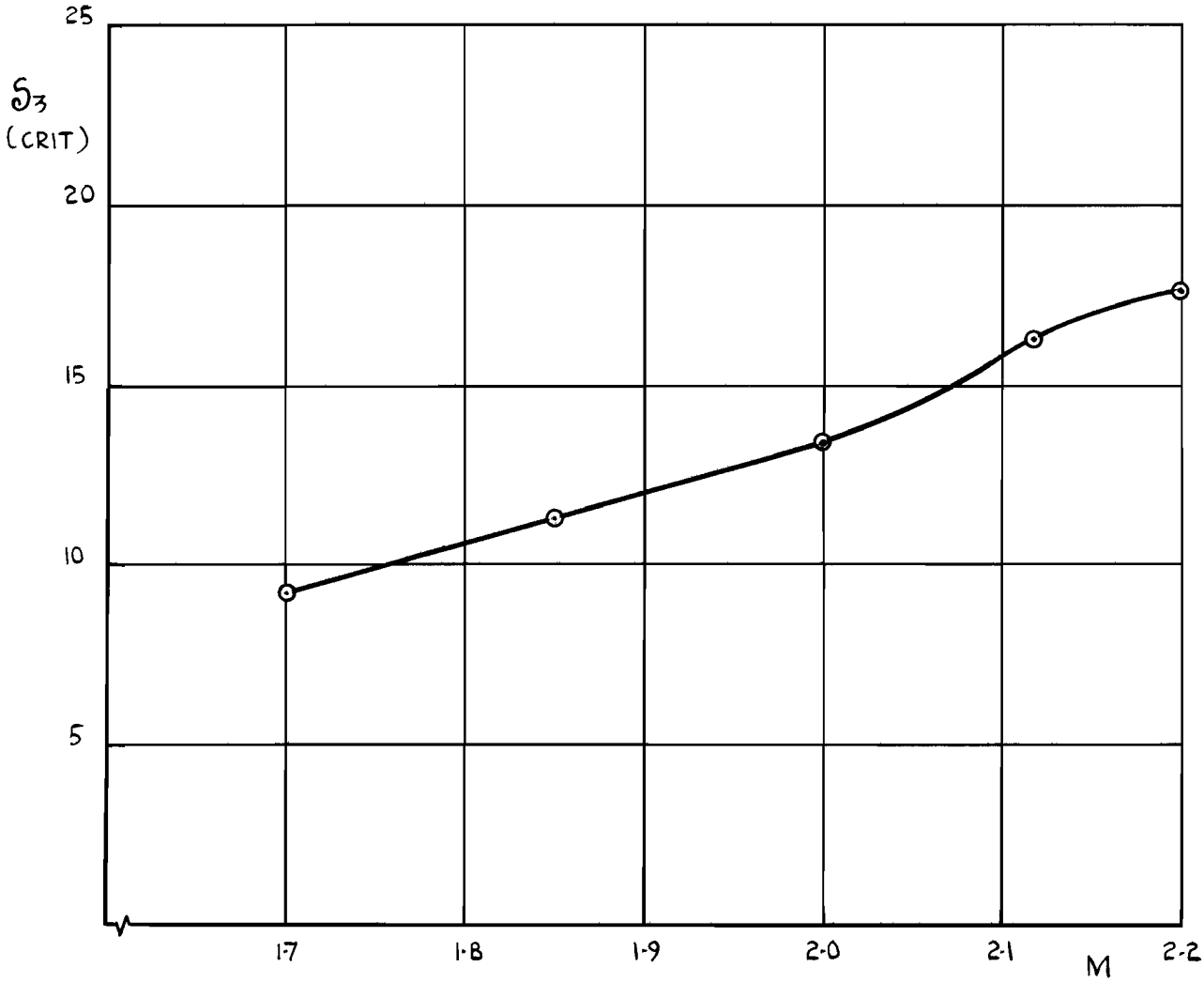

FIG. 11. CRITICAL RAMP ANGLE — VARIATION WITH MACH NUMBER

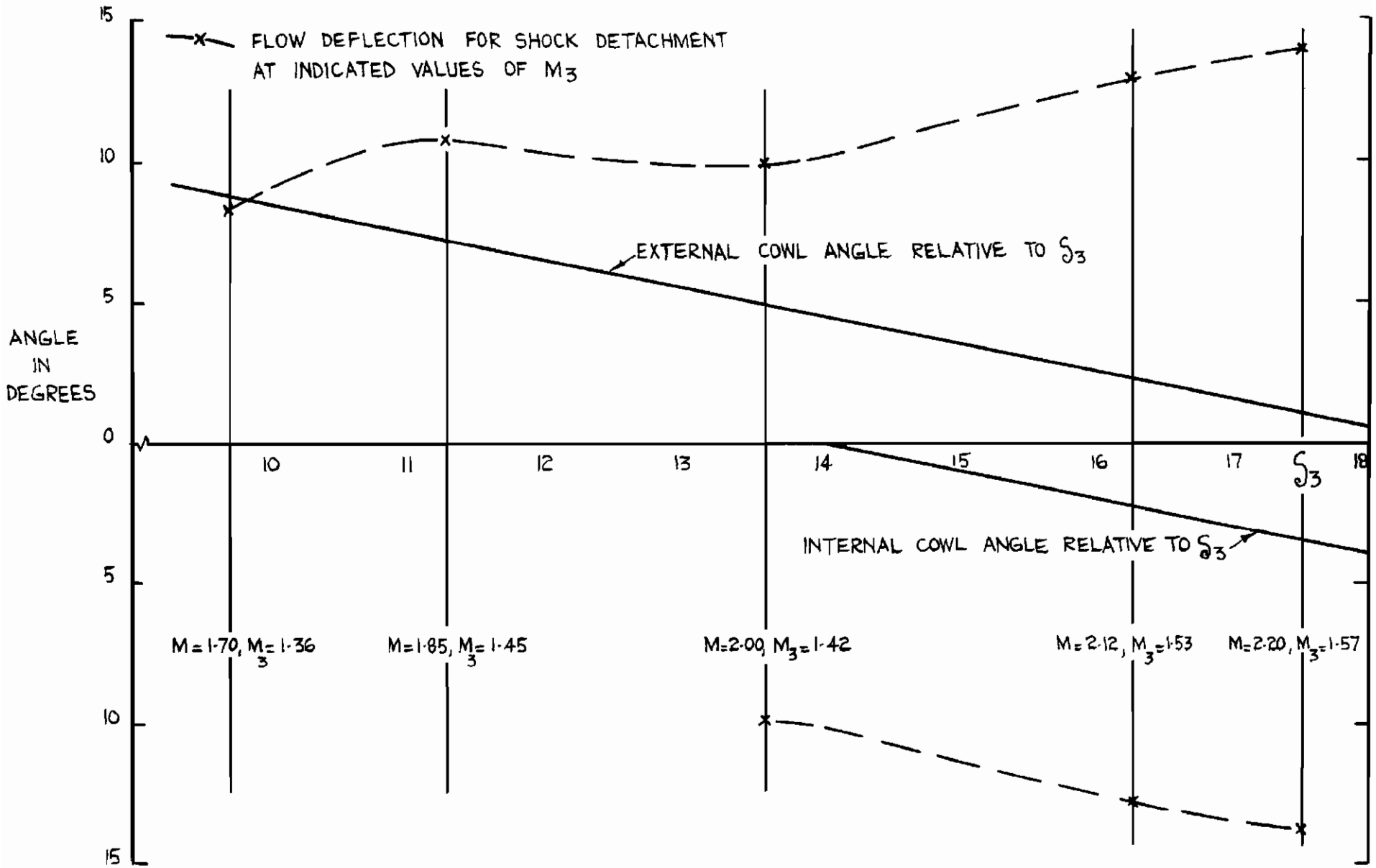

FIG. 12. POSSIBILITIES OF SHOCK DETACHMENT AT COWL LIP.

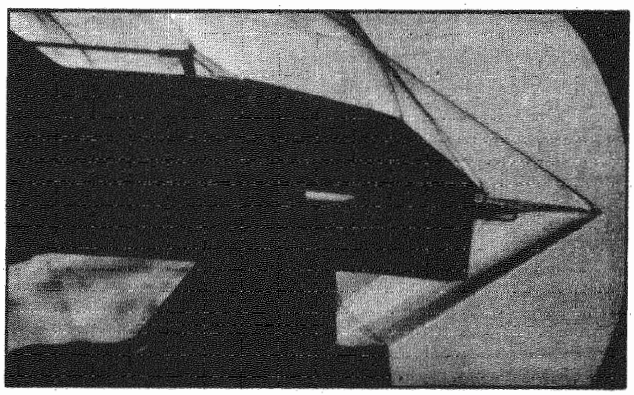

FIG. 13 SCHLIEREN PHOTOGRAPH - MAXIMUM INLET FLOW AT M = 1.70, $\delta_3 = 9.7^{\circ}$

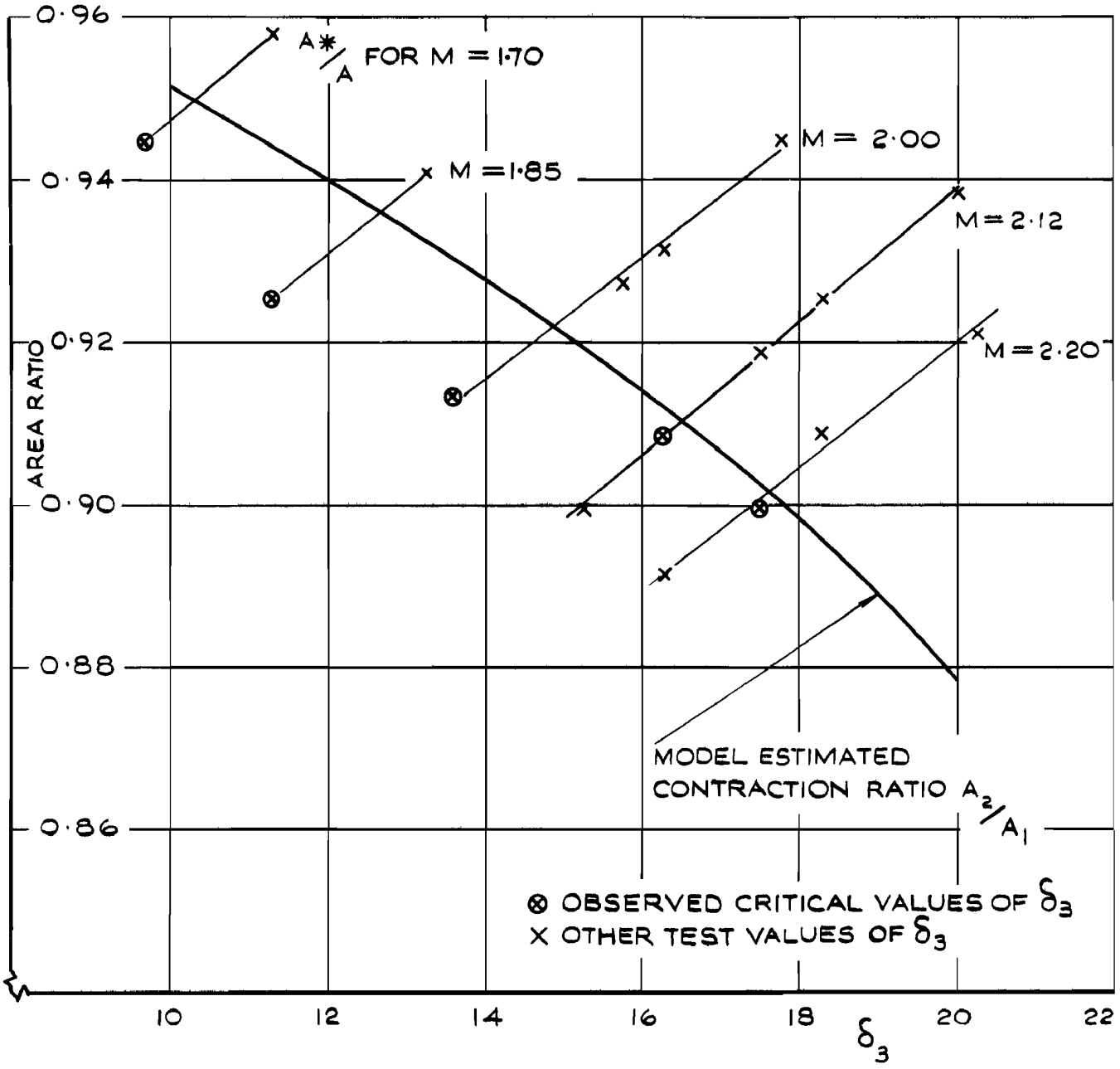

FIG 14 AREA RATIOS REQUIRED TO CHOKE FLOW DOWNSTREAM OF NORMAL SHOCK

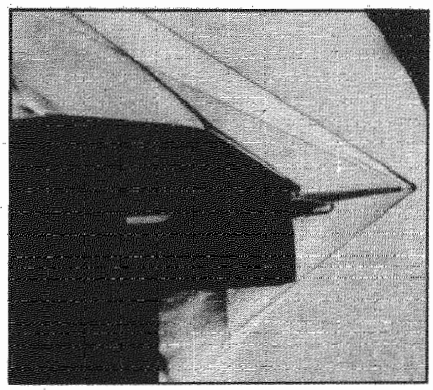

(a) $\delta_3 = 15.25^0$

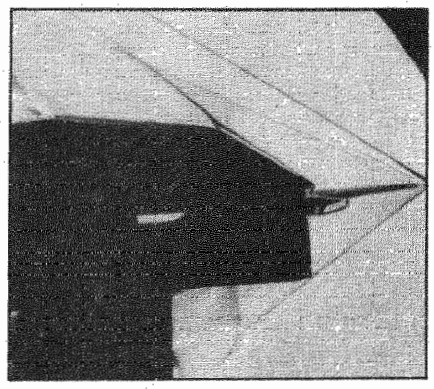

(b) $\delta_3 = 16.25^0$

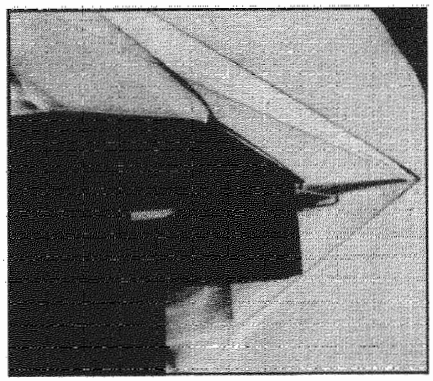

(c) $\delta_3 = 17.50^0$

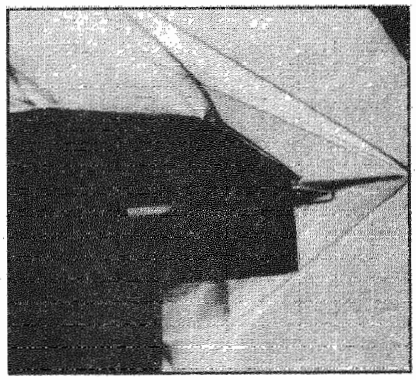

(d) $\delta_3 = 18.25^0$

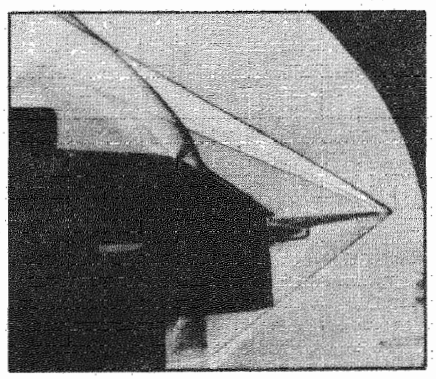

(e) $\delta_3 = 20.00^0$

(a) $m_b/m_i = 0$

FIG.15 SCHLIEREN PHOTOGRAPHS - M = 2.12, SPLITTER I

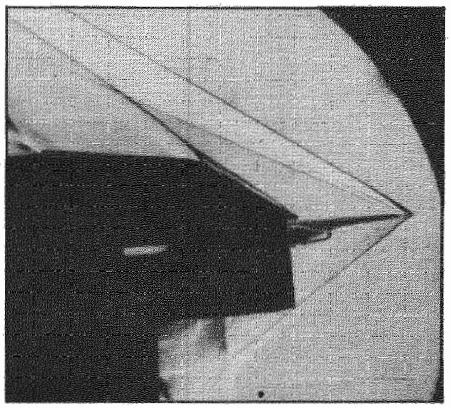

(a) $\delta_3 = 15.25^0$

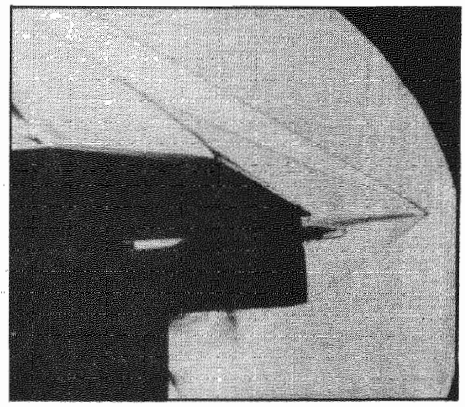

(b) $\delta_3 = 16.25^0$

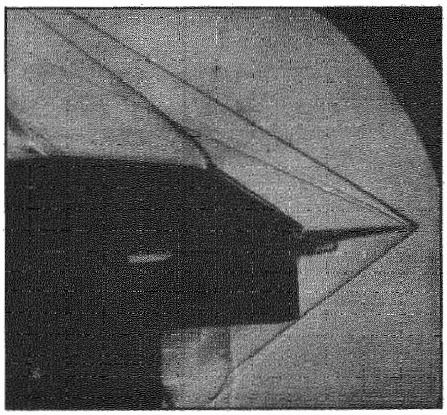

(c) $\delta_3 = 17.50^0$

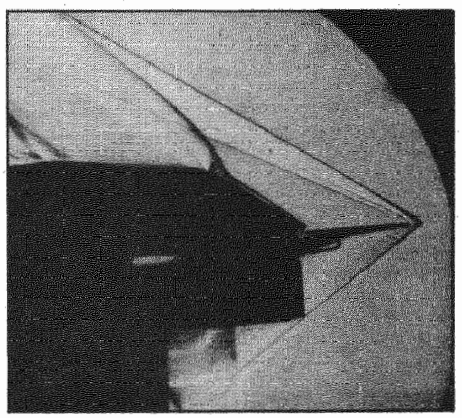

(d) $\delta_3 = 18.25^0$

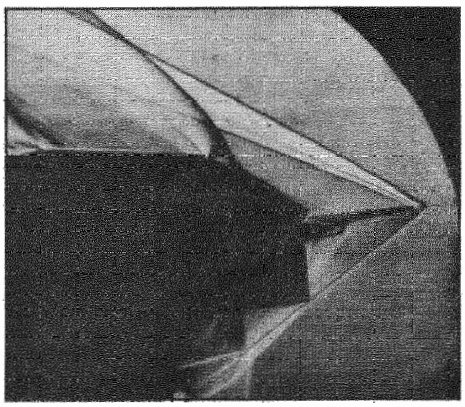

(e) $\delta_3 = 20.00^0$

(b) $m_b/m_i \approx 0.04$

FIG.15 (CONC)

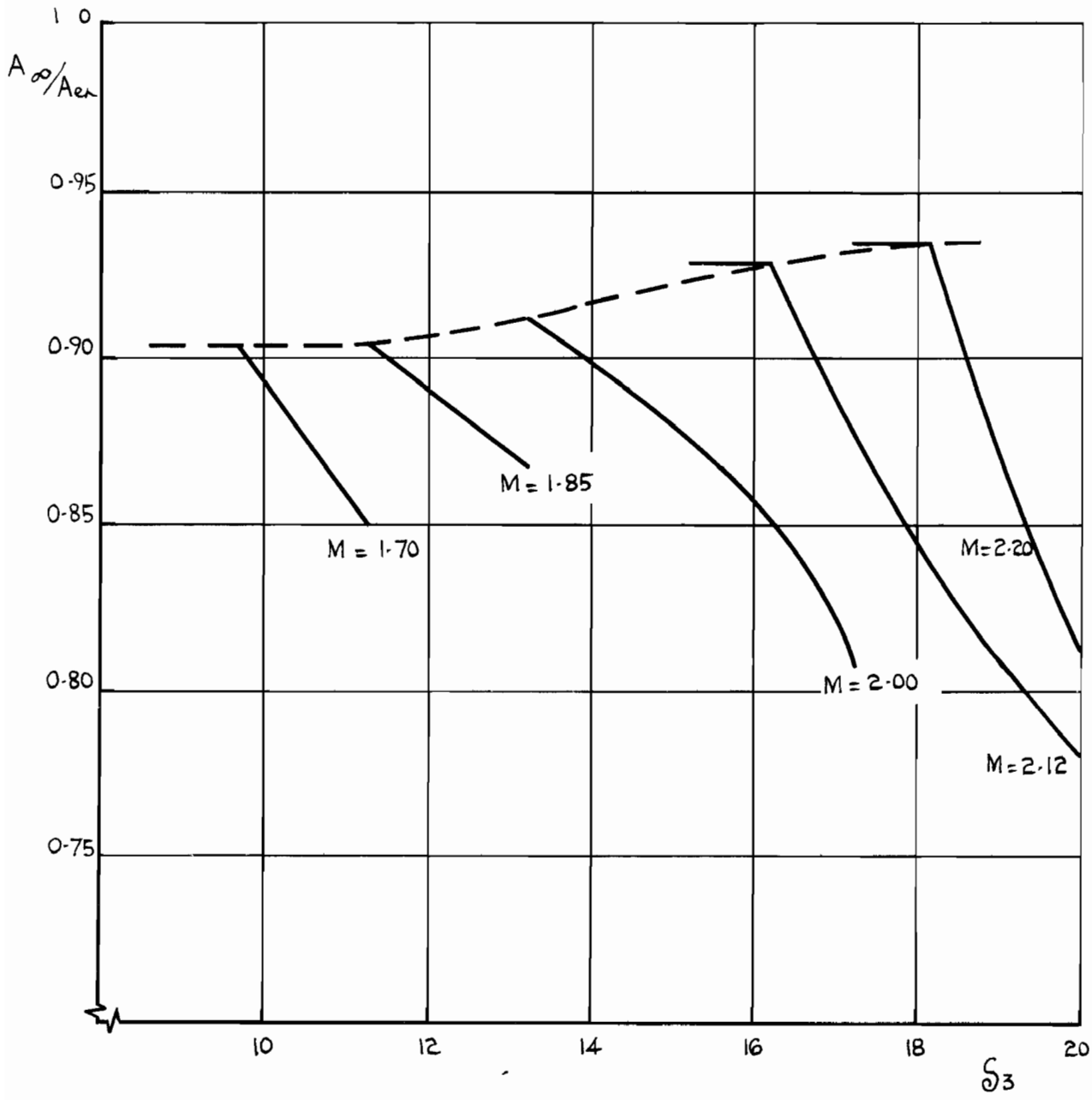

FIG. 16. MASS FLOW RATIO – VARIATION WITH δ_3 AT CONSTANT VALUES OF MACH NUMBER.

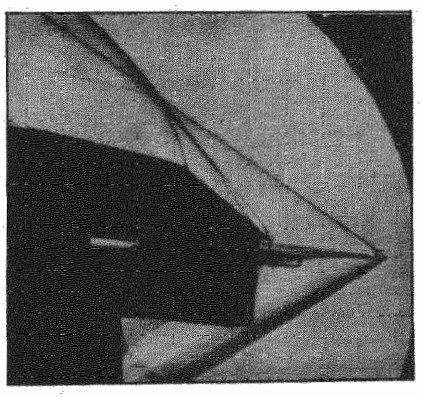

(a) M = 1.70, $\delta_3 = 9.7^0$

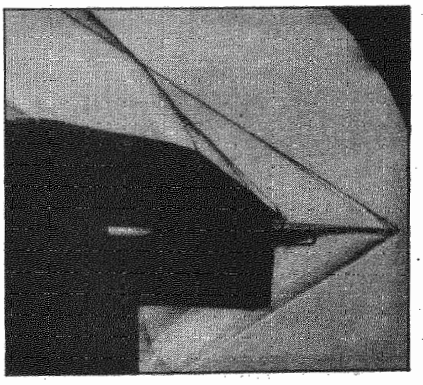

(b) M = 1.85, $\delta_3 = 11.3^0$

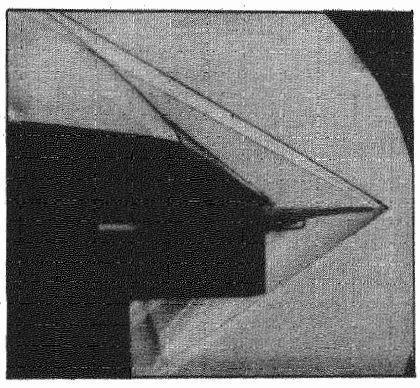

(c) M = 2.00, $\delta_3 = 13.6^0$

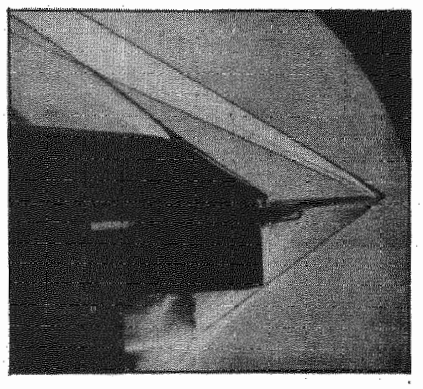

(d) M = 2.12, $\delta_3 = 16.25^0$

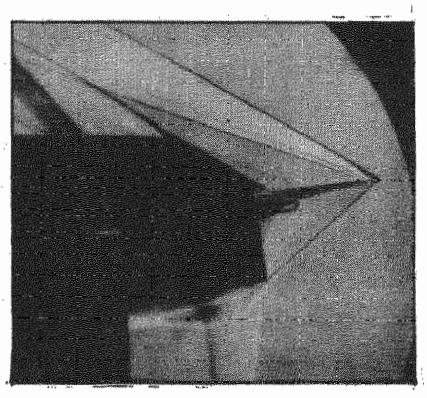

(e) M = 2.20, $\delta_3 = 17.50^0$

FIG.17 SCHLIEREN PHOTOGRAPHS - INTAKE AT FULL FLOW

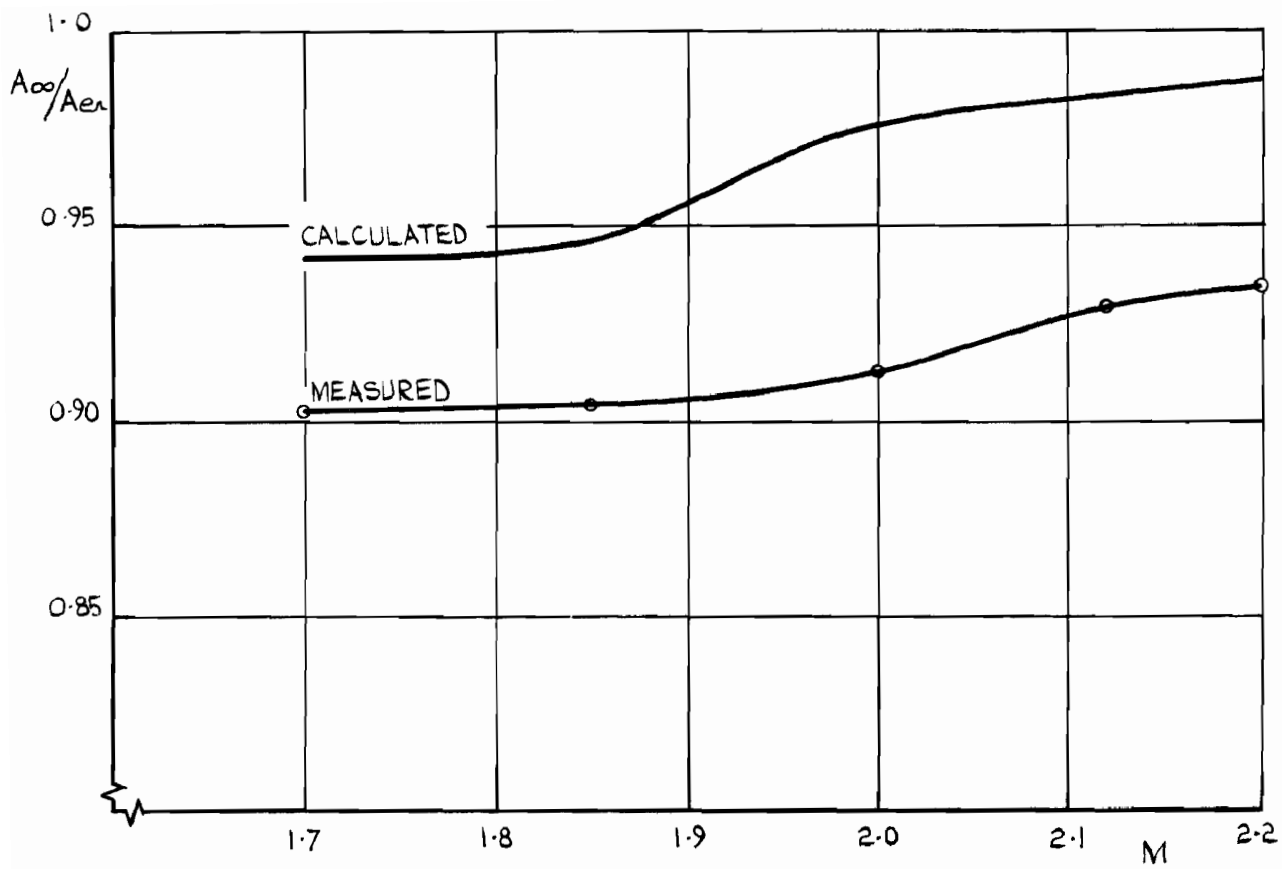

FIG. 18. MAXIMUM VALUES OF MASS FLOW WHEN DEFLECTION IS BY 7° WEDGE ONLY.

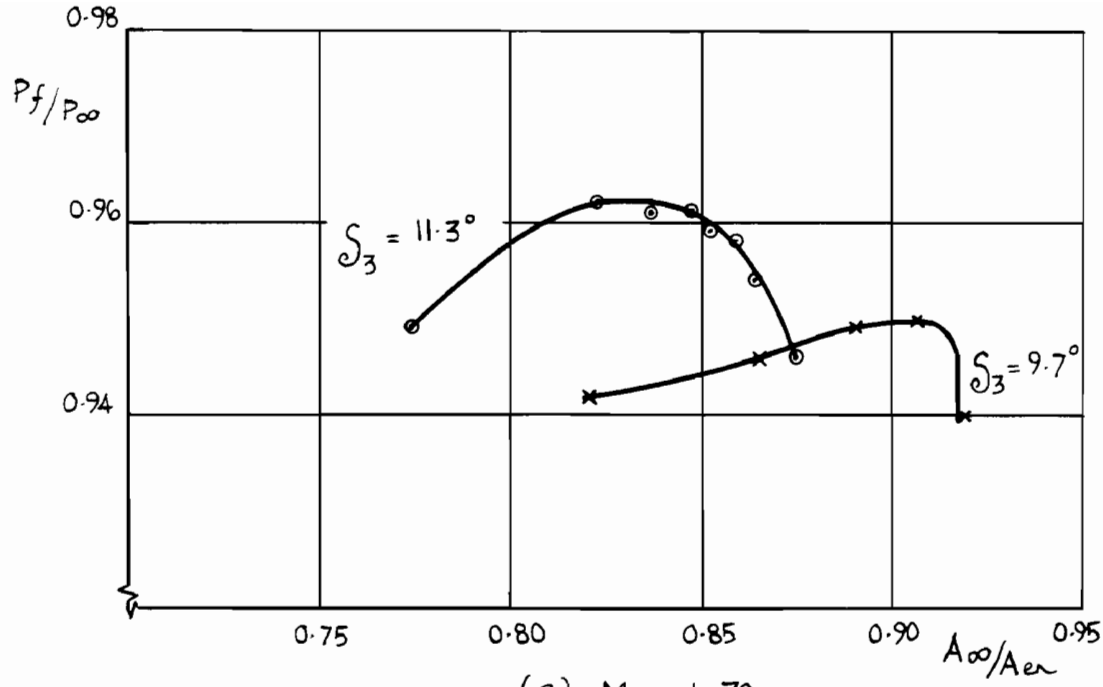

(a) M = 1·70

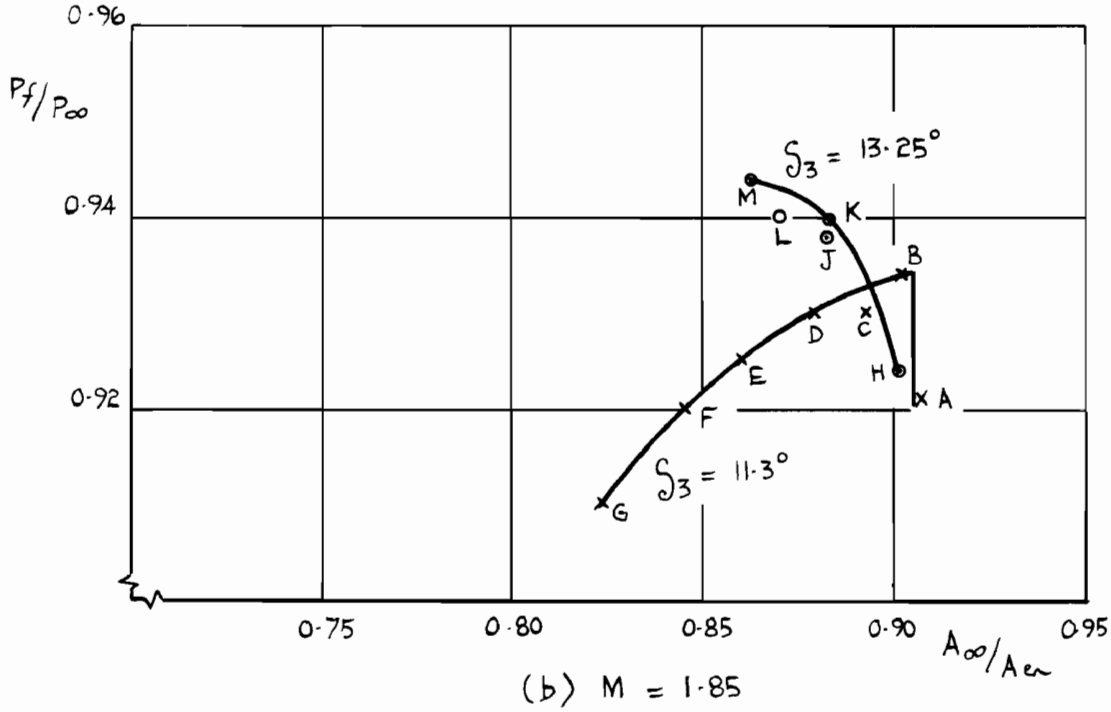

(b) M = 1·85

FIG. 19. TYPICAL PRESSURE RECOVERY CHARACTERISTICS FOR VARIOUS VALUES OF M & δ_3 – SPLITTER I.

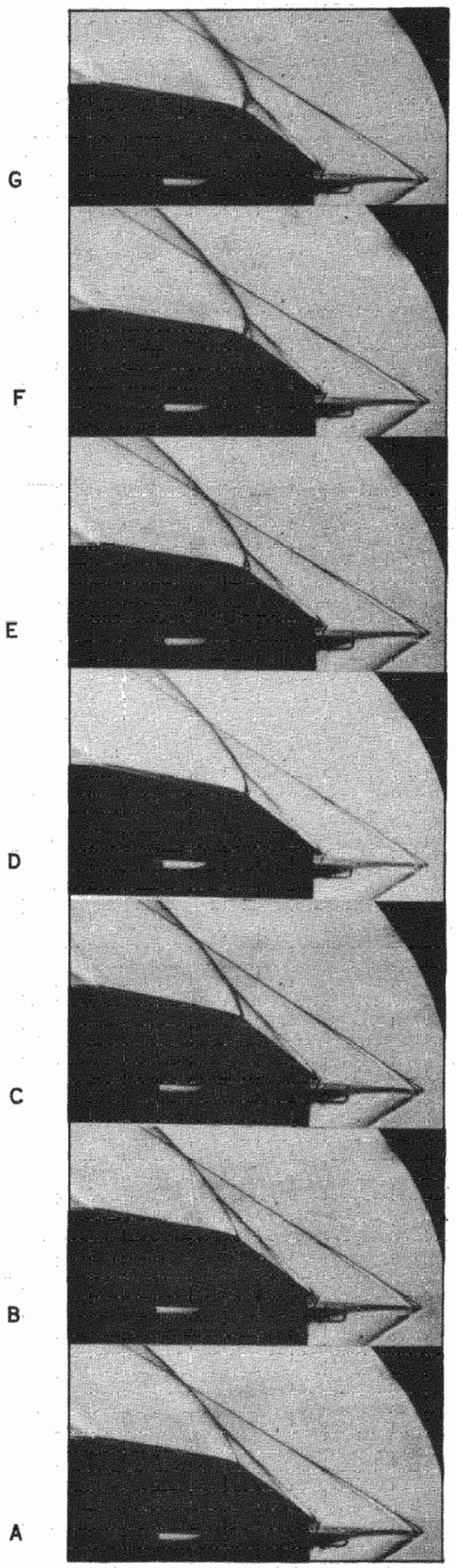

$\delta_3 = 11.3^0$

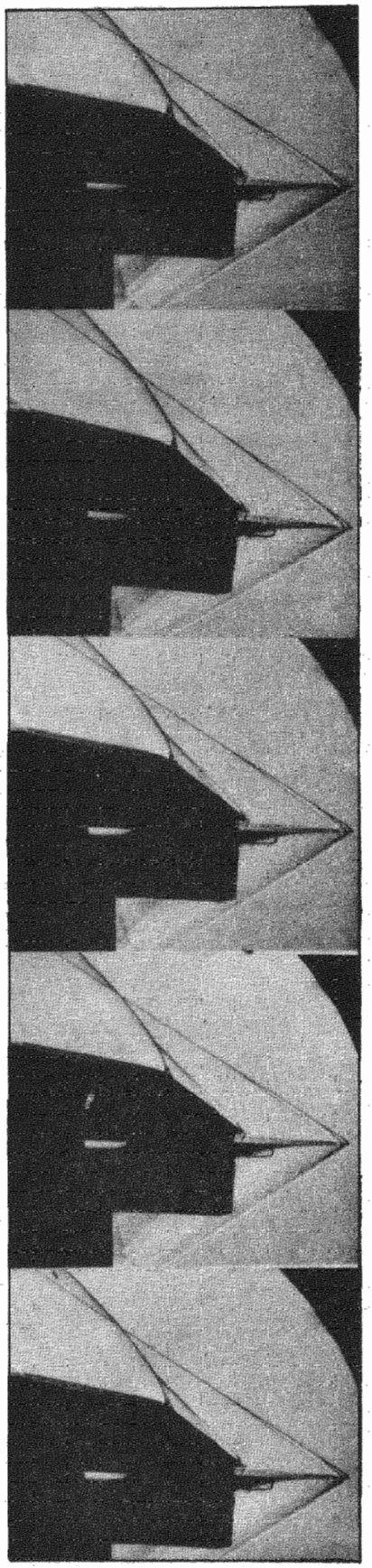

$\delta_3 = 13.25^0$

(c) SCHLIEREN PHOTOGRAPHS - M = 1.85

FIG. 19 (CONTINUED)

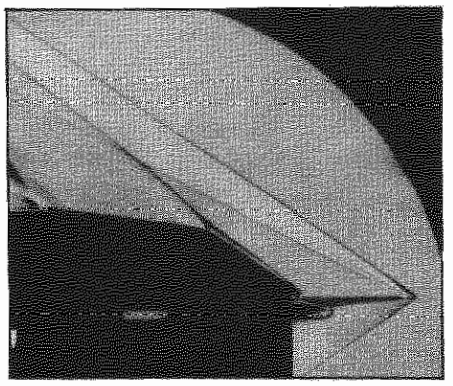

A

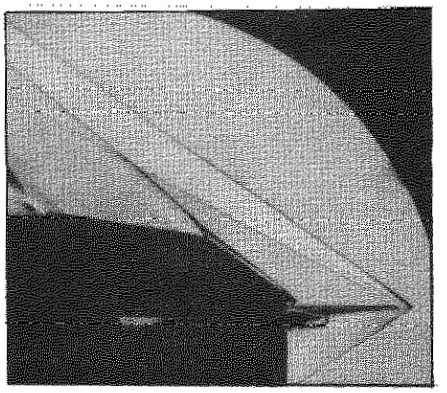

B

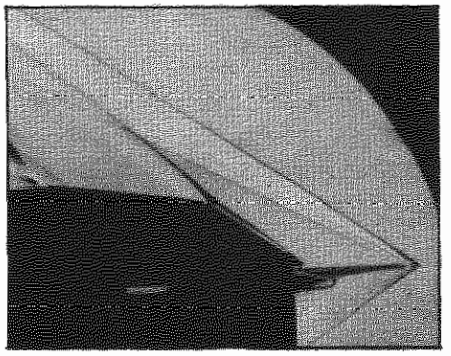

C

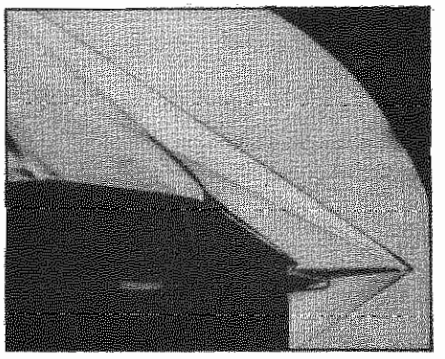

D

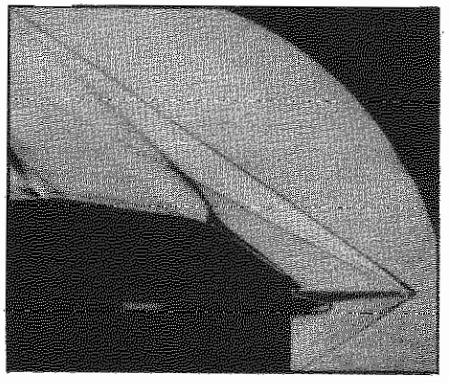

E

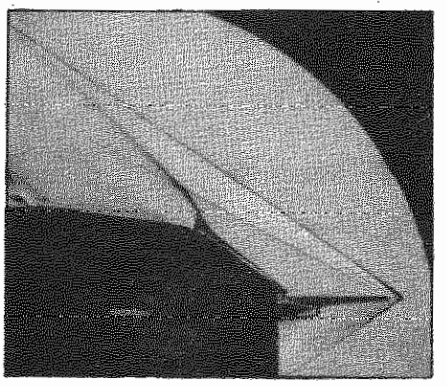

F

(f) SCHLIEREN PHOTOGRAPHS - M = 2.12 $\delta_3 = 15.25^{\circ}$

FIG.19 (CONTINUED)

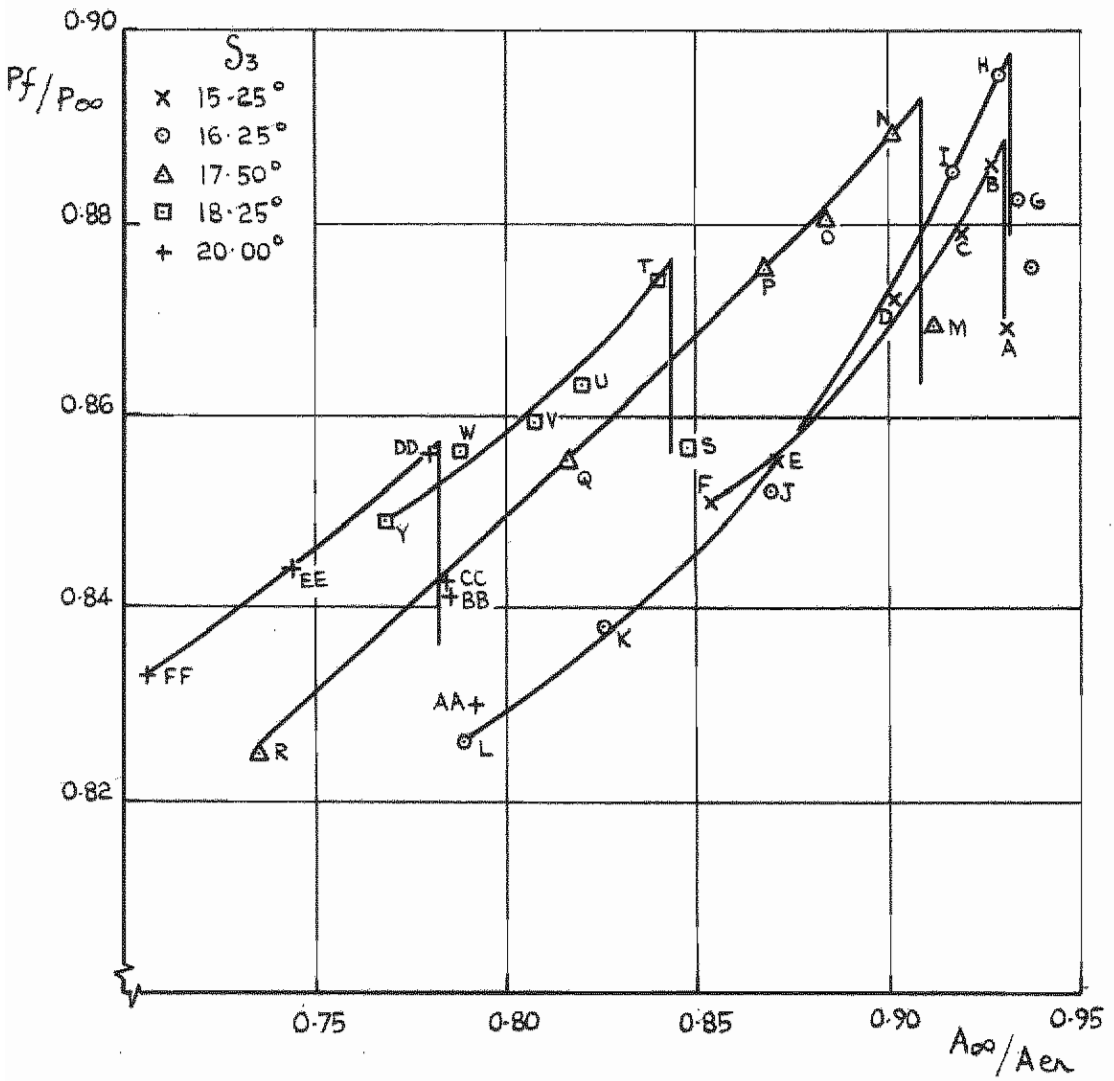

(e) M = 2·12

FIG. 19 (CONT.)

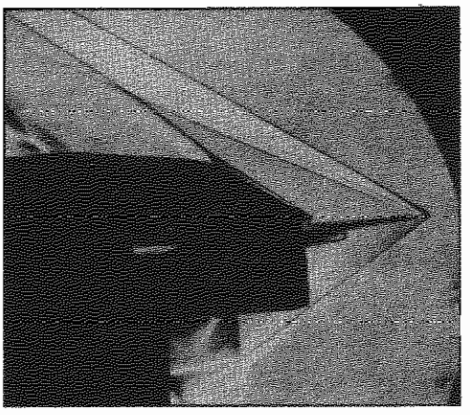

G

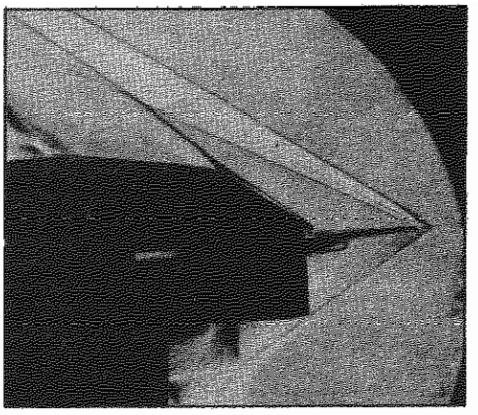

H

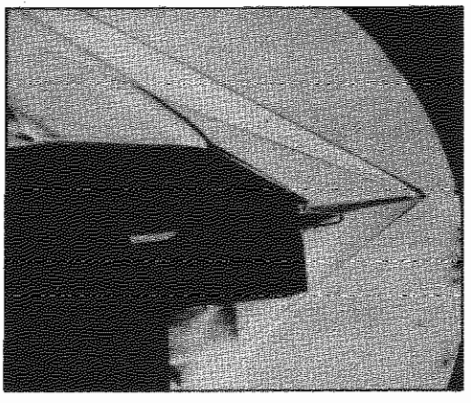

I

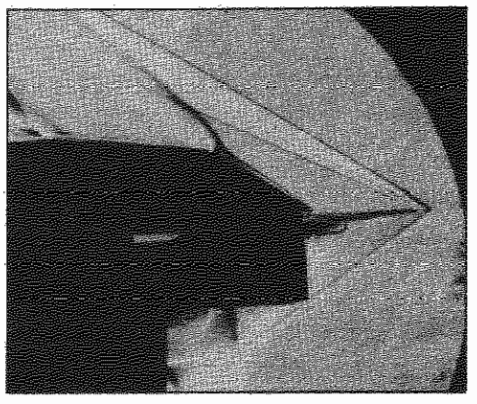

J

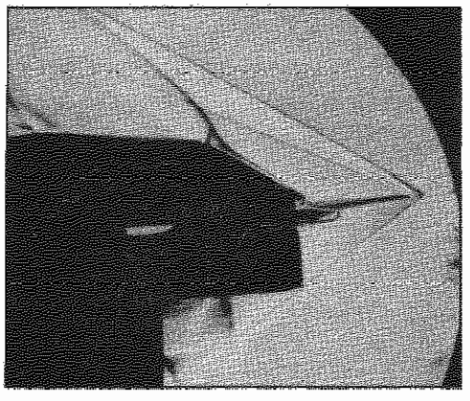

K

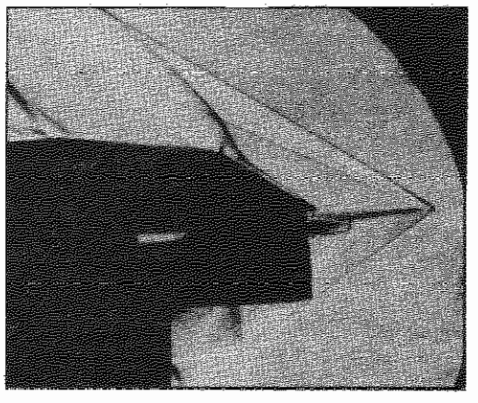

L

(g) $M = 2.12, \quad \delta_3 = 16.25^0$

FIG.19 (CONTINUED)

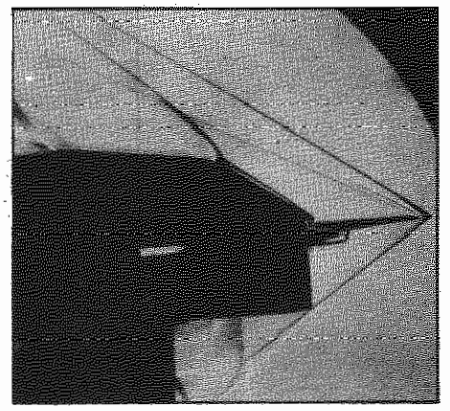

M

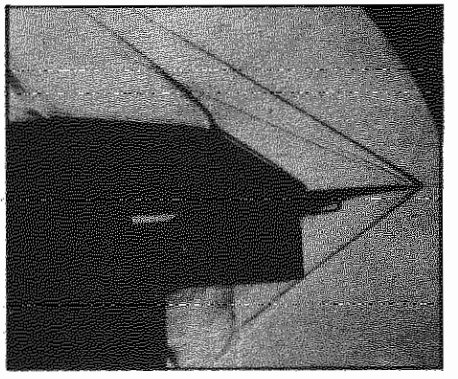

N

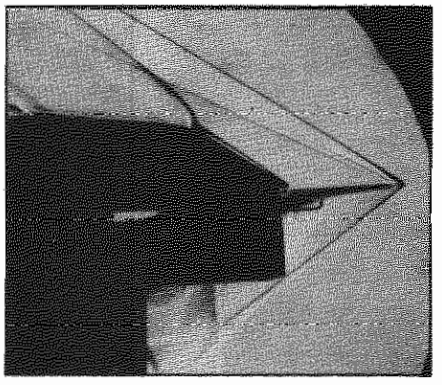

O

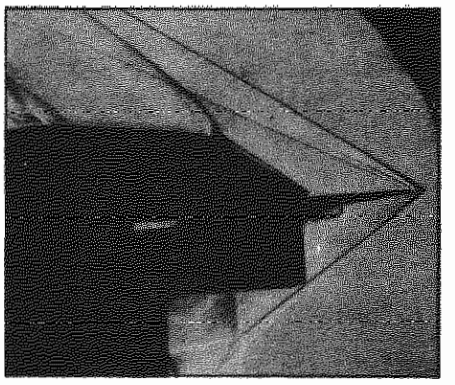

P

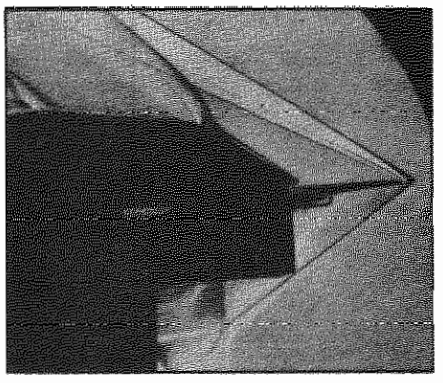

Q

R

(h) $M = 2.12, \quad \delta_3 = 17.50^0$

FIG. 19 (CONTINUED)

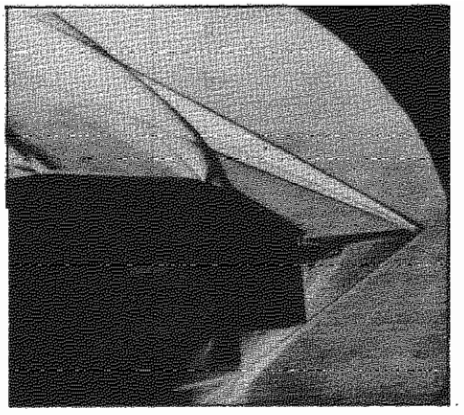

AA

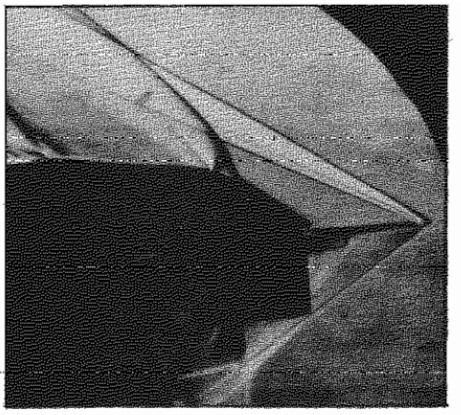

BB

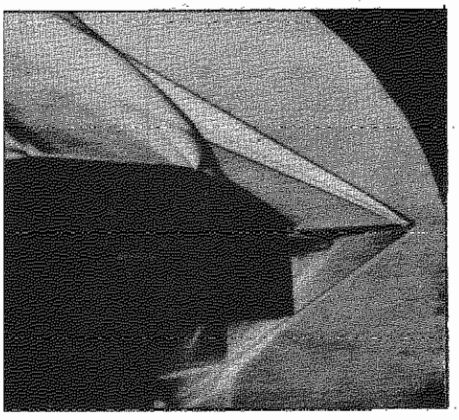

CC

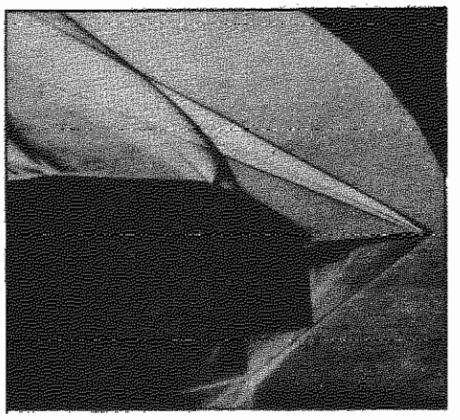

DD

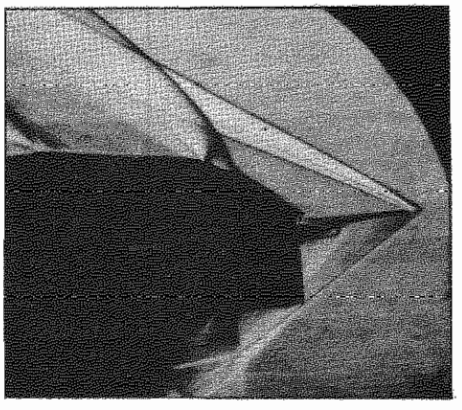

EE

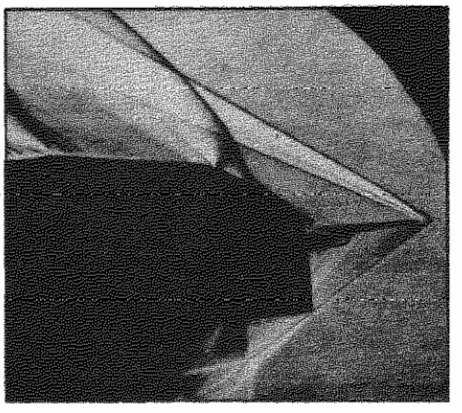

FF

(j) $M = 2.12, \quad \delta_3 = 20.0^{0}$

FIG.19 (CONTINUED)

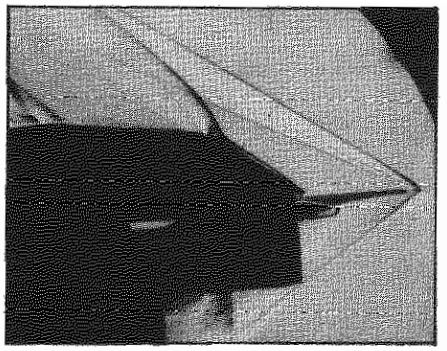

S

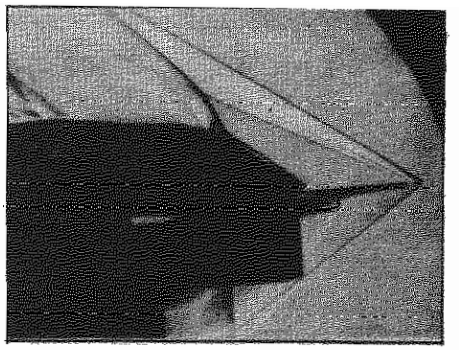

T

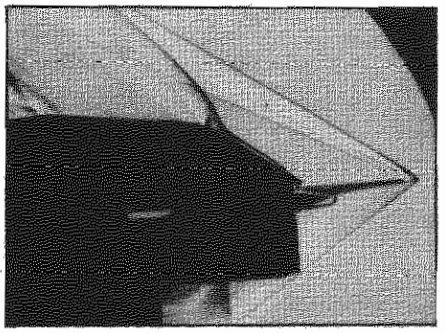

U

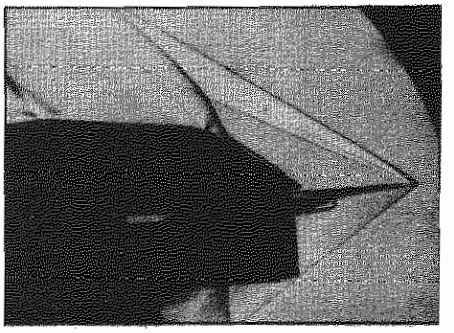

V

W

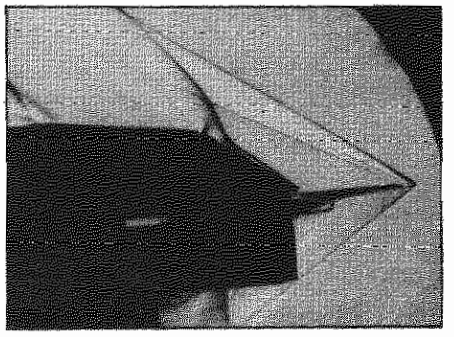

Y

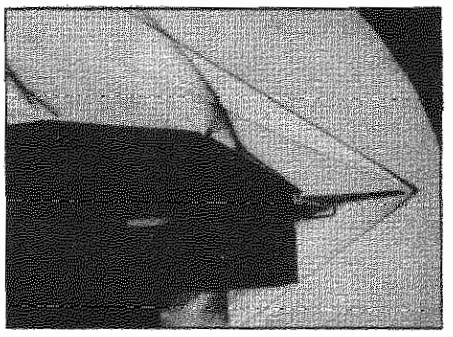

(i) $M = 2.12$, $\delta_3 = 18.25^0$

FIG.19 (CONTINUED)

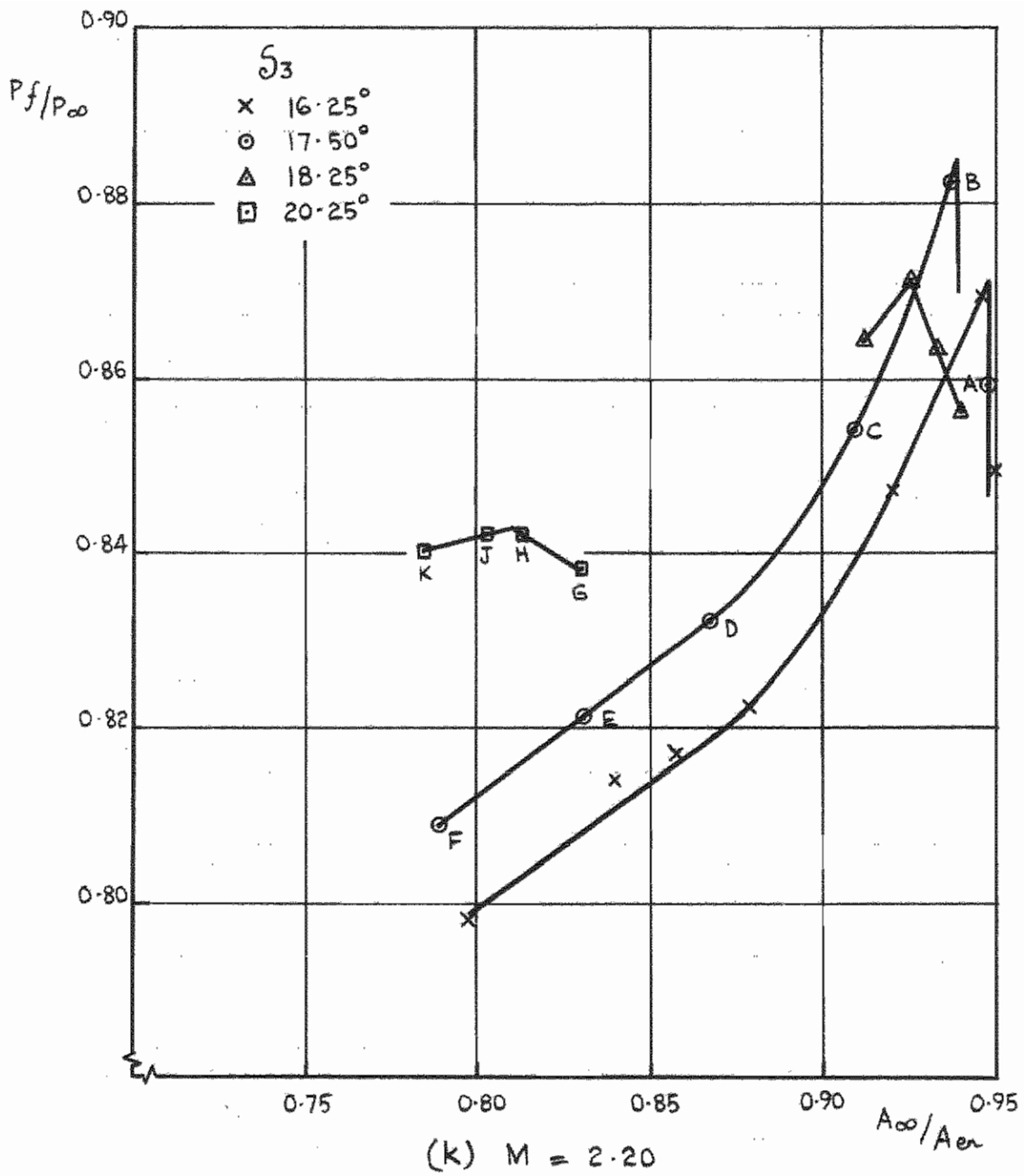

(k) M = 2·20

FIG. 19. (CONT)

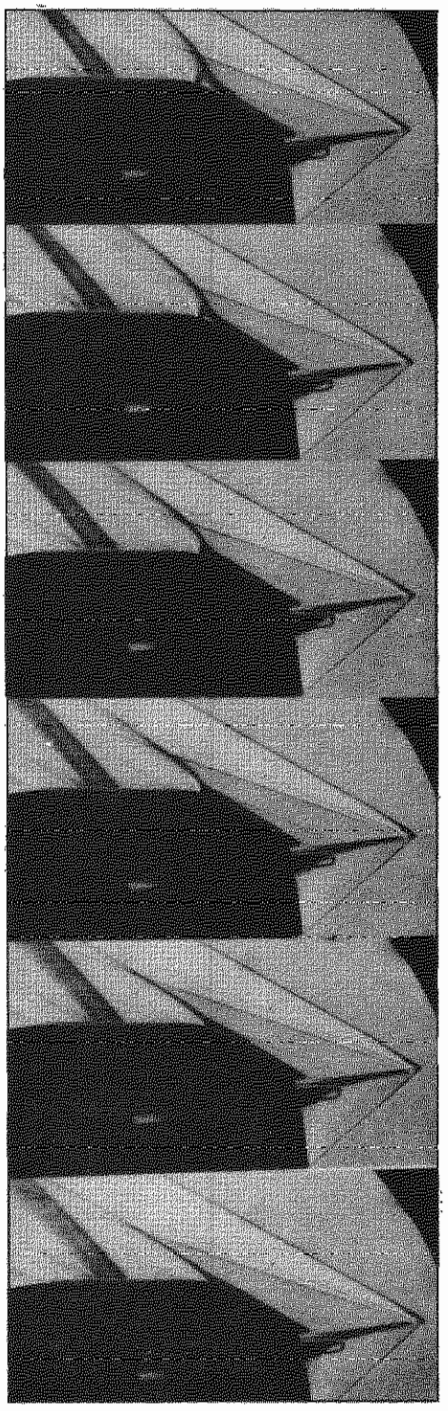

$\delta_3 = 17.50^0$

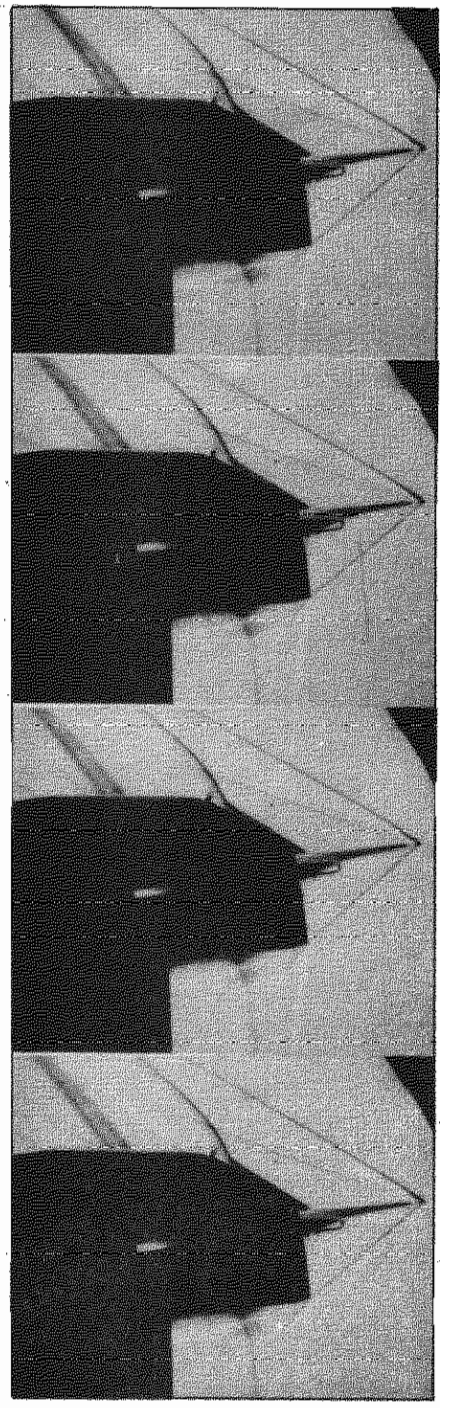

$\delta_3 = 20.25^0$

(1) SCHLIEREN PHOTOGRAPHS - M = 2.20

FIG.19 (CONCLUDED)

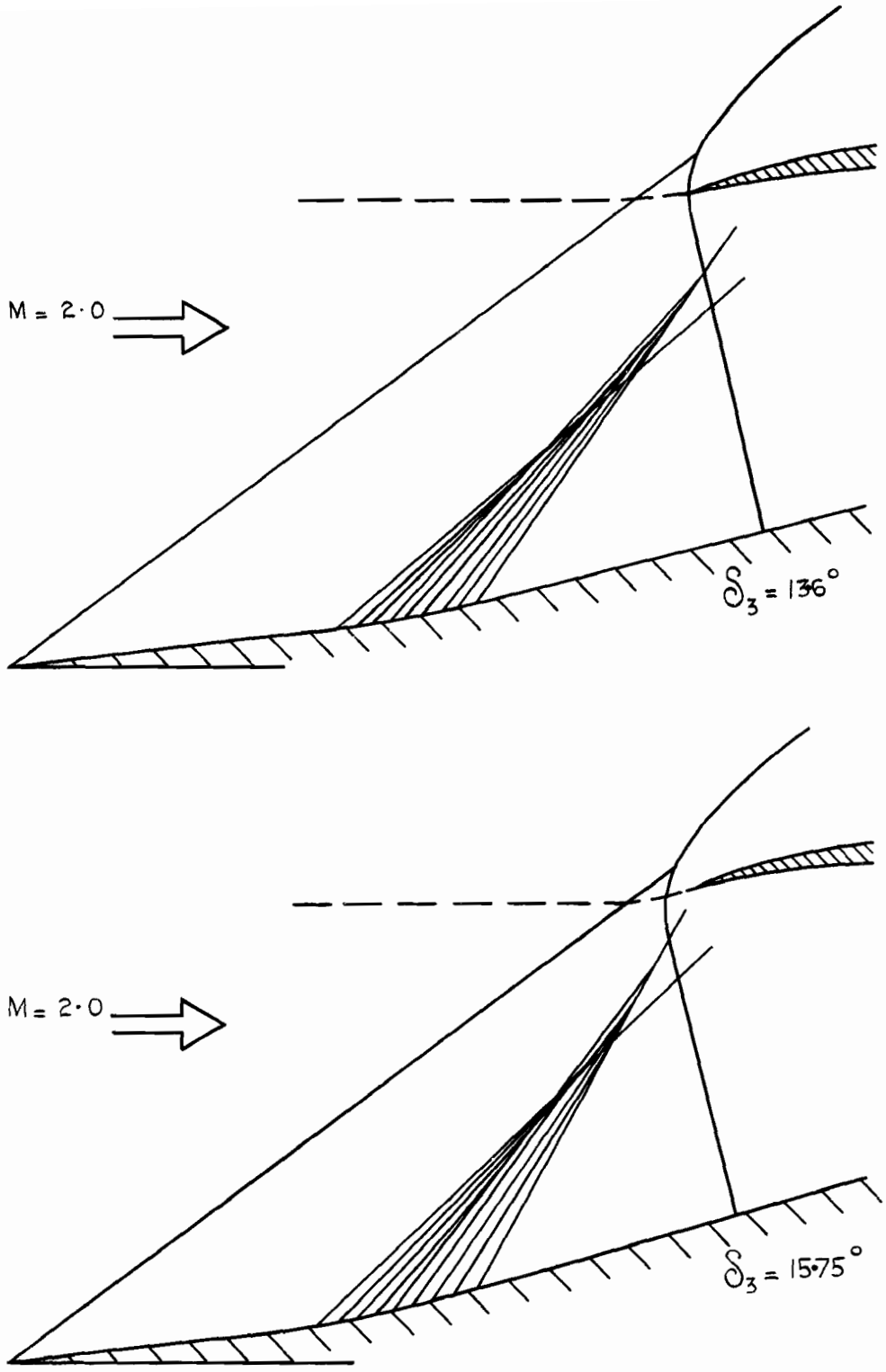

FIG. 20. SKETCHES SHOWING SHOCK SYSTEMS AT M = 2·0.
(ISENTROPIC COMPRESSION DRAWN AS DISCREET 1° SHOCKS)

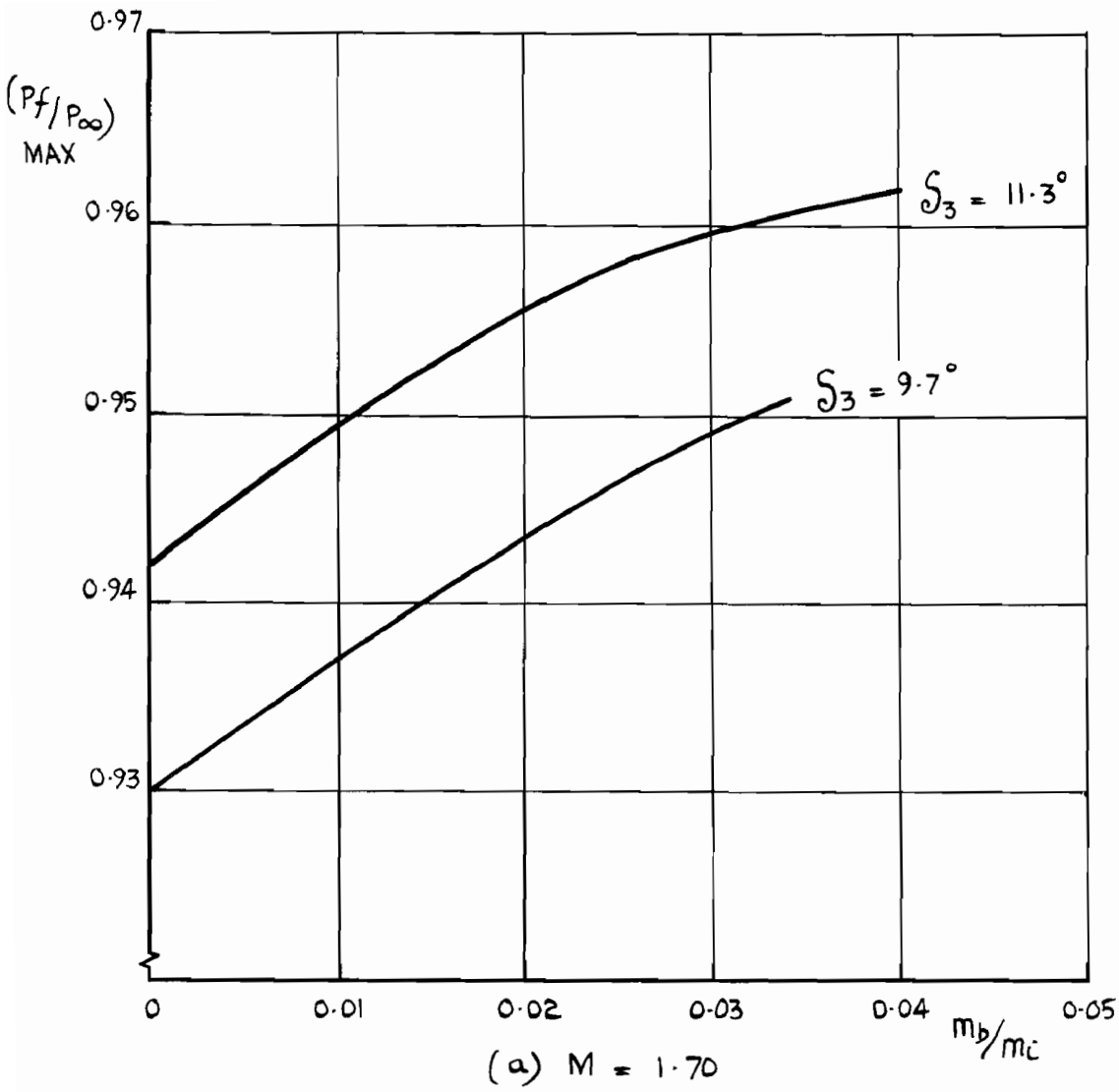

FIG. 21. MAXIMUM PRESSURE RECOVERY – VARIATION WITH THROAT BLEED FLOW, δ_3 & M – – SPLITTER I.

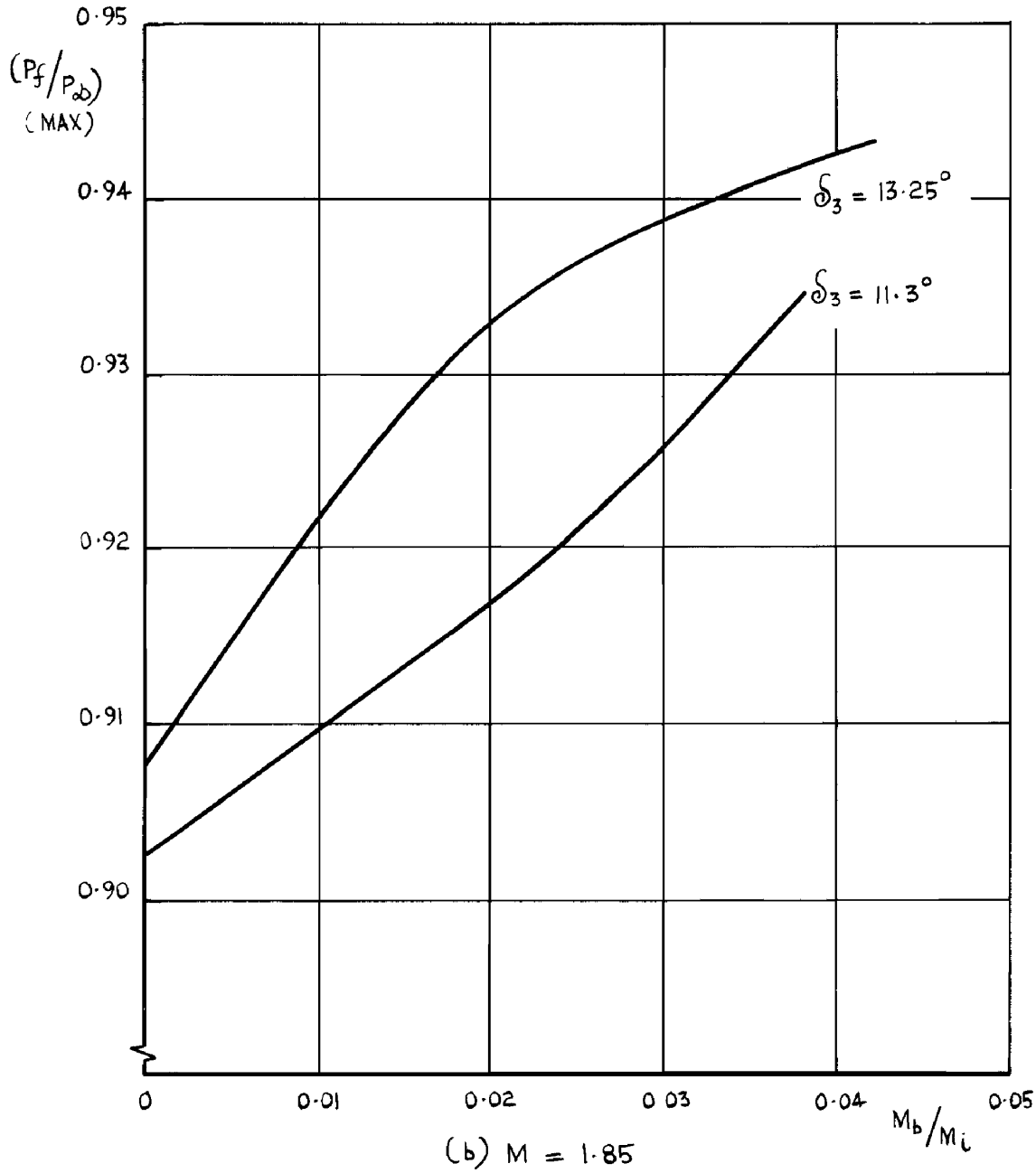
0·95
(P_f/P_{ab})
(MAX)
0·94
0·93
0·92
0·91
0·90
$\delta_3 = 13{\cdot}25°$
$\delta_3 = 11{\cdot}3°$
0
0·01
0·02
0 03
0·04
0·05
M_b/M_i
(b) M = 1·85

FIG. 21 (CONT.)

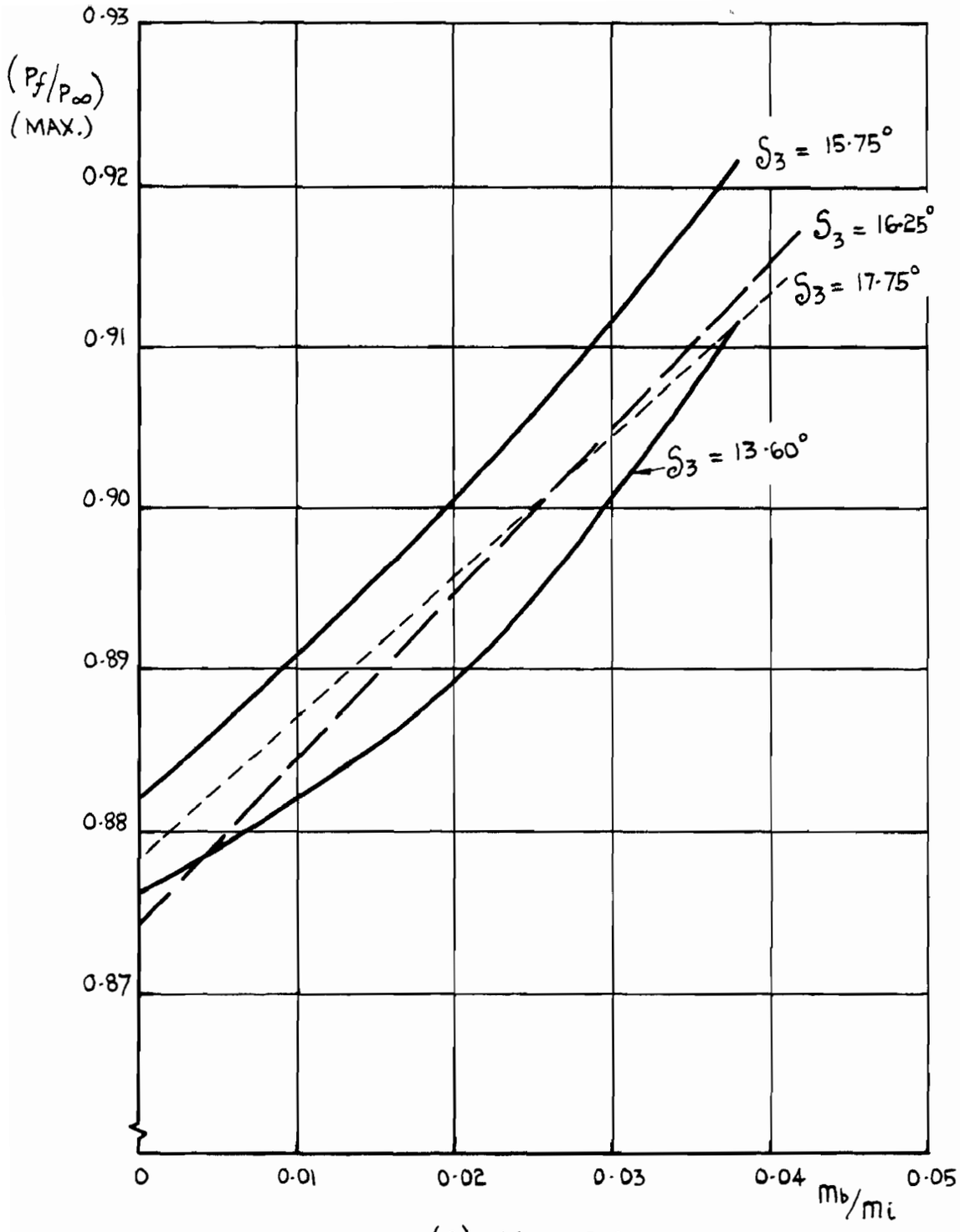

(c) M = 2·00.

FIG. 21. (CONT.)

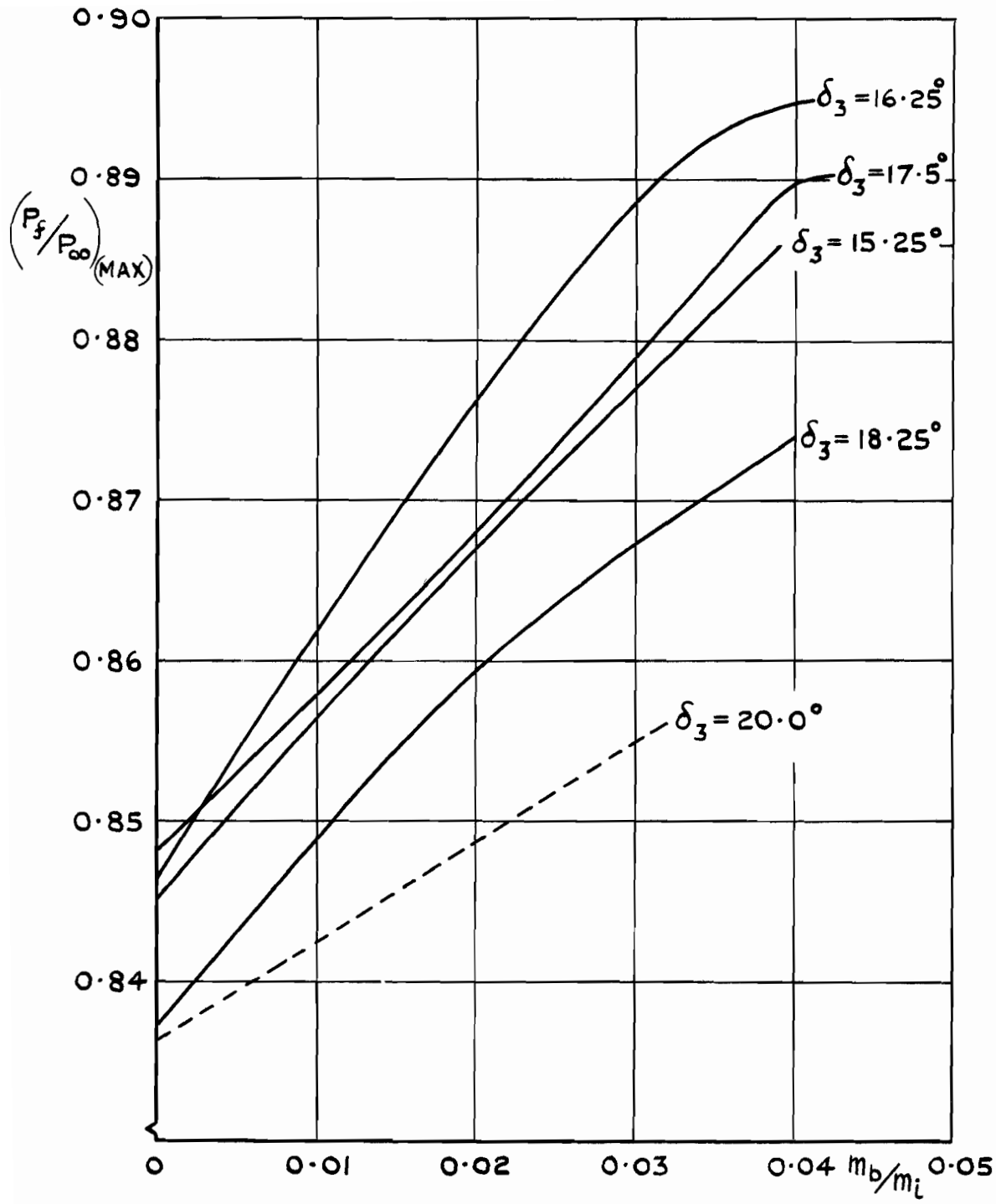

(d) M = 2·12

FIG. 21 (CONT.)

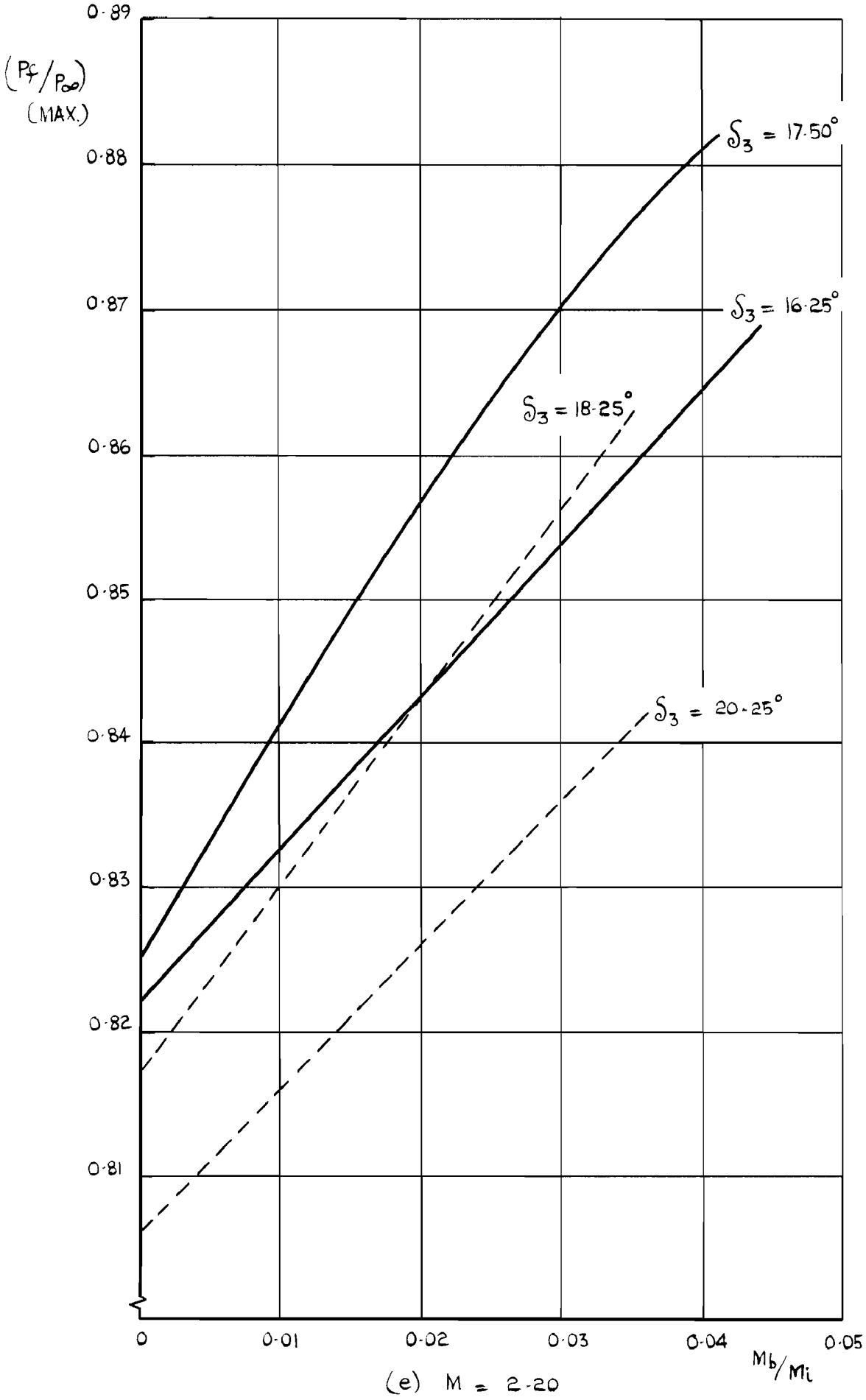

(e) M = 2·20

FIG. 21 (CONCLUDED.)

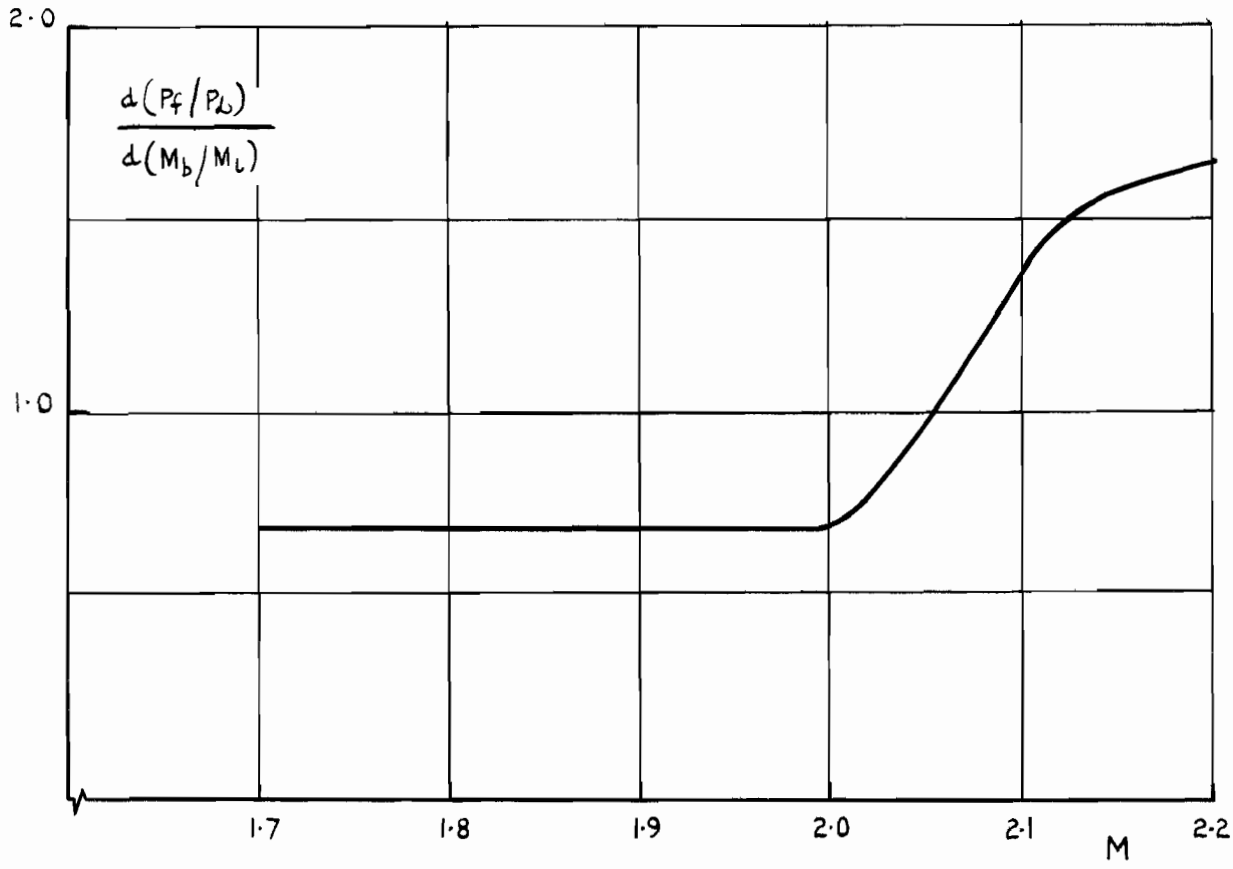

FIG. 22 VARIATION OF EXCHANGE RATE WITH MACH NUMBER FOR CRITICAL RAMP ANGLE SETTINGS

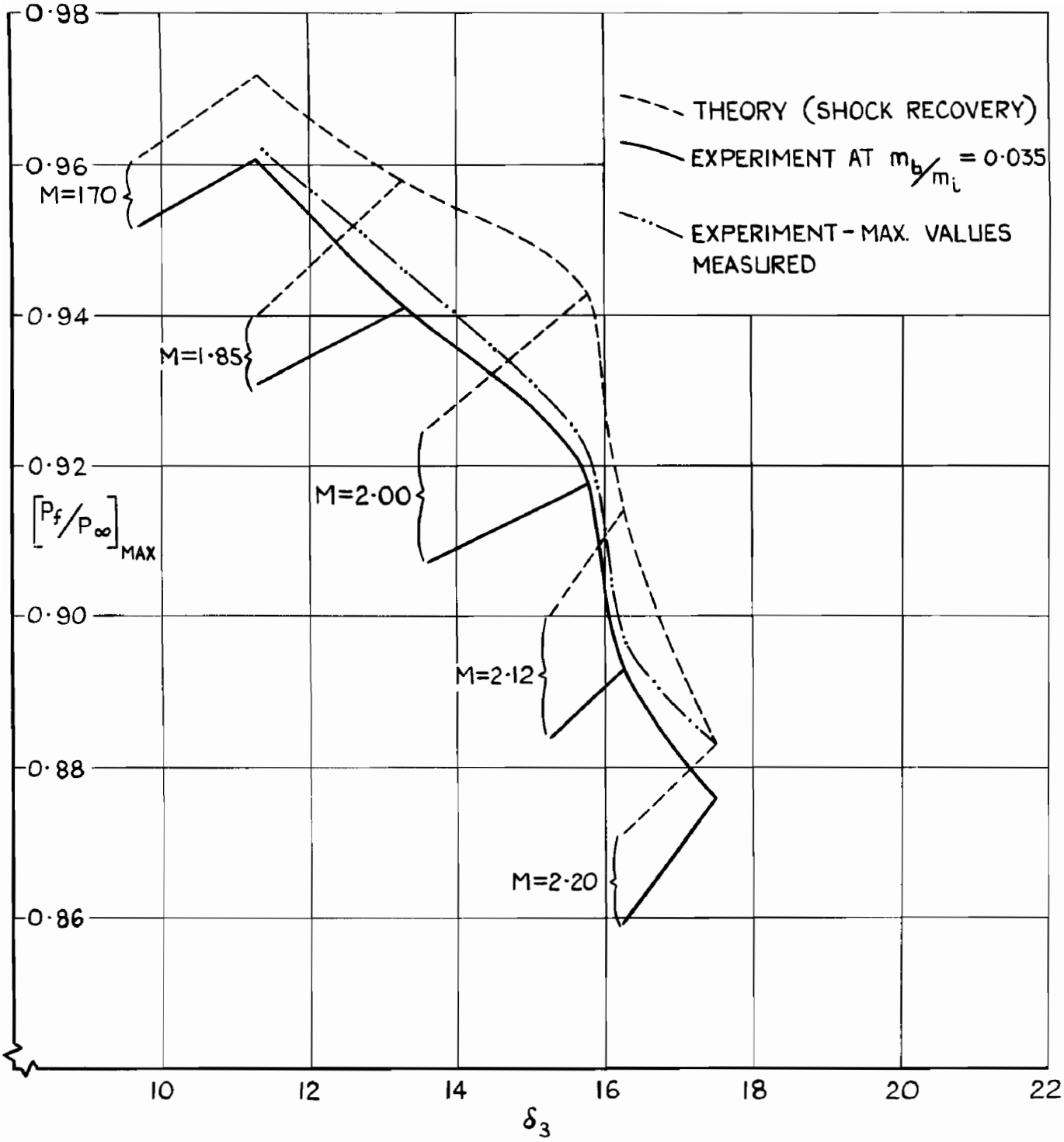

FIG. 23 SUMMARY OF PRESSURE RECOVERY—VARIATION WITH M & δ_3

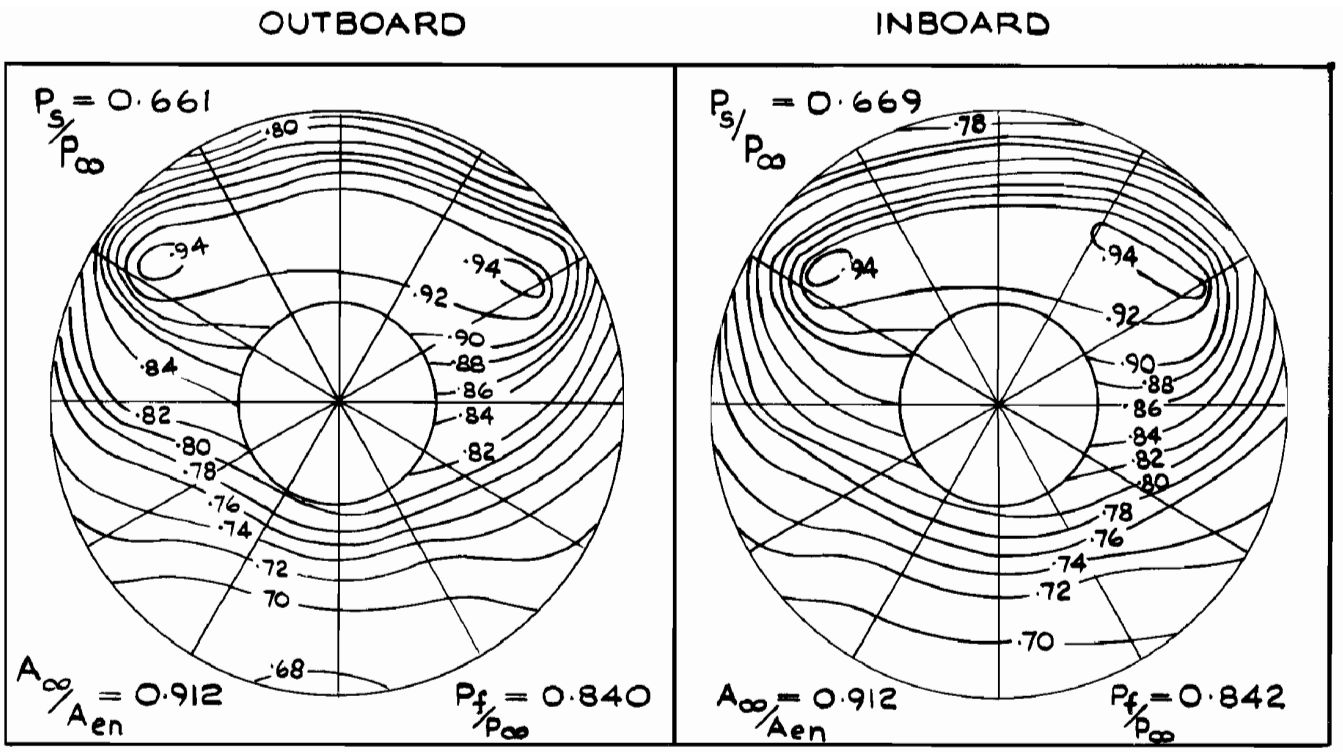

FIG.24(a) NO BLEED

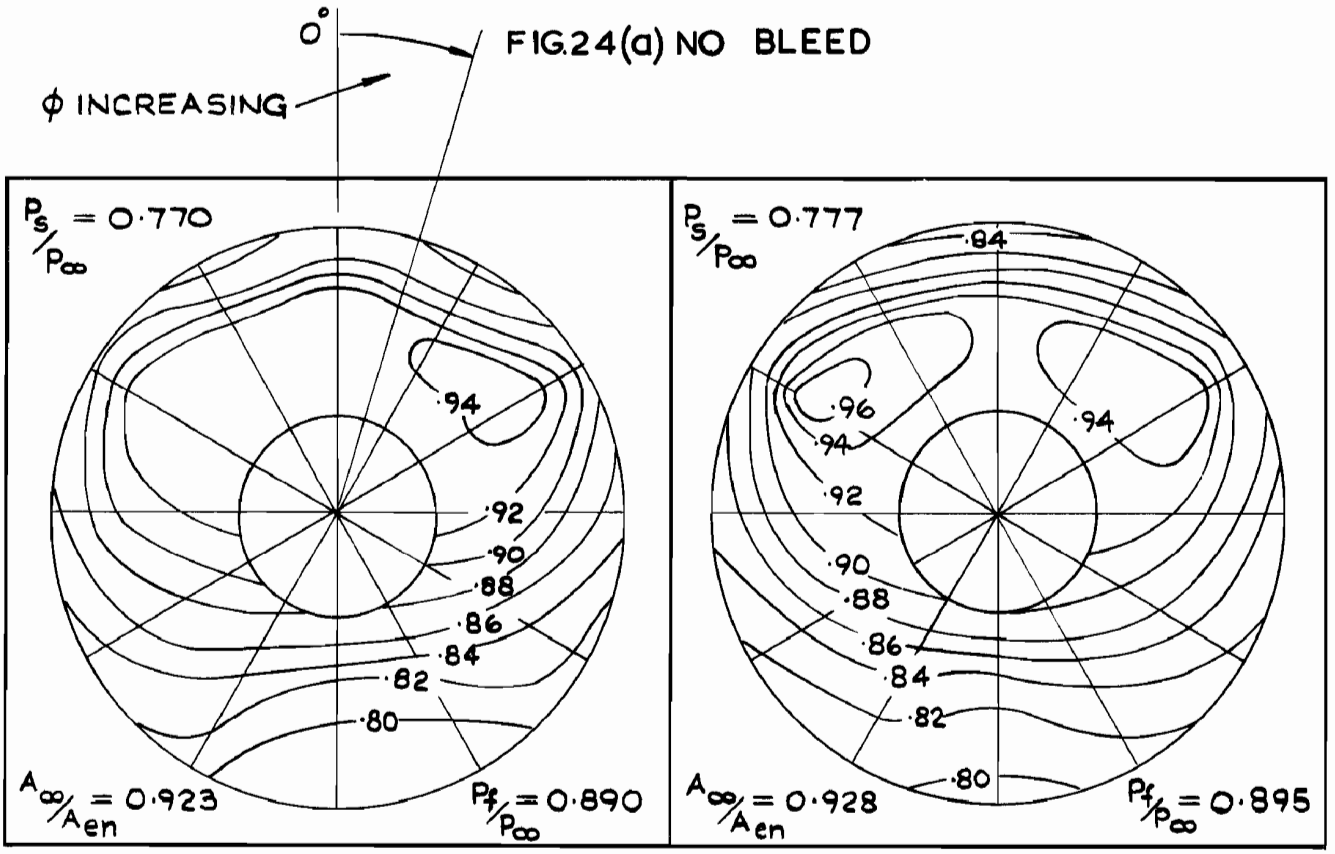

FIG.24(b) $m_b/m_i = 0.042$

FIG. 24 DISTRIBUTIONS OF PRESSURE RECOVERY

$M = 2.12$, $\delta_3 = 16.25°$, SPLITTER I

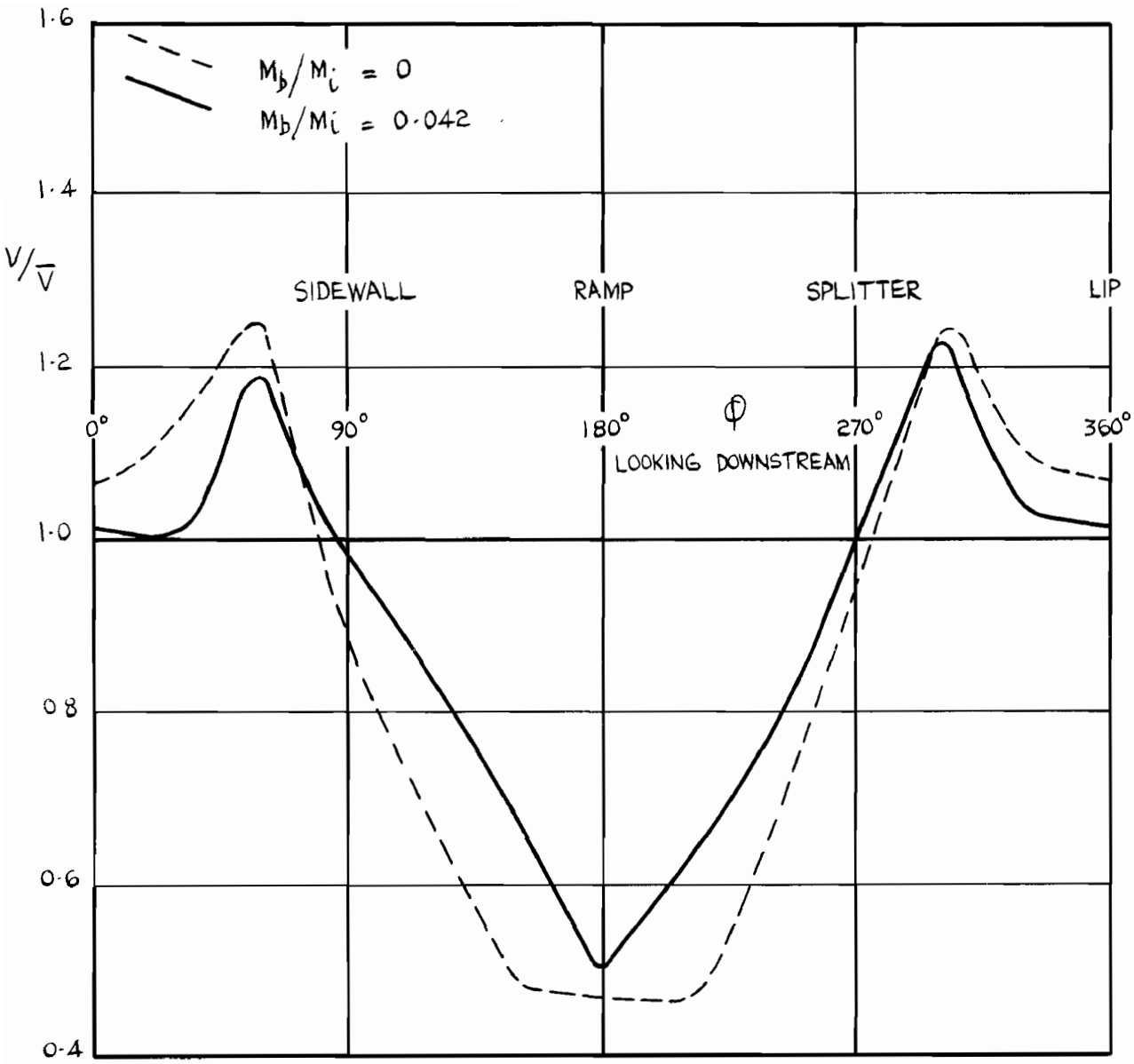

FIG. 25. CIRCUMFERENTIAL DISTRIBUTION OF $V/\bar{V}$ AT $r/R = 0{\cdot}798$, $M = 2{\cdot}12$, $\delta_3 = 16{\cdot}25^\circ$.

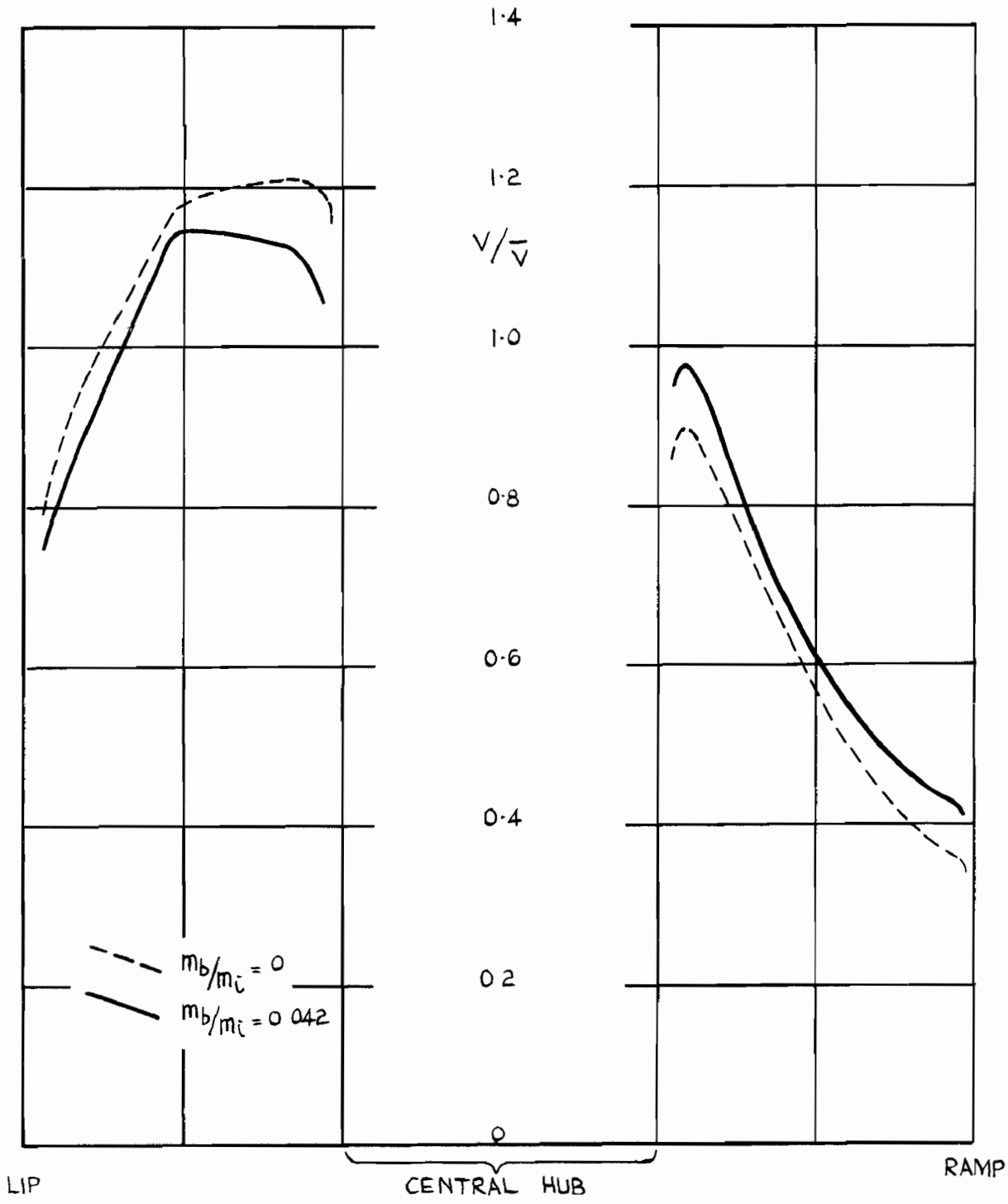

FIG. 26. DISTRIBUTION OF $V/\bar{V}$ ACROSS A VERTICAL DIAMETER, $M = 2 \cdot 12$, $\delta_3 = 16 \cdot 25^\circ$.

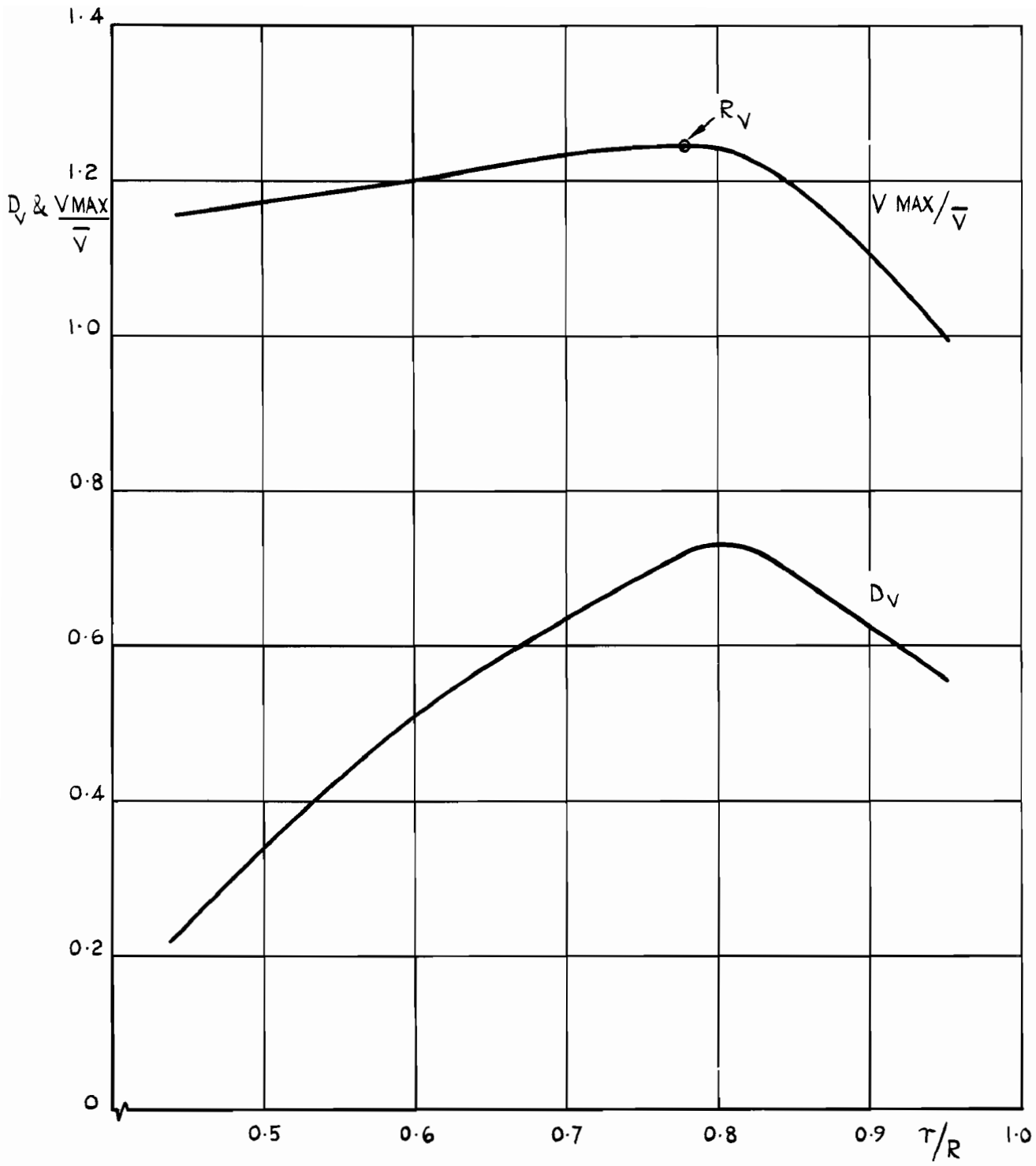

FIG. 27. DISTORTION PARAMETERS D_V & $V_{MAX}/\bar{V}$ – VARIATION WITH r/R, $M = 2 \cdot 12$, $\delta_3 = 16 \cdot 25$, $m_b/m_i = 0 \cdot 042$, SPLITTER I

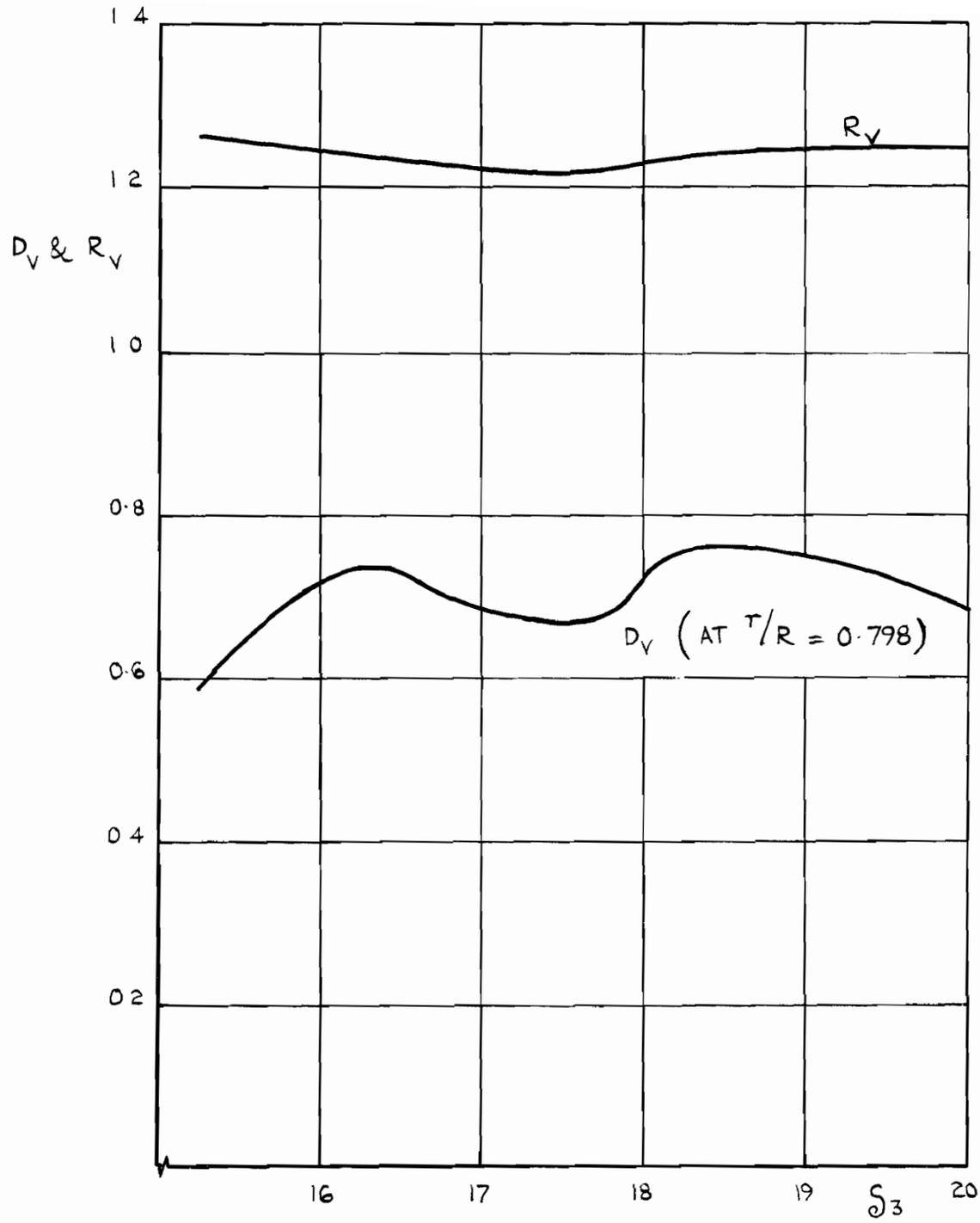

FIG. 28. DISTORTION PARAMETERS D_V & R_V – VARIATION WITH δ_3, M = 2·12, $m_b/m_i \simeq$ 0·04, SPLITTER I

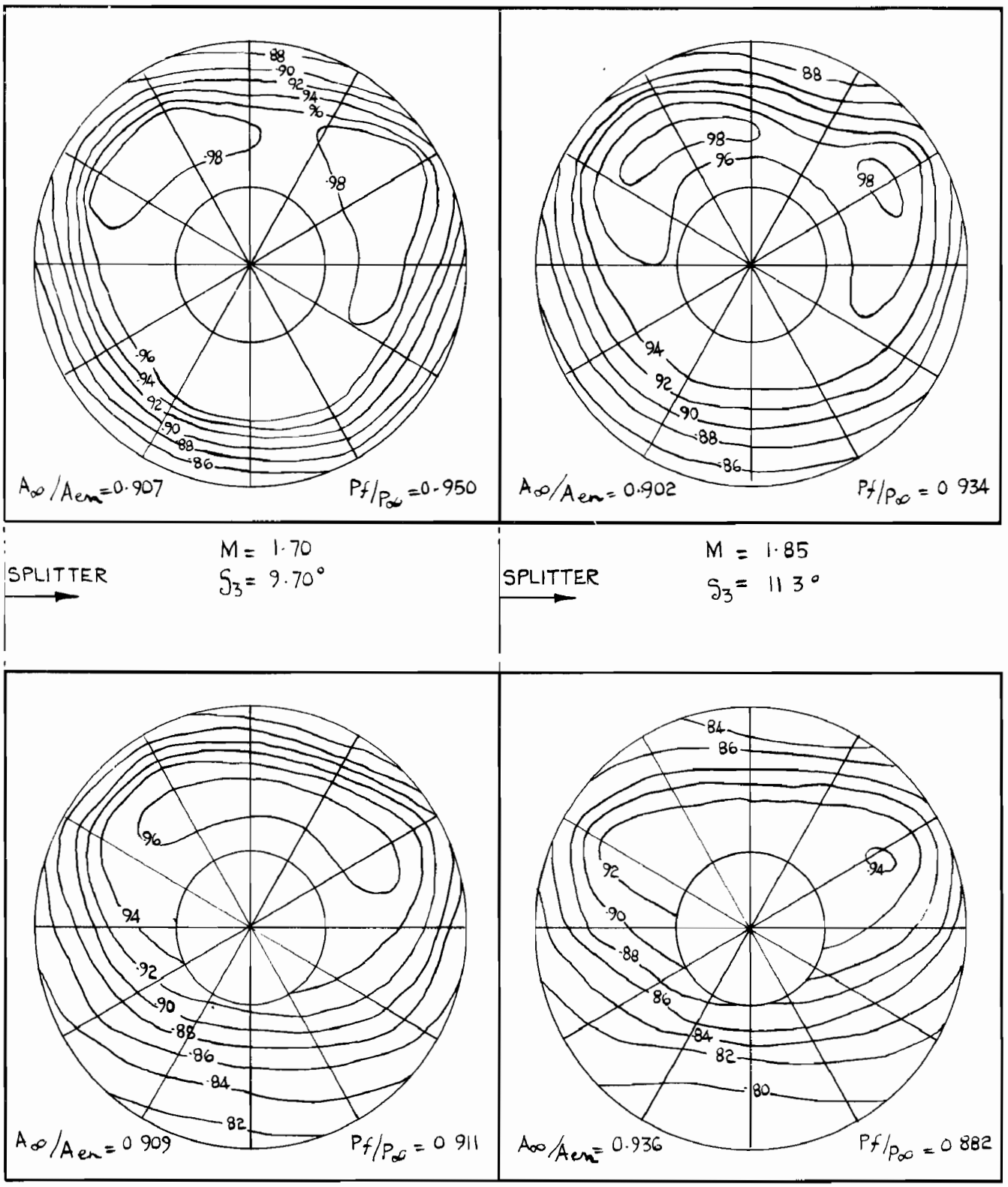

FIG. 29. PRESSURE RECOVERY DISTRIBUTIONS-INBOARD DUCT EACH WITH $m_b/m_i \simeq 0 \cdot 04$ AT THE POINT OF MAXIMUM P_f/P_∞.

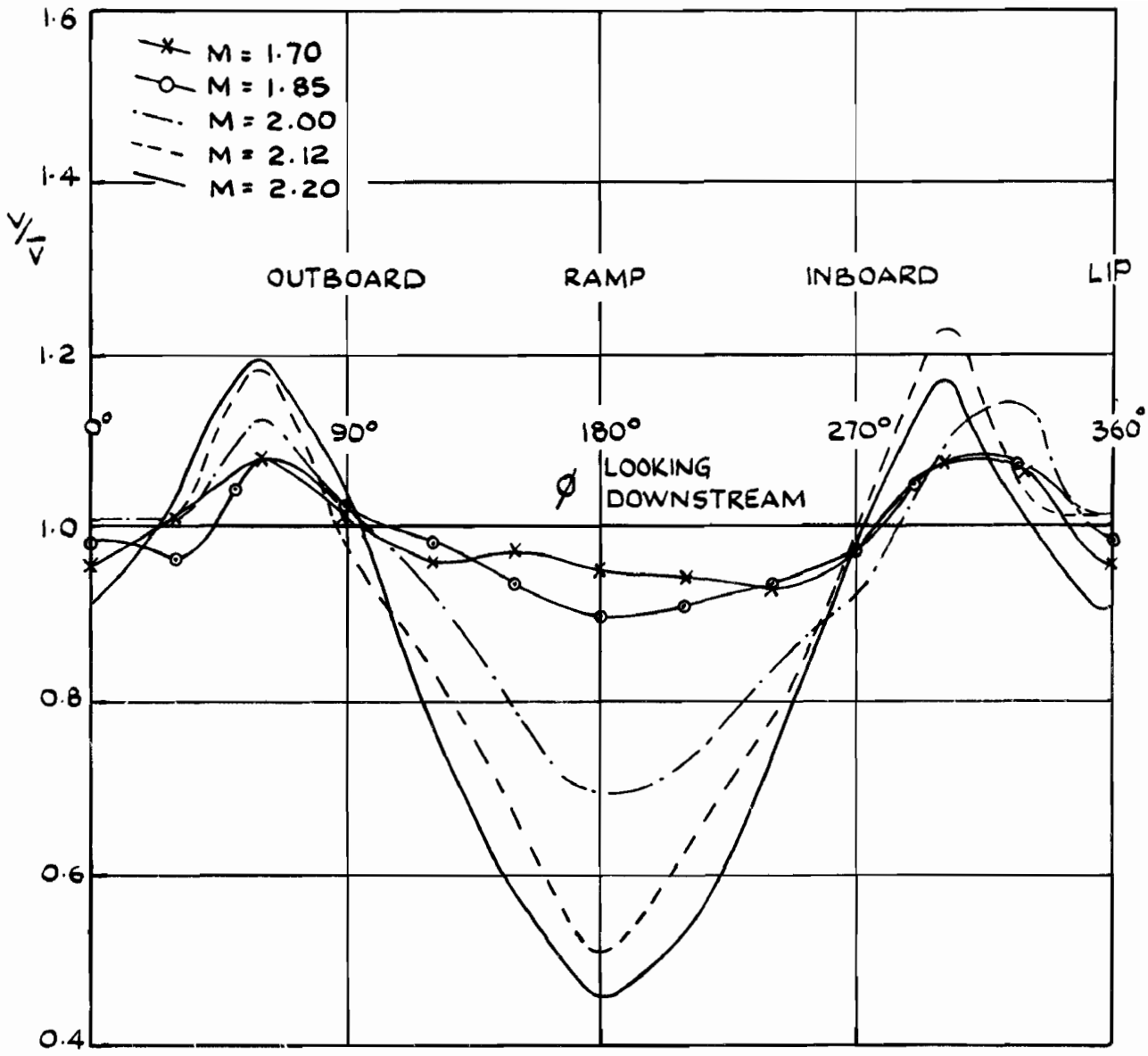

FIG. 30 CIRCUMFERENTIAL DISTRIBUTION OF $V/\bar{V}$ AT r/R = 0·798 – VARIATION WITH MACH. NUMBER. $m_b/m_i \simeq 0{\cdot}04$, SPLITTER I

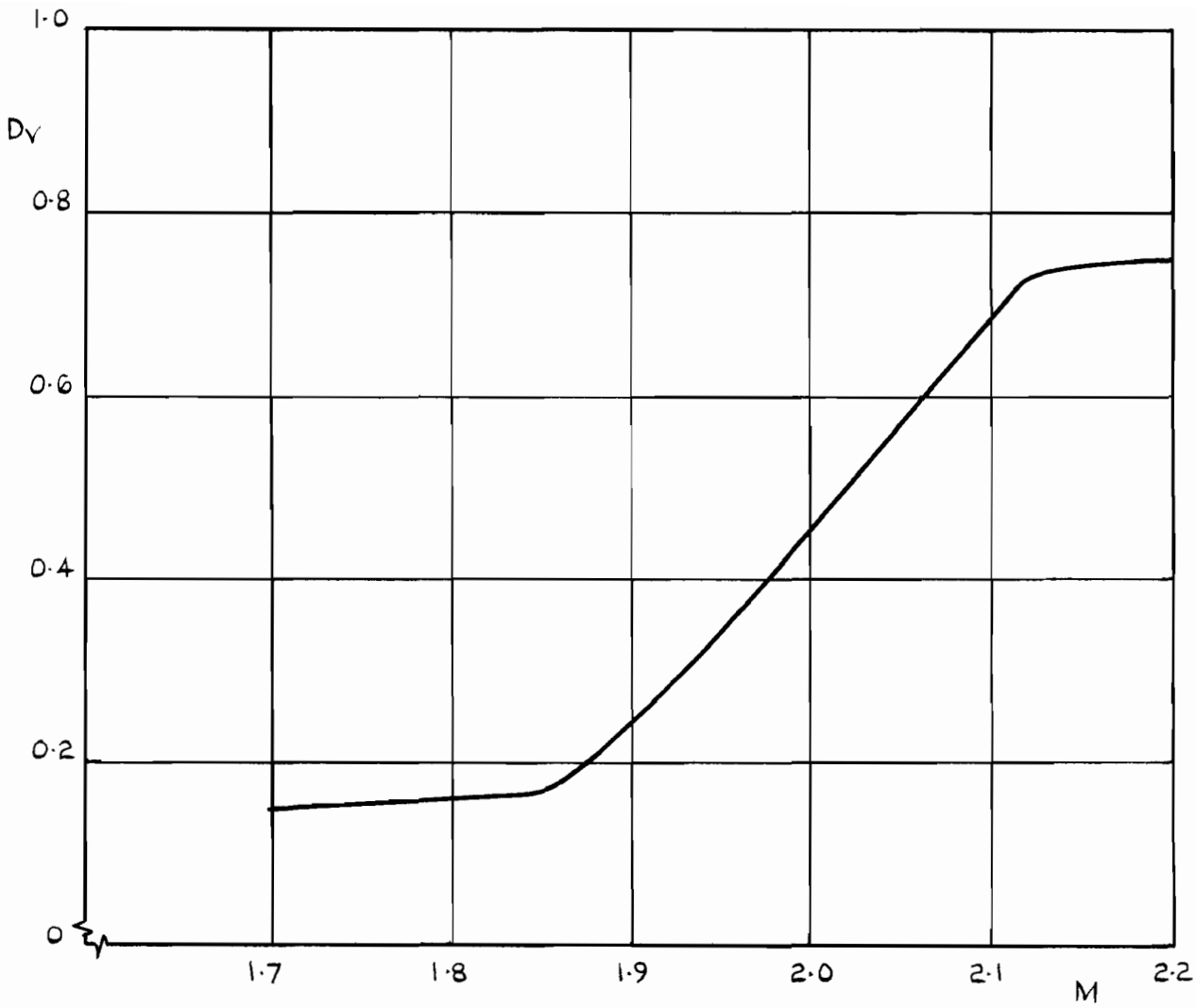

FIG. 31 DISTORTION PARAMETER Dv - VARIATION WITH MACH NUMBER $r/R = 0{\cdot}798$, $m_b/m_i \simeq 0{\cdot}04$, SPLITTER I.

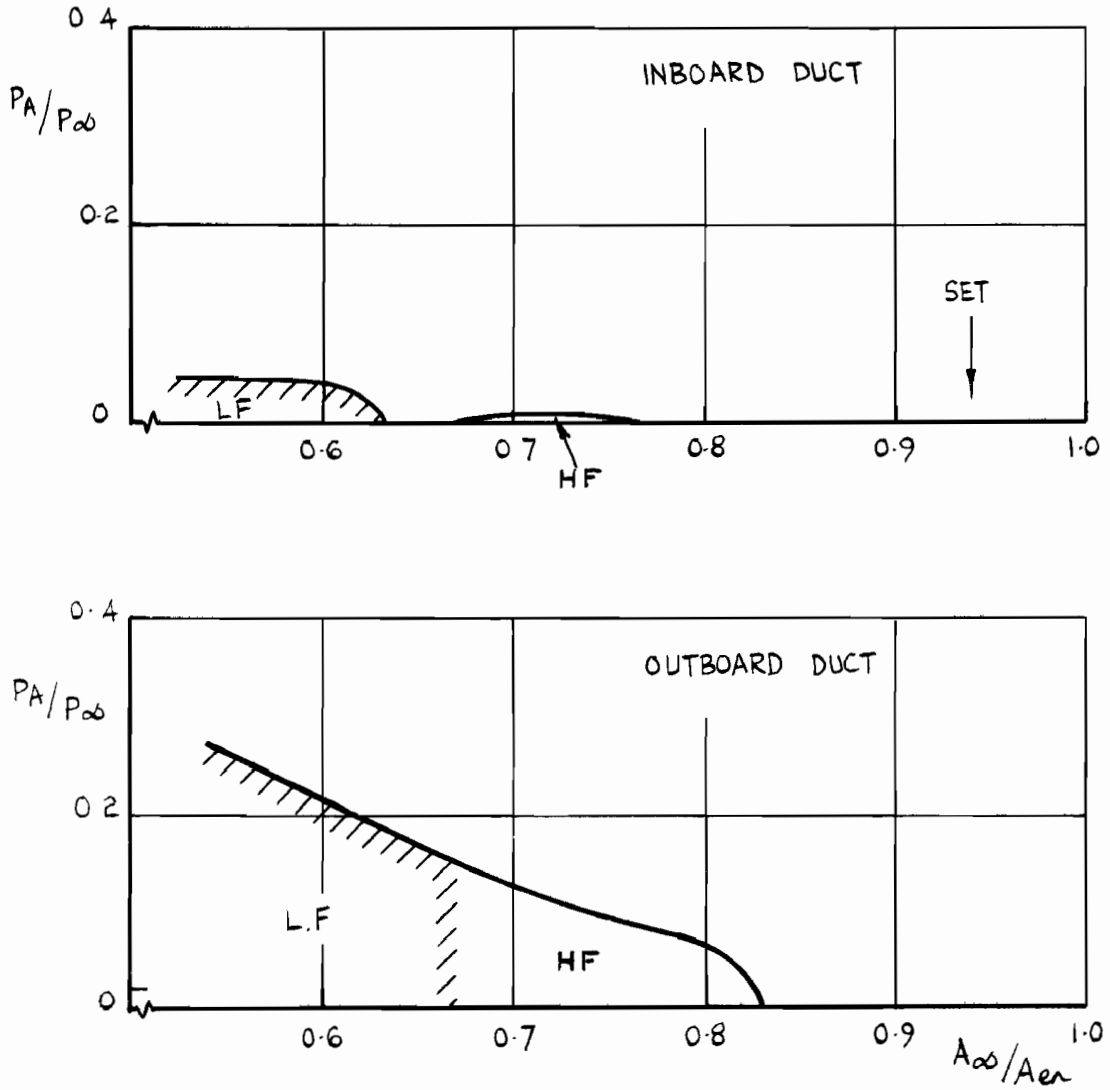

(a) M = 1 70, $\delta_3 = 9 \cdot 7°$

NOTE:- MASS FLOW THROUGH OUTBOARD DUCT VARIES. THROTTLE OF INBOARD SET TO PASS FULL FLOW. P_A/P_∞ VALUES FOR BOTH OUTBOARD AND INBOARD DUCTS ARE PLOTTED AGAINST MASS FLOW RATIO OF OUTBOARD DUCT

FIG. 32. FLUCTUATING PRESSURE AMPLITUDES. $m_b/m_i \simeq 0 \cdot 04$, SPLITTER I.

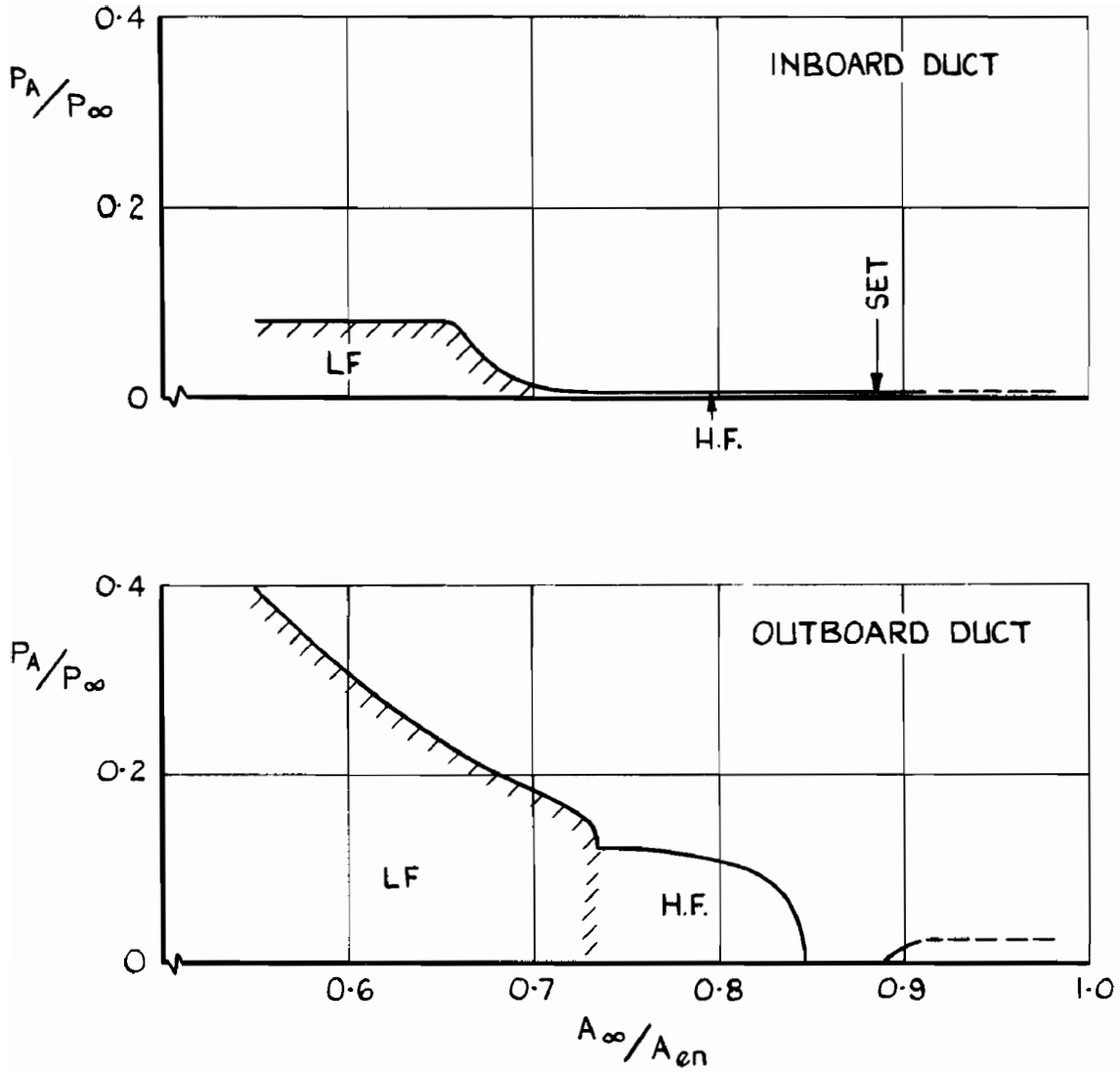

(b) $M=1{\cdot}85$, $\delta_3 = 11{\cdot}3°$

FIG. 32 (CONT)

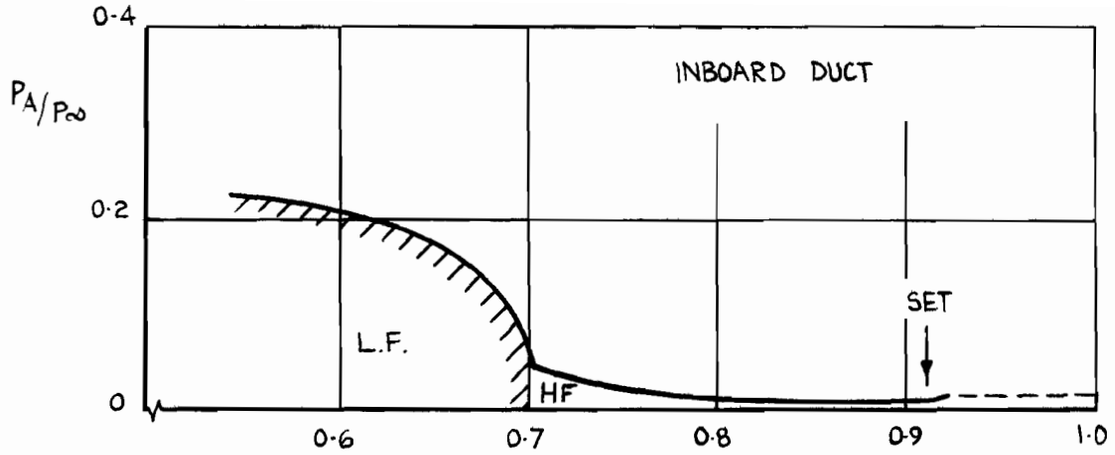

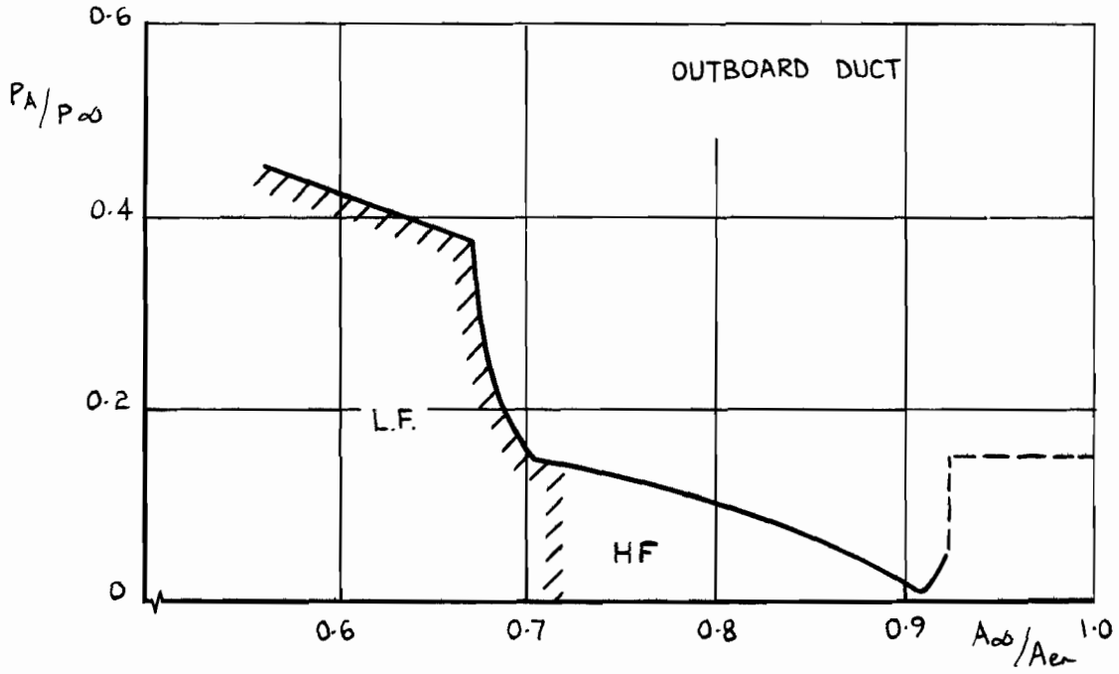

(c.) M = 2·00, δ_3 = 13·6°

FIG. 32 (CONT.)

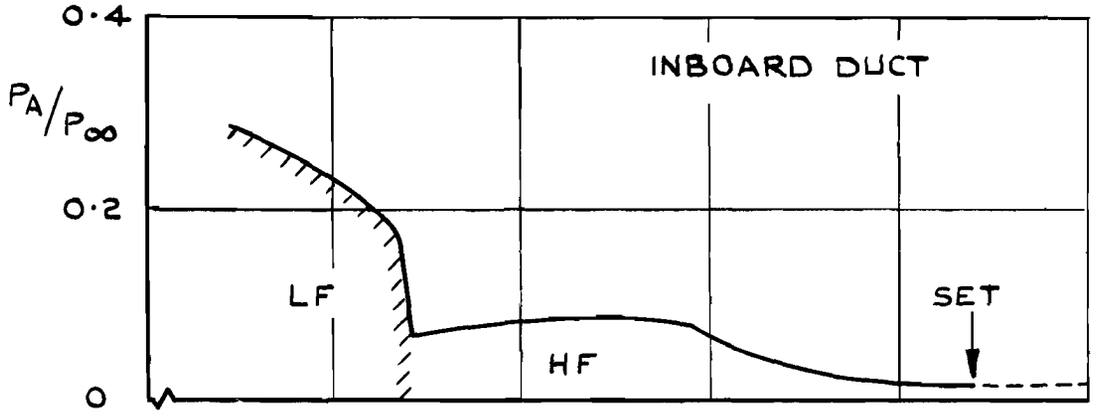

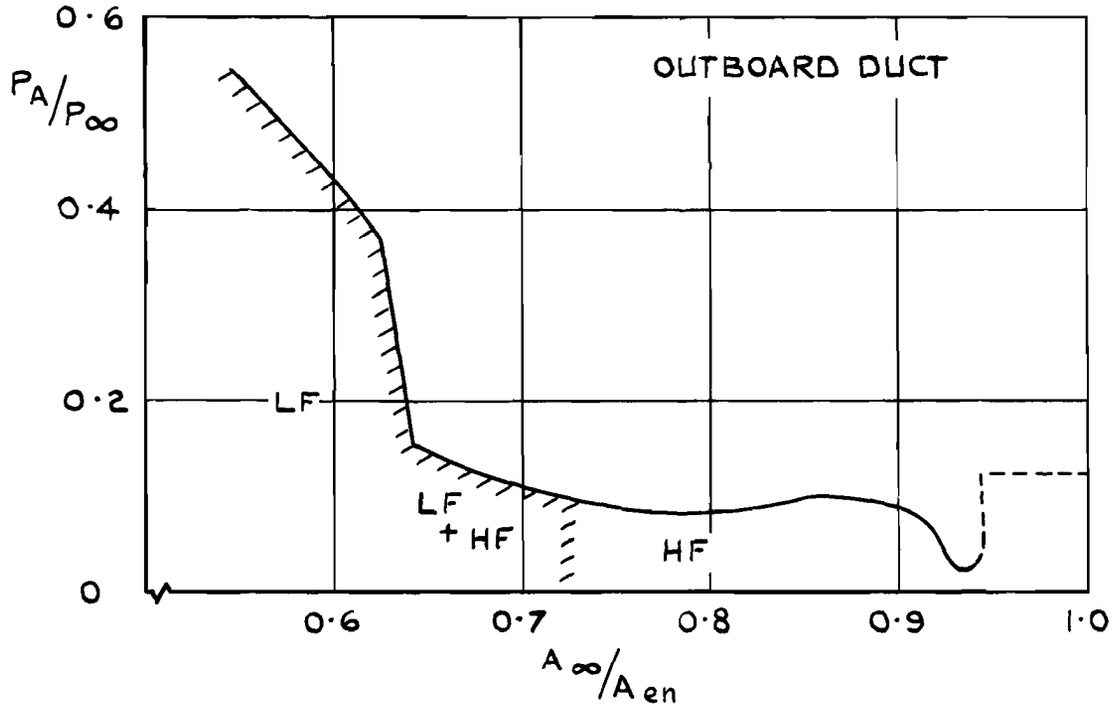

FIG. 32(d) $M = 2{\cdot}12$, $\delta_3 = 16{\cdot}25°$

FIG. 32 (CONT.)

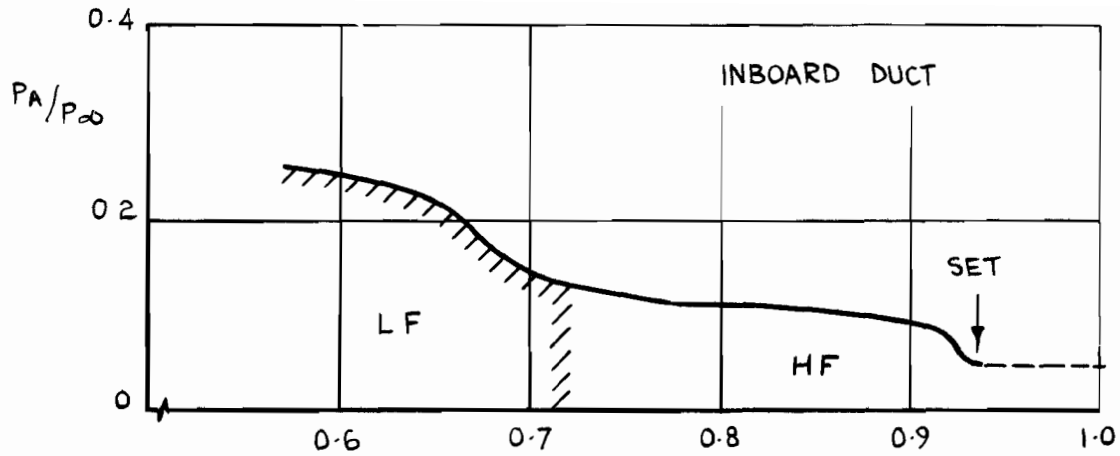

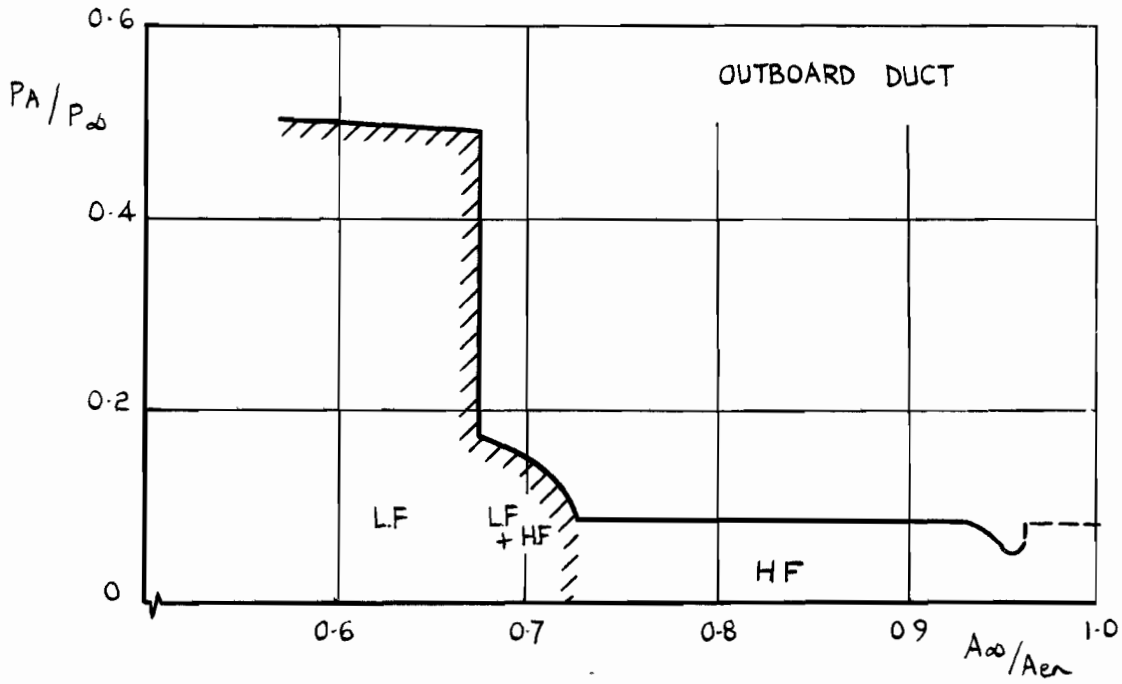

(e) $M = 2{\cdot}20$, $\delta_3 = 17{\cdot}50^\circ$

FIG. 32. (CONCL.)

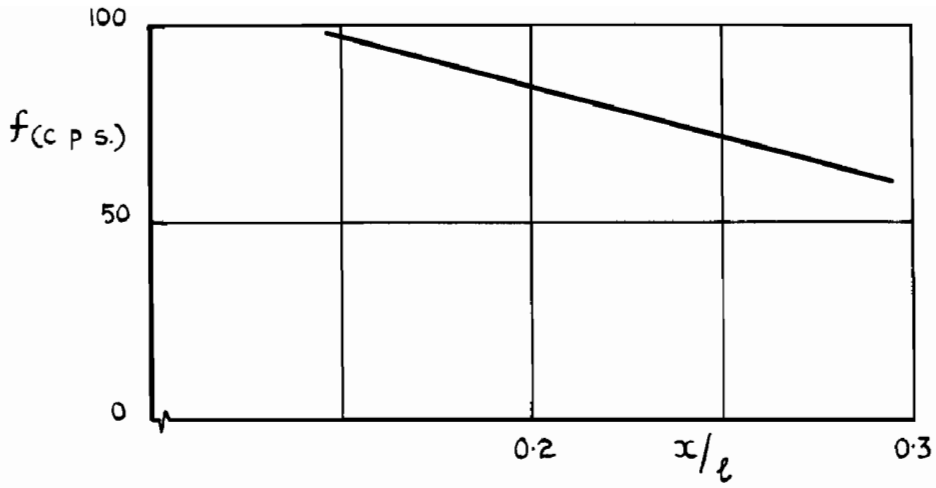

NOTE :- THE CURVE IS THE MEAN FOR SEVERAL SETS OF RESULTS FOR MACH NUMBERS OF 2·0, 2·12, & 2·20. THE SCATTER IS ABOUT ± 10 c p.s.

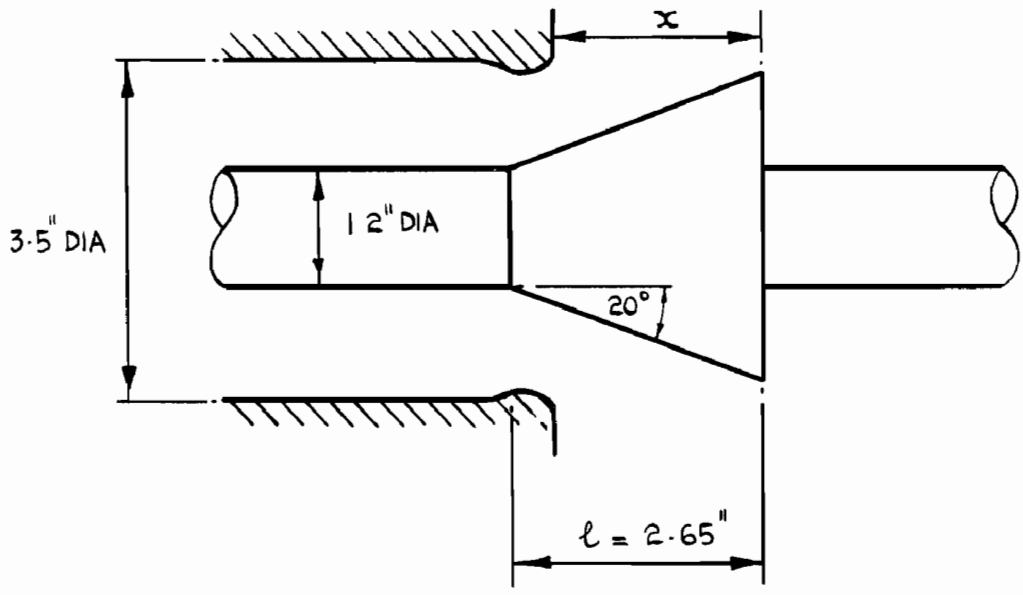

THROTTLE DETAILS.

FIG. 33. FREQUENCY OF L.F. OSCILLATION – VARIATION WITH THROTTLE POSITION.

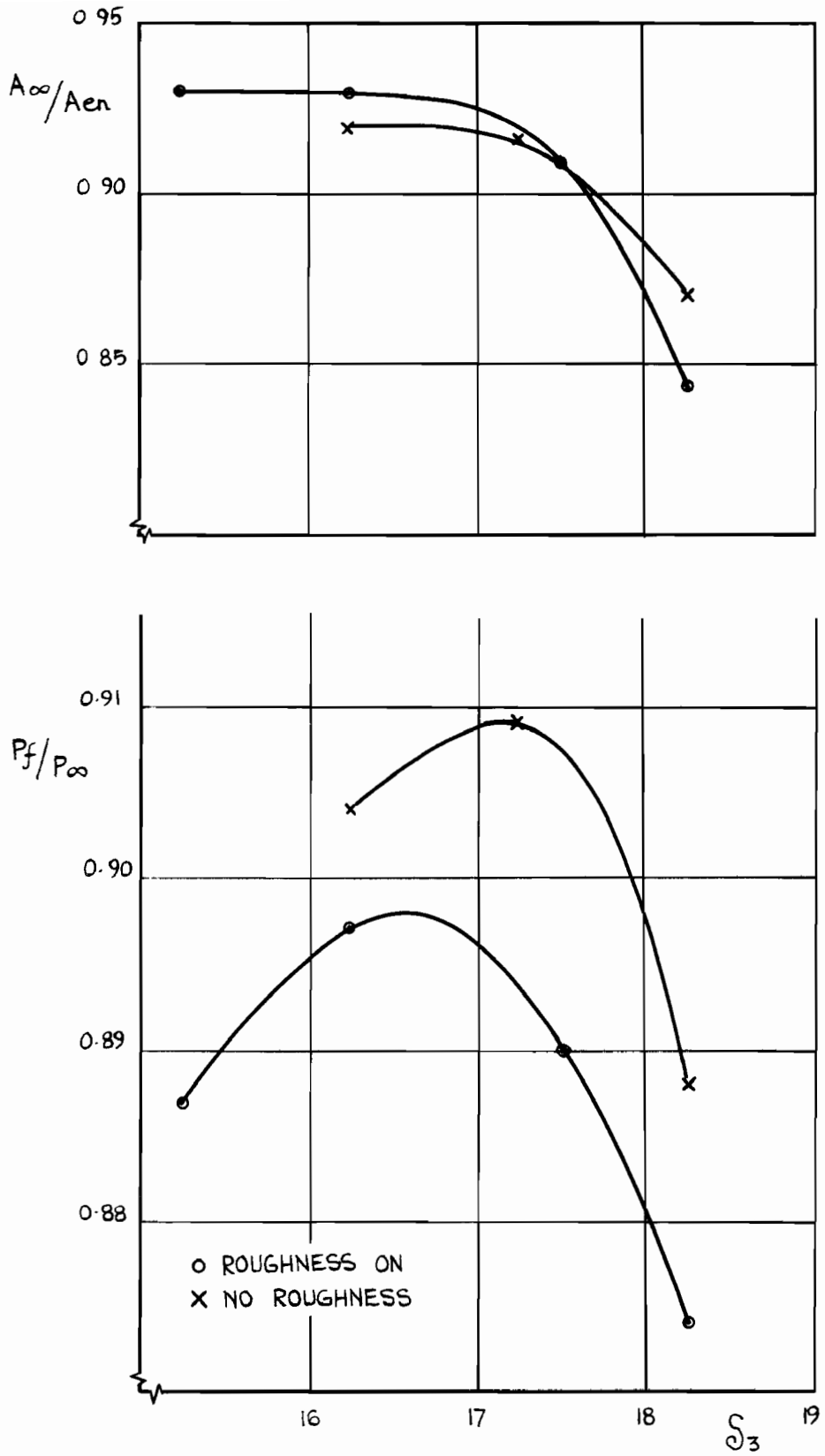

FIG. 41 EFFECTS OF TRANSITION ON MAXIMUM VALUES PRESSURE RECOVERY & MASS FLOW AT M = 2·12 – VARIATION WITH δ_3, $m_b/m_i \simeq 0{\cdot}04$, SPLITTER I.

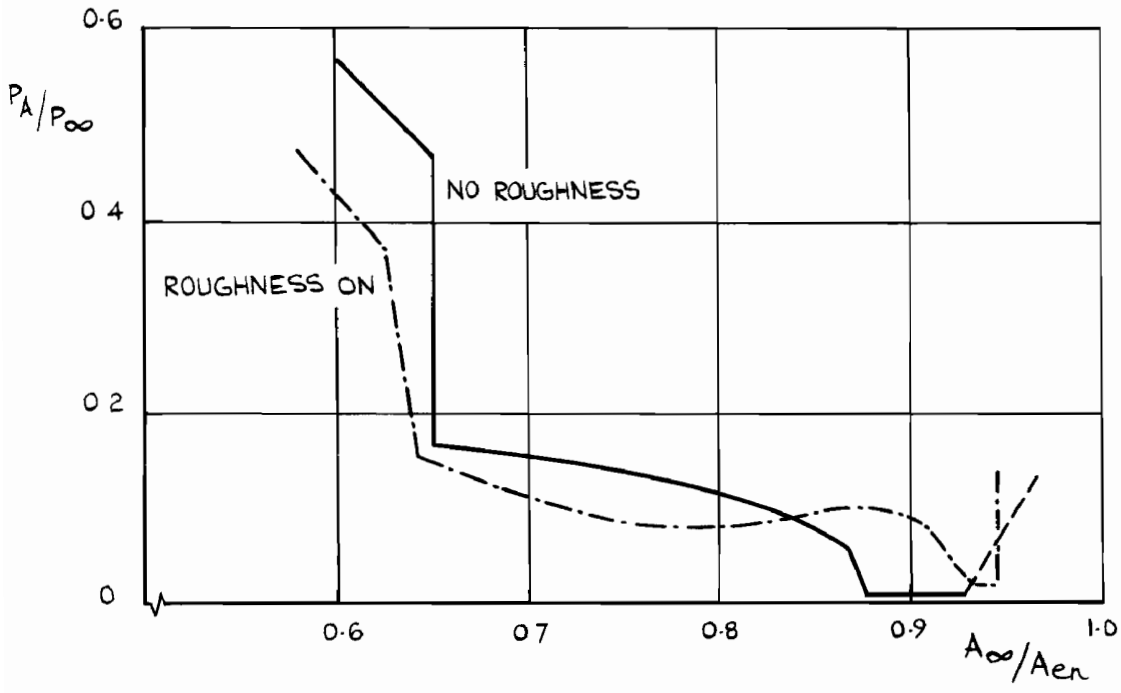

FIG. 42 FLUCTUATING PRESSURE AMPLITUDES.
$M = 2{\cdot}12$, $\delta_3 = 16{\cdot}25^\circ$, $m_b/m_i \simeq 0{\cdot}04$, SPLITTER I.

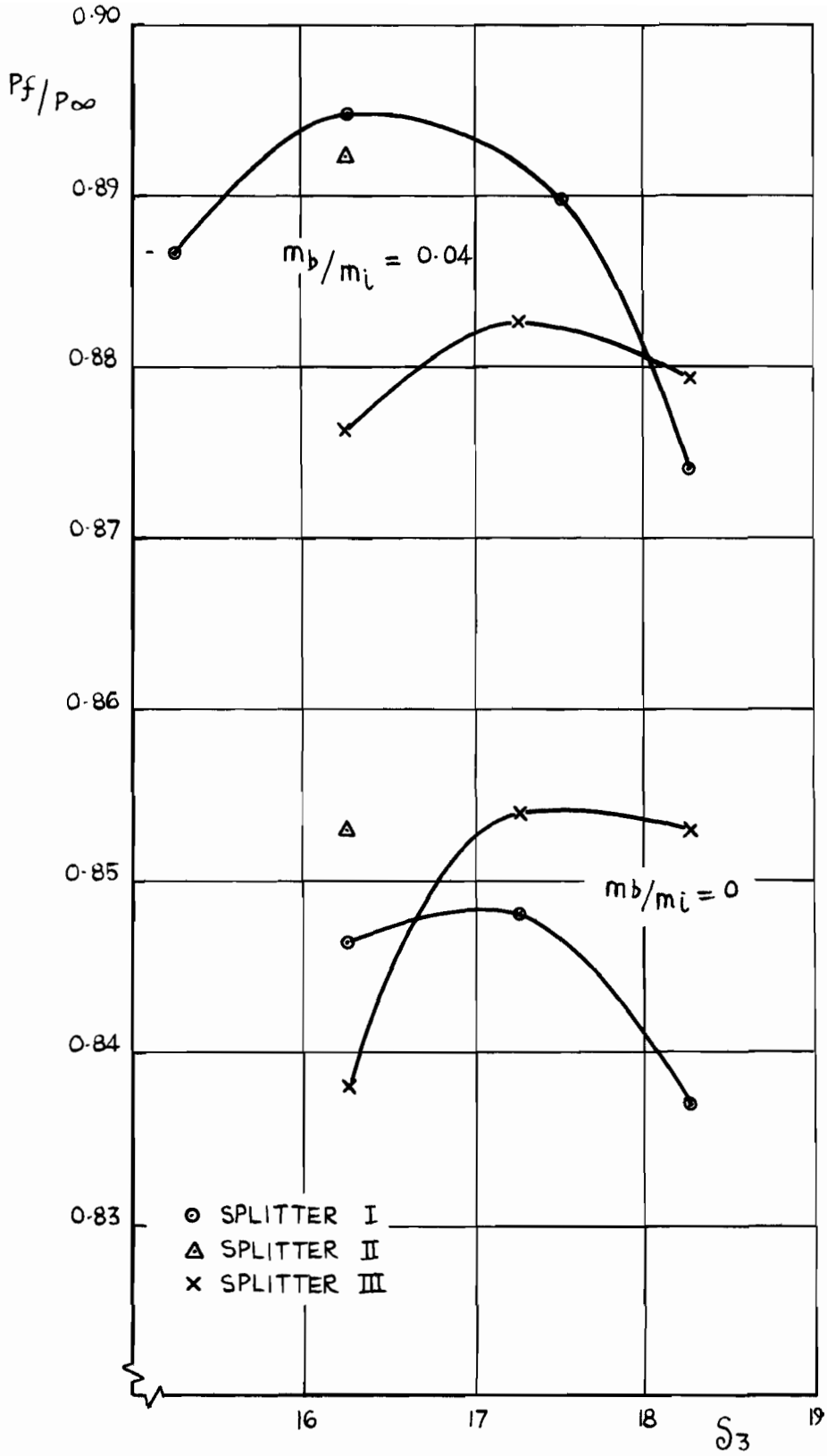

FIG. 43 MAXIMUM VALUES OF PRESSURE RECOVERY – VARIATION WITH δ_3 FOR THE THREE SPLITTER DESIGNS, M = 2·12.

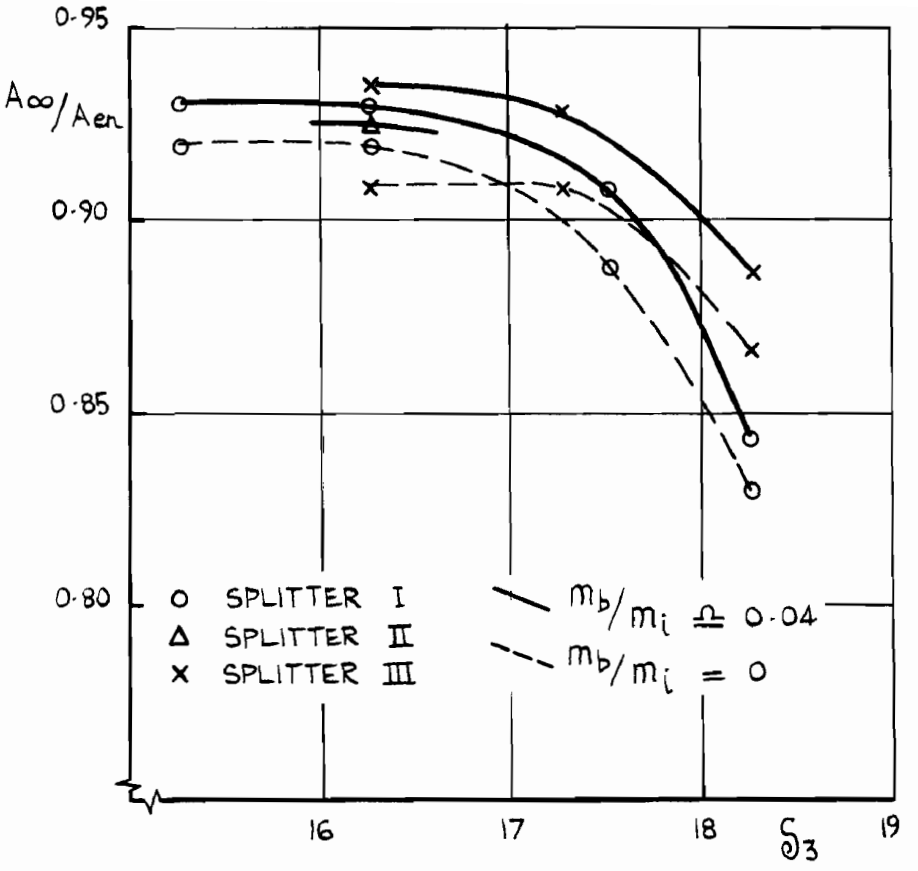

FIG. 44. MAXIMUM VALUES OF MASS FLOW RATIO – VARIATION WITH δ_3 FOR THE THREE SPLITTER DESIGNS

M = 2·12

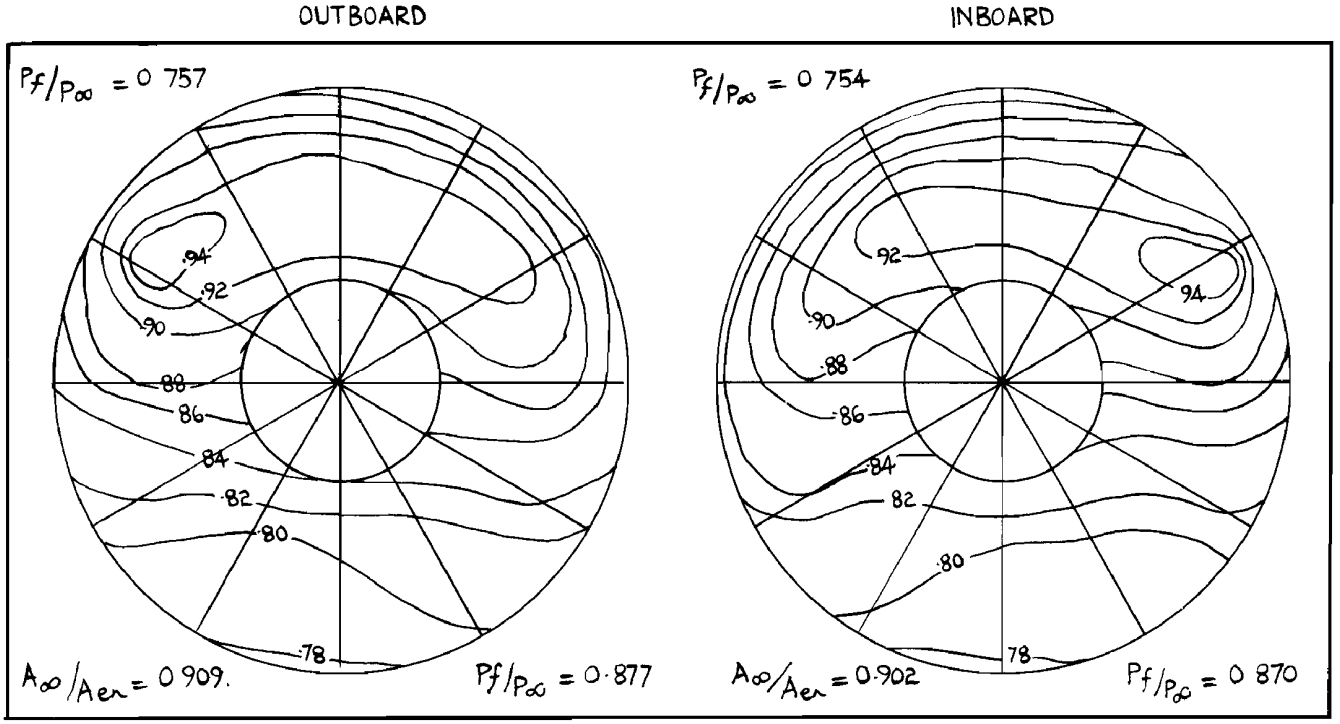

(b) SPLITTER III

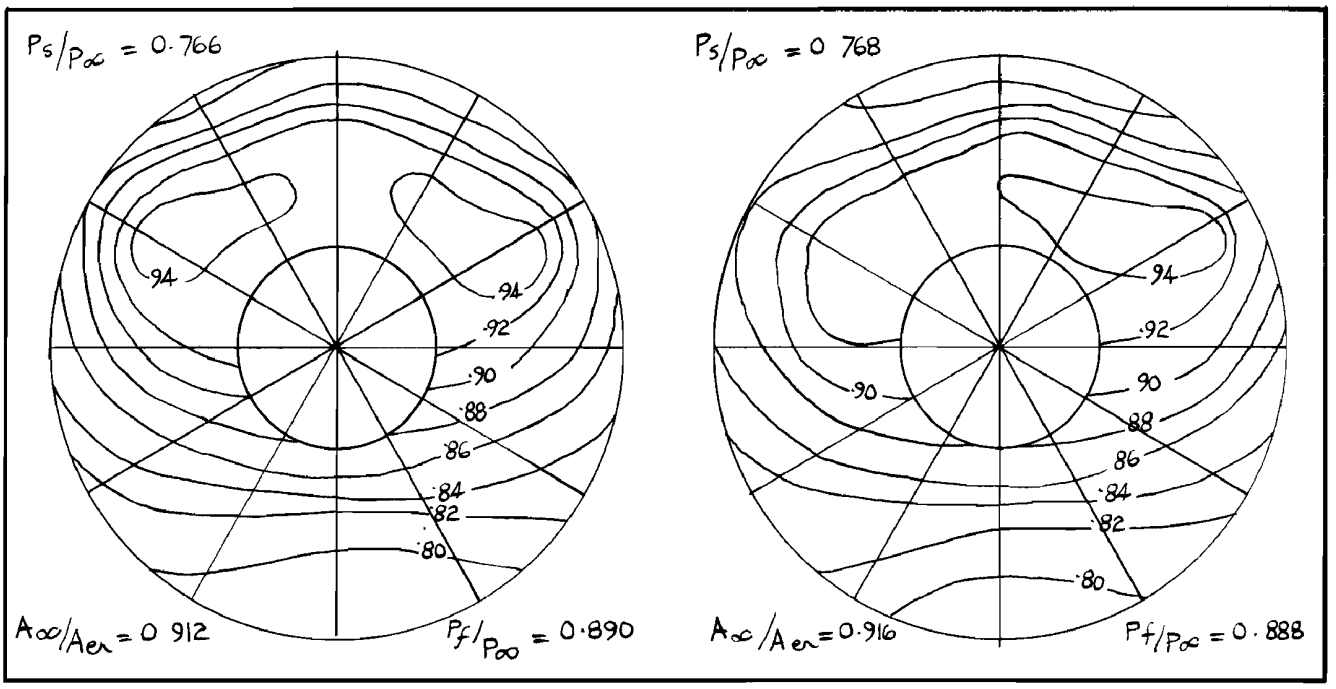

(a) SPLITTER II

FIG. 45. PRESSURE DISTRIBUTIONS, M = 212, $\zeta_3 = 16 \cdot 25^\circ$, $m_b/m_i \simeq 0 \cdot 04$

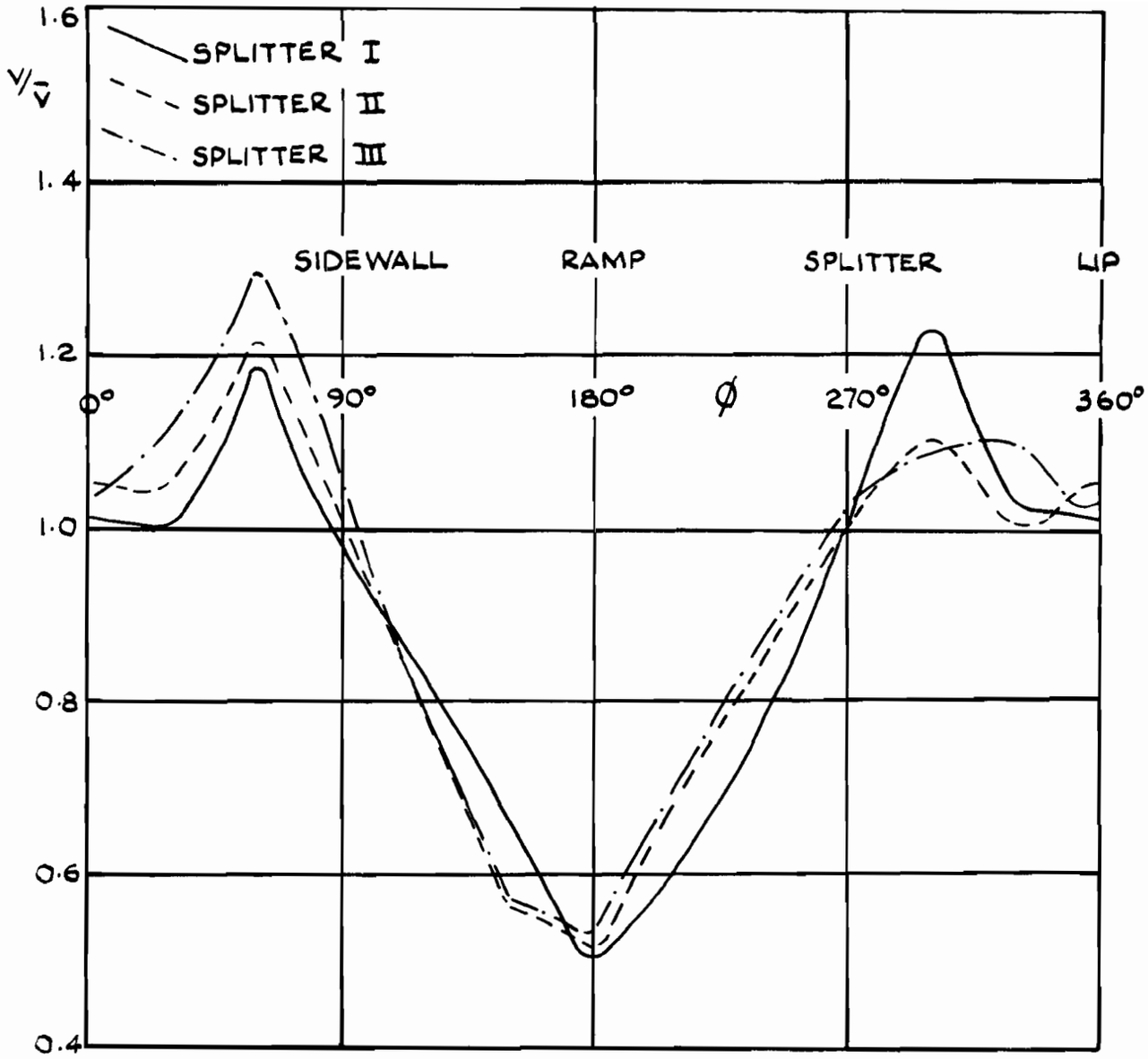

FIG. 46 CIRCUMFERENTIAL DISTRIBUTIONS OF $V/\bar{V}$ AT $r/R = 0.798$, $M = 2.12$, $\delta_3 = 16.25°$, $m_b/m_i \simeq 0.040$

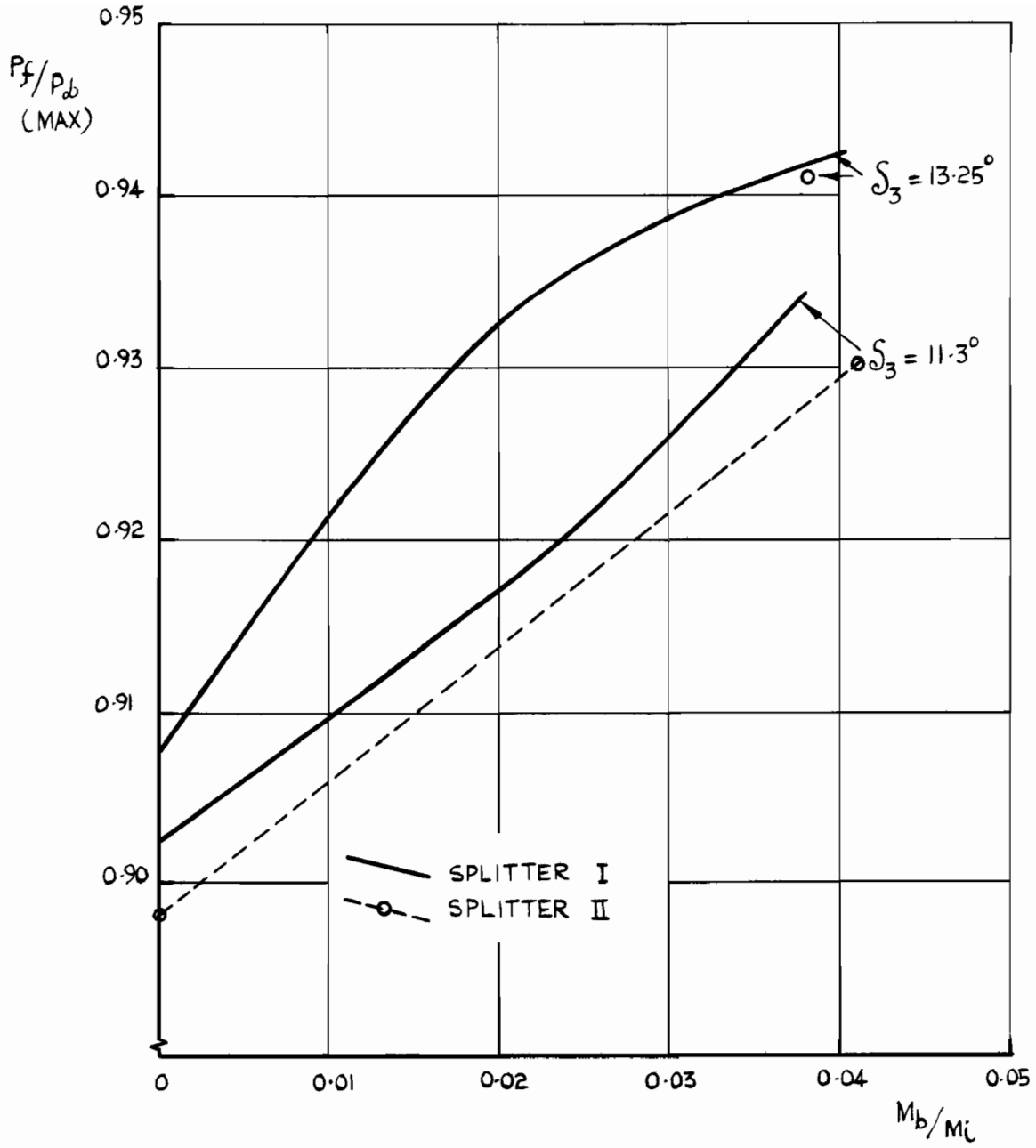

FIG. 47. MAXIMUM PRESSURE RECOVERY - VARIATION WITH THROAT BLEED FLOW & δ_3. M = 1·85.

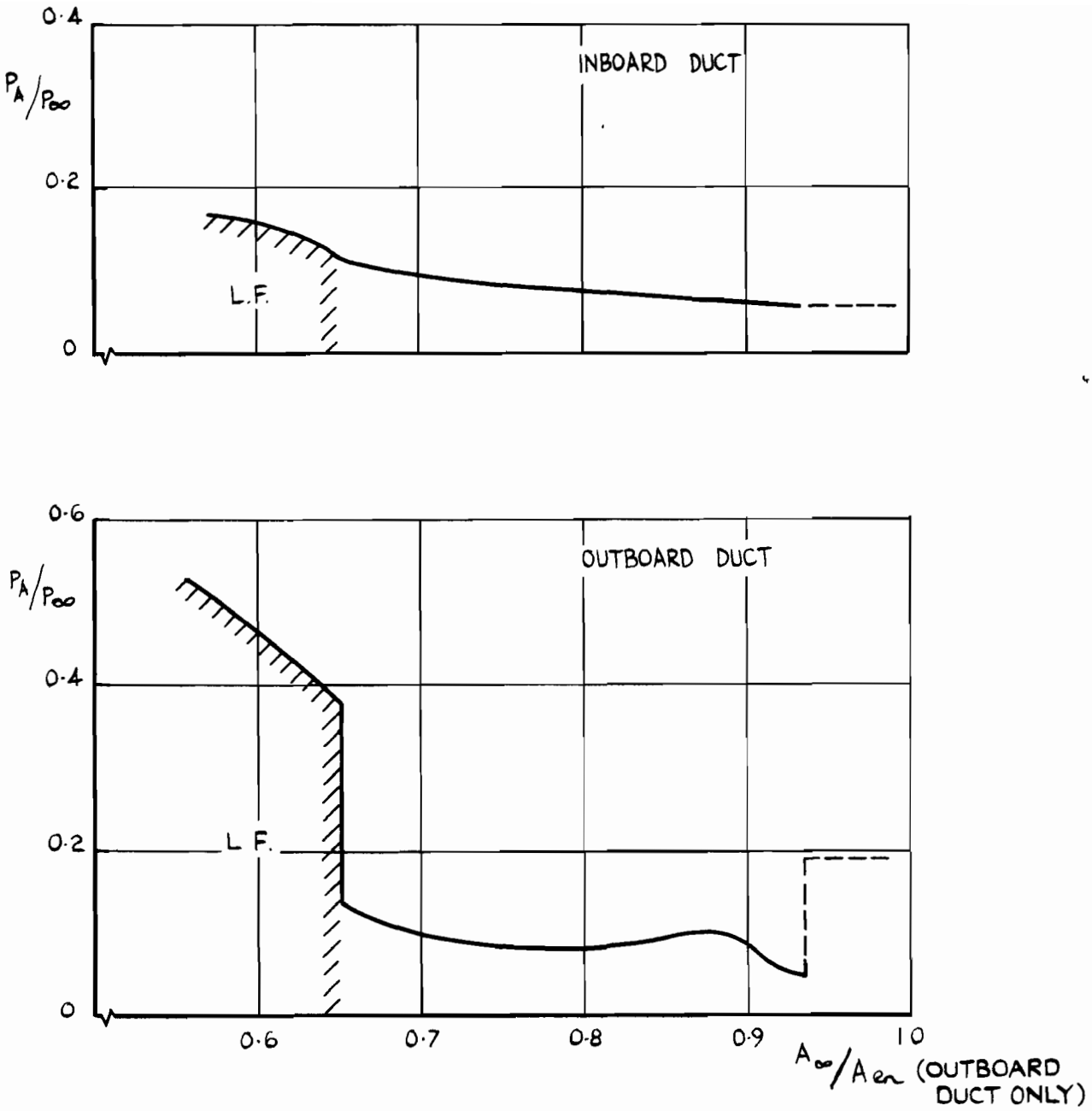

SEE FIG. 32 FOR EXPLANATORY NOTE.

FIG. 48. FLUCTUATING PRESSURE AMPLITUDES, SPLITTER II
$M = 2{\cdot}12$, $\delta_3 = 16{\cdot}25^\circ$, $m_b/m_i \simeq 0{\cdot}04$.

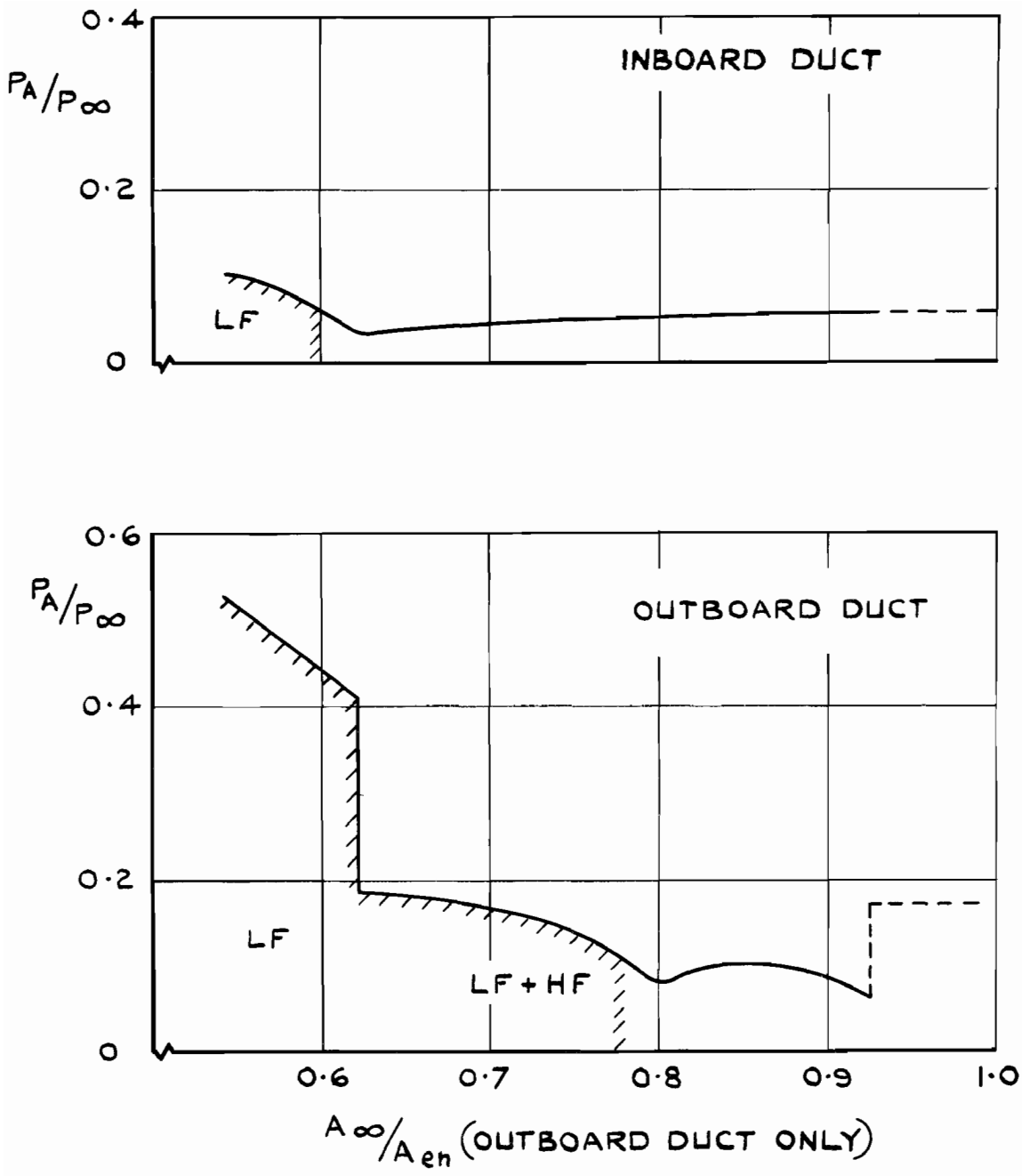

SEE FIG. 32 FOR EXPLANATORY NOTE

FIG. 49 FLUCTUATING PRESSURE AMPLITUDES, SPLITTER III, M = 2·12, δ_3 = 16·25°, m_b/m_i 0·04

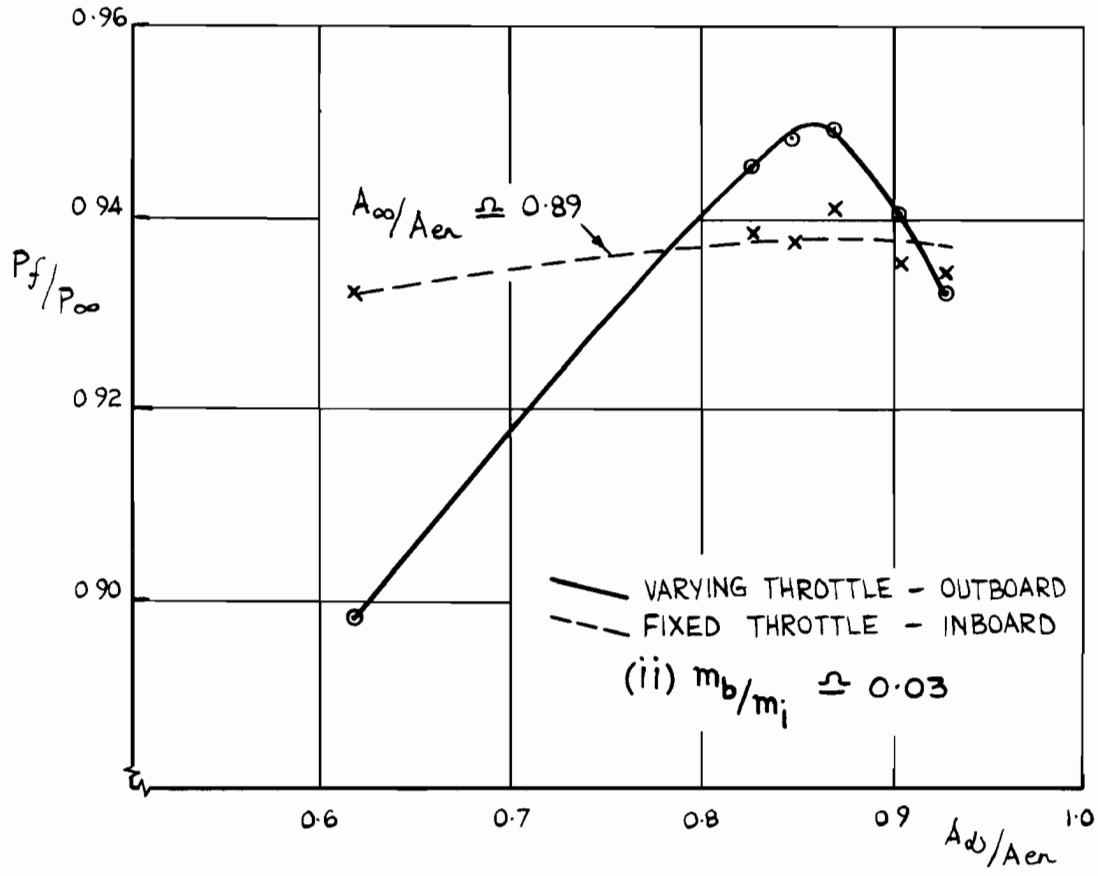

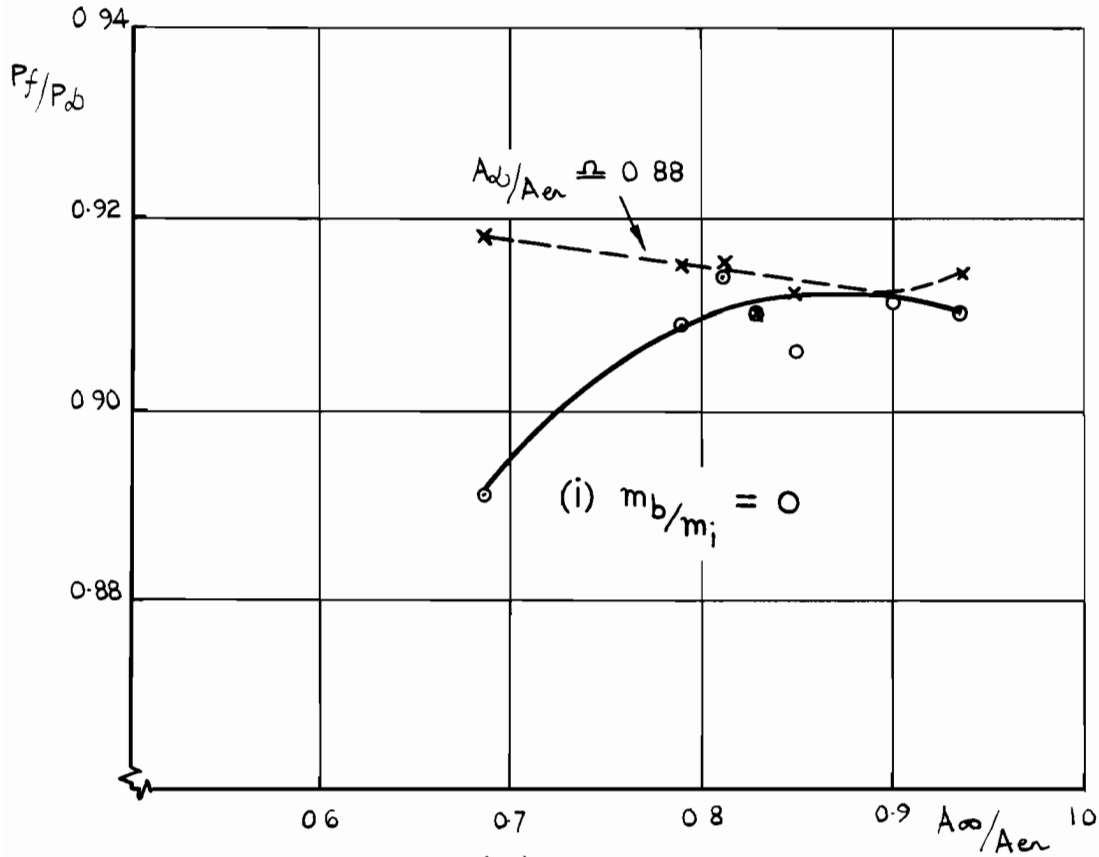

(a) M = 1·70

FIG.50 CURVES SHOWING INTERFERENCE EFFECTS. THESE (ARE DESCRIBED IN SECT. 4·2 .)

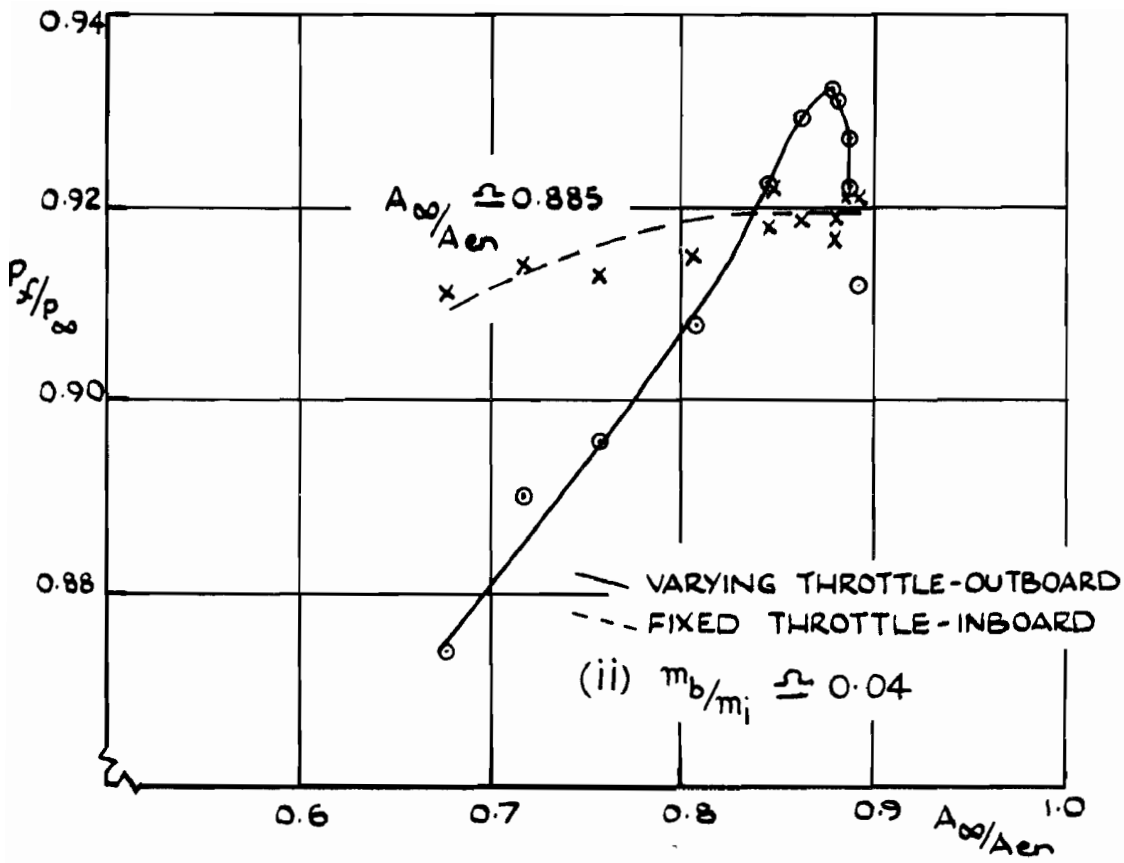

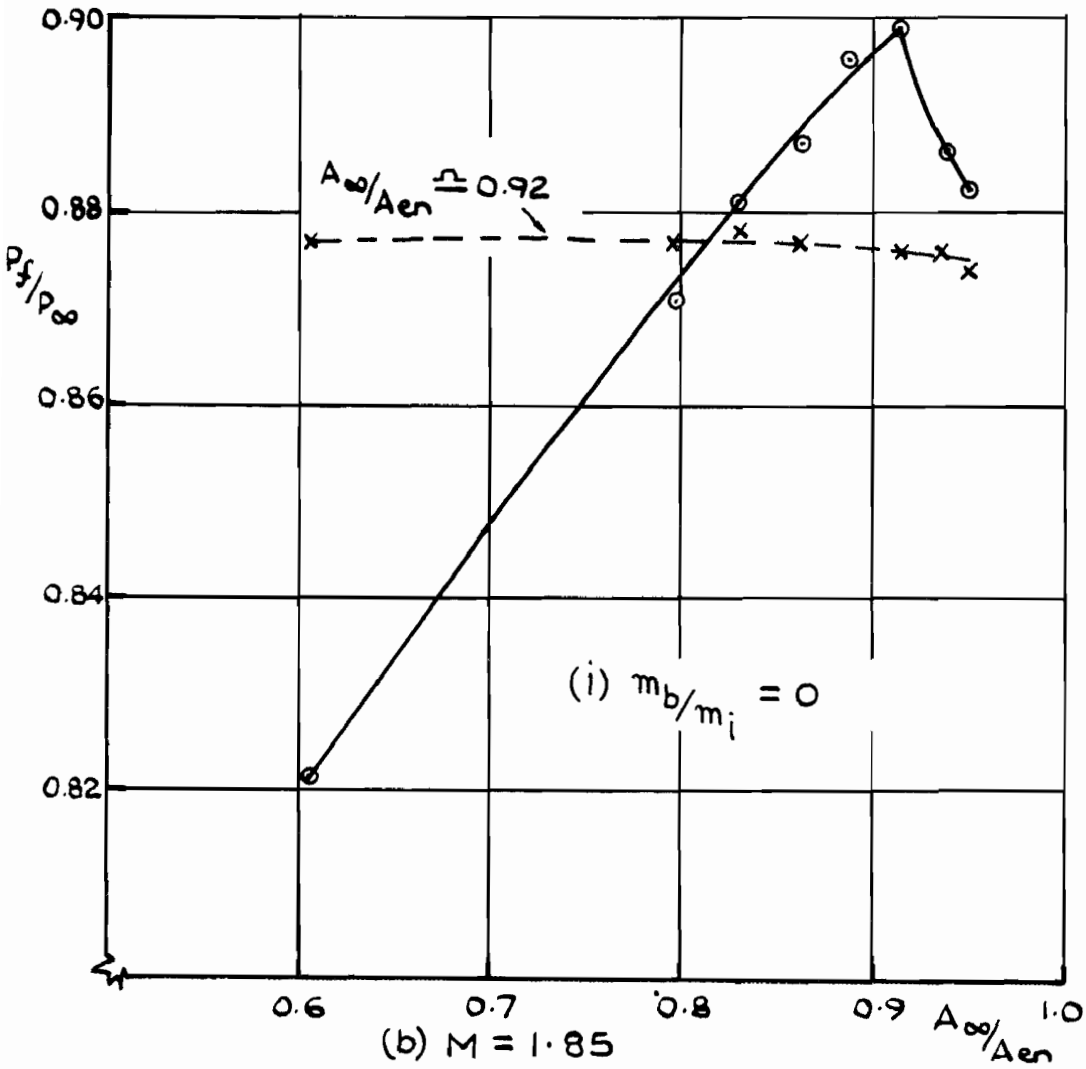

(b) M = 1·85

FIG. 50. (CONT)

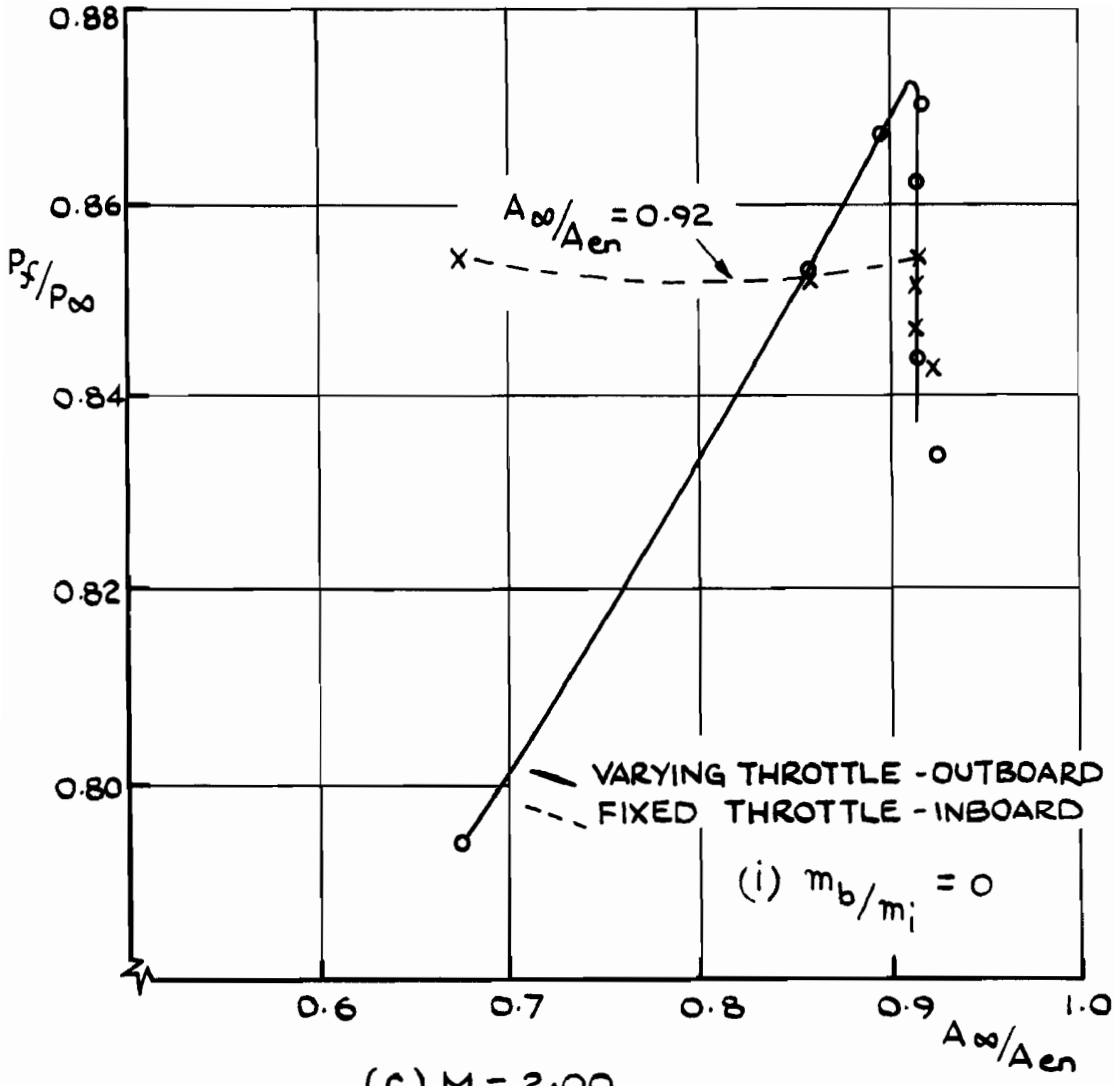

(c) M = 2·00

FIG. 50 (CONT)

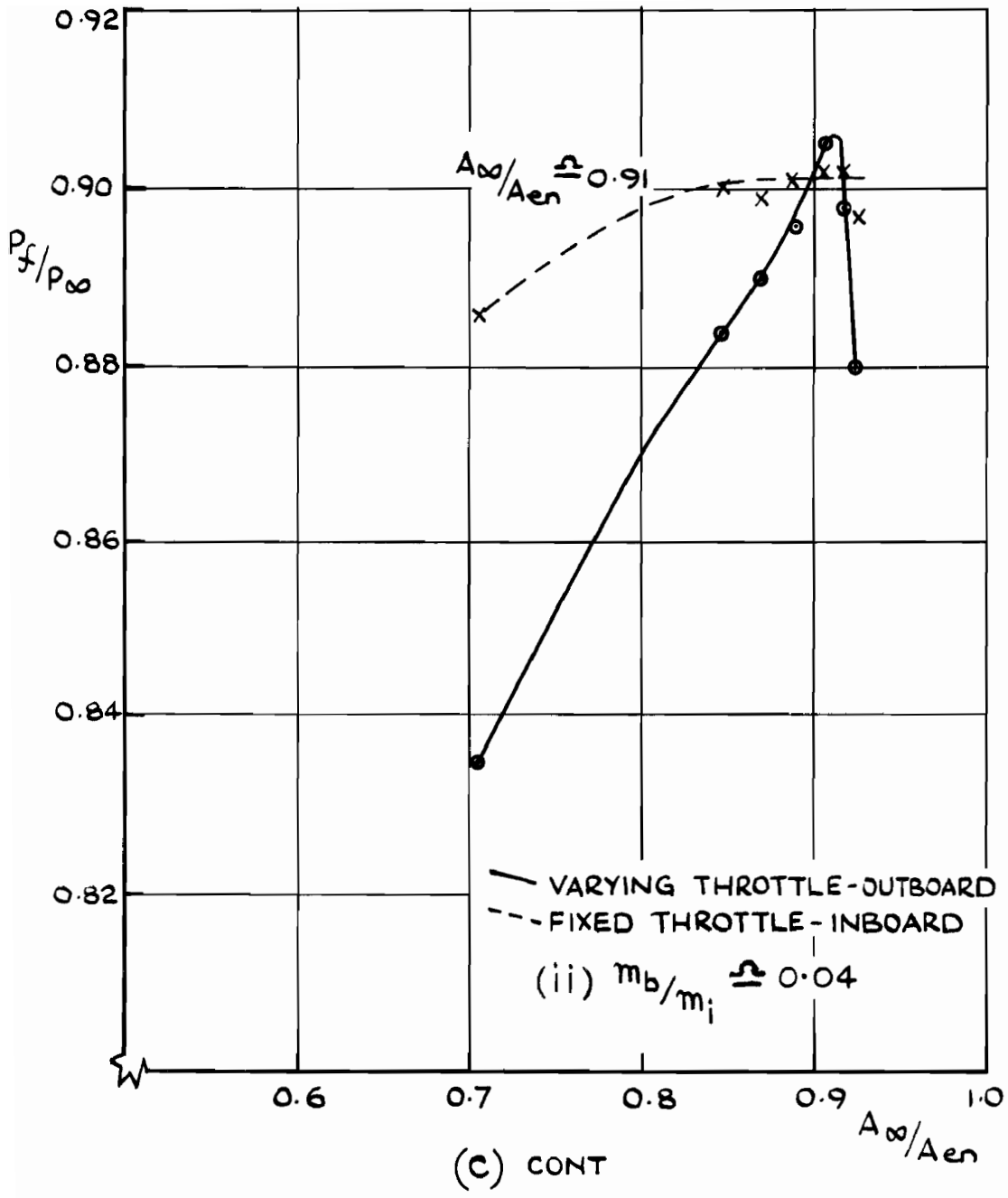

(C) CONT

FIG. 50 (CONT.)

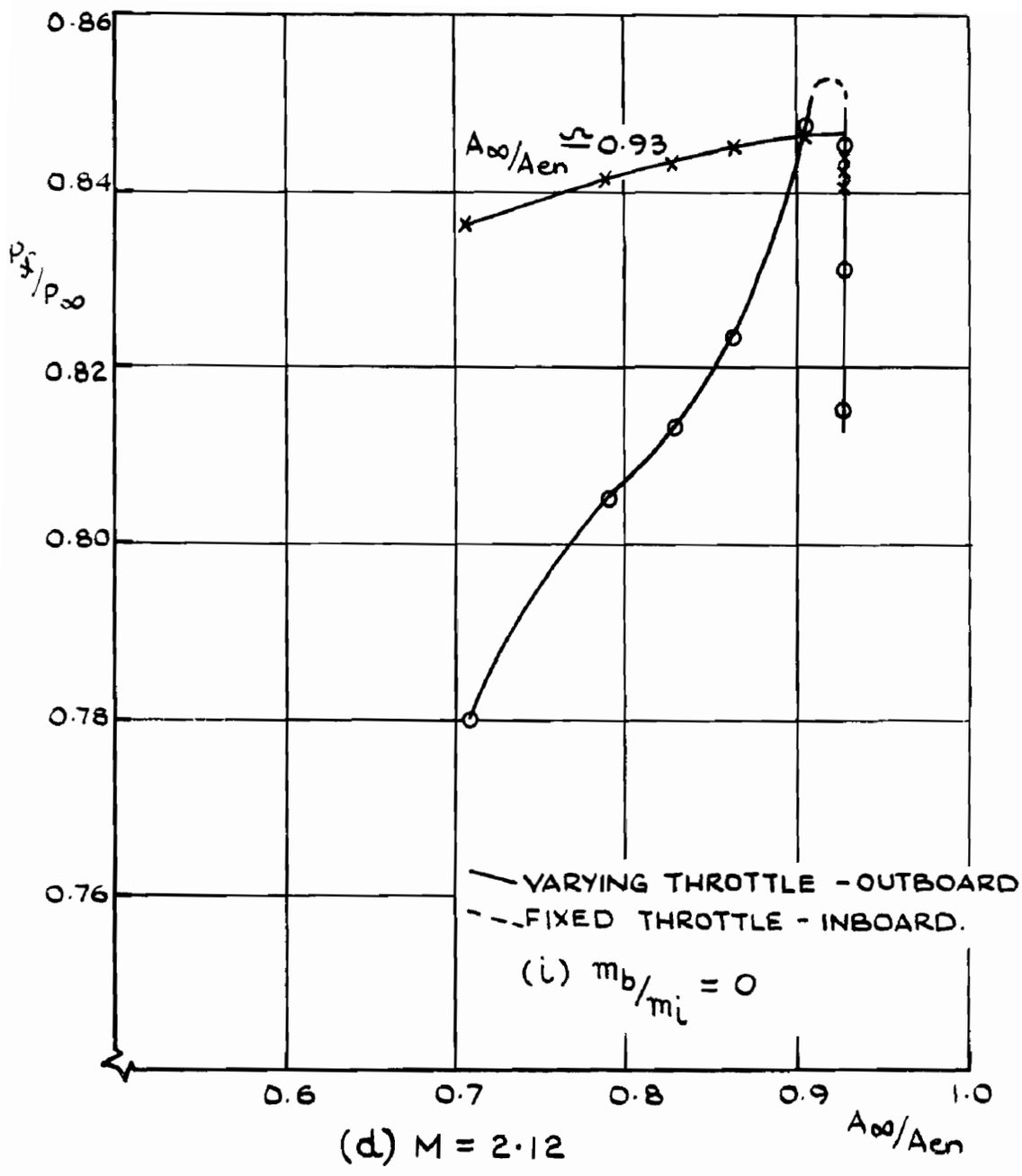

(d) M = 2·12

FIG. 50. (CONT)

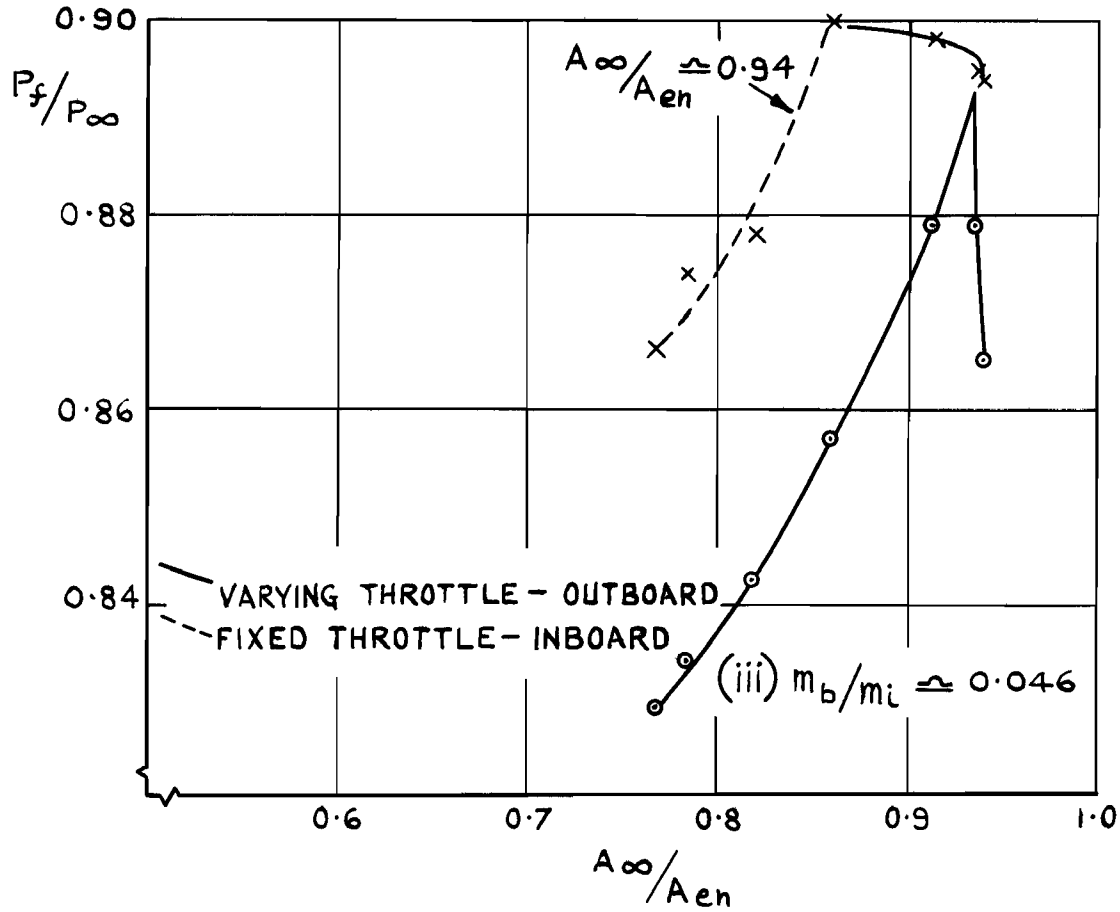

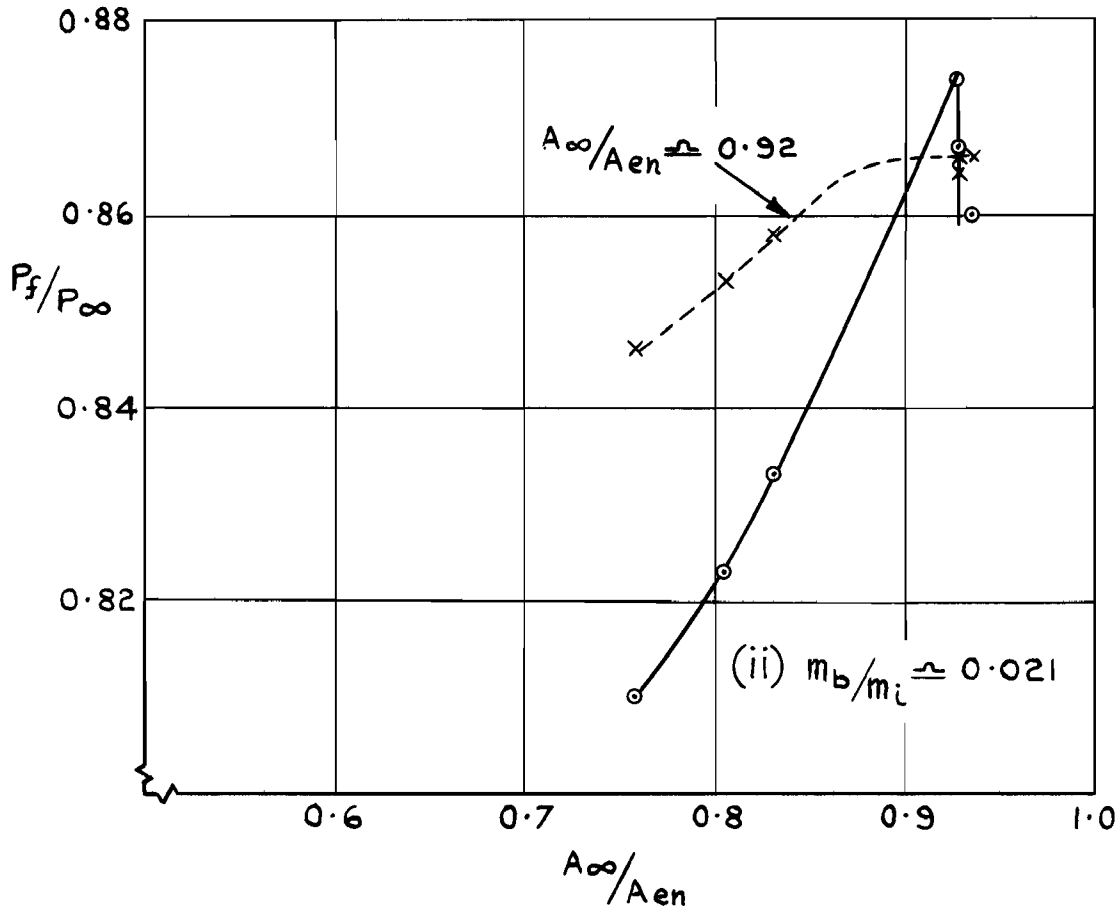

FIG. 50 (d) CONT.

FIG.50 (CONT.)

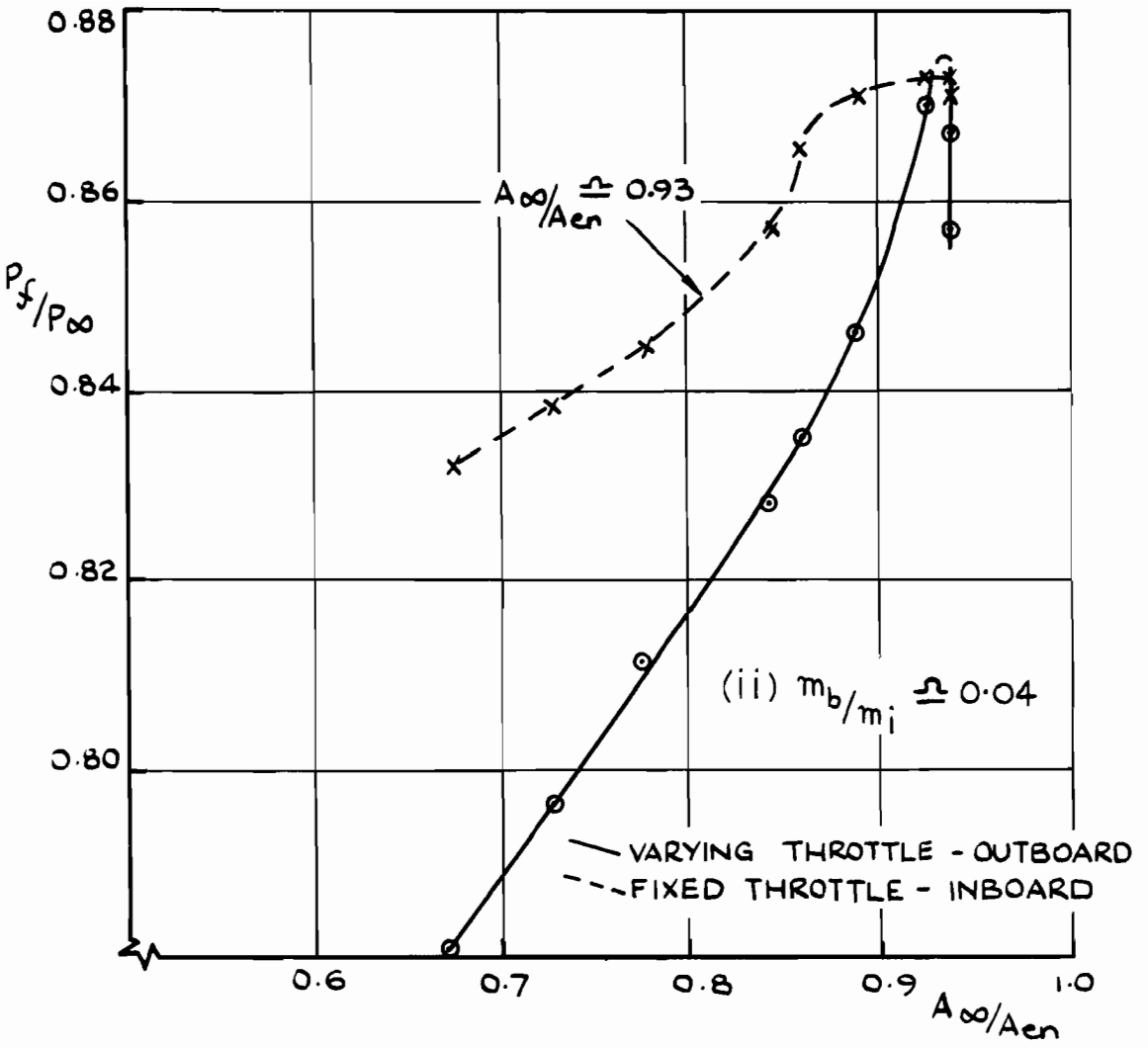

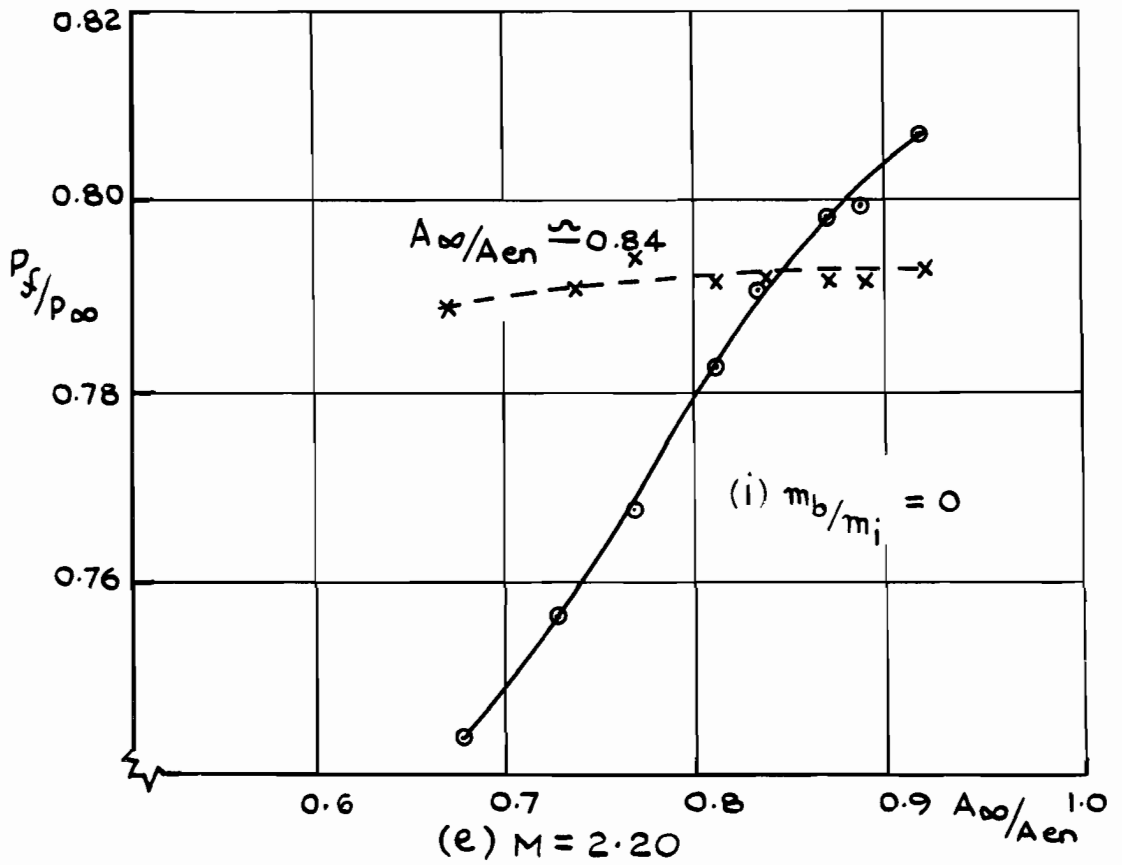

(e) M = 2·20

FIG. 50 (CONCL)

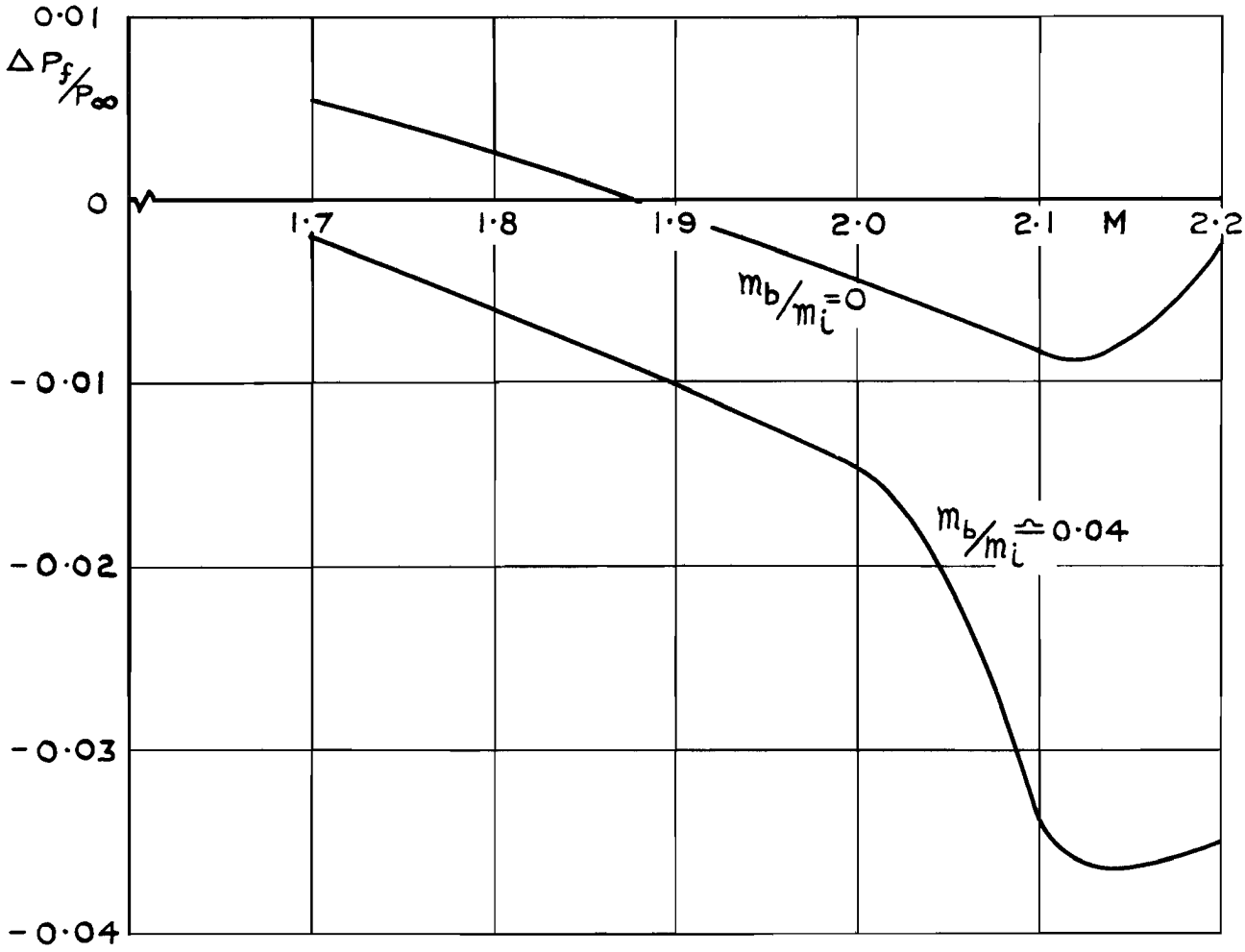

FIG.51 CHANGES OF PRESSURE RECOVERY IN INBOARD DUCT FOR A MASS FLOW RATIO IN OUTBOARD DUCT 20 % BELOW MAXIMUM

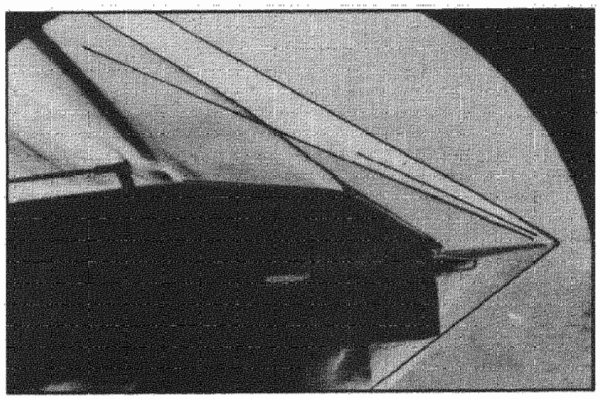

FIG. 52 (a) BOTH DUCTS RUNNING FULL
(PICTURES ARE SIMILAR BOTH WITH & WITHOUT THROAT BLEED FLOW)

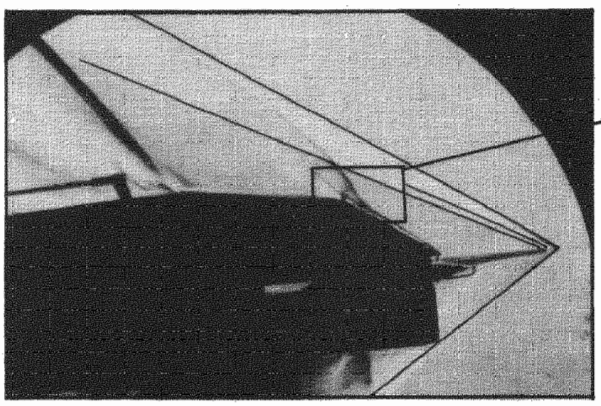

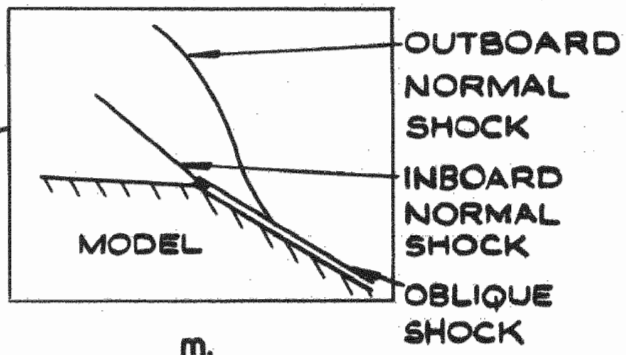

FIG. 52 (b) $m_b/m_i = 0$
OUTBOARD THROTTLED $A_\infty/A_{en} = 0{\cdot}788$

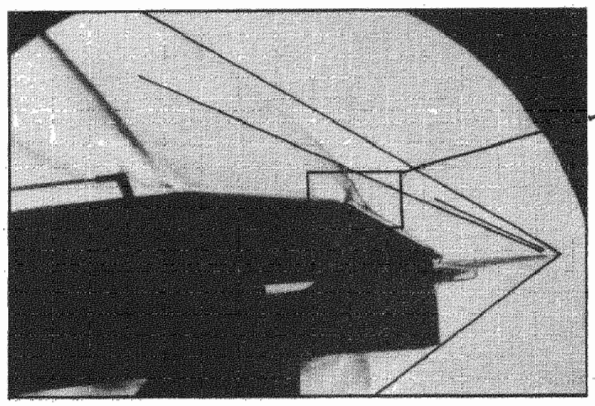

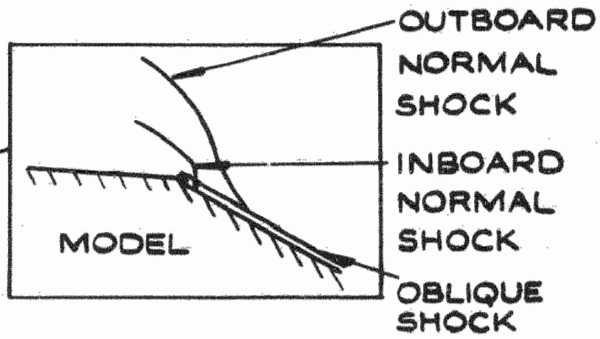

FIG. 52 (c) $m_b/m_i \simeq 0{\cdot}04$
OUTBOARD THROTTLED $A_\infty/A_{en} = 0{\cdot}781$

FIG. 52 SCHLIEREN PHOTOGRAPHS –
(CONDITIONS AS INDICATED IN FIG. 53)

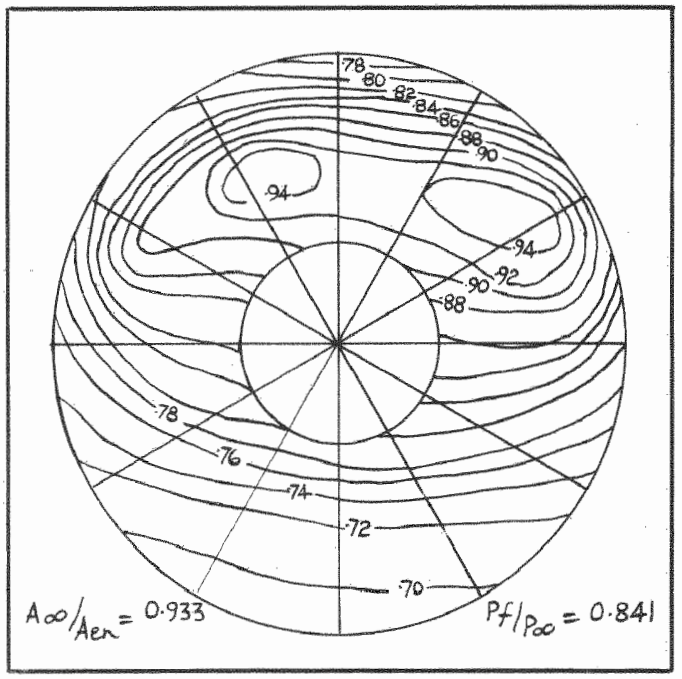

(a) NO BLEED

OUTBOARD A_∞/A_{en} = 0·788

NOTE:- FULL FLOW INBOARD

$A_\infty/A_{en} \simeq 0{\cdot}93$

∴ REDUCTION IN FLOW IS ZERO.

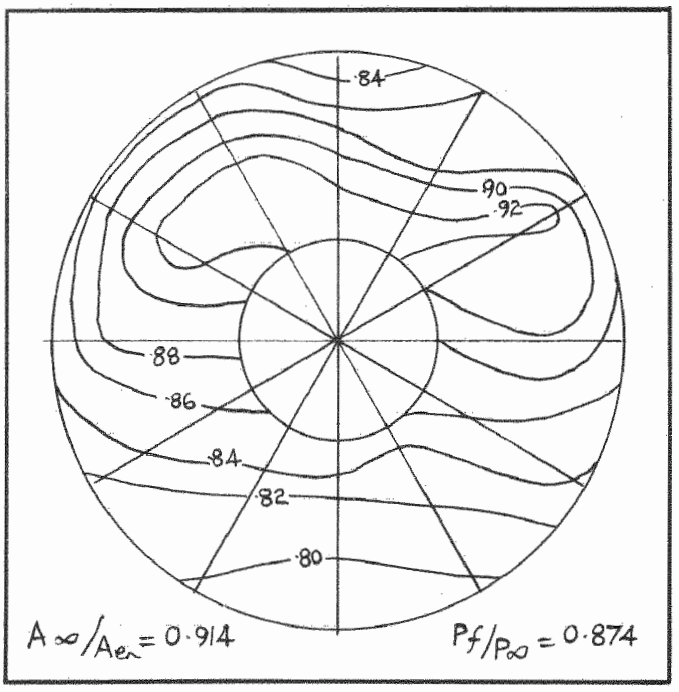

(b) $m_b/m_i \simeq 0{\cdot}04$

OUTBOARD A_∞/A_{en} = 0·781

NOTE:- FULL FLOW INBOARD

$A_\infty/A_{en} \simeq 0{\cdot}94$

∴ REDUCTION IN FLOW $\simeq$ 0·028

FIG. 53. PRESSURE DISTRIBUTIONS IN THE INBOARD DUCT WITH THROTTLE SET TO PASS MAXIMUM FLOW $M = 2{\cdot}12$, $\delta_3 = 16{\cdot}25^\circ$, SPLITTER I.

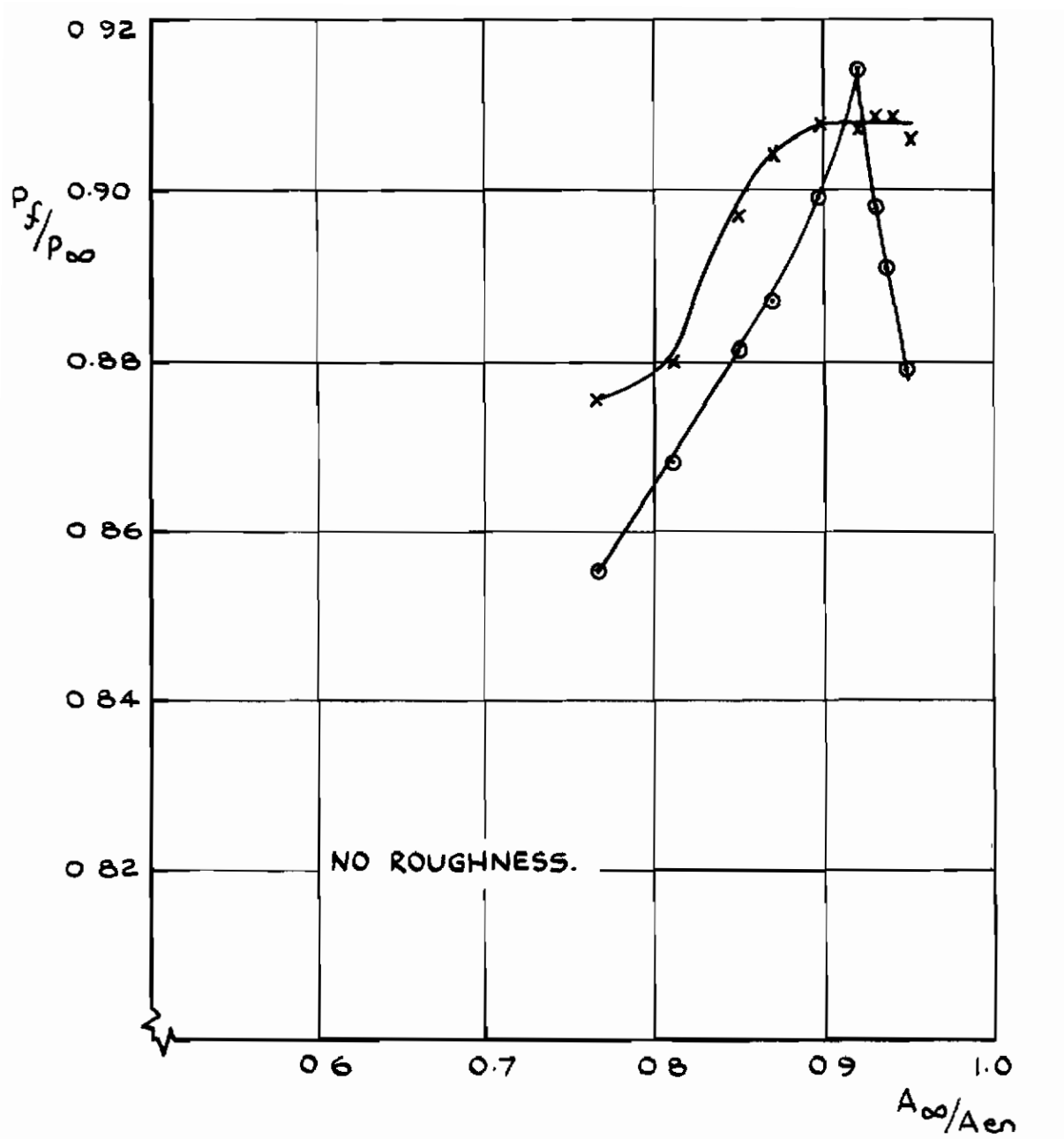

FIG 54. CURVES SHOWING INTERFERENCE EFFECTS $M = 2 \cdot 12$, $\delta_3 = 17 \cdot 25°$, $M_b / M_i \simeq 0 \cdot 04$

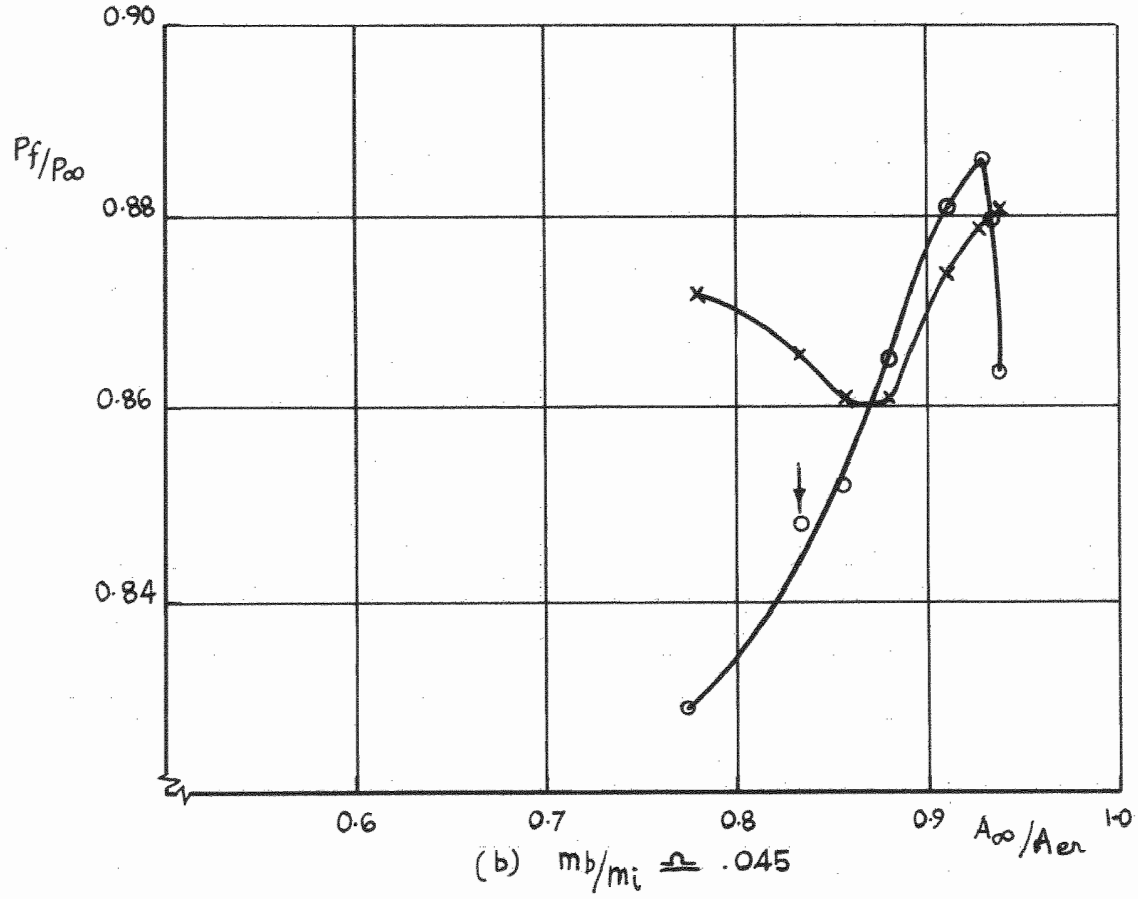

(b) $m_b/m_i \simeq .045$

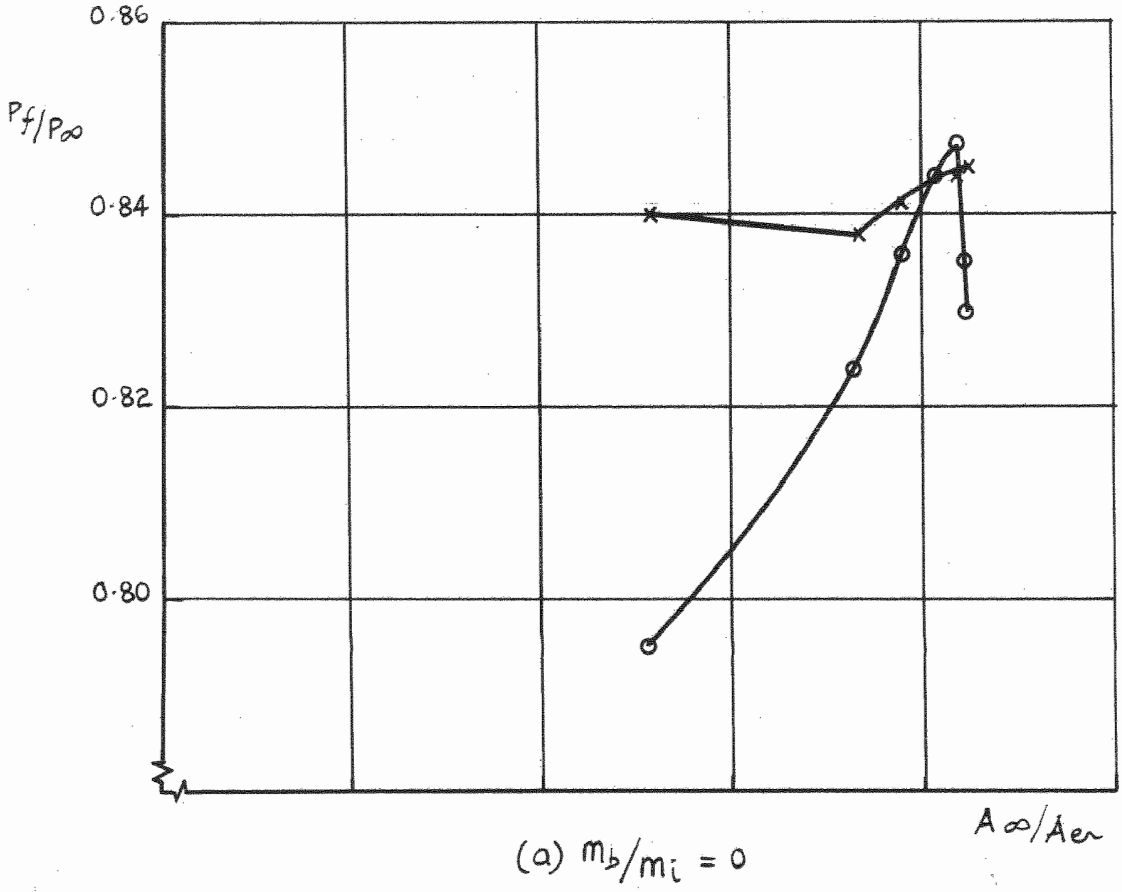

(a) $m_b/m_i = 0$

FIG. 55. CURVES SHOWING INTERFERENCE EFFECTS. SPLITTER II $M = 2 \cdot 12$. $\delta_3 = 16 \cdot 25^\circ$.

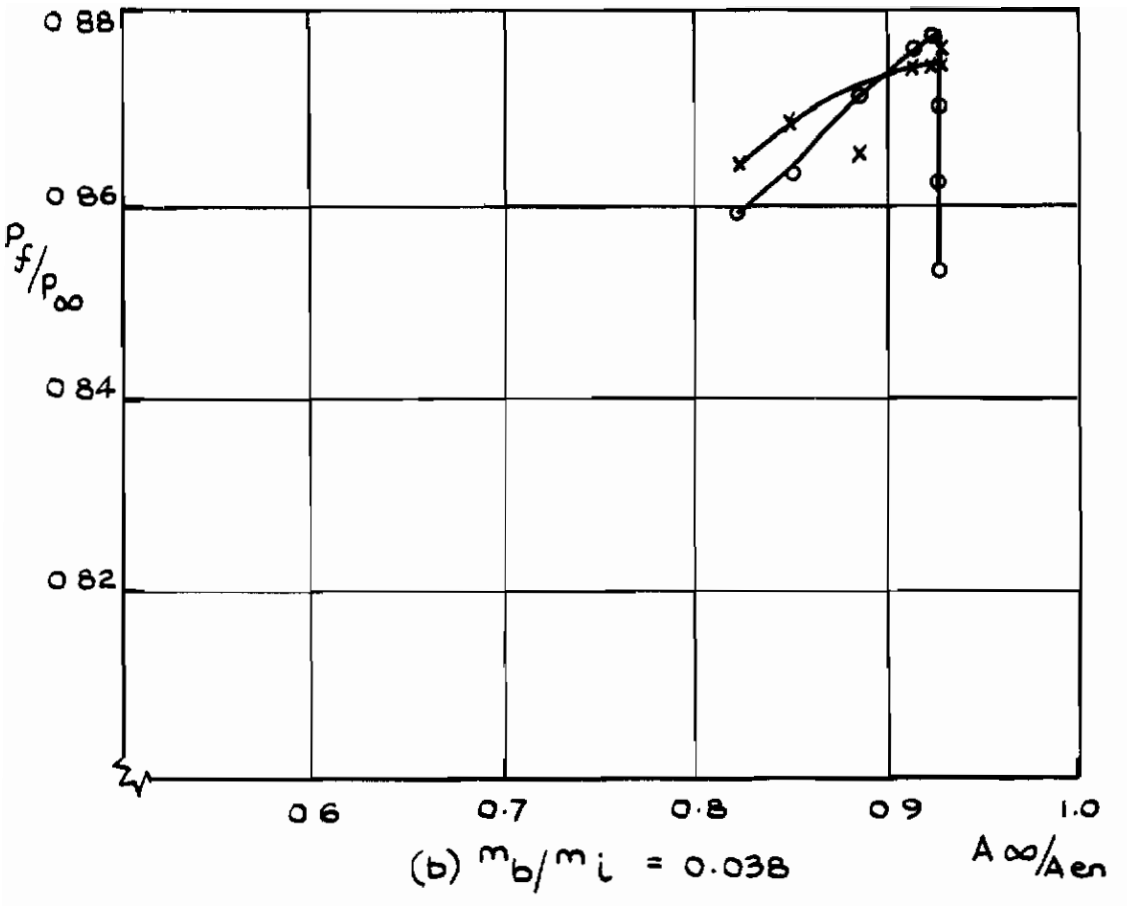

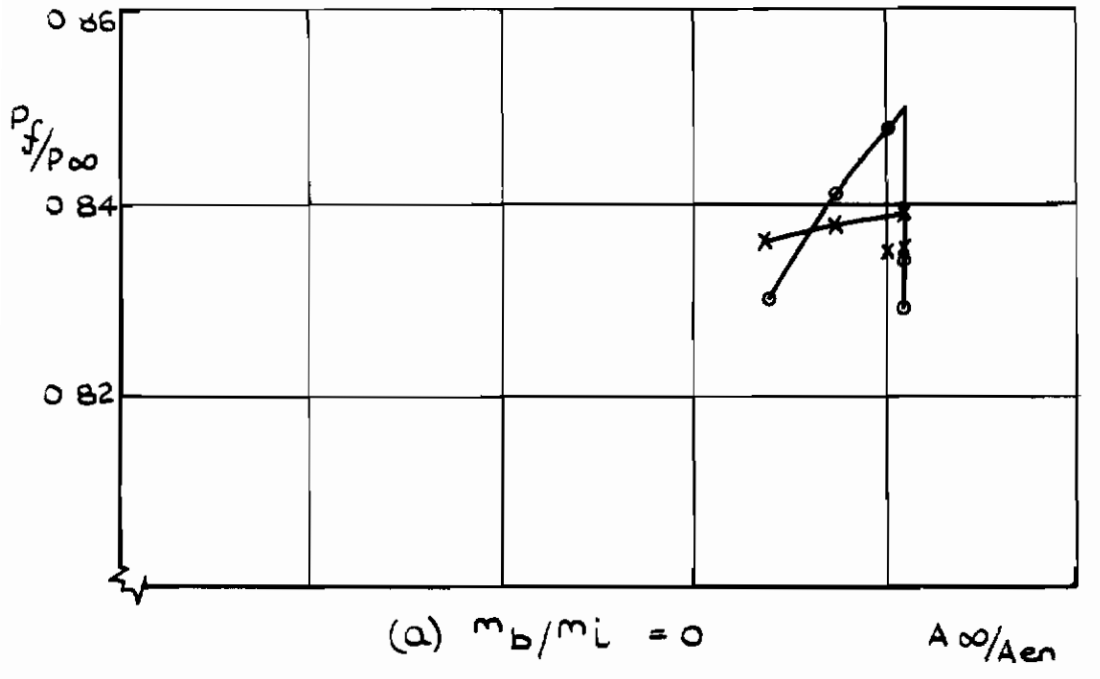

FIG. 56 CURVES SHOWING INTERFERENCE EFFECTS

SPLITTER III. M = 2·12, δ_3 = 16·25°

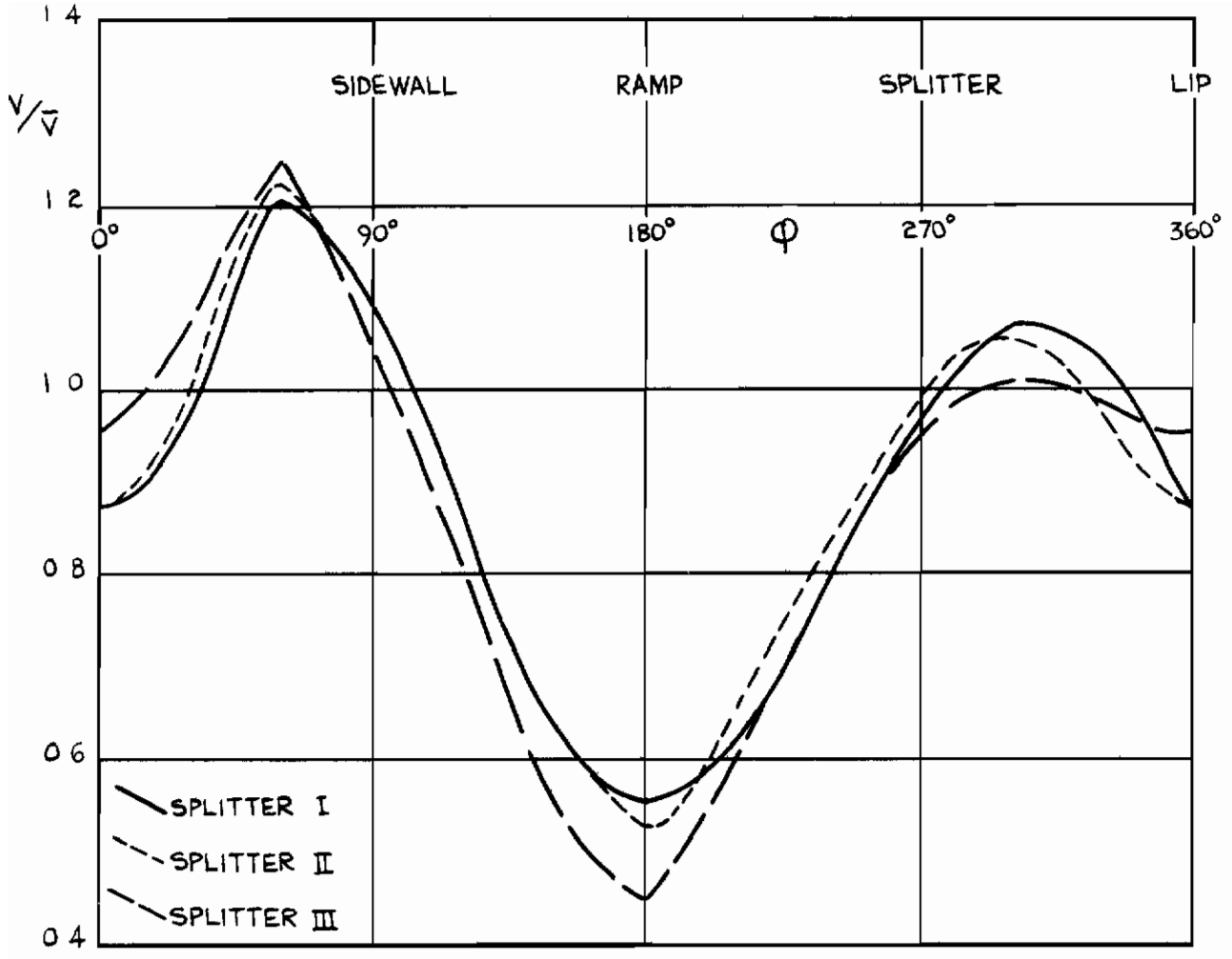

FIG. 57 VELOCITY DISTRIBUTIONS IN INBOARD DUCT AT $r/R = 0 \cdot 877$, $M = 2 \cdot 12$, $\delta_3 = 16 \cdot 25^\circ$, $m_b/m_i \simeq 0\ 04$.

INBOARD DUCT A_∞/A_{en} — FULL

OUTBOARD DUCT $A_\infty/A_{en} \simeq 0 \cdot 83$

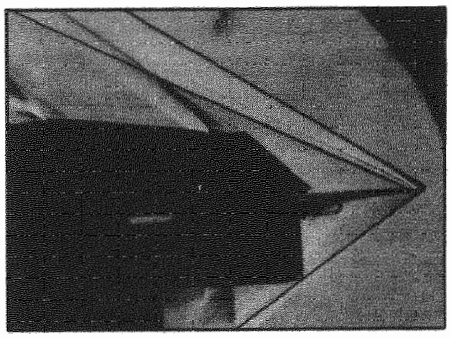

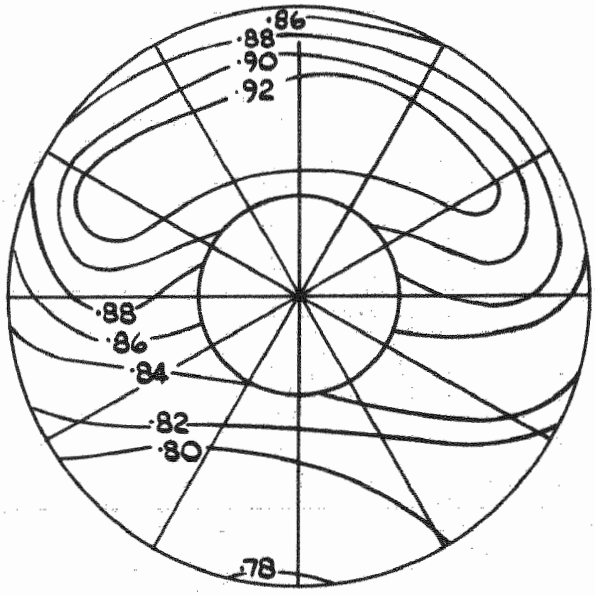

m_e/m_i	0·867
m_b/m_i	0·044
m_{sv}/m_i	0

P_f/P_∞	0·876	A_∞/A_{en}	0·911

(a) SPILL VENT O

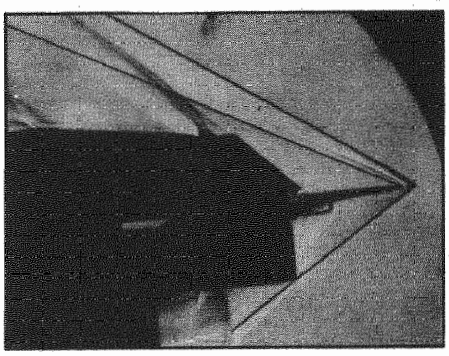

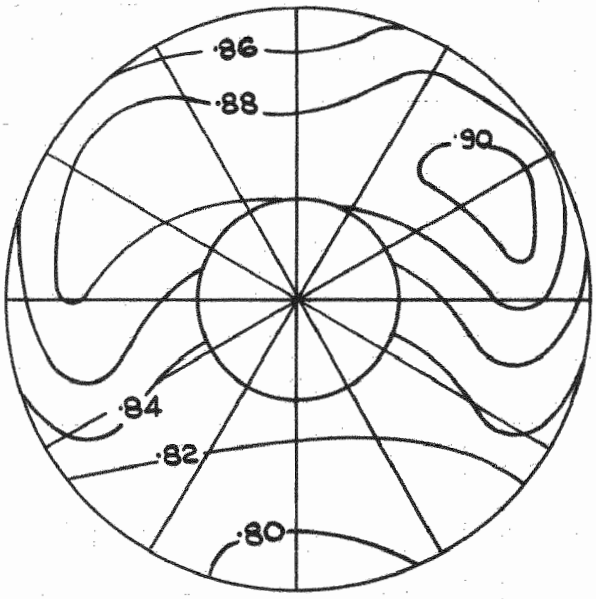

m_e/m_i	0·795
m_b/m_i	0·053
m_{sv}/m_i	0

P_f/P_∞	0·863	A_∞/A_{en}	0·848

(b) SPILL VENT O

FIG. 58 PRESSURE DISTRIBUTIONS FOR THE OUTBOARD DUCT AND SCHLIEREN PHOTOGRAPHS, CORRESPONDING WITH LETTERED POINTS ON FIG. 59

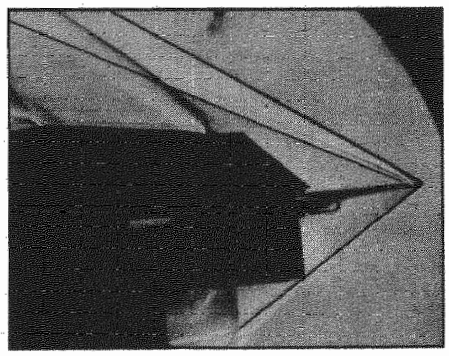

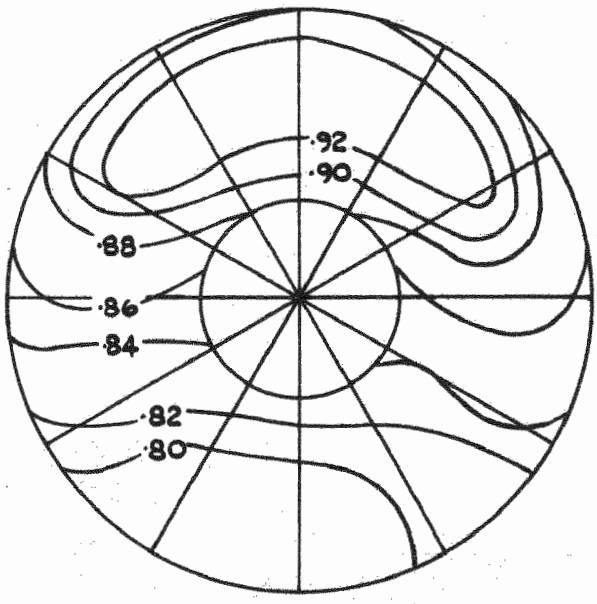

m_e/m_i 0·799

m_b/m_i 0·034

m_{sv}/m_i <0·078

p_f/p_∞ 0·878	A_∞/A_{en} <0·911

(c) SPILL VENT 1

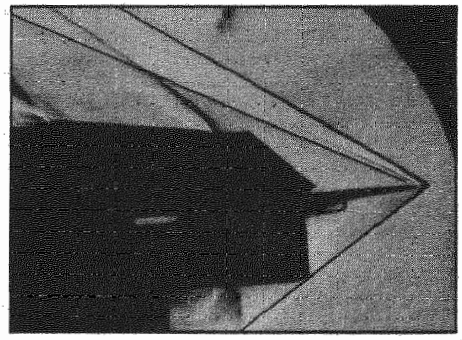

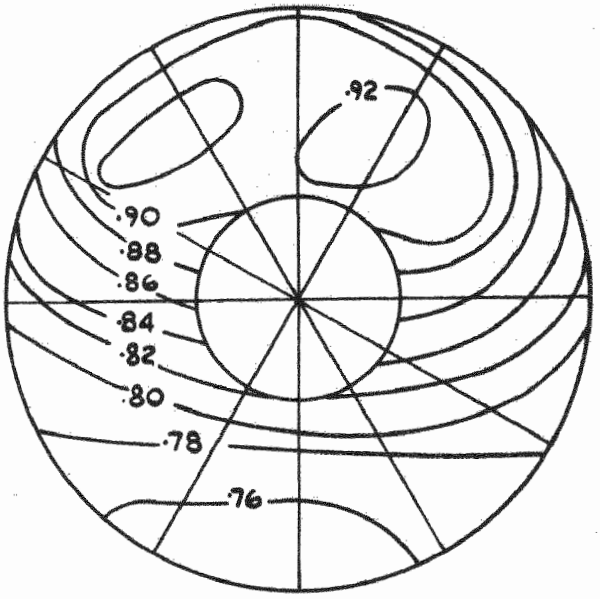

m_e/m_i 0·781

m_b/m_i 0·032

m_{sv}/m_i 0·113

p_f/p_∞ 0·868	A_∞/A_{en} 0·926

(d) SPILL VENT 2

FIG. 58 (CONT'D)

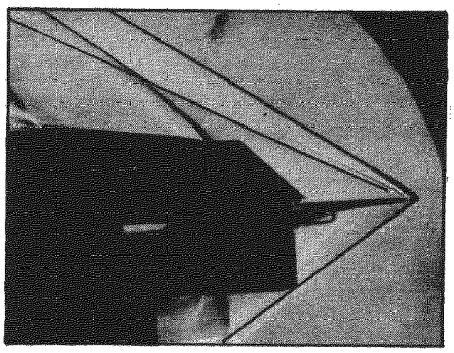

m_e/m_i 0·743

m_b/m_i 0·023

m_{sv}/m_i 0·160

P_f/P_∞ 0·832	A_∞/A_{en} 0·926

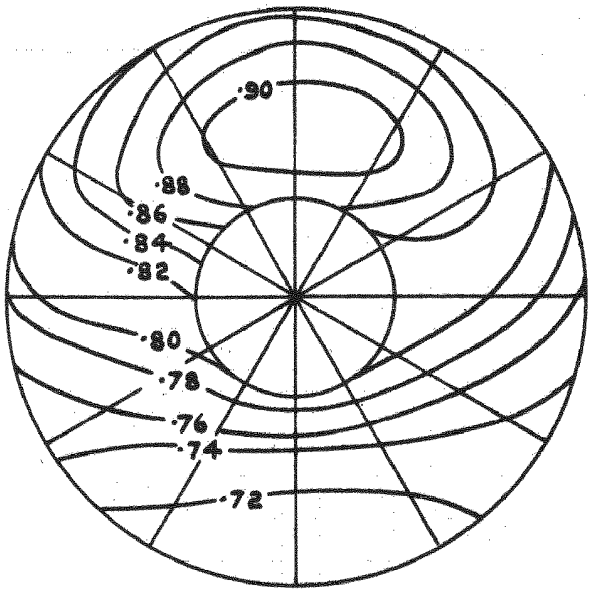

(e) SPILL VENT 3.

FIG. 58 (CONCL)

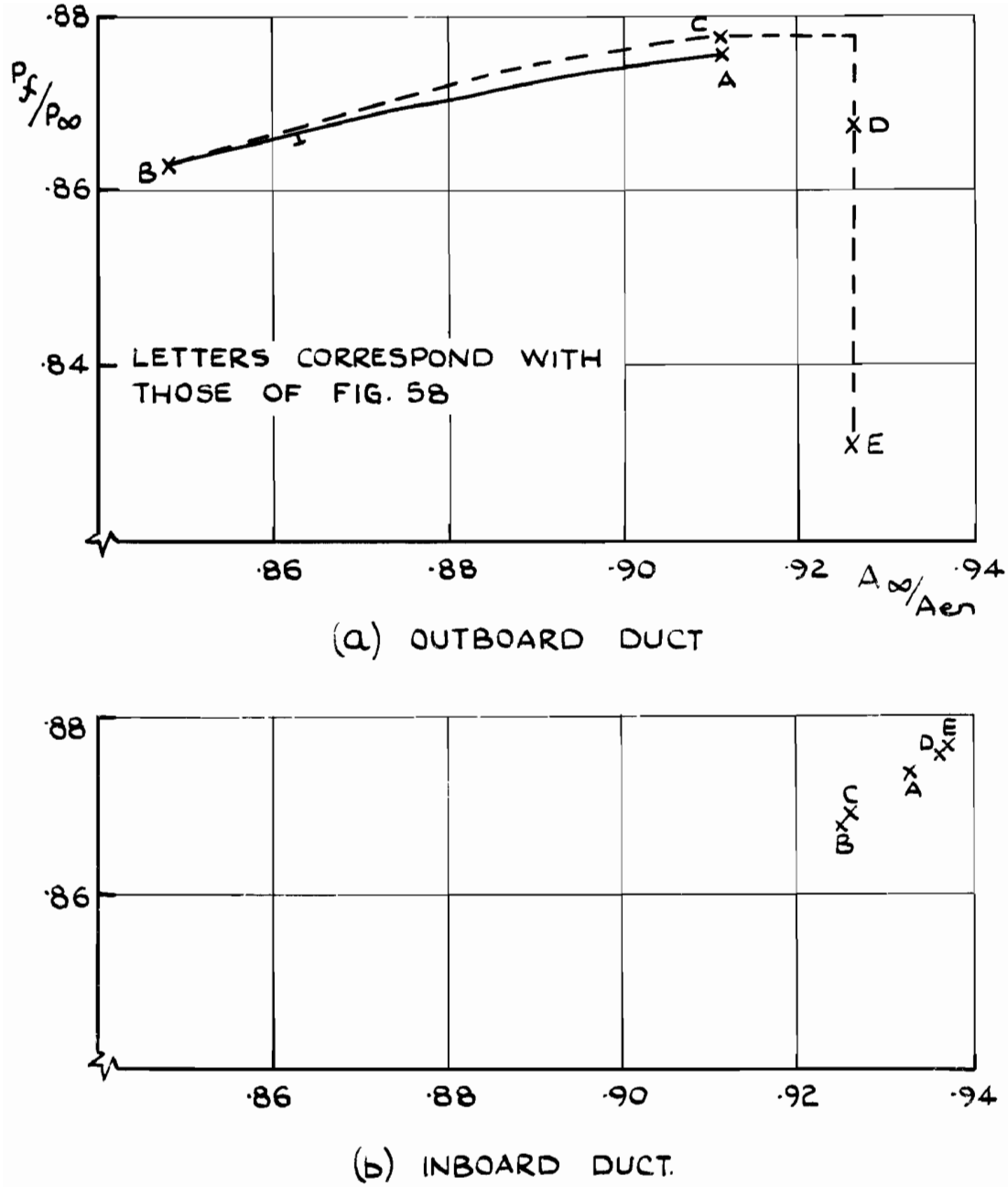

FIG. 59 PRESSURE RECOVERY— VARIATION WITH MASS FLOW RATIO, SHOWING EFFECTS OF OPENING SPILL VENTS. $M = 2{\cdot}12$, $\delta_3 = 16{\cdot}25°$, SPLITTER III

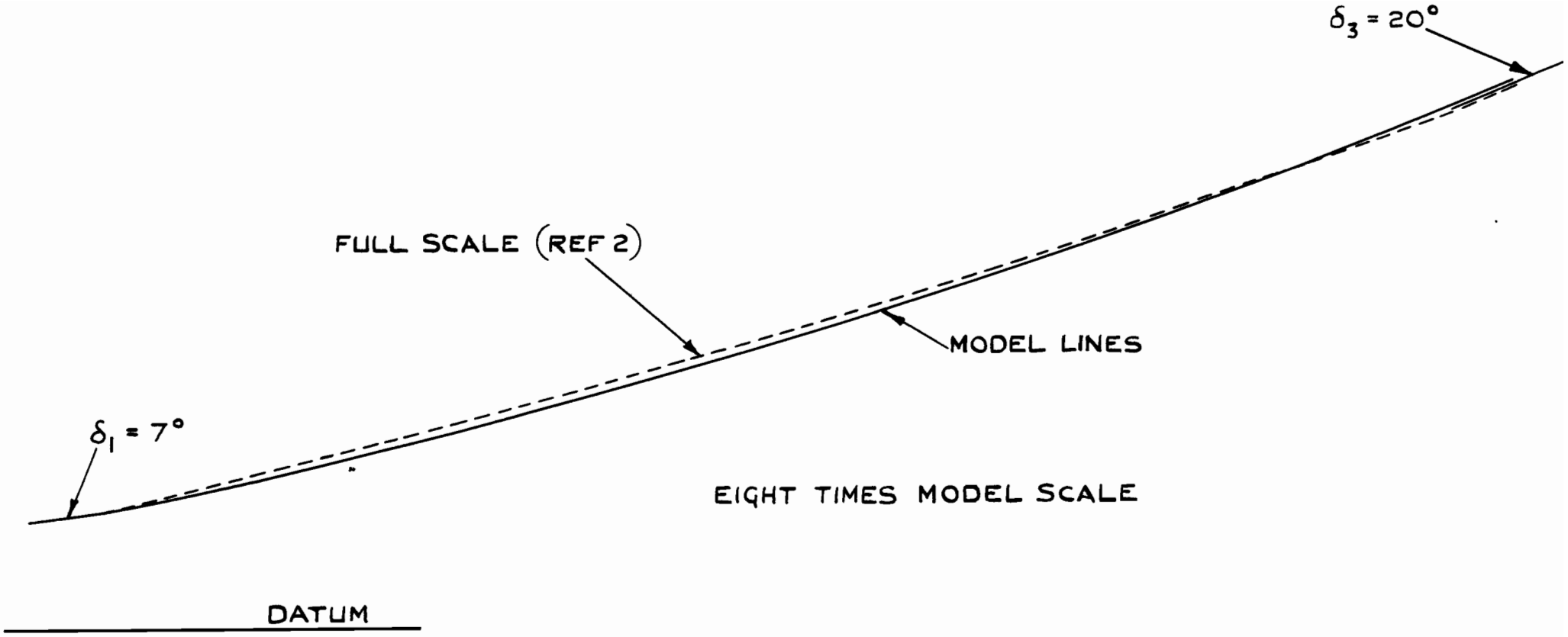

APPENDIX SKETCH A. COMPARISON OF COMPRESSION GEOMETRY

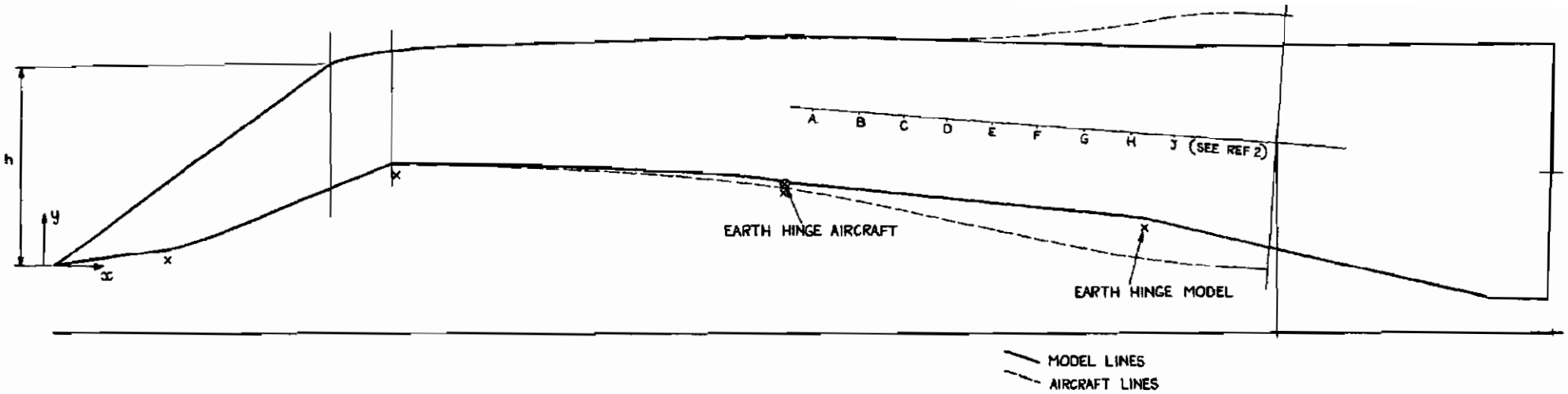

APPENDIX SKETCH B – COMPARISON OF MODEL AND AIRCRAFT DIFFUSER LINES

Printed in England for Her Majesty's Stationery Office by the Royal Aircraft Establishment, Farnborough. Dd.125875.K4.

A.R.C. C.P. No.944
April 1966

Dobson, M.D.

533.697.2 :
533.6.011.5

WIND TUNNEL TESTS ON A RECTANGULAR, TWIN DUCT, VARIABLE GEOMETRY AIR INTAKE AT SUPERSONIC SPEEDS

Tests have been made in the 3 ft x 3 ft supersonic wind tunnel on a rectangular twin duct air intake, which has variable geometry, over the Mach number range 1.7 to 2.2. The design Mach number of the intake was 2.12 and tests included an investigation of the effects of the variable geometry, throat bleed flow, transition fixing, splitter design and after-spill for conditions of equal and unequal throttling of the ducts.

Pressure recovery, duct mass flow and bleed mass flow were measured and the amplitude and frequency of pressure fluctuations were recorded.

(Over)

A.R.C. C.P. No.944
April 1966

Dobson, M.D.

533.697.2 :
533.6.011.5

WIND TUNNEL TESTS ON A RECTANGULAR, TWIN DUCT, VARIABLE GEOMETRY AIR INTAKE AT SUPERSONIC SPEEDS

Tests have been made in the 3 ft x 3 ft supersonic wind tunnel on a rectangular twin duct air intake, which has variable geometry, over the Mach number range 1.7 to 2.2. The design Mach number of the intake was 2.12 and tests included an investigation of the effects of the variable geometry, throat bleed flow, transition fixing, splitter design and after-spill for conditions of equal and unequal throttling of the ducts.

Pressure recovery, duct mass flow and bleed mass flow were measured and the amplitude and frequency of pressure fluctuations were recorded.

(Over)

A.R.C. C.P. No.944
April 1966

Dobson, M.D.

533.697.2 :
533.6.011.5

WIND TUNNEL TESTS ON A RECTANGULAR, TWIN DUCT, VARIABLE GEOMETRY AIR INTAKE AT SUPERSONIC SPEEDS

Tests have been made in the 3 ft x 3 ft supersonic wind tunnel on a rectangular twin duct air intake, which has variable geometry, over the Mach number range 1.7 to 2.2. The design Mach number of the intake was 2.12 and tests included an investigation of the effects of the variable geometry, throat bleed flow, transition fixing, splitter design and after-spill for conditions of equal and unequal throttling of the ducts.

Pressure recovery, duct mass flow and bleed mass flow were measured and the amplitude and frequency of pressure fluctuations were recorded.

(Over)

DETACHABLE ABSTRACT CARDS

Maximum mean pressure recoveries recorded were generally up to 2½% below the theoretical shock recovery. Recovery increases with the introduction of throat bleed and is dependent to some extent on transition of the boundary layer, bleed slot position and splitter design. At reduced duct mass flows both pressure recovery and distribution may be restored to "full flow" levels by careful use of afterspill.

Unequal throttling produces interference effects on the "unthrottled" duct by the "throttled" duct. These effects may be eliminated by the use of afterspill in the "throttled" duct.

Maximum mean pressure recoveries recorded were generally up to 2½% below the theoretical shock recovery. Recovery increases with the introduction of throat bleed and is dependent to some extent on transition of the boundary layer, bleed slot position and splitter design. At reduced duct mass flows both pressure recovery and distribution may be restored to "full flow" levels by careful use of afterspill.

Unequal throttling produces interference effects on the "unthrottled" duct by the "throttled" duct. These effects may be eliminated by the use of afterspill in the "throttled" duct.

Maximum mean pressure recoveries recorded were generally up to 2½% below the theoretical shock recovery. Recovery increases with the introduction of throat bleed and is dependent to some extent on transition of the boundary layer, bleed slot position and splitter design. At reduced duct mass flows both pressure recovery and distribution may be restored to "full flow" levels by careful use of afterspill.

Unequal throttling produces interference effects on the "unthrottled" duct by the "throttled" duct. These effects may be eliminated by the use of afterspill in the "throttled" duct.

© *Crown Copyright 1967*

Published by
HER MAJESTY'S STATIONERY OFFICE

To be purchased from
49 High Holborn, London W.C.1
423 Oxford Street, London W.1
13A Castle Street, Edinburgh 2
109 St. Mary Street, Cardiff
Brazennose Street, Manchester 2
50 Fairfax Street, Bristol 1
35 Smallbrook, Ringway, Birmingham 5
7-11 Linenhall Street, Belfast 2
or through any bookseller

C.P. No. 944

S.O. CODE No. 23-9017-44